UNCERTAINTY QUANTIFICATION IN WIND FARM FLOW MODELS

JUAN PABLO MURCIA

PH.D. THESIS

DECEMBER 2017

DTU Wind Energy
Department of Wind Energy

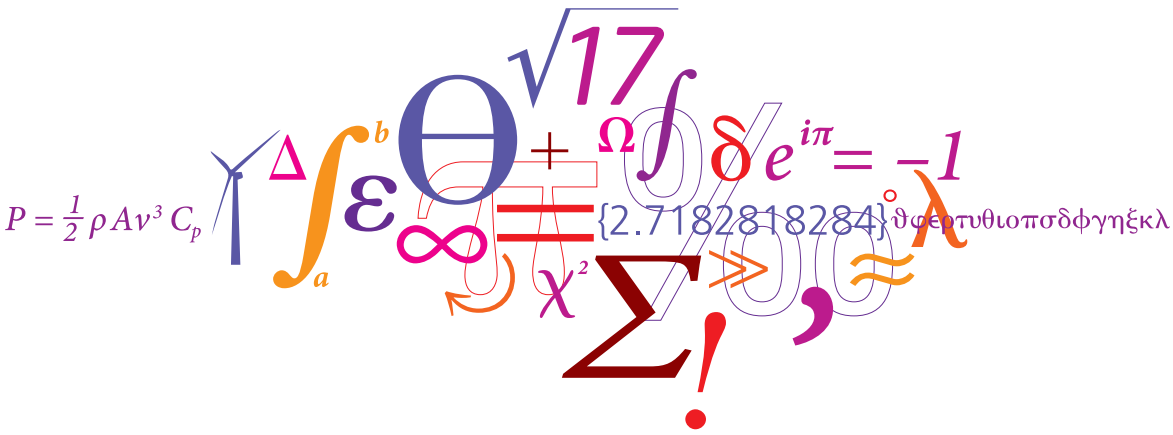

This document was typeset with XeLaTeX. The book design is based on the Tufte-LaTeX document class and the DTU Compute PhD thesis template.

DTU Wind Energy
Technical University of Denmark
Building 125
Risø Campus
Frederiksborgvej 399
4000 Roskilde
Denmark
Phone +45 2339 7790
jumu@dtu.dk

Preface

This thesis is submitted in partial fulfillment of the requirements for the Ph.D. degree from the Technical University of Denmark (DTU). The research work presented in this thesis was conducted during the period from December 2013 to December 2016 at the Department of Wind Energy, in the Aeroelastic Design (AED) and Resource Assessment Modelling (RAM) Sections.

I wish to express my sincere gratitude to my supervisor Senior Researcher Pierre-Elouan Réthoré for his support, patience and for all the brain storming sessions that have marked my research interest for many years to come. I will also like to thank him for the opportunity to be a part of his team in such interesting topics as it is Uncertainty Quantification.

I would also like to express my gratitude to Professor John Sørensen, Senior Scientist Anand Natarajan, Assistant Professor Søren Andersen for many useful conversations and for all their valuable suggestions.

I would like to thank my colleagues, fellow students and friends at the department for providing an amiable environment with room for humor, interesting discussions and collaboration.

Finally, I would thank my family and friends for their support.

Juan Pablo Murcia
Roskilde, December 2016

Summary

This thesis formulates a framework to perform uncertainty quantification within wind energy. This framework has been applied to some of the most common models used to estimate the annual energy production in the planning stages of a wind energy project. Efficient methods to propagate input uncertainties through a model chain are presented and applied to several wind energy related problems such as: annual energy production estimation, wind turbine power curve estimation, wake model calibration and validation, and estimation of lifetime equivalent fatigue loads on a wind turbine. Statistical methods to describe the joint distribution of multiple variables are applied to the description of the wind resources at a given location. A new method to predict the performance of an aeroelastic wind turbine model, and its corresponding uncertainty, is presented. This approach helps understand the uncertainty in the lifetime performance of a wind turbine under realistic inflow conditions. Operational measurements of several large offshore wind farms are used to perform model calibration and validation of several stationary wake models. These results provide a guideline to identify the regions in which a model fails to make accurate predictions, and therefore help guide research and development to focus on areas with the biggest uncertainty to lower costs of energy effectively.

Resumé

Denne afhandling opstiller en fremgangsmåde til at kvantificere usikkerheder indenfor vind energi. Fremgangsmåden benyttes på nogle af de mest almindelige modeller til bestemmelse af den årlige energi produktion i forbindelse med planlægningen af vind energi projekter.

Effektive metoder til at føre input usikkerheder igennem en modelkæde præsenteres og anvendes på flere relaterede vind energi problemer, såsom bestemmelse af årlig energi produktion, vindmøllers effektkurver, kalibrering og validering af kølvandsmodeller samt vurdering af udmattelseslaster i vindmøllens levetid. Statistiske metoder til beskrivelse af multivariable fordelinger er anvendt til beskrivelse af vind ressourcer på et givent sted.

En ny metode til at forudsige ydeevnen af en aeroelastisk vindmøllemodel, og de tilhørende usikkerheder, præsenteres. Denne tilgang øger forståelsen af usikkerheden af en vindmølles ydeevne under realistiske indstrømningsbetingelser.

Målinger fra flere fungerende offshore vindmølleparker er brugt til at kalibrere og validere flere stationære kølvandsmodeller. Disse resultater giver retningslinjeri forhold til at identificerer områder, hvor de enkelte modeller giver unøjagtive forudsigelser, og derfor understøtte forskning og udvikling til at fokusere på områder med størst usikkerhed for derved at sænke prisen af energi effektivt.

List of Publications

Papers included in this thesis

The following papers can be found in the appendices order according the topic. Here the articles are ordered chronologically.

Papers presented at peer-reviewed conferences

[1] Murcia et al. 2015. How many model evaluations are required to predict the AEP of a wind power plant?

[2] Murcia et al. 2015. A new method to estimate the uncertainty of AEP of offshore wind power plants applied to Horns Rev 1.

Paper submitted to peer-reviewed journal

[3] Murcia et al. 2016. Improved validation of stationary wake models using uncertainty propagation.

[4] Murcia et al. 2016. Uncertainty propagation through an aeroelastic wind turbine model using polynomial surrogates.

[5] Murcia et al. 2016. Wake model calibration based on SCADA data considering uncertainty in the inflow conditions.

Other publications not included in this thesis

The following publications have been prepared during the course of the PhD study as contributing author. They are omitted from this thesis.

Papers as contributing author presented at peer-reviewed conferences

[6] Wang et al. 2016. Multi-fidelity wake modelling based on Co-Kriging method.

Papers as contributing author submitted to or published in peer-reviewed journal

[7] Laan et al. 2015. The k-ϵ-f_P model applied to wind farms.

[8] Pavese et al. 2017. Design of a wind turbine swept blade through extensive load analysis.

[9] Meyer et al. 2016. Validation of a CFD model with a synchronised triple-lidar system in the wind turbine induction zone.

Contents

List of Figures

List of Tables

Abbreviations

AD	Actuator Disc 43, 44
AEP	Annual Energy Production 21, 22, 32, 36, 44, 52, 70, 100, 101
AL	Actuator Line 43, 44, 46
CDF	Cumulative Density Function 56, 59
CFD	Computational Fluid Dynamics 37
DBGS	Derivative Based Global Sensitivity Index 80–82
DBS	Derivative Based Sensitivity Index 81
DWM	Dynamic Wake Meandering 43, 44, 46
EEA	European Environment Agency 21
FFT	Fast Fourier Transformation 66
GUM	Guide to the expression of Uncertainty in Measurement 25
LCoE	Levelized Cost of Energy 21, 22, 31, 36, 70, 101
LES	Large Eddies Simulation 37, 43, 44, 46
LSE	Least Squared Errors 88, 89, 92, 93, 97
MAP	Maximum a Posteriori 90
MLE	Maximum Likelihood Estimation 88, 89, 94
PCE	Polynomial Chaos Expansion 72–77
PDF	Probability Density Function 23–27, 46, 52, 55, 56, 58, 63, 65
QoI	Quantity of Interest 36, 75
RANS	Reynolds Averaged Navier-Stokes 37, 43, 44
RBF	Radial Basis Function 77–80
RSS	Residual Sum of Squares 89
SCADA	Supervisory Control And Data Acquisition 45
UQ	Uncertainty Quantification 23, 101
WLSE	Weighted Least Squared Errors 88, 89, 92–94, 97
WRF	Weather Research & Forecasting Model 38
WSS	Weighted Sum of Squares 89

When asked how to deal with uncertainty in life one realizes that there are three options: to hide and avoid the external world, to live without considering consequences, or to understand the risks and try to get the most out of things.

Chapter 1

Introduction

After years of negotiations, all nations have signed an agreement to mitigate the effects of climate change in the UNFCCC COP21 Paris 2015[1]. The objective of the mitigation efforts is to keep the global temperature rise below 2°C above pre-industrial levels. The European Environment Agency (EEA) has established targets for reduction of greenhouse gases emissions to 20% in 2020, 40% in 2030 and at least 80% by 2050. These targets are implemented by increasing the share of the renewable energy sources in the total energy consumption up to 20% by 2020 and up to at least 27% by 2030 [10]. Wind energy is one of the main sources of renewable energy; in 2015 the total amount of wind energy capacity installed (63 GW) represented 50% of the total energy capacity installed world wide [11]. To fulfill these targets, it is required to continue decreasing the Levelized Cost of Energy (LCoE) for wind projects to competitive levels with respect to fossil fuels projects, a goal that has come true as onshore wind energy is cheaper than other energy options for some markets, see [12] for comparison of levelized cost of energy for different technologies.

[1] United Nations Framework Convention on Climate Change, Conference Of The Parties

[10] EEA. 2016

[11] GWEC. 2016

[12] Lazzard. 2015

The estimation of the cost of energy of a wind energy project takes into account parameters such as the Annual Energy Production (AEP), the operation and maintenance costs, the capital cost of the project, the interest rates and the expected lifetime of the project among others. In the planning stage of a wind project most of these variables are uncertain. Estimating the uncertainty in the prediction of the lifetime energy production of large wind plants is one of the main aspects that needs to improve in order to asses the financial viability of wind energy projects [13]. Optimized wind plant designs that minimize the cost of energy require an understanding of the uncertainty in the energy production, in the operation and

[13] Gass et al. 2011

maintenance costs, and in the lifetime of the project. The former two variables can be related to the lifetime accumulated fatigue damage in the structural components of every wind turbine in the project [14] among other additional parameters.

[14] Réthoré et al. 2013

1.1 Uncertainty Quantification in Wind Energy

Wind energy is a field in which the main variables have a natural stochasticity e.g. the long term wind resources on a site have variability caused by the yearly or longer term variability. Additionally, the estimation of the performance of a wind plant uses a combination of models such as a wind resource assessment flow model, a wind turbine model and a wake model. The accuracy of each of these models needs to be evaluated in order to be able to estimate the uncertainty in the AEP and the LCoE of a wind energy project. Additionally, part of the evaluation of the viability of a wind energy project requires the estimation of the uncertainty in the AEP, which is usually given as the 90% quantile of its predicted distribution, P90. See figure 1.1. Wind energy has two problems that are central to the uncertainty quantification field: the natural variability in some of the variables and the possibility that the models are not perfect under all the possible conditions. The following sections define the vocabulary of uncertainty quantification.

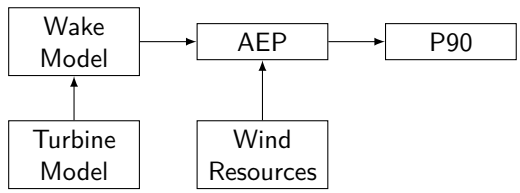

Figure 1.1: Model structure for typical AEP estimation.

1.2 Basic definitions

The estimation of the accuracy of the predictions of a computational model is a key problem in modern sciences and engineering. This problem needs to account for the aspects of the system that are not well known and for the stochastic behaviors in some of the modeled variables. The term *Uncertainty* is ambiguous because it refers to both of these problems: the stochastic behavior and the lack of

knowledge [15]. In this thesis, a variable is said to be uncertain if it is modeled as a stochastic variable.

[15] Oberkampf et al. 2002

Aleatoric uncertainty is used to describe the stochasticity or inherent variability in a variable. Aleatoric uncertainties can not be reduced as they are intrinsic to the reality being modeled. An example of a variable that has aleatoric uncertainty is the wind speed at a given height and location over the years. Variables with aleatoric uncertainty are represented with a Probability Density Function (PDF).

Epistemic uncertainty is used to refer to variables that are not well known. This type of uncertainty could be reduced if time and money are spent in better understanding, measuring or modeling the variable. An example of epistemic uncertainty is the uncertainty related to any measurement. A high quality instrument produces measurements with narrower tolerances. Variables with epistemic uncertainties can be represented using an uniform PDF.

Error is defined as the difference between a variable and its true value. Errors are the product of imperfect measurements or imperfect models. Errors can not be known and therefore need to be modeled as uncertain variables.

The purpose of Uncertainty Quantification (UQ) is to gain insight about the accuracy and precision of a model, and to understand what are the consequences in the predictions of having stochastic variables in the model chain. More specifically, a model with UQ will help make informed decisions by estimating the probability distributions of the predictions. A robust UQ framework can be the tool for certification tasks and can help decision makers to identify the aspects that require further research and investment in order to improve the accuracy in the predictions.

1.3 Modeling and Measuring Reality

In this section we define the variables and terminology used when referring to a modeling and measuring campaign. This section also identifies the different sources of uncertainty that could be introduced into a modeling chain. Figure 1.2 describes the process of measuring and modeling reality.

A model tries to capture the real process that relates the true input variables $\mathbf{x}$ to the true output variables $\mathbf{y}$. The model receives additional parameters $\boldsymbol{\theta}$ to make a prediction: $\mathcal{M}(\mathbf{x}, \boldsymbol{\theta})$. The model parameters are defined as independent of the inputs. Models are not perfect and therefore there is a difference between the true outputs and the model predictions: the model prediction error, $\boldsymbol{\varepsilon}_{\mathcal{M}}$.

On the other hand, measurements of the inputs, $\tilde{\mathbf{x}}$, and of the outputs, $\tilde{\mathbf{y}}$, are performed. The difference between the true variables and the measurement is called measurement error, $\boldsymbol{\varepsilon}_{\mathbf{x}}$ or $\boldsymbol{\varepsilon}_{\mathbf{y}}$. Note that the diagram represents the measurement and modeling process for a single realization of the true inputs and outputs.

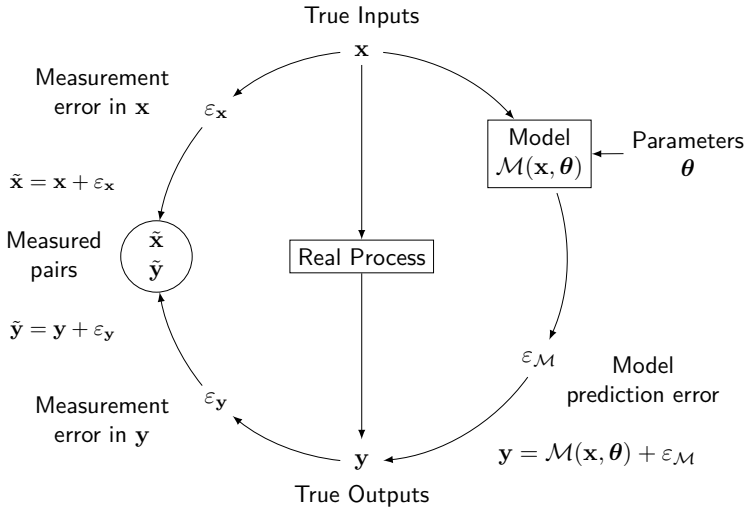

Figure 1.2: Measuring and modeling reality. Diagram modified from [16].

[16] Huard et al. 2006

Physical uncertainty or natural variability is an aleatoric uncertainty caused by the stochastic nature of a variable. It is referred to as residual variability because it cannot be reduced. The physical uncertainty may be present in the true input and output variables. The natural variability is characterized by the PDF of the true variable: $f(\mathbf{x})$ or $f(\mathbf{y})$.

Measurement uncertainty is a mixed of aleatoric and epistemic uncertainties. It is caused by the imperfection of every measurement process due to signal noise, dynamical response of the sensor, calibration issues, faulty set-up of experiment racks, etc. This type of uncertainty introduces biases and noise in the measurements therefore it has a mixed behavior between aleatoric and epistemic uncertainty. Measurement uncertainty is present in the observed variables, $\tilde{\mathbf{x}}$ and $\tilde{\mathbf{y}}$, and it is characterized by the PDF of the measurement errors: $f(\boldsymbol{\varepsilon}_{\mathbf{x}})$ or $f(\boldsymbol{\varepsilon}_{\mathbf{y}})$.

The Guide to the expression of Uncertainty in Measurement (GUM) [17] classifies measurement uncertainties into two groups: *Type A measurement uncertainty* represents the component of the uncertainty that can be estimated from multiple independent repetitions of the measurement using the standard error of the mean which is a consequence of the central limit theorem. *Type B measurement uncertainty* represents the epistemic uncertainty in the measurements due to the instrument or measurement process. Type B measurement uncertainty is estimated by assuming a PDF based on experience about the instrument performance such as calibration errors, signal drifts, data acquisition errors, etc. Type B uncertainty estimation relies on the information given by the manufacturer and by the standardization agencies. Combining the information from the Type A and B sources of measurement uncertainties gives an estimation of the PDF of the measurement errors.

[17] ISO et al. 2008

Parameter uncertainty is the epistemic uncertainty that captures the lack of knowledge about the true value of the parameters used in the model. The model parameters can represent physical constants or simply tunning parameters that need to be calibrated using measurements. The parameter uncertainty is characterized by the PDF of the parameters, $f(\boldsymbol{\theta})$.

Model uncertainty is an epistemic uncertainty caused by the imperfection of the model. The model uncertainty reflects the regions in which the assumptions in the model are a good representations of reality and the regions in which there is a lack of physics in the model. The model uncertainty is characterized by the PDF of the model prediction error $f(\boldsymbol{\varepsilon}_{\mathcal{M}})$ and it depends on the input variables. [2]

[2] An example of the dependence of model uncertainty on the inputs is Newton's theory of gravity. It can be used to design a wind turbine but it should not be used to calculate the location of a GPS device using satellite triangulation. The validation region of Newton's theory depends on the speed of the bodies studied.

Statistical uncertainty is the epistemic uncertainty due to the limited sample size of any variable. Observations are in many cases scarce and limited for both measurements and simulations, therefore the PDF of a variable cannot be determined exactly. If additional observations are provided then the statistical uncertainty may be reduced. The statistical uncertainty appears in every uncertain variable modeled with a PDF, such as the measurements, $f(\mathbf{x})$ or $f(\mathbf{y})$, as well as in the model predictions, $f(\mathcal{M}(\mathbf{x}, \boldsymbol{\theta}))$.

1.4 Framework for Model Verification, Validation and Uncertainty Quantification

This section gives the definitions, objectives and the key review references for each of the steps of a model verification, validation and uncertainty quantification (VV&UQ) process. For more details about the framework readers are referred to [18][19].

[18] Oberkampf et al. 2010
[19] Oberkampf et al. 2004

Model verification: To evaluate the accuracy of the model to solve the mathematical problem. The verification step has two objectives: *Solution verification* consists in quantifying the numerical accuracy of the representation and solution of the mathematical problem. Code verification consists in assessing the reliability of the implementation. A review of methodologies for estimation of numerical errors in complex models can be found in [18].

Input uncertainty elicitation: To identify the different sources of uncertainty; to define a mathematical structure to represent them and their correlation structure; and to fit their joint PDF $f(\mathbf{x})$. Since the input variables are measured it is required to take into account measurement uncertainties and statistical uncertainties. A review of the methods to describe multi-dimensional correlated PDF can be found in [20].

[20] Biller et al. 2006

Uncertainty propagation or uncertainty analysis: To determine the uncertainty in the model prediction that is produced by the inputs and parameters uncertainties. The outcome of this process is the PDF of the model output given a PDF of the inputs, $f(\mathcal{M}(\mathbf{x}, \boldsymbol{\theta}))$, see Figure 1.3. This process is the core of the uncertainty quantification problem as it is a requirement for following steps such as sensitivity analysis, model calibration and model validation. A survey of methods for uncertainty propagation can be found in [21].

[21] Helton et al. 2003

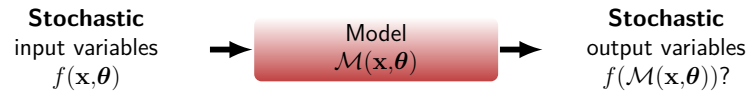

Figure 1.3: Propagation of uncertainty problem.

Sensitivity analysis: To detect which sources of uncertainty have the largest impact on the variation of the outputs. Consequently, sensitivity analysis can help the modeler simplify the UQ problem by identifying the variables whose uncertainty can be neglected. A review of the different methods used to perform sensitivity analysis can be found in [22].

[22] Saltelli et al. 2000

Model calibration: To determine the values of the model parameters given a set of measurement pairs, $(\tilde{\mathbf{x}}, \tilde{\mathbf{y}})$. The result of a calibration process is the joint PDF associated to the parameters, $f(\boldsymbol{\theta})$. This PDF quantifies both the lack of knowledge about the true value and the natural variability in the parameters. The PDF of the parameters is also a consequence of the measurement uncertainties in the measured pairs. A review of model calibration is given in [23].

[23] Tarantola. 2005

Model validation: To estimate the model prediction error given a set of measurement pairs, $(\tilde{\mathbf{x}}, \tilde{\mathbf{y}})$. The result of a validation process is the PDF of the model prediction error as a function of the true input variables $f(\boldsymbol{\varepsilon}_{\mathcal{M}}) = f(\zeta(\mathbf{x}))$. The change of notation from $\boldsymbol{\varepsilon}_{\mathcal{M}}$ to $\zeta(\mathbf{x})$ represents the fact that the model prediction error distribution can be estimated a priori on an unvalidated input case using the previous validation efforts.The validation process is performed in different validation points in the input space in order to identify the region in which the model is accurate enough for the application. The limits of the validation region depend on the user tolerance to model uncertainty. For some general examples of model validation refer to [24], [25].

[24] Roy et al. 2011
[25] Higdon et al. 2004

Model Assessment: To perform model selection and/or model combination to minimize the total output uncertainty. In model combination each model contributes information to the final prediction with the objective of minimizing a cost function defined based on the final output uncertainty and the computational cost. A survey of model combination is presented in [26].

[26] Peherstorfer et al. 2016

1.5 Problem statement

Uncertainty in the predicted performance of a wind plant depends on the uncertainty in the wind resource estimation and in the uncertainty of each of the models in the model chain. The primary questions this thesis seeks to answer are:

- What is the effect of the different turbulent inflow conditions in the performance of a wind turbine?
- How does the wake model prediction errors affect the estimation and the uncertainty in the annual energy production of an arbitrary wind plant?

- Can the uncertainty of a simplified wake model be capture through a calibration process?
- How can we establish a systematic procedure for model validation in wind energy?

1.5.1 Methodology

In order to answer these questions the following methods were researched:

- Statistical methods to handle the typical correlated PDFs that are observed in the atmospheric variables.
- Efficient methods to propagate input uncertainties through non-linear models and to perform sensitivity analysis.
- Methods to post-process the operational data from an offshore wind plant to define calibration and validation datasets. This methods include the estimation of the measurement uncertainties.
- Model calibration and model validation methods based on datasets that have uncertainties in both inputs and outputs.

1.6 Contributions

The main focus of this thesis was the development of key concepts related to the uncertainty quantification in wind energy. The main contribution of this thesis to the field are:

VV&UQ framework: A model verification, validation and uncertainty quantification has been applied to the wind plant performance problem.

Stochastic surrogate of an aeroelastic wind turbine model: A methodology to build stochastic surrogates of the aeroelastic model of a wind turbine has been developed. These surrogates help understand the uncertainty in the wind turbine model under realistic inflow conditions [4].

[4] Murcia et al. 2016

Wake model validation and calibration: Wake model calibration and validation procedures have been implemented using several databases of operational measurements from offshore wind plants. This

technique could improve the practice of the wind energy industry in terms of model development and evaluation because it helps to identify the regions in which a model fails to make accurate predictions [3] [5].

[3] Murcia et al. 2016
[5] Murcia et al. 2016

1.7 Thesis Structure

Each chapter of this thesis contains a literature review, an overview of the most important concepts, illustrative examples and corresponding sub-conclusions. Chapter 2 discusses the different model chains used in wind energy and gives an overview of the previous uncertainty quantification efforts done on each of the submodels. Chapter 3 presents the different options to handle multidimensional stochastic variables with different correlation structures. Additionally, this chapter explains the basic methodology to generate a sample from such distributions. Chapter 4 presents the different methods for efficient propagation of uncertainty and sensitivity analysis. Chapter 5 contains the formulation to perform model calibration and validation. These two techniques are grouped as they share a similar problem structure. Relevant examples and applications on wind energy are given for each method presented. Overall conclusions and perspectives on future work are presented in Chapter 6. The articles forming the research content of the thesis are found as appendices.

Chapter 2

Wind Plant Flow Modeling

Wind energy in the world is growing at an accelerated pace and large wind plants and wind plant clusters[1] are being developed on sites with good wind resources. This scenario is happening for offshore in the North Sea and the coasts of UK, and for onshore in China, USA and Brazil [11][2]. Some examples of such large projects are:

- Gansu (China, 2010 and 2012): 6000 MW wind energy complex consisting of 60 wind plants.
- Shepherds Flat (USA, 2012): 845 MW plant composed of 338 turbines.
- Ventos de Santa Joana complex (Brazil, 2015): 439 MW distributed over 15 wind plants.
- London Array (UK, 2013): 630 MW offshore plant composed of 175 wind turbines.
- Gwynt y Môr (UK, 2015): 576 MW offshore plant composed of 160 wind turbines.

The large wind project developers are continuously dropping the price of energy in their bids for the development of new wind energy projects. An example of this improvement can be seen in the offshore European market. DONG Energy bid €72.7/MWh for Borssele I and II 700 MW offshore wind plant (Holland) in 2016, while for Anholt 400 MW offshore wind plant (Denmark) the bid was €140/MWh in 2010 [27]. Vattenfall dropped this price even lower to €49.9/MWh for Kriegers Flak 600 MW offshore wind plant (Denmark) [28]. This reduction of the biding price requires an accurate estimation of the LCoE. As it was mentioned in the Introduction

[1] A wind plant cluster or complex is a site with several wind plants

[11] GWEC. 2016

[2] It is important to remark that most modern wind energy projects are onshore. Only ~12 GW out of the total ~433 GW installed wind power available by the end of 2015 are offshore [11]

[27] DONG. 2016

[28] Vattenfall. 2016

chapter, the estimation of the cost of energy of a wind energy project takes into account parameters such as the AEP, the operation and maintenance costs, the capital cost of the project, the interest rates and the expected lifetime of the project among others.

2.1 Structure of a Wind Plant Flow Model

The estimation of the performance of a wind plant uses a combination of models such as a wind resource assessment flow model, a wind turbine model and a wake model, see Figure 2.1. The wind resource assessment flow model predicts the local long term wind resources at each wind turbine site. The flow model captures the effect of the terrain, obstacles and elevation in the surroundings of the wind plant and on each turbine. The wind turbine model predicts the power and loads given the local inflow conditions (including wakes produced upstream). The wake model modifies the inflow conditions for each turbine operating behind the wake(s) of other turbines using the turbine model and the atmospheric inflow conditions.

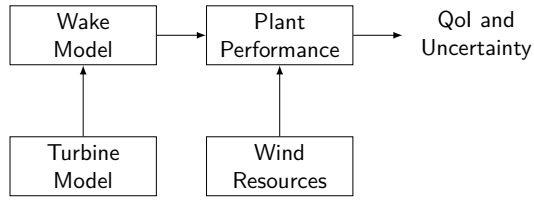

Figure 2.1: Model chain structure for typical wind plant performance estimation.

2.2 Quantities of Interest

There are three groups of quantities of interest (QoI) that are studied using wind plant flow models: energy production, wind turbine loads and cost of energy.

2.2.1 Energy Production

The annual energy production (AEP) is the most common measure of wind plant performance used in wind project planning. The AEP represents the expected mean energy production during a certain return period, usually the lifetime of the project (∼20 years). This

means that the AEP is proportional to the expected power production under all the possible atmospheric conditions during the lifetime of the project. An equivalent QoI to the AEP is the power plant capacity factor (CF) that normalizes the AEP by the energy that would be produced in a year if the plant constantly produced the rated power.

AEP of a single wind turbine

The distribution of the long term wind resources at the location and the hub height of a turbine is characterized by the joint probability density function $f(\mathbf{x})$. Traditionally, the wind conditions are represented by the wind speed and wind direction averaged over a time step Δt of usually 10 min or 1 hour: $\mathbf{x} = [U, \theta]$. The AEP of a single wind turbine, $\mathrm{AEP_T}$, is estimated by computing the expected power production over the long term distribution of the wind resources, see equation 2.1. The constant n_t represents the number of time steps in a year and a factor for change of units, i.e. $n_t = 8760$ for 10 min averages and for AEP in [MWh].

$$\mathrm{AEP_T} = n_t\,\Delta t\,\mathbb{E}(P_\mathrm{T}) = n_t\,\Delta t \int_{\Omega_\mathbf{x}} P_\mathrm{T}(\mathbf{x})\,f(\mathbf{x})\,d\mathbf{x} \tag{2.1}$$

AEP of a wind plant

The local wind resources at each wind turbine location $f(\mathbf{x}_i)$ are needed in order to estimate the AEP of each turbine $\mathrm{AEP}_{\mathrm{T}i}$ individually. The total plant $\mathrm{AEP_P}$ is estimated using the equation 2.2. This equation includes the wake losses for each turbine as a function of its local wind conditions: $\eta_i(\mathbf{x}_i)$. In practice, the wake losses on a turbine depend on the operational conditions of the wake generating turbine.

$$\mathrm{AEP_P} = \sum_{i=1}^{N_\mathrm{T}} \mathrm{AEP}_{\mathrm{T}i} = \sum_{i=1}^{N_\mathrm{T}} n_t\,\Delta t \int_{\Omega_\mathbf{x}} P_{\mathrm{T}i}(\mathbf{x}_i)\,\eta_i(\mathbf{x}_i)\,f(\mathbf{x}_i)\,d\mathbf{x}_i \tag{2.2}$$

Time series wind resources

Time dependent estimation of the energy production of the plant is starting to gain importance in wind energy. In this method a time series of the weather conditions for a long time period, such as 20 years can be used as an input to the energy production model of

the plant. The wind plant model evaluates the energy production for each timestamp t_j.

$$\mathrm{AEP_P} = \frac{1}{20} \sum_{j=1}^{20n_t} \sum_{i=1}^{N_\mathrm{T}} \Delta t \, P_{\mathrm{T}i}\big(\mathbf{x}_i(t_j)\big) \, \eta_i\big(\mathbf{x}_i(t_j)\big) \tag{2.3}$$

Additional atmospheric variables can also be consider as part of the wind resources such as the air density (ρ), the turbulence intensity at hub height (I), the turbulence length scale (λ), the shear exponent at hub height (α) or the atmospheric boundary layer stability (Obukhov length L). The time series method has the advantage of capturing the correlation of the additional atmospheric parameters when all of them are estimated per time step. Advanced methods for multidimensional correlations are required to describe the distribution of the different atmospheric conditions by the pdf function $f(\mathbf{x}) = f(U, \theta, \rho, I, \lambda, L)$. Refer to chapter 3 for these methods.

An alternative energy production QoI is the instantaneous power production of each turbine $P_{\mathrm{T}i}(t)$ or the wind plant $P_\mathrm{P}(t)$. This QoI is used when the models are developed to fully capture the dynamic response of each turbine e.g. to design control strategies for individual WT or for the over-all wind plant control (i.e. down-regulation). Full versions of these models are unsteady and require a wind turbine model that handles the control strategy, the unsteady aerodynamics and the structural vibration of the wind turbine in a fully coupled *aero-servo-elastic* code.

2.2.2 Wind Turbine Loads

The second group of QoI are related to the loads that the components of each wind turbine will experience through a given period of time. The lifetime equivalent fatigue load (L_eq) is a measure of the wear that a component of a wind turbine will experience during its expected lifetime of 20 years. L_eq are required for the design of modern wind turbines and for the selection of the wind turbine for a particular wind energy project i.e. wind plant sitting.

The damage equivalent fatigue loads (D_eq) are computed using a rainflow counting algorithm to determine the number of load cycles n_L with their corresponding load range S_L in a given reference period (10-min or 1 hour) of turbine response. The damage equivalent fatigue load is obtained using the fatigue properties of the materials i.e. Wöhler exponent m for example, see equation 2.4 [29]. The reference number of load cycles N_ref is used to obtain a 1Hz damage

[29] Miner. 1945

equivalent fatigue loads, and it is based on the number of 1Hz cycles in the reference period: $N_{\text{ref}} = 600$ for 10 minutes or $N_{\text{ref}} = 3600$ for 1 hour reference periods.

$$D_{\text{eq}} = \left[\frac{\sum n_L S_L^m}{N_{\text{ref}}} \right]^{\frac{1}{m}} \tag{2.4}$$

The lifetime equivalent fatigue load of a component is the accumulated D_{eq} over the joint probability of the wind conditions felt by the turbine during the expected 20 years of operation, see equation 2.5. Where n_t is the number of reference periods in a year, and $N_{\text{L,eq}}$ is the number of 1Hz load cycles that the component will experience in its lifetime, usually 10^7. In contrast to the estimation of AEP, the L_{eq} requires the inclusion of additional atmospheric parameters to properly describe the turbulent inflow acting on the turbine. Additionally, an aero-servo-elastic turbine model that is able to predict instant loads on the wind turbine components is required. Wind turbine design standards [30] define additional conditions a turbine experiences (e.g. normal operation, idle, etc.) and they should be included in equation 2.5.

[30] IEC 61400-1. 2005

$$L_{\text{eq}} = \left[\frac{20 n_t}{N_{\text{L,eq}}} \int_{\Omega_{\mathbf{x}}} [D_{\text{eq}}(\mathbf{x}_i)]^m \; N_{\text{ref}} \, f(\mathbf{x}_i) \, d\mathbf{x}_i \right]^{1/m} \tag{2.5}$$

In this case, the flow model and the wake model are used to estimate the wind conditions at the location of each wind turbine: $\mathbf{x}_i$. The wake model is used to estimate the turbulent and waked inflow for each turbine for a given observed inflow. An aero-servo-elastic turbine model of each turbine predicts the D_{eq}.

Another QoI are the extreme loads a wind turbine component will experience during its operational lifetime. This problem is considerably more complicated. First, it requires the estimation of the extreme wind conditions that will occurred in the location during the lifetime. Second, it requires the estimation of the maximum instantaneous load that the component will experience in the extreme wind conditions.

2.2.3 Cost of Energy

If the objective of the wind plant model is to assess the total economical and financial balance of a wind energy project the most common QoI is the cost of energy (CoE). CoE is defined as the rate between the initial capital cost (ICC) of the wind plant and the

expected annual energy production. The cost of energy is a rough estimation of the price at which the wind energy project will produce energy over the expected project lifetime. The CoE disregards the change of value in money[3] and the difference between fixed costs and variable costs such as operation and maintenance costs.

[3] The change of value in money in time is due to financial interest rates and inflation rates

$$\mathrm{CoE} = \frac{\mathrm{ICC}}{AEP} \tag{2.6}$$

The levelized cost of energy (LCoE) is defined as the ratio of the total levelized annual cost of the project and the AEP. LCoE accounts for aspects like the fixed charge rate (FCR), the annual land lease cost (LLC), the levelized operation and maintenance cost (OMC) and the levelized replacement/overhaul cost (ROC). This Quantity of Interest (QoI) takes into account the balance of the cashflows over time and then redistributed the net present value of the project (NPV) into annual fix value payments. Cost models need to be added to a wind plant flow model in order to make predictions in terms of LCoE for a wind energy project [31]. Note that the OMC and ROC models use the L_{eq} as a measure of wear of the components and to estimate their lifetime [14].

[31] Fingersh et al. 2006

[14] Réthoré et al. 2013

$$\mathrm{LCoE} = \frac{\mathrm{FCR} \times \mathrm{ICC} + \mathrm{LLC} + \mathrm{OMC} + \mathrm{ROC}}{\mathrm{AEP}} \tag{2.7}$$

2.3 Wind resource assessment

Wind resource assessment consists in predicting the distribution of wind resources at a given location on the site. This predictions are based on observation/measurements of the wind resources in a nearby location or on numerical models. A survey of the methodologies applied in wind resource assessment can be found in [32][33][34].

[32] Ayotte. 2008

[33] Landberg et al. 2003

[34] Sanz Rodrigo et al. 2016

The wind atlas methodology is the core of the flow model used to estimate the wind resources on each wind turbine location based on the measurements in another nearby location [35]. This methodology consists in predicting the distribution of the generalized wind climate by removing the effects of the terrain, roughness, roughness changes, obstacles and mean stability from the wind resources at the reference point. This generalized climate is then used used to predict the wind resources at each turbine location by including the effects of terrain, roughness and mean stability of the new locations. See figure 2.2.

[35] Troen et al. 1989

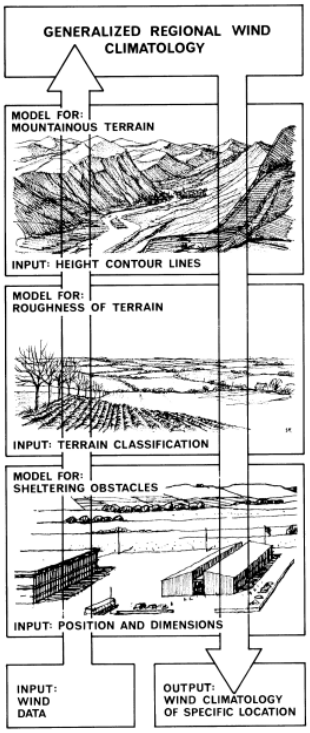

Figure 2.2: Wind atlas methodology. From [35].

2.3.1 Flow Model

The linearized Reynolds Averaged Navier-Stokes (RANS) flow models such as the spectral BZ model of WAsP [36], the LinCom model of WAsP Engineering [37], MS-Micro (MS3DJH/3) [38] among others are widely used because of their computational speed. Linearized flow models have proven to be accurate for the prediction of neutral flows over smooth roughness terrains with reduced slope hills. These class of models have been the industry standard for 30 years.

[36] Troen. 1990
[37] Dunkerley et al. 2001
[38] Taylor et al. 1983

Models based on the solution of the fully non-linear RANS equations are now available in research and commercial Computational Fluid Dynamics (CFD) codes such as Ellipsis 3D [39] in WAsP CFD, MSFDPBL [40], Fluent and OpenFoam [41]. These family of models vary in complexity and accuracy, but these models have been developed to be used in complex terrain where the assumptions of the linear models have been proven to not hold.

[39] Sørensen. 1995
[40] Ayotte et al. 1995
[41] Balogh et al. 2012

A third group of flow models fully resolves the largest turbulent structures in the flow. Large Eddies Simulation (LES) models have started to be used for flow modeling because they produce

time series of the wind resources and therefore naturally handle the correlation between the wind resources in multiple locations. LES models have the limitation of their high computation requirements; nevertheless they are applicable to the estimation of wind resources in the present [42].

[42] Wood. 2000

Finally, mesoscale weather models, i.e. Weather Research & Forecasting Model (WRF), can be used to generate the long term weather resources of the generalized climate over large areas. Coupling the atmospheric weather models and the micro scale LES flow models is currently a topic of research [34], that promises to obtain the benefits of the long term time series of the resources from the weather forecast models, and of the smaller dynamical scales of the LES flow models.

[34] Sanz Rodrigo et al. 2016

2.3.2 Uncertainty in the Flow Model

Clerc et. al [43] presented an empirical methodology to perform uncertainty quantification of the flow model for wind energy resources assessment. The results of this article are applicable to the industry standard linearized flow models. These models estimate the wind conditions at the wind turbine locations by computing the speed-up (Sp) and turning (Tu) effects due to the terrain, obstacles and land use with respect the observed wind resource on a meteorological mast.

[43] Clerc et al. 2012

$$U_{\mathrm{T}_i} = Sp\,U \qquad \theta_{\mathrm{T}_i} = Tu + \theta \tag{2.8}$$

A statistical model to estimate the speed-up errors based on a validation campaign on a large database of meteorological masts pairs is presented in [43], see figures 2.3. Uncertainty models for the speed-up are build from empirical relationships.

[43] Clerc et al. 2012

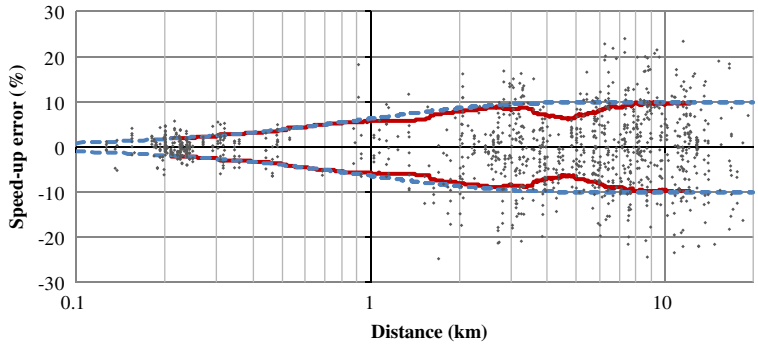

Figure 2.3: Speed up errors as a function of distance between the two sites from multiple site-site cross-validation. From [43].

Flow Model Speed-up Uncertainty:

The flow model uncertainty presented in [43] is an empirical model for the errors in the speed-ups predicted by linearized flow models as a function of the distance between the reference measurement site and each of the locations. This models assumes that the distributions of the errors of the speed-ups (ϵ_{Sp}) are correlated between different wind direction bins:

$$\epsilon_{Sp} \sim (\mathbf{0}, \mathbb{C}_{Sp}) \tag{2.9}$$

In the literature at the present time there is not a model for the error of the turning component of the flow model. This is mainly because of the difficulty of considering the spatial decorrelation in the wind direction. A discussion of this aspect in offshore wake model validation is presented in the next section.

Several studies have been published about flow model validation in complex terrain. For example, several validation campaigns have been conducted for WAsP and it has been concluded that the uncertainty in the wind atlas methodology grows as a function of the difference in the ruggedness indexes between observation and prediction locations [44].

[44] Mortensen et al. 2006

Some of the major micro meteorological experiments on complex flow are the Askevin hill experiment [45], the Bolund hill experiment [46] performed by Risø/DTU, the Alaiz test site [47] and the Benakanahalli experiment [48]. In these experiments detailed measurement were taken with multiple met masts and/or remote sensing devices (SONAR and LIDAR) to fully characterize the flow.

[45] Mickle et al. 1988
[46] Berg et al. 2011
[47] Chávez Arroyo et al. 2014
[48] Berg et al. 2012

These experiments have been used to validate different flow models [49] and [50]. A summary of the results is presented in the IEA-Task 31 Wakebench international project results overview article [51]. The uncertainty related to the flow models in complex terrain has not been fully understood. A review of flow modeling and validation can be found in [34].

[49] Bechmann et al. 2011
[50] Koblitz et al. 2014
[51] Sanz Rodrigo et al. 2014
[34] Sanz Rodrigo et al. 2016

Similar experiments and validation campaigns are being conducted to determine the effect of stability such as the daily atmospheric boundary layer experiments (GABLS) [52]. The results have shown that there are still large uncertainties associated to modeling the daily ABL cycle.

[52] Svensson et al. 2011

2.4 Wind Turbine Wake

The flow behind a wind turbine is a complex unsteady aero-servo-elastic problem that requires understanding of aerodynamics, fluid-structure interaction for non-rigid bodies and control. It is nevertheless, a key aspect in modern wind energy project planning to be able to predict the modified flow structure in which downwind turbines will operate. This flow structure is necessary to design the layout and select the wind turbines in the plant. A number of reviews on the different aspects of wind turbine wakes can be referred to, such as [53][54][55][56][34][57]. The present overview of the main features of the wake flow is based on these reviews (further individual references are omitted).

[53] Sanderse et al. 2011
[54] Crespo et al. 1999
[55] Snel. 2003
[56] Sørensen. 2011
[34] Sanz Rodrigo et al. 2016
[57] Göçmen et al. 2016

The flow behind a wind turbine can be divided into two regions: near and far wake. The near wake starts right after the turbine and extends to 1-5 turbine diameters downstream (depending on the ambient turbulence intensity and the operational conditions of the wind turbine). The near and far wake regions are depicted in Figure 2.4.

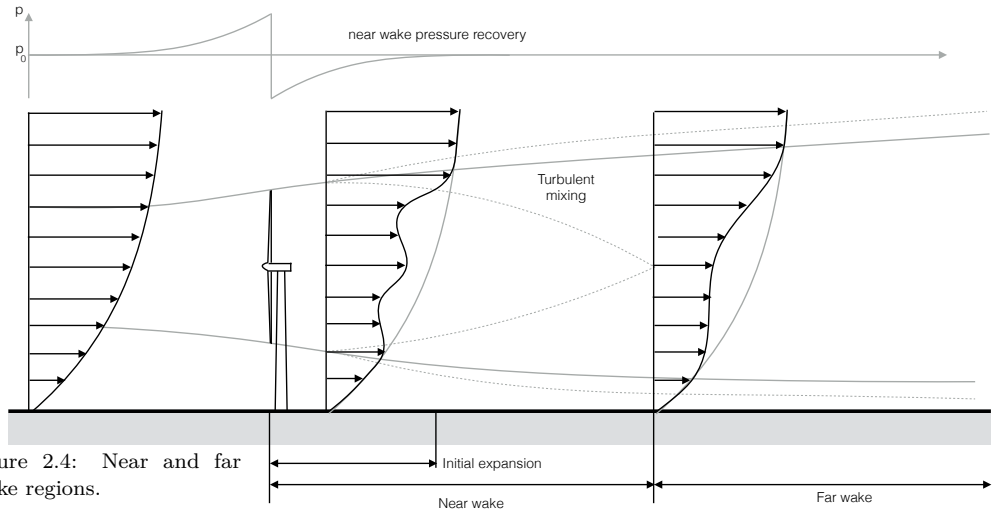

Figure 2.4: Near and far Wake regions.

Near wake

In the near wake region, the flow is three dimensional, unsteady and characterized by the rotor-flow dynamic interaction. Since the turbine extracts momentum/energy from the flow, there exist steep gradients of pressure and axial velocity in front and behind the

rotor's plane; in particular there is a sudden pressure drop at the turbine's disc-plane.

The velocity difference between the air inside and outside the wake generates the wake shear layer that grows thicker as it moves downstream. The wake shear layer is an important source of turbulence production because of the large velocity gradients. This generation of turbulent eddies is responsible of mixing the fast outer wake flow with the slow inner wake flow. The near wake ends at the point where the wake shear layer reaches the center of the wake (wake axis), see Figure 2.4. Detailed modeling of the near wake flow under real atmospheric boundary layer and rotor orientation conditions is critical for modeling unsteady/transient wind turbine operation and to predict the dynamic load distribution on the turbine. On the contrary, the near wake flow has reduce influence on the energy production of a wind plant because the turbines are not placed inside the near wake region of other turbines. This restriction is applied in order to avoid the reduced power production and higher fatigue loading.

Far wake

In the far wake, the wake is characterized by the distribution of velocity deficit and of turbulence intensity. These distributions can be approximated as axisymmetrical functions. In this region the effects of the wake generating turbine are limited to general operational parameters such as thrust force coefficient and tip-speed ratio. As the wake moves downstream, the turbulence mixing accelerates the wake recovery in terms of reducing both the velocity deficit and the small scale turbulence fluctuations (small turbulent eddies). In this process the wake expands at a rate that depends on the inflow turbulence intensity, the ABL profile, the land roughness and the topographical effects. The deviations from axisymmetry and shape preserving (sel-similarity) behavior of the wake are due to asymmetric flow conditions such as: shear in the atmospheric boundary layer, ground effects, large scale atmospheric turbulent structures and dynamic behavior of the wake.

In addition to the mechanical turbulence produced by the turbine and by the shear layer in the edge of the wake, the far wake flow is under the influence of the large-scale atmospheric turbulence structures. These large eddies are not modified with the interaction with the rotor and induce meander in the wake as it is convected

downstream. The meandering of the wake means that there is a dynamic vertical and horizontal translation center of the wake.

A wind turbine operating behind a wake with meandering operates under a dynamical wake location and hence under changing partial wakes and yaw-misalignment conditions. Wake meandering is one of the main sources of uncertainty in wind plant power production and load predictions under atmospheric conditions, the reason is that the meandering of the wake contributes to the reduction of the time-averaged velocity deficit whereas significantly increases the unsteady loading on the downstream turbines in a process described as apparent added turbulence [58].

[58] Larsen et al. 2008

Wind plant flow

The flow inside a wind plant is considerably more complicated than the single wind turbine wake case. In general, turbines inside the plant will produce less power and experience higher fatigue loads, due to the reduced wind speed and the higher turbulence intensities inside the plant. The flow inside a wind plant has dynamical interactions of multiple wakes in both velocity deficits and turbulence levels. In order to predict the power production and the loads on a turbine, it is required to understand how a turbine operates under such complex inflow conditions. The wake interaction can be observed in figure 2.5. Although, this picture is not representative of operational conditions, since the wind speed is low and most turbines are not operating [59].

Figure 2.5: Photograph of the Horns Rev 1 danish offshore wind farm taken the 12th of February 2008 at around 10:10 UTC seen from the south [59].

[59] Hasager et al. 2013.

2.4.1 Wind Plant Flow Models

Wind plant flow model classification consist in separating stationary models used for AEP predictions from dynamic models used to predict instant power and fatigue loads. An overview of the different wake model and their assumptions is presented in table 2.1, while figure 2.6 shows the computational effort and the amount of physics included in each wake model family.

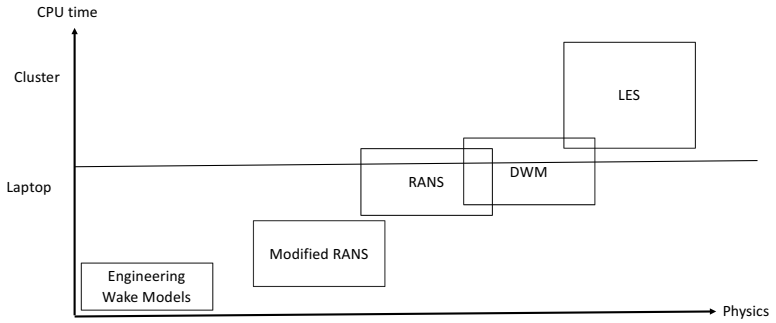

Figure 2.6: Wake model classification diagram.

Stationary wake models can be divided into engineering models that use empirical relations to predict single wake axial velocity deficits and added turbulence intensities, and into coupled wind plant models that use numerical methods to solve the RANS equations, or a simplified version of them. In general, stationary wake models predict the velocity deficit in the wake and its recovery as the wake moves further downstream from the wake generating turbine. Stationary wake models rely on the estimation of the turbulent kinetic energy in the wake as an intermediate QoI to model D_{eq}, by assume a dependency between the inflow turbulence intensity at hub height with the fatigue loads on the different components of a turbine [60].

[60] Frandsen. 2007

Dynamical wake models consider the multiple scales of turbulence, and as a consequence require larger computational time. Some example of dynamic wake models are: LES and the Dynamic Wake Meandering (DWM). The DWM is based on small scale turbulence filters and uses an aeroelastic turbine model to capture the dynamic turbine response. LES models rely on distributing the axial forces actuating on the rotor into the flow the rotor disc for Actuator Disc (AD), or over the blades chord center line for the Actuator Line (AL).

Stationary Wake Models

Model	QoI	Turbine Model	Flow/Wake Assumptions
Mesoscale: Fitch [61] Volker [62]	AEP	$C_T(U)$, $P(U)$	Wind plant modeled as an internal boundary layer (IBL)
Engineering: Jensen [63] Frandsen [64] Gaussian [65] FLORIS [66]	AEP	$C_T(U)$, $P(U)$	Empirical, axisymmetric, self-similar velocity deficit
Semi-empirical Engineering: Larsen [67] Ainslie [68] Madsen [69]	AEP	$C_T(U)$, $P(U)$	Thin shear layer RANS, axisymmetric self-similar velocity deficit, no pressure gradients outside the wake, mixing length turbulence closure
Added Turbulence: Frandsen [70] Quatron [71] Hassan [72] Crespo [73] Chamorro [74]	$I_W(x,r)$	$C_T(U)$	Empirical, axisymmetric, self-similar wake generated turbulence intensity
Modified RANS: FUGA [75], UPMWAKE [76] WAKEFARM [77]	AEP	$C_T(U)$, $P(U)$, AD	Linearized RANS or Parabolized RANS, prescribed pressure gradients outside the wake or near wake boundary condition, turbulence closure.
RANS: Van Der Laan [78] Cabezon [79] El Kasmi [80] Gomez [81]	AEP	$C_T(U)$, $P(U)$, AD	RANS with turbulence closure, forces uniformly distributed or radially dependent

Dynamic Wake Model

Model	QoI	Turbine Model	Flow/Wake Assumptions
DWM: Larsen [82] Madsen [69] Keck [83]	P(t), AEP, D_{eq}, L_{eq}	Aeroelastic	Small turbulent scales filter, Meandering induced by large turbulent scales, Wake added small scale turbulence
LES: [84] **AD:** Nilsson [85] Wu [86] Sørensen [87] **AL:** Churchfield [88] Ivanell [89] Troldborg [90] **AL-Aeroelastic:** Andersen [91] **Full rotor:** Heinz [92]	P(t), D_{eq}	AD, AL, AL-Aeroelastic, Full rotor	Fully resolved large scales, Small scales (Subgrid) turbulence model

Table 2.1: QoI for different types of wind plant models

2.4.2 Uncertainty in the Wake Model

Supervisory Control And Data Acquisition (SCADA) data from wind plants is available to the project developers and operators, and such data could be used to evaluate the performance of wake models. SCADA data analysis presents challenges such as the detection and filtering of normal wind turbine operation cases for each individual turbine. This is a complex task taking into account that such databases are composed of hundreds of sensors that have to be verified for quality, calibrated and filtered for normal conditions [93][94]. Wake model comparisons with the operational data from various sites have been performed in several studies, a review of the experimental data for wake model validation can be found in [95].

[93] Réthoré et al. 2009
[94] Barthelmie et al. 2009
[95] Barthelmie et al. 2013

Small wind plants/single turbine sites:

- Nibe turbines (ETSU) [96]
- Sexbierum wind farm (TNO) [97]
- Tjæreborg turbine (Risø/DTU) [98]
- Nordtank 500 turbine (Risø/DTU) [99]
- Wieringermeer wind farm (ECN) [100]

Large wind plants:

- Vindeby 1-3 (Risø/DTU) [101][102]
- Horns Rev 1 (DONG/Vattenfall) [103][104][105][106]
- Middlegrunden 1-2 (Middelgrundens Vindmøllelaug) [107][14][108]
- Nysted (DONG/Vattenfall) [94][103][109][110][106]
- NoordZee/Egmond Aan Zee (NoordZeeWind B.V.) [111]
- Lillgrund (Vattenfall) [112][113][106]
- North Hoyle (RWE npower renewables) [106]
- London Array (DONG) [110]
- Anholt (DONG) [110]

Plant to plant interaction:

- Nyested and Rødsand II (E.ON/SEAS-NVE) [114][115][110][106]
- Walney (Walney 1 and Walney 2) (DONG) [110]

In most of these validation databases the undisturbed inflow conditions can not be measured for all wind directions. The inflow conditions are usually point observations from a meteorological mast that do not capture the spatial variability of the inflow conditions throughout the whole plant. The inflow information is even scarcer for offshore SCADA databases. For these cases, the inflow conditions are inferred from a single or a group of undisturbed wind turbines. One of the main challenges for

wake model validation is the large uncertainties on the inflow conditions for the SCADA observations.

Moriarty et. al [105] published the results of the wake model benchmarking campaign (IEA Task 31 Wakebench). This study concluded that there is no clear improvement in the power production prediction of wake models of higher fidelity when compared with the operational data of large offshore wind farms. This is explained as an effect of the large uncertainties in the undisturbed inflow conditions in the validation datasets. The higher fidelity wake models are expected to accurate simulate the wake characteristics, but even the most sophisticated model can fail to reproduce the flow if the provided inputs are erroneous or deficient. Most of the studies disregarded the effect of the measurement uncertainty and rely on grouping the measurements into inflow wind speed and wind direction bins.

The combination of wakes and terrain effects is still a research topic but model comparison/validation in such conditions suffers of even larger uncertainties about the inflow conditions because of the non-uniformity of flow conditions and the non-linear interactions between wake and terrain flows [116].

In general, all the wake models require the undisturbed wind speed and wind direction, and in some degree the ambient turbulence intensity and atmospheric stability. Dynamic wake models such as DWM [82] and LES-AL [90] models require a turbulent inflow field that can be generated using a precursor simulation or a wind field simulation generated using a spectral turbulence model [117].

Wind Direction Uncertainty

Gaumond proposed a wind direction error post-processing as a tool to improve the comparison of the power predictions of stationary wake models to SCADA databases [118]. This approach proposes a correction for the power of a wake operating turbine based on the PDF of the difference between the reference wind direction and the local wind direction. The PDF of the local wind direction error ($\varepsilon_\theta \approx \theta_{\text{ref}} - \theta_{\text{np}}$) can be fitted to a normal distribution: $f(\varepsilon_\theta) = \text{Normal}(0, \sigma_\theta)$.

$$P_{\text{T corrected}}(\theta) = \int_{-\infty}^{\infty} P_{\text{T}}(\theta + \varepsilon_\theta)\, f(\varepsilon_\theta)\, \mathrm{d}\varepsilon_\theta \tag{2.10}$$

The post-processing methodology for wind direction uncertainty was deemed necessary in order to be able to compare the stationary model predictions with SCADA measurements of real wind farms binned in narrow wind direction sectors (less than 5°).

At the same time, this correction does not modify the accuracy of stationary models when the data is grouped into wider wind direction sectors [118]. This approach resolves the limitations presented by Barthelmie [95] regarding the comparison of wake deficits from stationary models with measurement under atmospheric turbulence. However, this approach does not consider the correlation between local wind direction

[105]
[116] Politis et al. 2012
[82] Larsen et al. 2008
[90] Troldborg et al. 2007
[117] Mann. 1998
[118] Gaumond et al. 2014
[118] Gaumond et al. 2014
[95] Barthelmie et al. 2013

errors nor the effect of yaw miss-alignment in wake development, as presented in [119]. Further modifications need to be considered regarding these aspects.

[119] McKay et al. 2013

Ott [75] proposed a further correction to include non-stationarity in the reference wind direction measurements. These variations are trends inside the averaging time period. Note that these variations are also due to large turbulent scales. In this report Ott argues that theses tendencies can be estimated by computing the change between two consecutive time averaged reference wind directions ($\Delta\theta$).

[75] Ott et al. 2014

The local wind direction error can then be estimated by combining both of these sources of uncertainty in wind direction are considered in a post-processing process. This methodology was used to validate RANS simulations of different wind farms with SCADA data grouped in narrow wind direction sectors in [7].

[7] Laan et al. 2015

$$f(\varepsilon_\theta) \sim \text{Normal}\left(0, \sqrt{\sigma_\theta^2 + \sigma_{\Delta\theta}^2}\right) \tag{2.11}$$

Uncertainty in individual turbine inflow conditions:

Due to the spatial and temporal decorrelation the inflow conditions of each individual turbine in a plant will have an *error* with respect to the reference instrument. This phenomena affects both the wind speed and the wind direction. The correlation between these variables depend on the distance between the points. A decrease in the correlation of the wind direction occurs for wind turbines operating deep inside the plant. A statistical model for the wind direction error in multiple sensors in a wind plant due to spatial decorrelation can be built by assuming a multivariate normal distribution.

$$\begin{aligned} f(\varepsilon_\theta) &\sim \text{Normal}(0, \mathbb{C}_\theta) \\ f(\varepsilon_U) &\sim \text{Normal}(0, \mathbb{C}_U) \end{aligned} \tag{2.12}$$

2.5 Wind Turbine Performance

The power production, the thrust force and the fatigue loads on a wind turbine depends on the turbulent inflow conditions it experiences. Traditionally, the power curve is used to characterize the power production of the wind turbine as a function of the wind speed at hub height. The thrust coefficient curve as a function of the wind speed at hub height is also used in order to estimate the wake the turbine generates. These curves are published by the manufactures.

In reality the actual performance of a turbine can depend on other atmospheric variables such as the turbulence intensity, shear exponent of the atmospheric boundary layer, among others. This section gives

an overview of the methods to estimate the performance of a turbine in realistic atmospheric conditions.

2.5.1 Binning method for power and thrust curve

The most common method to capture the performance of a wind turbine is using power and thrust curves based on the hub height wind speed. The IEC 61400-12 standard [120][121] defines the steps to characterize the power performance of a wind turbine based on observations from a near-by meteorological mast. Here, the inflow is the mean wind speed at hub height corrected for density variations. This methodology consists in binning the observations with respect to the hub height wind speed to obtain the mean power at each bin. This method proposes the standard error as the associated uncertainty to the mean power.

[120] IEC 61400-12-1. 2005

The standard error is a consequence of the central limit theorem and it is defined as the ratio of the standard deviation by the squared root of the number of observations: $\mathbb{S}(P)/\sqrt{N}$.

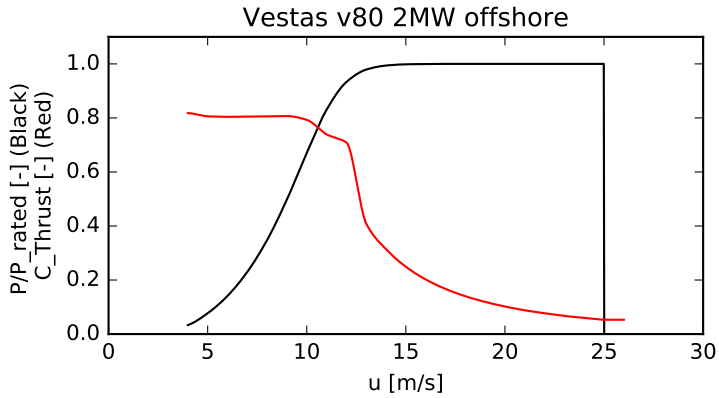

Figure 2.7: Official power curve and thrust curve for Vestas v80.

2.5.2 Effect of wind speed shear on the power curve

A redefinition of the power curve based on the rotor equivalent wind speed has been proposed in [122] in order to capture the effect of the ABL wind speed profile in the power curve. The rotor equivalent wind speed uses the definition of power coefficient to define a wind speed that contains the equivalent kinetic energy over the full rotor disc.

[122] Wagner et al. 2011

$$P = \frac{1}{2}\rho A U^3 C_P \qquad U_{eq} = \frac{1}{A}\left(\int_A U^3 dA\right)^{\frac{1}{3}} \tag{2.13}$$

2.5.3 Effect of turbulence on the power curve

Power curves depend on the turbulence intensity distribution of the site. Power curves are usually reported for a reference turbulence intensity of 10%, this reference turbulence intensity defines the PDF of turbulence intensity as a function of the wind speed [30]. A turbine that operates on a site with a higher reference turbulence intensity will have a different power curve. An experimental power curve that shows the effect of the

[30] IEC 61400-1. 2005

turbulence intensity is presented in figure 2.8. The main trend of the effect of turbulence intensity is seen, but there is considerable uncertainty in the hub height wind speed measurements because the meteorological mast is located 2 km away from the turbine.

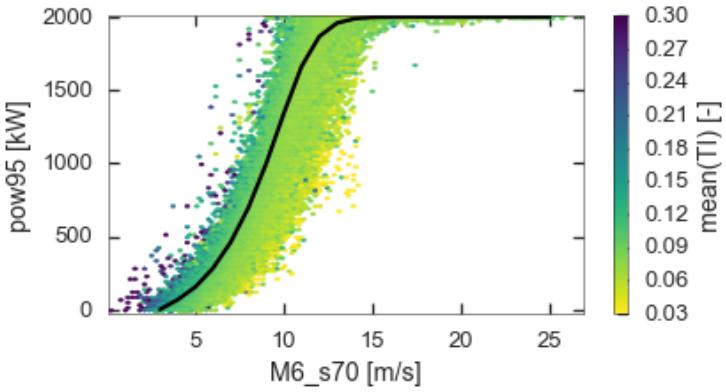

Figure 2.8: Example of the influence of turbulence intensity on a measured power curve.

The turbulence renormalization method considers the effect of the measured turbulence intensity at hub height by predicting an ideal zero turbulence power curve [123]. This curve is obtained by assuming an ideal performance on each of the operation regions. This means that the power will extract maximum C_P in region II and rated power in region III, see equation 2.14. In this equation u represents the instantaneous rotor averaged wind speed.

[123] Clifton et al. 2014

$$P_{\text{ideal}}(u) = \begin{cases} \frac{1}{2}\rho A u^3 C_{P,max} & \text{for } P_{\text{ideal}}(u) < P_{\text{rated}} \\ P_{\text{rated}} & \text{for all other cases} \end{cases} \tag{2.14}$$

Finally the turbulence renormalization process uses the experimental zero turbulence power curve and the assumption of normally distributed instantaneous wind speed ($f(u) = \mathcal{N}(U_{eq}, I\,U_{eq})$) to predict the power curve correction at a given hub height turbulence intensity.

$$P(U_{eq}) = \int P_{\text{ideal}}(u)\, f(u)\, du \tag{2.15}$$

Figure 2.9 presents an example of the effect of turbulence intensity on power and thrust curves with renormalization method. The turbulent fluctuations around the mean wind speed have different effects on the power curve depending on the region of operation. For cases near the rated wind speed, the turbulent fluctuations will force the pitch mechanism to regulate the power output; this effect produces a lower 10-min mean power than otherwise expected using the ideal zero-turbulence power curve. The turbulent fluctuations around and above rated wind speed have the effect of increasing the 10-min mean power; this is due to the fact that the power is proportional to the cube of the instantaneous wind speed, therefore, there is an extra amount of energy in comparison to the original power curve.

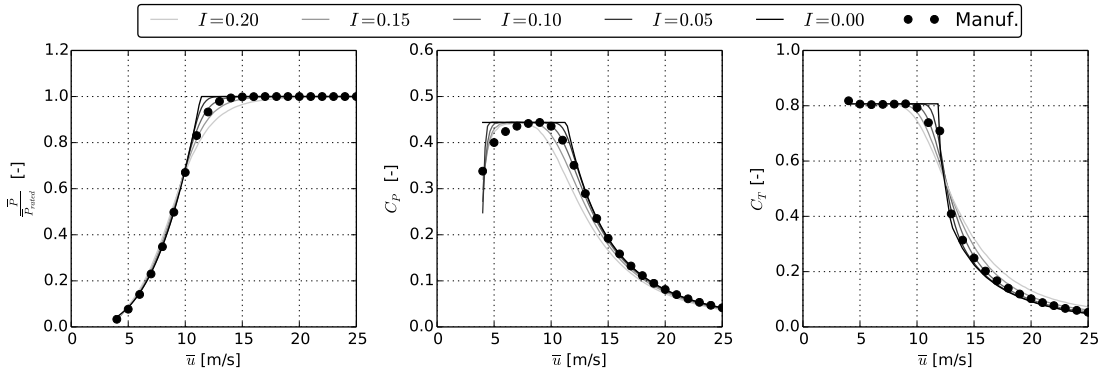

Figure 2.9: Example of the influence of turbulence intensity on power and thrust curves with renormalization method for Vestas v80.

2.5.4 Aeroelastic turbine model

Aeroelastic turbine models are the standard tool for design of wind turbines. In these models the dynamics of the structure are captured using an structural model of the turbine; while the unsteady aerodynamics are captured using the quasy-stationary blade element momentum (BEM) method with a dynamic stall model. The dynamical stall model describes the forces that act on the turbine and their unsteady interaction with the flow; additionally such models contain a controller. For a review on this topic refer to [124].

[124] Hansen et al. 2006

The main advantage of using an aeoelastic model to capture the turbine response is that it captures the unsteady power, thrust coefficient and loads of the turbine to realistic turbulent inflow conditions as the turbulent fields generated using a spectral turbulence model such as Mann's turbulence model [117]. Figure 2.10 shows the general turbulent inflow inputs variables and turbine performance outputs of an aeroelastic model. Here, the variable TIR represents the turbulent inflow realization, and it represents the variability due to having different turbulence structures in the inflow field.

[117] Mann. 1998

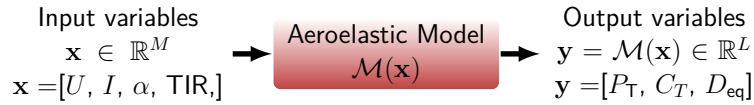

Figure 2.10: Inputs and outputs for an aeroelastic model.

Several aeroelastic codes exist. Benchamarking campaigns have compared their predictions but due to the large number of input variables required, it is hard to pin-point the main differences between the codes [125]. Although the code inter-comparison has improved significantly in the latest decade, the main differences remain to be caused by the turbulent inflow conditions, the airfoil aerodynamics used in the model and the structural damping [126][127].

[125] Simms et al. 2001

[126] Buhl Jr et al. 2006
[127] Vorpahl et al. 2014

2.5.5 Surrogate of an aeroelastic turbine model

Since the response of the turbine to the turbulent inflow field is highly non-linear, it has been proposed to use surrogates of the turbine response in order to capture the mean power, the thrust coefficient and D_{eq} as a function of the rotor averaged wind speed, wind shear and turbulence intensity [128] [129]. In these articles the random forest method is used as a surrogate, but other methods for supervised machine learning problem can be applied such as response surfaces [130], Co-Kriging [131], among others.

[128] Clifton et al. 2013
[129] Clifton et al. 2014
[130] Toft et al. 2016
[131] Abdallah et al. 2015

2.5.6 Uncertainty in wind turbine model

The power curve has been identified as a main source of uncertainty in the prediction of power production of individual turbines due to the fact that the flow is oversimplified and important aspects such as mean wind speed vertical profile (wind shear), directional changes over height (wind veer) and turbulence intensity vertical profile are ignored [122]. A comparison of the measured mean power and the predicted power using the three methods of power curve mentioned in this section has concluded that surrogate based power curves that capture the effect of additional atmospheric variables give considerable better results [123].

[122] Wagner et al. 2011
[123] Clifton et al. 2014

Abdallah concluded that the uncertainty in the aerodynamic data (airfoil aerodynamic polars) used by any aeroelastic tool has a considerable effect on the estimation of the extreme loads on a wind turbine [132]. This agrees with the expected effect on the predicted loads characterized by the uncertainty factors given in the standards [30].

[132] Abdallah et al. 2015
[30] IEC 61400-1. 2005

An additional source of uncertainty in the prediction of the thrust coefficient and D_{eq} on the different components of a turbine is the turbulent inflow realization. This uncertainty is not negligible when the inflow parameters are known (i.e. hub height wind speed, turbulence intensity, shear exponent). Many studies have analyzed the difficulties of studying fatigue and extreme loads under different turbulent inflow realizations [133] [134].

[133] Moriarty. 2008
[134] Agarwal et al. 2009

Surrogate techniques of computational expensive models are promising for wind plant model uncertainty reduction as the uncertainty in the prediction of thrust and power propagates through the wind plant model.

Further additional advantages can be obtained using a surrogate model for the mean power, thrust coefficient and D_{eq} response for a turbine operating inside a plant. This surrogate will predict the dependency of the turbine performance on the rotor averaged wind speed, rotor averaged turbulence intensity, wind shear (or another atmospheric boundary layer model) and a wind speed deficit at different locations. Such a model could improve the prediction capacity of simple stationary wake models but could also accelerate the computational time of dynamic models. This approach was proposed in the database of partial wakes used in Risø's TopFarm wind plant optimization platform [14].

[14] Réthoré et al. 2013

2.6 Uncertainty in AEP - A mental example

As an example, in an offshore wind plant the wind resources of the site can be represented by the PDF of the wind direction and wind speed at hub height $f(U, \theta)$. This distribution is commonly discretized by a histogram with normalized frequency $f_{ij} \approx f(U_i, \theta_j)$. The wake model uses the layout of the plant to predict the power production as a function of wind speed and wind direction, $\mathrm{P}_{ij} \approx \mathrm{P}(U_i, \theta_j)$. The wake model requires a wind turbine model which is usually the power and the thrust coefficient curves (as well as the rotor diameter and hub height). The AEP can then be computed as the expected value of the power production times a proportional constant (a) that considers the additional losses and the averaging time of the variables i.e. 10 minutes:

$$\mathrm{AEP} = a\,\mathbb{E}(\mathrm{P}) = a \sum_{i,j} f_{ij}\mathrm{P}_{ij} \tag{2.16}$$

Assume that we know the error in the prediction of the power production for a given wind speed and wind direction due to the wake model and the turbine model. In this hypothetical scenario one could predict the true power production for those conditions:

$$\mathrm{P}_{ij\,\mathrm{true}} = \mathrm{P}_{ij} + \epsilon_{\mathrm{P}_{ij}} \tag{2.17}$$

The error on the AEP (ϵ_{AEP}) will be the expected value of the wake model error weighted by the wind resources:

$$\mathrm{AEP}_{\mathrm{true}} = a \sum_{i,j} f_{ij}(\mathrm{P}_{ij} + \epsilon_{\mathrm{P}_{ij}}) = \underbrace{a \sum_{i,j} f_{ij}\mathrm{P}_{ij}}_{\mathrm{AEP}} + \underbrace{a \sum_{i,j} f_{ij}\epsilon_{\mathrm{P}_{ij}}}_{\epsilon_{\mathrm{AEP}}} \tag{2.18}$$

The wind resources represent the longterm corrected variability in the wind, therefore there is an intrinsic uncertainty in them due to the yearly variability. Imagine that we could track the weather on the site for hundreds of years, then we could produce several realizations of the wind resources during 20 consecutive years; f_{ij}^k represents a single realization. The AEP and its error will be different for each one of these weather resources realizations.

$$\mathrm{AEP}_{\mathrm{true}}^k = a \sum_{i,j} f_{ij}^k(\mathrm{P}_{ij} + \epsilon_{\mathrm{P}_{ij}}) = \underbrace{a \sum_{i,j} f_{ij}^k\mathrm{P}_{ij}}_{\mathrm{AEP}^k} + \underbrace{a \sum_{i,j} f_{ij}^k\epsilon_{\mathrm{P}_{ij}}}_{\epsilon_{\mathrm{AEP}}^k} \tag{2.19}$$

The uncertainty in the AEP, and therefore the P90, can then be obtained form the histogram of the different realizations of the corrected AEP:

$$f(\mathrm{AEP}_{\mathrm{true}}) = \mathcal{N}\big(\mathbb{E}(\mathrm{AEP}^k + \epsilon_{\mathrm{AEP}}^k), \mathbb{V}(\mathrm{AEP}^k + \epsilon_{\mathrm{AEP}}^k)\big) \tag{2.20}$$

This example is relevant since it explores two concepts that are central in this thesis: the natural variability in some variables and the possibility that the models are not perfect for all the possible conditions.

2.7 Summary

This chapter has given an overview of the different models used in wind farm flow modeling. References are given for the main publications that have estimated the prediction errors of each model on a validation database. From this survey the following conclusions can be made:

- There is a need to understand the uncertainty in the wind resources flow model in more details. Clerc [43] has presented empirical distributions of the model prediction errors of the speed-up factor. This methodology only applies to linearized flow models and does not include information about the errors in the wind direction.
- There is a need to build a statistical model for the wake model prediction error. This validation process needs to consider the measurement uncertainties in the inflow conditions present in the SCADA databases of large offshore wind plants. This is the objective of the article [3]. This article can be found in appendix D.
- There is a need for a statistical model to predict the uncertainty in the power and thrust curves for realistic inflow conditions. A methodology to achieve this is presented in the article [4]. The methodology is also used to estimate D_{eq} in different components of a turbine. This article is available in chapter B.

[43] Clerc et al. 2012

[3] Murcia et al. 2016

[4] Murcia et al. 2016

Chapter 3

Input uncertainty

The initial step of any model uncertainty quantification study starts by defining the PDF of the input variables of the model. In general this process requires measurements, theoretical knowledge about the underlying physics of the variables and understanding of the theory of probabilities and statistics. This chapter summarizes the methods to describe the most common multivariate distributions that are relevant for wind energy applications. A review of this field can be found in [20]. This chapter assumes that the reader is familiar with basic statistics/probability concepts; a good introductory reference is [135].

[20] Biller et al. 2006

[135] Grinstead et al. 2012

3.1 Parametric probability density functions

The most common method to represent an uncertain variable is to use a parametric PDF, which are distributions with an analytical expression for their PDF given as a function of some hyperparameters[1]. The most important probability density functions are the normal and the uniform distributions. In the wind energy field, it is very common to refer to the Weibull distribution to characterize the PDF of the wind speed at given location. Lognormal distributions are also commonly used to characterize the uncertainty of variables that have to be positive by definition. A summery of the parameters of these distributions is given in table 3.1.

[1] Note that we refer to hyperparameters of a distribution to make a distinction to the parameters of a model.

Table 3.1: Important PDFs. $\Gamma(x)$ is the Gamma function.

Distribution	Notation	PDF: $X \sim f(x)$	Mean: $\mathbb{E}(X)$	Variance: $\mathbb{V}(X)$
Uniform	$\mathcal{U}(a,b)$	$1/(b-a)$	$(a+b)/2$	$(b-a)^2/12$
Normal	$\mathcal{N}(\mu,\sigma)$	$\frac{1}{\sigma\sqrt{2\pi}}\, e^{-\frac{(x-\mu)^2}{2\sigma^2}}$	μ	σ^2
LogNormal	$\mathcal{LN}(\mu,\sigma)$	$\frac{1}{x\sigma\sqrt{2\pi}}\, e^{-\frac{(\ln x-\mu)^2}{2\sigma^2}}$	$e^{\mu+\sigma^2/2}$	$(e^{\sigma^2}-1)e^{2\mu+\sigma^2}$
Weibull	$\mathcal{W}(k,A)$	$\frac{k}{A}\left(\frac{x}{A}\right)^{k-1} e^{-(x/A)^k}$	$A\,\Gamma(1+\frac{1}{k})$	$A^2\left[\Gamma\big(1+\frac{2}{k}\big)-\big(\Gamma\big(1+\frac{1}{k}\big)\big)^2\right]$

A note on notation:

In this thesis we use capital letters to denote random variable and lower case letters to denote variables, a lower case with a subindex denotes a sample and bold cases are used for denoting vectors (multiple variables). For example $\mathbf{X} \sim f(\mathbf{x})$ means that the random variables $\mathbf{X}$ are distributed with the PDF given by the function $f(\mathbf{x})$. If a sample of the random variable is obtained a similar notation can be used $\mathbf{x}^* \sim f(\mathbf{x})$. In an analog way but for single variables, the notation $X \sim f(x)$ indicates the PDF of the random variable X, while $x^* \sim f(x)$ represent a sample.

3.1.1 Fitting a distribution to observations and the effect of the statistical uncertainty

Several methods to estimate the hyperparameter of a distribution given an independent sample of the variable. The method of moments consists in estimating the parameters that make the statistical moments of the distribution equal to the statistical moments estimators of the observations. The maximum likelihood estimation (MLE) method consists in finding the hyperparameters that maximizes the product of the PDF of the observations for the given hyperparameter. Another alternative method consists in performing fitting a function to the empirical Cumulative Density Function (CDF) of the sample by minimizing the least-squared errors. Methods for model calibration and how to estimate the uncertainty of the calibration are discussed in more details in Chapter 5. All the fitting methods will give a different estimation of the hyperparameters and therefore are part of the total uncertainty in the stochastic variables.

An additional aspect to consider when fitting a distribution to a sample is the statistical uncertainty. This uncertainty is the effect of having only a reduced number of observations. As an example a random sample of Weibull distribution is fitted using MLE for different sample sizes, see figure 3.1. It can be seen how the MLE estimation is able to reconstruct the true hyperparameters of the distribution as the number of observation increases.

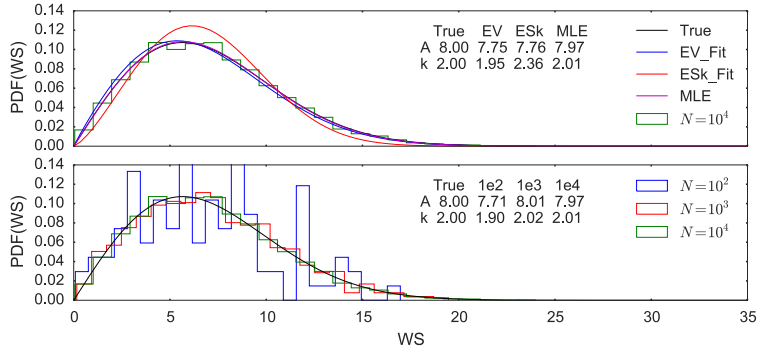

Figure 3.1: Statistical uncertainty on a Weibull distribution fit.

(top) A 10^4 random sample of $\mathcal{W}(k, A)$ is fitted using three different methods: method of moments for mean and variance (EV), method of moments for the mean and skewness (ESk) and maximum likelihood estimation (MLE).

(bottom) MLE for random samples of different sizes.

3.1.2 Multivariate normal distribution

The most common parametric multivariate distribution is the multivariate normal. This distribution is widely use in most of the methods related to uncertainty quantification because it describes the distribution of multiple normal variables as well as the correlations between them. The correlation structure captured by the multivariate normal distribution is a linear correlation and therefore it can only capture random variables that show linear trends between them. The distribution is defined by the vector of means μ and by the covariance matrix $\mathbb{C}$:

$$\mathbf{X} \sim \mathcal{N}(\mu, \mathbb{C}) \tag{3.1}$$

The correlation structure in a multivariate normal distribution is better represented by the correlation matrix, a matrix whose elements are the Pearson correlation coefficient between every pair of variables. An example of a sample from a four dimensional normal distribution can be seen in figure 3.3. This figure shows a two dimensional histogram for every two pairs of variables in the lower diagonal, and the one dimensional histograms represent the marginal distribution of the variables[2]. The correlation matrix for this example is presented in figure 3.2. Note that the correlation matrix determines whether there is a positive, negative or no trend between every pair of variables.

[2] The marginal distribution neglects any relationships among variables.

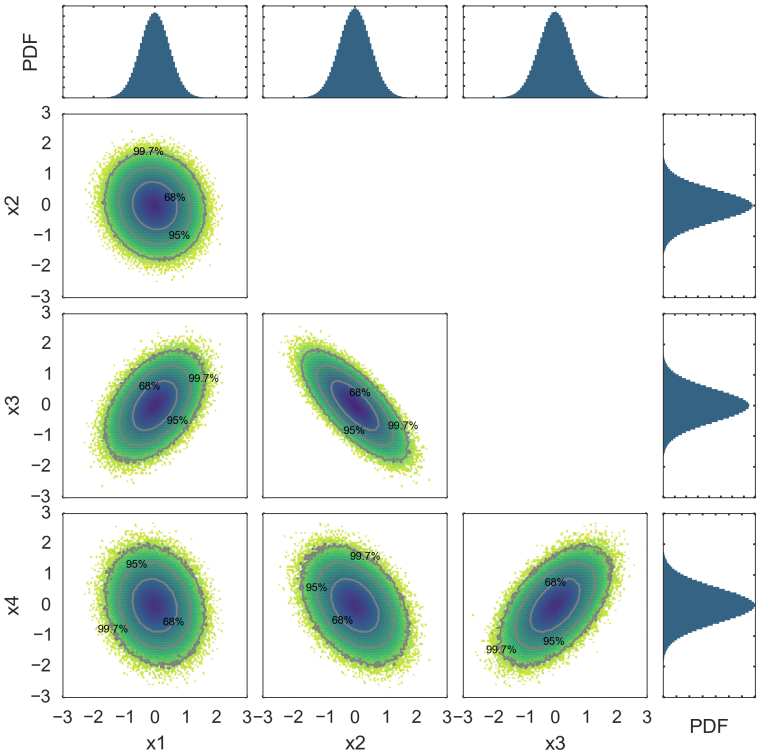

Figure 3.3: A 10^6 Halton sample of a multivariate normal distribution.

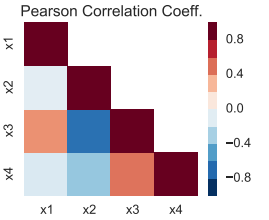

Figure 3.2: Corresponding correlation matrix to figure 3.3.

3.2 Iso-probabilistic transformations

Iso-probabilistic transformations are used to handle multiple uncertain inputs with non-normal marginal distributions and non-linear correlation structures between them. These transformations are a change of variables from the correlated variables into a set of identically distributed and independent variables $\mathbf{w}$. The notation of these transformations and their inverse is given in 3.2. The iso-probabilistic transformations $R(.)$ have the property of conserving the integration of any function $h(\mathbf{x})$ with respect the PDF, $f(\mathbf{x})$, over the input variables space $\Omega_{\mathbf{x}}$. See equation 3.3.

$$\mathbf{x} = R(\mathbf{w}) \quad \longleftrightarrow \quad \mathbf{w} = R^{-1}(\mathbf{x}) \tag{3.2}$$

$$\int_{\Omega_x} h(\mathbf{x}) f(\mathbf{x}) d\mathbf{x} = \int_{\Omega_w} h\big(R(\mathbf{w})\big) f(\mathbf{w}) d\mathbf{w} \tag{3.3}$$

In this section only the most important transformations are discussed; these transformations can be mixed in order to define more complex dependency structures [20]. The inverse transformation is a basic unidimensional transformation from any distribution into a uniform variable; this transformation is the basis for all iso-probabilistic transformations. The Rosenblatt transformation considers the cases in which the marginal distribution of each individual variable is defined in a sequential conditional dependency with respect the other variables [136]. The Cholesky decomposition is the transformation used to decorrelate multivariate normal distributions. The generalized Nataf transformation can be used to transform correlated non-normal inputs into a multivariate independent normally distributed variables [137].

[20] Biller et al. 2006

[136] Rosenblatt. 1952

[137] Li et al. 2008

3.2.1 Inverse transformation

Let x be a single input variable with a probability density function $f(x)$ and a corresponding cumulative density function $F(x)$. An unitary uniform variable, $w \sim \mathcal{U}(0,1)$, can be defined using the properties of $F(\mathbf{x})$; the inverse transformation is defined in equation 3.4. Numerical approximations can be used to define $F^{-1}(w)$ for those distributions that do not have an analytical form; see [138] for details of this implementation.

[138] Feinberg et al. 2015

$$w = F(x) \quad \longleftrightarrow \quad x = F^{-1}(w) \tag{3.4}$$

The importance of the inverse transformation:

The inverse transformation is the cornerstone of all the methods related to uncertainty quantification. This transformation can be used to change the distribution of the variable from any arbitrary distribution to the unitary uniform distribution. Furthermore, the inverse transformation can be used sequentially and transform any distribution into a more familiar distribution such as the standard normal distribution.

3.2.2 Cholesky decomposition

Let the input variables be distributed as a multi-dimensional normal distribution $\mathbf{x} \sim \mathcal{N}(\boldsymbol{\mu}, \mathbb{C})$; with mean $\boldsymbol{\mu}$ and covariance $\mathbb{C}$. The Cholesky decomposition consists in decomposing the covariance matrix into a lower diagonal matrix product, $\mathbb{C} = \mathbb{L}\mathbb{L}^T$, where $\mathbb{L}$ is a lower diagonal matrix. This decomposition is always possible because the covariance matrix is positive definite. The isoprobability transformation for multi-dimensional normal distribution into an independent normally distributed variables $\mathbf{v}$ is given in 3.5.

$$\mathbf{v} = \mathbb{L}^{-1}\mathbf{x} \quad \longleftrightarrow \quad \mathbf{x} = \mathbb{L}\mathbf{v} \tag{3.5}$$

Cholesky decomposition:

The Cholesky decomposition is the method that makes handling multivariate normal distribution easy. Using this transformation one can decorrelate the variables into non-correlated standard normals.

3.2.3 Nataf transformation

Nataf transformation consists of three steps: (1) Transform each input variable $\mathbf{x}$ into an uniform distributed variable using the inverse transformation, these uniform variables are correlated $\mathbf{v}$. (2) Transform $\mathbf{v}$ into a multivariate correlated normal variables $\mathbf{w}$ using the inverse transformation, and (3) transform $\mathbf{w}$ into a set of independent normally distributed variables $\mathbf{z}$ using the Cholesky decomposition, see equation 3.6.

In equation 3.6, $F_i(x_i)$ is the CDF of the i-th input variable and $\Phi(w)$ is the CDF of the standard normal distribution.

$$\begin{aligned} v_i = F_i(x_i) \quad &\longleftrightarrow \quad x_i = F_i^{-1}(v_i) \\ w_i = \Phi^{-1}(v_i) \quad &\longleftrightarrow \quad v_i = \Phi(w_i) \\ \mathbf{z} = \mathbb{L}^{-1}\mathbf{w} \quad &\longleftrightarrow \quad \mathbf{w} = \hat{\mathbb{L}}\mathbf{z} \end{aligned} \tag{3.6}$$

The main limitation with this approach is that the covariance of the multivariate correlated normal variables $\mathbf{w}$ might not reflect the details of the correlation in the actual variables $\mathbf{x}$ [139]. Some authors have proposed methods to determine the optimal correlation matrix in the normal $\mathbf{w}$ space that will approximate the correlation in the non-normal input variables [137].

[139] Lebrun et al. 2009

[137] Li et al. 2008

When to use the Nataf transformation?

The Nataf transformation is used when there is enough information/data to be sure that the variables are non-Normally distributed but there is not enough information to describe their correlation in details. That means that this method is used when the marginal distributions of each variable can be characterized but only the Pearson correlation coefficient between them is known.

3.2.4 Rosenblatt transformation

Let the set of input variables $\mathbf{x}$ have a sequential conditional dependency such that the distribution of the i-th input variable x_i is given by the F_i whose hyperparameters[3] $\boldsymbol{\vartheta}_i$ are themselves functions of the previous input variables:

$$x_i \sim f_i(x_i|\boldsymbol{\vartheta}_i = \boldsymbol{\vartheta}_i(x_0, x_1, \ldots, x_{i-1})) \tag{3.7}$$

[3] The term hyperparameter refers to the set of parameters that determine a parametric probability density function. E.g. the mean and standard deviation for a normal distribution.

The Rosenblatt transformation consists in using the inverse transformation in sequence to transform the variables into a set of uncorrelated unitary uniform variables [136], see equation 3.8.

[136] Rosenblatt. 1952

$$\begin{aligned} w_i &= F_i(x_i|\boldsymbol{\vartheta}_i = \boldsymbol{\vartheta}_i(x_0, x_1, \ldots, x_{i-1})) \\ x_i &= F_i^{-1}(w_i|\boldsymbol{\vartheta}_i = \boldsymbol{\vartheta}_i(x_0, x_1, \ldots, x_{i-1})) \end{aligned} \tag{3.8}$$

When to use Rosenblatt transformation?

The Rosenblatt transformation is the most natural way to capture the correlation between multiple non-Normal variables. This sequence of conditionally dependent distributions are widely used in wind energy and can be constructed using moving window distribution fits. Some example of such distributions are:

- The wind rose is a sequential conditional distribution: the distribution of the wind direction is independent, while the parameters of the Weibull distribution of the wind speed depend on the value of the wind direction.
- The normal turbulence model [30] describes the wind speed as an independent Weibull distribution while the turbulent fluctuation in the streamwise direction follows a LogNormal distribution whose parameters depend on the value of the wind speed.

[30] IEC 61400-1. 2005

3.2.5 Copulas

Additionally, recognizing that each marginal distribution can be transform into correlated unitary uniform variables $v_i = f(x_i)$, lead to the proposal of copula theory. A copula is an iso-probabilistic transformation that does not modify the marginal distributions of each individual variable, but that defines correlation structures in their corresponding uniform space; see equation 3.9. The copula C or its copula density $\mathscr{C}$ are analytical expressions for the most common types of copulas such as Gaussian, Frank, Clayton or Gumbel copulas. For these expressions refer to [140].

[140] Nelsen. 2007

$$
\begin{aligned}
F(\mathbf{x}) &= C\Big(F_1(x_1), \ldots, F_D(x_D)\Big) \\
f(\mathbf{x}) &= \frac{\partial\, C\Big(F_1(x_1), \ldots, F_D(x_D)\Big)}{\partial x_1, \ldots, \partial x_D} \\
f(\mathbf{x}) &= \mathscr{C}\Big(F_1(x_1), \ldots, F_D(x_D)\Big) \prod_{i=1}^{D} f(x_i)
\end{aligned}
\tag{3.9}
$$

When to use Copulas?

Copulas are used when the amount of data is not enough to build a Rosenblatt distribution and when the NATAF method fails to capture the correlation structures.

Illustrative example

Figure 3.4 shows three different two dimensional correlated distributions. All of them share a similar Pearson correlation coefficient, but it can be seen that the correlation structures are very different. In particular Rosenblatt and copulas are very useful to describe the joint distribution of non-Normal variables.

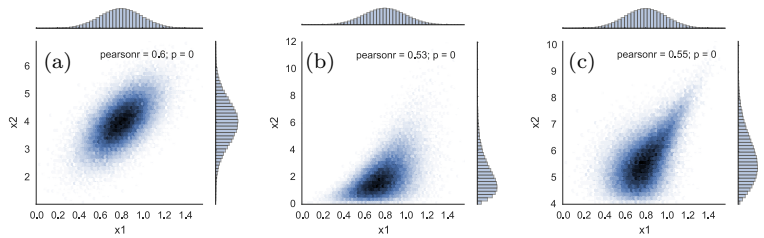

Figure 3.4: Examples of a 10^4 Halton sample of 2D $f(\mathbf{x})$ with different correlation structure but similar Pearson correlation coefficient and its p-value*:

(a) 2D normal
$x_1 \sim \mathcal{N}(0.8, 0.2)$
$x_2 \sim \mathcal{N}(4, 0.8)$
$\rho = 0.6$

(b) Rosenblatt:
$x_1 \sim \mathcal{N}(.8, .2)$
$x_2|x_1 \sim \mathcal{W}(2, 2(x_1 + 0.3)^2)$

(c) Joe Copula:
$x_1 \sim \mathcal{N}(0.8, 0.2)$
$x_2 \sim \mathcal{W}(2, 2)$
$\theta = 2$

*p-value is the probability of finding the Pearson correlation coefficient in the sample of a distribution with null correlation

3.3 Sampling methods

In order to obtain a sample from any arbitrary distribution it is required to define the transformation from the variables $\mathbf{x}$ into their unitary uniformly uncorrelated variables $\mathbf{v}$; this can be achieved using iso-probabilistic transformations. A sample can be generated in the unitary uniform space (unitary hypercube) and then transformed back into the desired distribution.

Several sampling methods can be used to generate a sample in the unitary hypercube. Factorial design of experiments, Box-Behnken designs or central composite designs define points that cover the unitary hypercube, but these methods are avoided for large number of dimensions because the number of model evaluations grows to the power of the number of dimensions.

Pseudo-random sample is the most used method to generate a sample from the independent unitary uniforms in large numbers of dimensions.

Different sampling techniques have been designed in order to reduced the required number of samples to cover a multidimensional space such as:

Quasi-MC methods define a sequence of numbers that fully cover the unitary hypercube. The points are not random and their locations are defined using prime numbers. Some examples are Hammersley sequence [141], Halton sequence [142] and Sobol sequence [143].

[141] Hammersley. 1960
[142] Halton. 1960
[143] Sobol'. 1967

Latin hypercube sample (LHS) divides the hypercube into a number of regions with the same probability and then uses semi-random sample inside each regions [144]. Modifications of the sampling inside the regions have been proposed to maximize the minimum distance between points or to reduce the correlation between variables.

[144] McKay et al. 2000

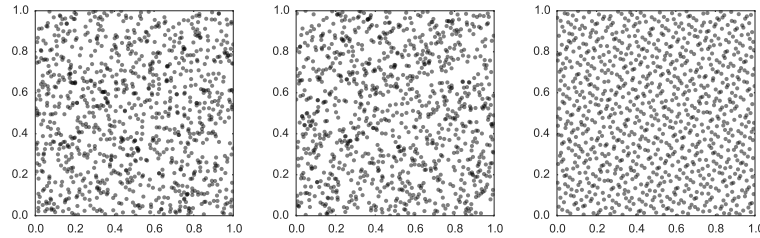

Figure 3.5: Examples of 1000 sample of the 2D hypercube: (a) Pseudo-Random (b) LHS (c) Halton.

3.4 Non-parametric multidimensional distributions

Non-parametric distributions are methods to describe the joint probability distribution based on an observation sample. These methods rely on the mixture or superposition of multiple distributions. One of the most important non-parameteric distributions methods is the mixture of multivariate normals. In this method the joint probability function is approximated as the mixture of N_k multivariate normal distributions, each of these distributions has a frequency of occurrence α_j and its own mean vector, covariance function $\mathbb{C}_j$ and where $\phi(\mathbf{x}|\mu_j, \mathbb{C}_j)$ is its corresponding multivariate normal density. Several algorithms for selection exist to determine the hyperparameters $(\alpha_j, \mu_j, \mathbb{C}_j)$ and the optimal number of distributions N_k to be used; refer to [145].

[145] McLachlan et al. 2004

A generalization of the mixture of distributions method is the Kernel density estimation (KDE)[4]. In this method an individual distribution is added for every observation in the sample. Each of these distributions has a maximum at the location of the observation and share the same hyperparameters that controls the region of influence or bandwidth $\boldsymbol{\vartheta}$: $K(\mathbf{x} - \mathbf{x}_j^*|\boldsymbol{\vartheta})$. Several distributions can be used such as uncorrelated normal, exponential and others, see [20].

[4] A Kernel refers to a distributions that is defined in terms of the distance to the observation.

[20] Biller et al. 2006

$$
\begin{aligned}
f(\mathbf{x}) &\approx \sum_{j=1}^{N_k} \alpha_j \phi(\mathbf{x}|\mu_j, \mathbb{C}_j) \\
f(\mathbf{x}) &\approx \frac{1}{N} \sum_{j=1}^{N} K(\mathbf{x} - \mathbf{x}_j^*|\boldsymbol{\vartheta})
\end{aligned}
\tag{3.10}
$$

Non-parametric multidimensional distributions:

KDE and mixtures models are very attractive methods to describe a multidimensional joint distribution. The main drawback is that these techniques are purely data driven and therefore they do not contribute to better understanding of the physics of the correlations between variables. This means that non-parametric distribution can not be used to generalize on what the distributions should look like on other datasets.

These types of distributions have been suggested for wind resource assessment in [146] and [147]. This methods have the potential to reduce the statistical uncertainty in the wind resources by not making assumptions on what distribution family represents each variable.

3.5 Expert elicitation

For those cases where there are no measurements highlighting the variability of some variables a common practice is to perform an expert elicitation. A survey on this topic is presented in [148]. In this process a group of experts is gathered and a series of surveys are used to aggregate the information about the uncertainty in the variables and their correlations. This process gives an estimation of the joint PDF of the input variables, which is for most cases represented using a known multivariate distribution such as a multivariate normal distribution. Alternative methods that rely on graphical input from the expert have been proposed [149]. Note that expert elicitation should only be used when there is no measurements as these methodologies can give overconfident assessments of the actual variability [148].

[146] Carta et al. 2008

[147] Zhang et al. 2013

3.6 Summary

This chapter has given an overview of the different methods to handle the joint distributions of multiple variables. Several examples of UQ problems that use this distributions can be found in `https://github.com/jp5000/Examples_PhD_thesis` [DOI:10.5281/zenodo.204786]. From this chapter the following conclusions can be made:

- The wind rose approach to represent the wind resources on a site can be improved by considering the joint distribution of wind speed and wind direction (or other additional atmospheric variables). This can be done using a Rosenblatt transformation or it can be a non-parametric distribution using KDE.
- The joint distribution of multiple inflow parameters and the sampling methods described in this chapter are used in the article [3]. This article can be found in appendix D.

[148] Morgan. 2014

Chapter 4

Propagation of Uncertainty

Propagation of uncertainty consists in finding the PDF of the outputs of a model produced by the joint PDF of the inputs and parameters. To simplify the notation, the uncertain parameters will be included as part of input variables and the model is assumed to have no prediction error. The propagation of uncertainty problem is depicted in Figure 4.1. This chapter formulates the methods for propagation of uncertainty that exist in the literature.

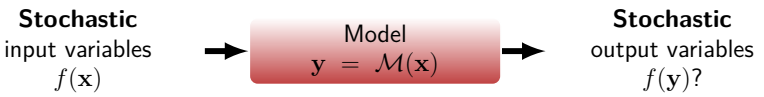

Figure 4.1: Propagation of uncertainty problem.

4.1 Analytical techniques/Convolution

Propagation of uncertainty can be performed analytically using the convolution function. The PDF of the outputs, $f(\mathbf{y})$, can be expressed using the convolution operation [150]. Here, the joint PDF of the inputs and the Dirac's function (δ) of the model and outputs give an expression for the joint PDF of the model outputs:

[150] Dietrich. 1991

$$f(\mathbf{y}) = \int_{\Omega_{\mathbf{x}}} \delta(\mathbf{y} - \mathcal{M}(\mathbf{x}))\, f(\mathbf{x})\, d\mathbf{x} \tag{4.1}$$

Two conditions make it difficult to obtain an analytical expression out of equation 4.1. Most of the models are too complicated to evaluate over all the input/parameter space and in most physical applications the joint PDF, $f(\mathbf{x})$, is too complicated to obtain an analytical expression for the integral. Only simple cases of uncertainty propagation can be found analytically: models that consists of linear combinations of independent and identically distributed inputs of well known PDF families (i.e. Normal, Chi-squared, among others) [150].

[118] Gaumond et al. 2014

Approximation of convolution:

The convolution equation can be approximated using a predefined design of experiments $\mathbf{x}^*$ that cover the input variables space $\Omega_{\mathbf{x}}$. A common approach in wind plant flow modeling is applying a convolution of the uncertain variable to a model to obtain an expected model output for given inputs. This approach has been used for wake models to consider the uncertainty in wind direction in [118]. This approximate approach consists in weighting the precomputed model evaluation databases with the probability of the desired evaluation point. See equation 4.2, where the constant b is normalization constant for the weights $(f(\mathbf{x}_j^*|\mathbf{x}))$ and its usually related to the space between the evaluation points and the number of points N. Note that this approach does not give the distribution of the outputs but it is a good approach to remove nuisance variables.

$$\mathbb{E}(\mathbf{y}|\mathbf{x}) = \int_{\Omega_{\mathbf{x}}} \mathcal{M}(\mathbf{x}+\boldsymbol{\varepsilon}_{\mathbf{x}})\, f(\boldsymbol{\varepsilon}_{\mathbf{x}})\, d\boldsymbol{\varepsilon}_{\mathbf{x}} \approx b \sum_{j=1}^{N} \mathcal{M}(\mathbf{x}_j^*)\, f(\mathbf{x}_j^*|\mathbf{x}) \quad (4.2)$$

More advanced methods exist that use the properties of the Fast Fourier Transformation (FFT) to approximate the convolution theorem.

4.2 Monte-Carlo simulations

Monte-carlo (MC) simulations are a numerical approach that uses random numbers to sample from PDFs. These methods are also used to evaluate integrals of complex multi-variate regions. MC simulations consists in generating a sample in the unitary hypercube and then use iso-probabilistic transformation to obtain a sample from the input distribution $(\mathbf{x}_1^*, ..., \mathbf{x}_N^*)$; finally, the model is executed for each of the observations in the sample, obtaining an output sample $(\mathcal{M}(\mathbf{x}_1^*), ..., \mathcal{M}(\mathbf{x}_N^*))$. Descriptive statistics can be calculated from the output sample such as the mean, variance, skewness, kurtosis or histograms. The main limitation of MC simulations is that the number of samples required to have convergence in the statistics of the output can become very large since the rate of convergence of the statistical moments of the output is $\propto N^{-1/2}$. Despite this limitation, Monte-Carlo simulations give the reference solution to any uncertainty propagation problem (that does not have an analytical solution) as it is easy to understand and to parallelize.

The curse of dimensionality:

The property that makes MC methods interesting is that the number of sample points required to achieve convergence in the estimation of the statistical moments of the output does not depend on the number of input uncertain variables.

The curse of dimensionality is the main problem of using factorial design of experiments to select the points of evaluation of a model. In a problem with 5 uncertain input variables, a factorial design of experiments with 10 levels for each dimension makes a total of 10^5 model evaluations.

The best performance of MC simulation is obtained when advanced sampling techniques (*Quasi-MC* or *LHS*) are used to define the evaluation points. This is important for problems with large number of inputs variables.

Example: Power law ABL vertical extrapolation

A common problem in wind resource assessment is the vertical extrapolation of the wind resources. This problem consists in taking measurements at a height and predicting the resources at different heights. In this example the empirical power law ABL model is used, equation 4.3, where H and U_H are the height and wind speed measurement.

$$U(z) = \begin{cases} U_H \left[\frac{z}{H}\right]^{\alpha} & \text{for } U_H > 1 \\ U_H & \text{for } U_H <= 1 \end{cases} \tag{4.3}$$

The measured wind speed at 80 [m] (U_{80}) follows a Weibull distribution and the shear exponent follows the conditional distribution proposed in [151]:

[151] Dimitrov et al. 2015

$$\begin{aligned} &f(U_{80}) = \mathcal{W}(A = 10, k = 2) \\ &f(\alpha|U_{80}) = \mathcal{N}\big(\mu(U_{80}) = 0.088(\ln(U_{80}) - 1), \sigma(U_{80}) = 1/U_{80}\big) \end{aligned} \tag{4.4}$$

A MC simulation is performed in order to predict the wind resources in multiple heights using the Rosenblatt transformation, a Halton sequence and a sample size of $N = 10^5$. The results are presented in figure 4.2. It can be observed that the correlation structure between shear and wind speed describes sites for which there is large variability in the shear exponent at low wind speeds. Additionally, it is evident that the wind speed at the prediction height (U_{120}) is highly correlated with the measured wind speed (U_{80}). The resulting distribution for the wind resources at 120 [m] height was fitted to a Weibull distribution $f(U_{120}) = \mathcal{W}(A = 10.49, k = 1.93)$ [m/s]. The distribution predicted if the mean shear coefficient is used to *shear-up* the scale coefficient at the measured point is less accurate: $\mathcal{W}(A = 10.37, k = 2.)$.

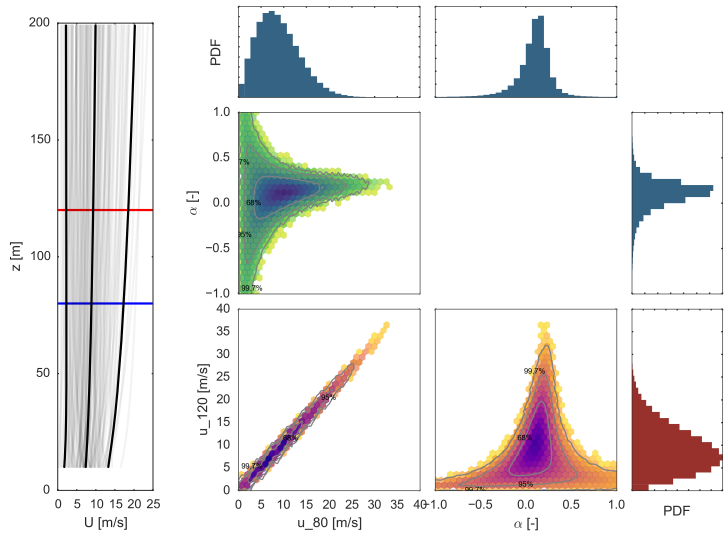

Figure 4.2: MC simulation for power law ABL. (left) 100 realizations of the ABL profile with the mean profile, and the 5% and 95% quantiles profiles. (right) Joint distribution of the inputs and and an example output $f(\mathbf{x}, \mathbf{y}) = f([U_{80}, \alpha, U_{120}])$.

4.3 Surrogate Models

Surrogate based uncertainty methods are designed for computationally expensive models. Since theses models are usually locally and globally non-linear; Taylor based methods can lead to large errors in the QoI statistics. For such models direct application of MC methods is prohibited due to the large number of simulations required. In this situation, the uncertainty propagation problem is applied to a surrogate model that consist in a mathematical model that replicates the behavior of the model over the input/parameter space of interest. Several options of surrogates have been proposed from different areas of mathematics, statistics, engineering and computer science; reviews of the different surrogate techniques can be found in [152] and [26]. In most of these techniques a limited number of model evaluations is used to train/build a surrogate. Additional model evaluations can be used to estimate the accuracy of the surrogate.

[152] Forrester et al. 2009
[26] Peherstorfer et al. 2016

The problem of building a surrogate model based on a set of model evaluations (or actual data) is also called supervised machine learning in modern applied statistics. Supervised machine learning algorithms can be grouped into three groups:

1. Generalized linear models are algorithms that fit the model evaluations as a linear combination of proposed basis functions. This type of models groups several of the most common used surrogates such as polynomials, piecewise polynomials splines and radial basis functions. Techniques for preforming sparse regression are very useful to avoid over fitting when building surrogates in large number of input variables and functional candidates. The detailed description of techniques like Ridge, least absolute shrinkage and selection operator (LASSO), least-angle regression (LAR), among others can be found in [153].

[153] Friedman et al. 2001

2. Algorithms based on the distance between points. These methods use the distance between point evaluations as one of the main parameters to determine the surrogate output; some examples are: radial basis functions (RBF), Gaussian process, support vector machines (SVM), among others [154].
3. Ensemble algorithms divide the problem into independent (or sequential) smaller regressions. Some examples are random forest (ensemble of decision trees), neural networks, bagging method, AdaBoost boosting algorithm, among others. A detail description of these methods can be consulted in [155].

[154] Smola et al. 2004

[155] Dietterich. 2000

4.3.1 Taylor series expansion

Taylor series expansion is the most traditional method for calculating the sensitivity of a model due to input and parameter variation. This is the basis for the uncertainty propagation methods proposed in the Guide to the expression of uncertainty in measurement (GUM) [17] and in the IEC 61400 standards for AEP uncertainty estimation [120].

[17] ISO et al. 2008

[120] IEC 61400-12-1. 2005

The Taylor series expansion consists in linearizing the model around the expected value of the inputs. The linearized model can be considered the simplest surrogate model possible. The Taylor expansion is given in equation 4.6; here, $\mathbb{J}$ represent the Jacobian matrix and $\mathbb{C}$ represents the covariance matrix[1]. In this method the inputs are assumed to follow a multivariate normal distribution $f(\mathbf{x}) = \mathcal{N}(\mu_{\mathbf{x}}, \mathbb{C}_{\mathbf{x}})$.

[1] The Jacobian contains the local sensitivities of the model with respect each of the variables at the expected value of the input: $\mathbb{J}_{j\,i} = \frac{\partial \mathcal{M}_j}{\partial x_i}|_{\mathbf{x}=\mu_{\mathbf{x}}}$

$$\mathbf{y}(\mathbf{x}) \approx \mathcal{M}(\mu_{\mathbf{x}}) + \mathbb{J}\,[\mathbf{x} - \mu_{\mathbf{x}}] \tag{4.5}$$

Depending on the complexity of the model the Jacobian can be calculated analytically, approximated numerically using a perturbation/finite differences scheme or generalized linear model regression techniques. Once the model has been linearized then the mean and variance of the output can be approximated from the mean and variance of the inputs, see equation 4.6. The final distribution of the output is also a multivariate normal because the linearized model does not modify the distribution shape: $f(\mathbf{y}) = \mathcal{N}(\mu_{\mathbf{y}}, \mathbb{C}_{\mathbf{y}})$. [2]

[2] The equation for the covariance of the output in equation 4.6 is the general version of the law of propagation of uncertainty.

$$\begin{aligned} \mu_{\mathbf{y}} &\approx \mathcal{M}\,(\mu_{\mathbf{x}}) \\ \mathbb{C}_{\mathbf{y}} &\approx \mathbb{J}\,\mathbb{C}_{\mathbf{x}}\,\mathbb{J}^T \end{aligned} \tag{4.6}$$

Several assumptions need to be checked in order to use GUM: (1) The non-linearity of the model can be neglected in the region covered by the input uncertainty. (2) The input variables can be approximated using a normal distribution. The critical issues with GUM approach are the treatment of asymmetric probability distributions and non-linearities in the model. For these cases, the expected value of the output variable can have a bias. Additionally, the variability in the output variable can be over estimated. Extensions to this approach consists in using a higher order Taylor expansions for propagation; expressions for second order Taylor expansion around the expected value for the first moment and for the second moment of the output can be found in literature [156].

[156] Mekid et al. 2008

On which cases should I use GUM?

This method can be used in problems where the input uncertainty represent only a small variability in comparison to the full scale of the problem, for such cases even in complex models the linearizion of the model is a good approximation.

For wind energy related problems such as the estimation of the uncertainty in AEP and LCoE for a wind plant the GUM method will not give an unbiased expected value of the output. The reason for this is that for non-linear models the expected output is not necessarily the evaluation of the model at the expected input $\mu_{\mathbf{y}} \neq \mathcal{M}(\mu_{\mathbf{x}})$. Furthermore this method can have biased estimation of the uncertainty in the output.

Significantly, most variables in wind energy have several layers of uncertainty. For example, the 10 minutes mean wind speed at a given site follows a Weibull distribution, but the measurement uncertainty related to a single observation of the wind speed follows a normal distribution. These different scales of uncertainty are related to the different scales of turbulence, and they are difficult to be characterized as a multivariate normal distribution.

GUM example: Log-law ABL vertical extrapolation

This example is a similar version of the vertical extrapolation of the wind resources problem, in which the measurements at a height are used to predict the resources at different heights. In this example the logarithmic ABL model with stability and ABL height is used, equation 4.7 [157]. Where u_* is the friction velocity, κ is the von Karman constant ($\sim$0.4), z_0 is the roughness height, L is the Obukhov length, z_i is the ABL height, and s is an auxiliary variable: $s = \left(1 - 12\frac{z}{L}\right)^{1/3}$.

[157] Peña et al. 2012

$$
\begin{aligned}
\psi\left(\frac{z}{L}\right) &= \begin{cases} -4.7\frac{z}{L} & \text{for L>0} \\ \frac{3}{2}\ln\left(\frac{1+s+s^2}{3}\right) - \sqrt{3}\arctan\left(\frac{2s+1}{\sqrt{3}}\right) + \frac{\pi}{\sqrt{3}} & \text{for L<0} \end{cases} \\
f_s\left(\frac{z}{z_i}\right) &= \begin{cases} 1 - \frac{z}{2z_i} & \text{for stable: L>0} \\ 1 & \text{for unstable: L<0} \end{cases} \\
U(z) &= \frac{u_*}{\kappa}\left[\ln\left(\frac{z}{z_0}\right) - \psi\left(\frac{z}{L}\right) f_s\left(\frac{z}{z_i}\right)\right]
\end{aligned}
\tag{4.7}
$$

The vertical extrapolation simplifies the equation by removing the dependency on the friction velocity. The uncertain parameters in this case are redefined in order to achieve an almost perfectly linear behavior: $\mathbf{x} = [U_H, \ln(z_0), 1/L, z_i]$ and a multivariate normal distribution is assumed. A negative correlation is assumed between $1/L$ and z_i as it is a well known fact that the atmospheric boundary layer height is reduced during stable conditions, and the positive correlation between the wind speed and the roughness considers ocean roughness increase with wind speed.

A MC simulation is performed in order to have a reference solution of the wind resources at multiple heights using a Halton sequence and a sample size of $N = 10^5$. In order to linearized the model a set of 15 simulations cover the region around the expected value. The results are presented in figures 4.3, 4.5 and 4.6. It can be observed that the definition of the uncertain variables makes this problem an ideal candidate for linearization. Finding the mean ABL profile under different conditions is relevant for wind resource assessment flow models, for a more theoretical approach refer to [158]. The main limitation of this example is the fact that the wind speeds are normally distributed.

[158] Kelly et al. 2010

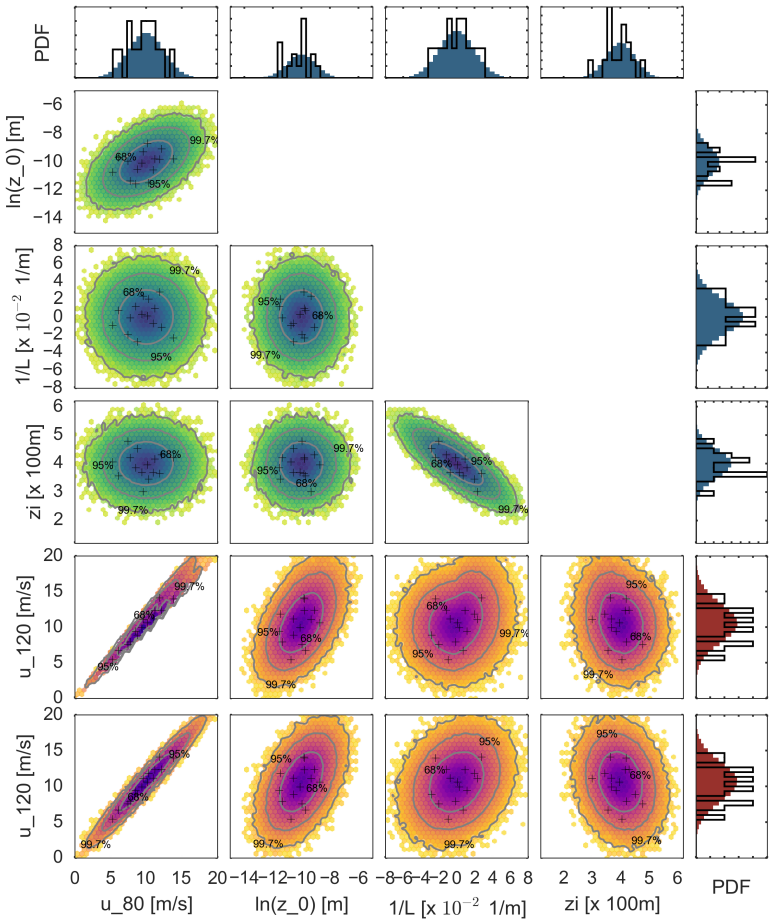

Figure 4.3: (colour histogram) 10^5 MC simulation. (+) points used to fit the PCE surrogate.

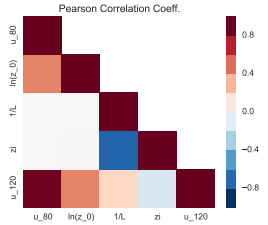

Figure 4.4: Corresponding correlation matrix to figure 4.3.

Figure 4.5: (colour histogram) 10^5 MC simulation on the linearized model. (+) points used to linearized the model.

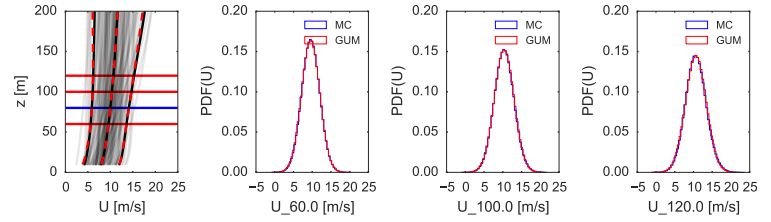

Figure 4.6: Comparison between MC and GUM predictions of the wind resources at different heights with the two methods.

4.3.2 Polynomial chaos expansions

Response surface surrogates consist in fitting an analytical expression to the model outputs; usually a polynomial function is proposed. Polynomial Chaos Expansion (PCE) is a technique for uncertainty propagation that consist in building a global polynomial response surface, with the particularity of using a polynomial basis based on $f(\mathbf{x})$. For an overview of the PCE methods refer to [159].

[159] Xiu. 2010

Consider a model with a single uncertain input x and a single output y. PCE consists of defining a polynomial family that is orthogonal with respect to the input distribution, $f(x)$. It is then required to define an inner product between two arbitrary functions, $g_1(x)$ and $g_2(x)$ with respect to the probability density function of the input $f(x)$ as:

$$\langle g_1, g_2 \rangle \equiv \int_{\Omega_\mathbf{x}} g_1(x)\, g_2(x)\, f(x)\, dx \tag{4.8}$$

The polynomial basis ($\phi_i(x)$ with polynomial orders $i = 0, 1, \dots$) is then constructed such that $\phi_0 = 1$ and all the polynomials are orthogonal:

$$\langle \phi_j, \phi_k \rangle = \delta_{jk} = \begin{cases} 1 \text{ if } j = k \\ 0 \text{ if } j \neq k \end{cases} \tag{4.9}$$

An important consequence of the orthogonality property is that all the polynomials in the orthogonal basis are orthogonal to the unitary function, see equation 4.10. For details on how to define new polynomial basis to an arbitrary input distributions refer to [160]. Orthogonal polynomial families with respect to the most important distributions are well known, see table 4.1.

[160] Gautschi. 1994

$$\langle 1, \phi_j \rangle = 0 \iff \int_{\Omega_\mathbf{x}} \phi_j(x)\, f(x)\, dx = 0 \quad \forall j > 0 \tag{4.10}$$

Table 4.1: Classical orthogonal polynomial families.

Distribution	Polynomial Family
Uniform	Legendre
Normal	Hermite

These polynomials are used to build an approximation of the output, see equation 4.11. Where c_j is the correspondent coefficient to $\phi_j(x)$ and M represents the truncation order of the PCE.

$$y(x) \approx \hat{y}(x) = \sum_{j=0}^{M} c_j\, \phi_j(x) \tag{4.11}$$

The orthogonality property makes the PCE an useful approach to propagate uncertainty because the statistical moments of the output can be derived directly from the coefficients:

$$\begin{aligned} \mathbb{E}(y) &= \int_{\Omega_\mathbf{x}} y(x)\, f(x)\, dx = \langle 1, y \rangle \approx \sum_{j=0}^{M} c_j \langle 1, \phi_j \rangle = c_0 \\ \mathbb{V}(y) &= \mathbb{E}(y^2) - \mathbb{E}(y)^2 = \sum_{j=1}^{M} c_j^2 \end{aligned} \tag{4.12}$$

When the problem has D input dimensions, the first step is to use an iso-probabilistic transformation to transform the input variables into an independent identically distributed space $\mathbf{w}$. A D-dimensional polynomial is constructed as the sum of the product between one dimensional polynomials for each of the uncorrelated variables, $\mathbf{w} = [w_0, \dots, w_{D-1}]$:

$$\mathbf{\Psi}_j(\mathbf{w}) = \phi_{l_0}(w_0) \times \cdots \times \phi_{l_{D-1}}(w_{D-1}) \tag{4.13}$$

The D-dimensional surrogate is written using a set of multiple indexes $\mathcal{I} \subset \mathbb{N}^D$. An element $J \in \mathcal{I}$ contains the order of the polynomial in each dimension: $J = [l_0, \dots, l_{D-1}]$. Additionally, the multiple indexes are enumerated, $J \leftrightarrow j \in \mathbb{N}$. A PCE with N_c terms can be written as: [3]

[3] This equation uses the iso-probability transformation notation $\mathbf{x} = R(\mathbf{w})$.

$$y(\mathbf{x}) = y(R(\mathbf{w})) \approx \sum_{j=0}^{N_c-1} c_j \, \mathbf{\Psi}_j(\mathbf{w}) \tag{4.14}$$

Two groups of methods exist to fit the PCE coefficients c_j:

Semi-Spectral projection consists in using quadrature rules to approximate the inner product definition of the c_j coefficients. A quadrature rule gives N_n nodes for model evaluation x_i and their corresponding weights ω_i, see equation 4.15 for the 1-dimensional quadrature. Gaussian quadrature rules are widely used because they are accurate for smooth function integration with respect a weight function $f(x)$. The location of the nodes depends on the truncation order.

$$c_j = \langle y, \phi_j \rangle \equiv \int y(x)\, \phi_j(x)\, f(x)\, dx \approx \sum_{i=0}^{N_n} \omega_i \, y(x_i) \tag{4.15}$$

There are several options to design more efficient truncation schemes in multidimensional problems: *Smolyak sparse grid collocation* proposes quadrature rules from the combination of lower order quadratures that significantly reduce the number of model evaluations required. *Adaptive sparse collocation* can be build by sequentially enriching the terms and their sparse quadratures from the full set of possible terms [161].

[161] Le Maître et al. 2010

Point collocation consists in fitting the c_j coefficients based on a sample of model evaluations. Traditionally, this fit can be done using least squares algorithm. A weighted least squares can be used to include information about the PDF of the input evaluation points $f(\mathbf{x}^*)$. Advanced generalized linear model regression algorithms can be used to obtain sparse PCE approximations that do not include all the possible interaction terms in the final surrogate; for examples refer to [162][163].

[162] Blatman et al. 2011
[163] Sudret. 2008

PCE example: Ishigami function

The Ishigami function was introduced in [164] as a test function for uncertainty propagation methods because it contains nonlinearities and in-

[164] Ishigami et al. 1990

teraction terms, see equation 4.16. The constants of the model are set as $a = 7$ and $b = 0.1$.

$$y = \sin(x_1) + a\,\sin^2(x_2) + b\,x_3^4\,\sin(x_1) \tag{4.16}$$

Figures 4.7 and 4.8 shows the model results for uncorrelated uniform input variables in the range $x_i \sim \mathcal{U}(-\pi, \pi)$ using a $N = 10^5$ MC simulation and a PCE approximation based on $N = 495$ simulations. The regression of the coefficients was done using the implementation of the LAR algorithm available in the Python libraries Scikit-learn [165] and chaospy [138].

[165] Pedregosa et al. 2011
[138] Feinberg et al. 2015

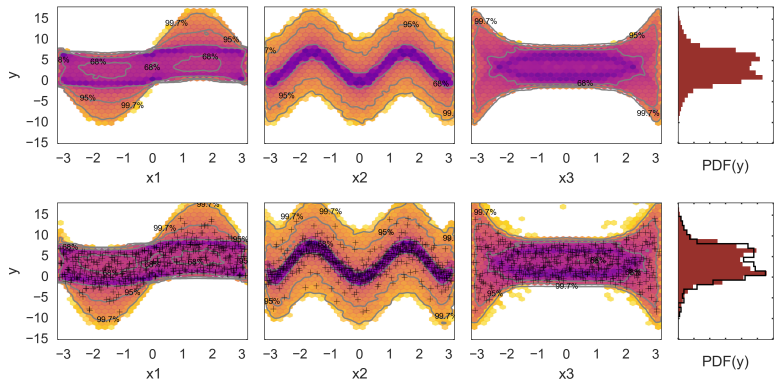

Figure 4.7: (top) 10^5 MC simulation on the Ishigami function (bottom) Sparse PCE surrogate fit of 495 simulations.

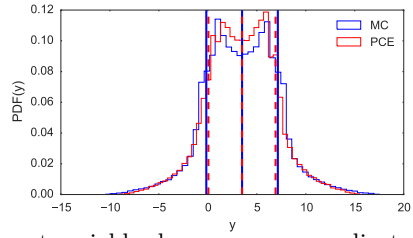

Figure 4.8: Comparison of $f(y)$ with 10^5 MC and 495 PCE.

When the input variables have a more complicated joint PDF including non-linear correlations, the Ishigami function can be quite challenging to surrogate due to its periodicity. To exemplify this, the Ishigami function is applied to a set of variables related to a wind resource assessment problem: 10 minutes mean wind speed ($x_1 = U$), 10 minutes mean wind direction ($x_2 = \theta$) and turbulence intensity. The turbulence intensity is modeled using the standard deviation of instantaneous streamwise wind speed scaled to have a valid range for the original Ishigami function $x_3 = \sigma_1/10$. The distribution for the streamwise turbulent fluctuations conditioned on the wind speed is described as the normal turbulence model in the IEC standards [30]. A reference turbulence intensity of 16% is used.

[30] IEC 61400-1. 2005

$$\begin{aligned} f(\theta) &= \mathcal{U}(-\pi, \pi) \\ f(U) &= \mathcal{W}(A = 8, k = 2) \\ f(\sigma_1|U) &= \mathcal{LN}(\mu_{\sigma_1} = \mu_{\sigma_1}(U), \sigma_{\sigma_1} = \sigma_{\sigma_1}(U)) \end{aligned} \tag{4.17}$$

$$\sigma_{\sigma_1} = \sqrt{\ln\left(\frac{\mathbb{V}(\sigma_1|U)}{\mathbb{E}^2(\sigma_1|U)} + 1\right)} = \sqrt{\ln\left(\frac{1.4^2}{(0.75U + 3.8)^2} + 1\right)}$$
$$\mu_{\sigma_1} = \ln\left(\mathbb{E}(\sigma_1|U)\right) - \frac{\sigma_{\sigma_1}^2}{2} = \ln\left(\mathrm{I}_{\mathrm{ref}}\left(0.75U + 3.8\right)\right) - \frac{\sigma_{\sigma_1}^2}{2} \tag{4.18}$$

Figures 4.9 and 4.10 show a $N = 10^5$ MC simulation and a PCE approximation based on $N = 495$ simulations for the Ishigami function when there are large correlations between the input variables. For the PCE the maximum possible polynomial order is set to be 8. The final surrogate is as good as in the case with uncorrelated input variables. It can be observed that the mean and the standard deviation (figure 4.11) of the output are well captured, but if the QoI is the prediction for a single input case then a more flexible global surrogate should be used such a reduced basis functions or Gaussian process.

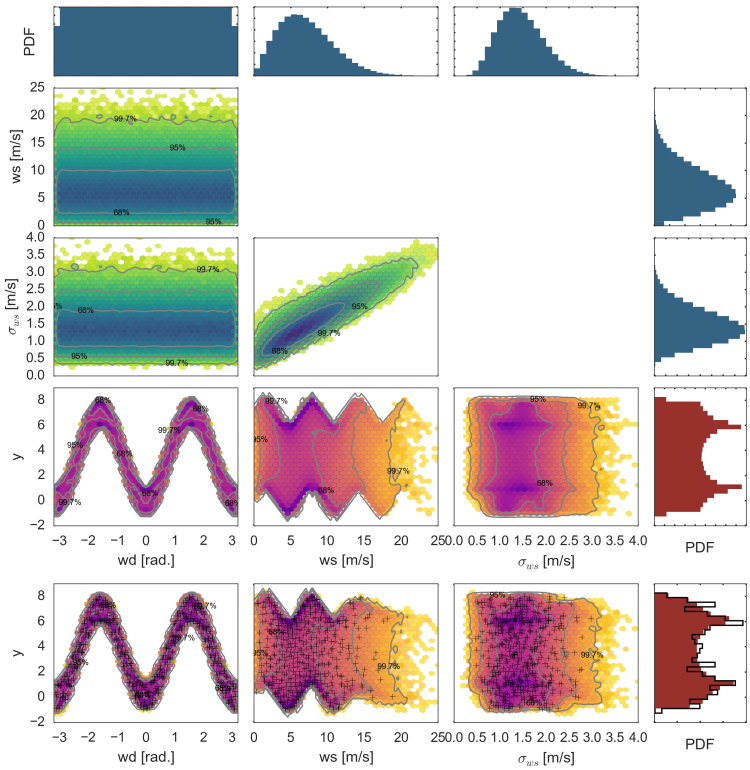

Figure 4.9: Predicted $f(y)$ with $N = 10^5$ MC simulations.

Figure 4.10: Predicted $f(y)$ with $N = 495$ PCE. Surrogate is evaluated at the same locations as with MC.

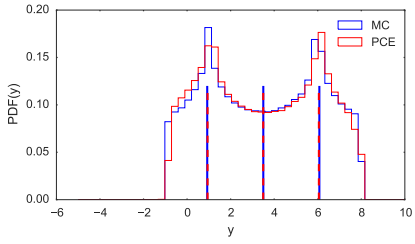

Figure 4.11: Comparison of $f(y)$ with MC and PCE, when the input variables are non-normal and correlated.

PCE example: Oakley and O'Haggan function

[166] Oakley et al. 2004

The Oakley and O'Haggan function is used to test the methods for intermediate number of uncertain input variables since it has 15 dimensions [166]. This function contains nonlinearities and interaction terms, see equation 4.19. This function is design to have 5 variables that are relatively important, 5 intermediate variables and 5 nuisance variables. This function is a good example for testing sensitivity analysis methods, as well as, reduction of problem dimensionality.

$$y(\mathbf{x}) = \mathbf{a_1}^T\mathbf{x} + \mathbf{a_2}^T \sin(\mathbf{x}) + \mathbf{a_3}^T \cos(\mathbf{x}) + \mathbf{x}^T\mathbf{M}\mathbf{x} \tag{4.19}$$

[4] In this example the input variables are correlated which it was not considered in the original article [166]

With this number of dimension it is difficult to present the joint distribution in a gridplot as it has been used for the previous examples[4]. Instead only the correlation matrix is used to illustrate the linear correlations between the different variables. For this case the input variables follow a multivariate normal distribution with null mean, unitary standard deviation but a correlation structure, see figure 4.12. Note that there is almost no linear correlation between the inputs and the output (last line of the correlation matrix); this is because of the periodicity in the output. This sort of dependency is not captured by the Pearson correlation coefficient. Figure 4.13 shows a $N = 5 \times 10^5$ MC simulation and a PCE based on $N = 2448$ simulations with a maximum polynomial order of 3.

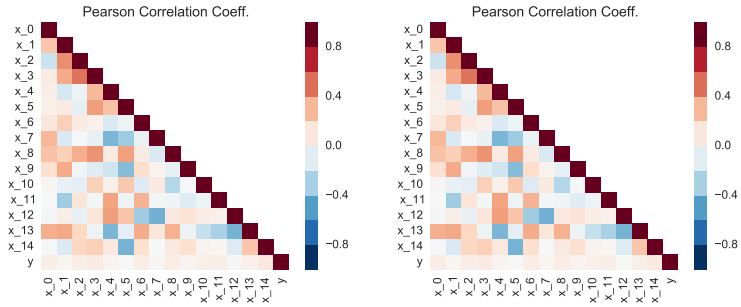

Figure 4.12: (left) MC simulation correlation matrix. (right) PCE correlation matrix.

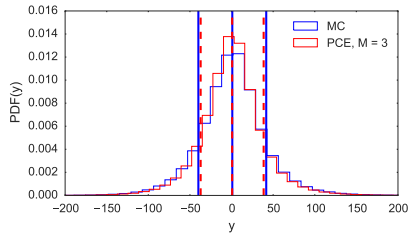

Figure 4.13: Comparison of $f(y)$ obtained with MC and PCE.

PCE as a generalization of GUM:

Think about PCE as a generalized version of the GUM that simplifies the model but that is able to capture most of its global properties. PCE becomes equivalent to GUM if the polynomials are forced to be of first order, and if the input uncertain variables are normally distributed.

PCE becomes very powerful for problems where the model is non-linear and where the distributions are non-normal. This makes it a very good candidate method for wind energy UQ problems.

One of the main limitations of this method is that the number of polynomial terms in the surrogate grows exponentially with the number of input variables. Even using sparse generalized linear model regression methods there is a limit in the number of uncertain variables this method can handle. The maximum number of dimensions for real applications is in the order of 100 variables with the most advanced methods PCE methods [167].

[167] Bigoni et al. 2016

4.3.3 Radial basis functions

Radial Basis Function (RBF) surrogates consist in approximating the model as a linear combination of simple functions that only depend on the radial distance from their definition node [168]. In this method a sample of the input $\mathbf{x}^*$ and its corresponding model evaluations $\mathbf{y}^* = \mathcal{M}(\mathbf{x}^*)$ are used to define the nodes of the RBFs, see equation 4.20.

[168] Broomhead et al. 1988

$$y(\mathbf{x}) \approx \sum_{j=1}^{N} c_j \, K(||\mathbf{x} - \mathbf{x}_j^*||) \tag{4.20}$$

Similarly to the response surface method, different calibration methods can be used to find the c_j coefficients. The most common approach consists in solving the least squares errors by solving the linear system of equation given by arranging the RBF evaluations into the Gram matrix $\mathbf{\Phi}$, see equation 4.21.

$$\begin{aligned} \mathbf{\Phi c} &= \mathbf{y}^* \\ \mathbf{\Phi}[i,j] &= K(||\mathbf{x}_i^* - \mathbf{x}_j^*||) \end{aligned} \tag{4.21}$$

Several radial functions can be used such as linear, cubic, among others. The most widely used RBF is the Gaussian RBF because it assures stability to the solution of the weights. The Gaussian RBF is given by the following equation:

$$K_G(||\mathbf{x} - \mathbf{x}_j||) = \exp\left(-\frac{||\mathbf{x} - \mathbf{x}_j||^2}{2\vartheta_G^2}\right) \tag{4.22}$$

The Gaussian RBF contains a hyperparameter ϑ_G that represents the radius of influence of each of the model evaluations in the input space. This hyperparameter is usually shared between all the RBFs and becomes a tunning parameter that controls how smooth is the resulting surrogate

[26] Peherstorfer et al. 2016

[26]. This hyperparameter needs to be defined by the user. Since the input variables $\mathbf{x}$ have different units and ranges, it is appropriate to use the RBF applied in the uniform space after an iso-probabilistic transformation $\mathbf{x}$. This means that all the variables are scaled in the range $[0, 1]$ and therefore the hyperparameter ϑ_G can be set to vary within [0,1].

$$y(\mathbf{x}) = y(R(\mathbf{w})) \approx \sum_{j=1}^{N} c_j \, K(||\mathbf{w} - \mathbf{w}_j^*||) \tag{4.23}$$

Greedy algorithm

Since the optimal radius of influence of the Gaussian RBF is unknown, one could model it as an uncertain variable. This means that for a set of observed model evaluations (training points) there will be a set of predictions for every evaluation location. This extra information can be translated into an estimation of the error in the surrogate. The user of the surrogate can expect the true model to be inside the confidence interval generated by the surrogate uncertainty. Surrogate models that give a confidence region for the prediction can be considered to be certified since their error can be reduced to a tolerable level using a *greedy algorithm* [169].

[169] Hesthaven et al. 2015

The first step is to build the surrogate uncertainty model is to define an expected range of influence in the hyperparameter. Since in the uniform space all variables vary between $[0, 1]$, then a good initial estimate is to define $f(\vartheta_G) \sim \mathcal{N}(0.5, 0.1)$. This estimation can be improved using the calibration techniques described in section 5.1.

The greedy algorithm can be summarized as:

1. Define an initial set of simulations based on extreme values of the inputs, and enrich it with a small random distribution of input points in the inner range. This initial condition should define the minimum number of simulations and it defines the initial condition for the algorithm.

2. Define the evaluation points where the surrogate is to be evaluated; it could be a large MC of the inputs.

3. Define the test values for the hyperparameters. A small sample of the hyperparameters can be obtained according to their distribution $f(\vartheta_G)$. This sample can vary as the distribution of the hyperparameter is reduced.

4. Estimate the evaluation point that has the largest variability according to the ensemble of RBFs. The standard deviation of the RBF ensemble is computed using the predictions done with each of the different hyperparameters.

5. Evaluate the model in that new point. Enrich the training data set.

6. Stop if the maximum surrogate standard deviation is lower than a tolerance value.

RBF example: Ishigami function

The same example of the Ishigami function applied to the $\mathbf{x} = [\theta, U, \sigma_1]$ of section 4.3.2 is to illustrate the greedy algorithm with certified RBF surrogates. In this example a sample of 10 hyperparameters was selected. The initial training set consisted of 58 values, 8 extreme values and 50 inner points generated using a Halton sequence. Figure 4.14 shows the mean and standard deviation of the ensemble of surrogates for the initial condition. Figure 4.15 shows the mean and standard deviation of the ensemble of surrogates after the greedy algorithm has enrich the training dataset to 250 points. Note how the standard deviation of the surrogates has been reduced. Figure 4.16 present the comparison of a 10^5 MC simulation and the RBF ensemble prediction. Note that the final RBF surrogate achieves a perfect surrogate with only 250 simulations.

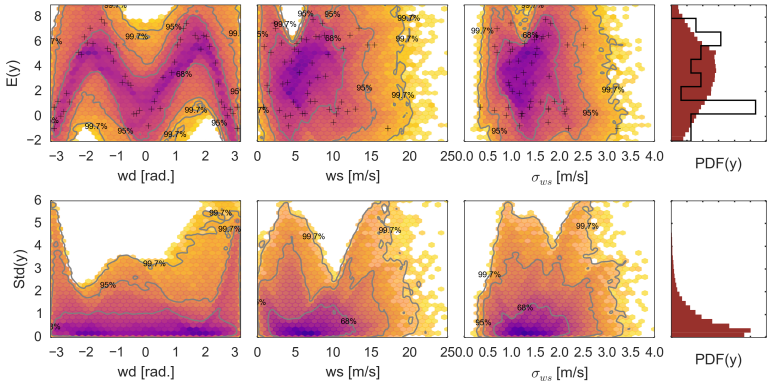

Figure 4.14: Mean and standard deviation of the output predicted with an RBF ensemble trained based on 57 model evaluations. Initial condition for the greedy algorithm.

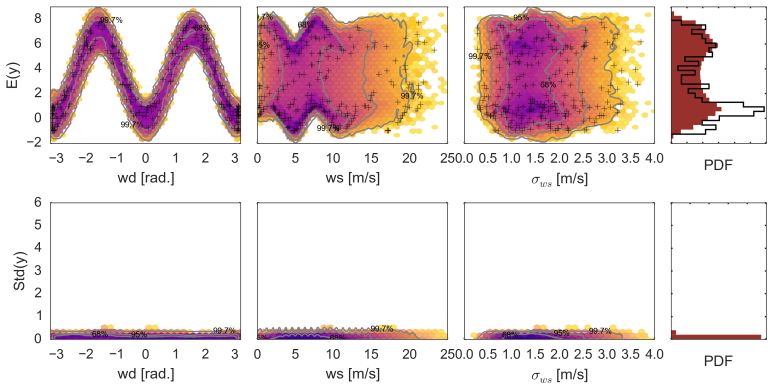

Figure 4.15: Mean and standard deviation of the output predicted with an RBF ensemble trained based on 250 model evaluations. After 193 added points by the greedy algorithm.

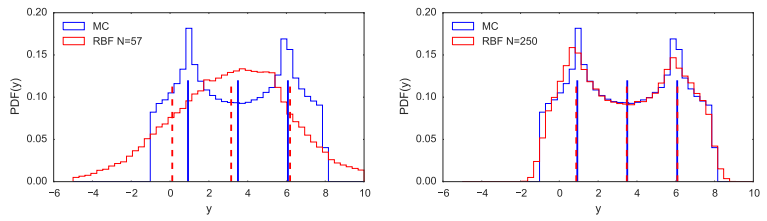

Figure 4.16: Comparison of $f(y)$ with RBF after the greedy algorithm.

PCE or RBF?

RBF is a good replacement for PCE when the output has several complex interaction terms. RBF surrogates are very flexible to interpolate complex models in multiple dimensions because their response is only driven by the number of know solutions. The flexibility of the RBF to interpolate the behavior of the model is both its advantage and its main problem. This flexibility makes it less accurate and therefore it will require a larger number of model evaluations than PCE for a large number of input dimensions. Note that the distance between points increases as the problem has additional dimensions. RBF is a good approach to build surrogates when the input variables are heavy tailed distributed and/or when they have complex correlation structures.

The greedy algorithm is an optimal approach to build a certified surrogate. It can be applied to several different surrogate methods that give an estimation of the surrogate error such as Gaussian process, or surrogates based on model ensembles.

4.4 Sensitivity Analysis

Sensitivity analysis is a required step after propagation of uncertainty because it helps to understand which uncertain input variables are responsible for the variability in the outputs. This means that an initial sensitivity analysis of a model is a powerful tool to select what variables are required to be considered as uncertain in future uses of the model. A sensitivity analysis is a necessary aspect of building a model, specially to those models that have large number of inputs/parameters. In general, having multiple input variables makes a model very flexible to capture any phenomena but it also makes it more sensitive to uncertainties in these multiple inputs/parameters.

4.4.1 Local sensitivity analysis

Local sensitivity analysis consists in finding the gradient of the model with respect to the inputs around a specific point in the input space[5]. This sensitivity can be non-dimensiona-lized using the variance of the input and output. This local Derivative Based Global Sensitivity Index (DBGS) represents the ratio of influence of a given input in the variance of the output, see equation 4.24. The main limitation of local sensitivity analysis is that it only represent the actual variability if the model can be linearized using a Taylor series approach. This equation represents the contribution of a single variable in the famous law of uncertainty propagation when normalized by the variance of the output.

[5] The Jacobian represents the local sensitivity analysis for models with multiple outputs

$$\mathrm{DBS}_i = \left(\frac{\partial \mathcal{M}}{\partial x_i}(\mu_{\mathbf{x}}) \right)^2 \frac{\mathbb{V}(x_i)}{\mathbb{V}(y)} \tag{4.24}$$

Global sensitivity analysis consists in giving a measure of how much of the variance in the output can be explained by the propagation of the uncertainty in each of the inputs. Global sensitivity is required when the model is non-linear and when the uncertainty in the inputs is large enough to explore regions with different model output local sensitivity. A review of the SA methods can be found in [170].

[170] Iooss et al. 2015

4.4.2 Screening methods

An estimate method to obtain global sensitivity analysis information based on the local sensitivity or gradients of the model. *Morris screening* estimates the local sensitivity using finite differences and it samples the input space using the Morris sequence [171]. Morris screening requires very few simulations and it can be used as a preliminary SA study. DBGS is obtained by the partial derivatives of the model evaluated at a MC sample of the input. This translates the local model sensitivities into global sensitivity measures [172].

[171] Morris. 1991

[172] Sobol' et al. 2009

$$\mathrm{DBGS}_i = \int_{\Omega_{\mathbf{x}}} \left(\frac{\partial \mathcal{M}}{\partial x_i}(\mu_{\mathbf{x}}) \right)^2 \frac{\mathbb{V}(x_i)}{\mathbb{V}(y)} f(\mathbf{x})\, \mathrm{d}\mathbf{x} \tag{4.25}$$

When the uncertainty in the variables is not large or when the model is linear, the DBGS and Derivative Based Sensitivity Index (DBS) converge to the same value.

4.4.3 Variance decomposition

Variance decomposition method consists in decomposing the variance of the output into contributions of variance of the output from each of the individual inputs, and from interaction terms of multiple combinations of inputs. Refer to [173] for further details. This method is the most recognized methods for global sensitivity analysis and it shares the same theory used in analysis of variance (ANOVA). Variance decomposition can be expressed in terms of the variance of the marginal expected value of a subset of input variables. Note that this decomposition is not a infinite series expansion, but it is just a recurrent use of Bayes theorem.

[173] Saltelli et al. 2010

$$\mathbb{V}(y) = \sum_{i=1}^{D} \mathbb{V}_i + \sum_{i=1}^{D} \sum_{j>i}^{D} \mathbb{V}_{ij} + \sum_{i=1}^{D} \sum_{j>i}^{D} \sum_{k>j}^{D} \mathbb{V}_{ijk} + \ldots + \mathbb{V}_{1,\ldots,D} \tag{4.26}$$

In this equation, $\mathbb{V}_i = \mathbb{V}\left(\mathbb{E}_{\forall x_l \neq x_i}\left(\mathcal{M}(\mathbf{x}|x_i)\right)\right)$ is the variance due the main effect[6]. The output variance due to the interaction between the i-th and j-th variables is $\mathbb{V}_{ij} = \mathbb{V}\left(\mathbb{E}_{\forall x_l \neq x_i, x_j}\left(\mathcal{M}(\mathbf{x}|x_i, x_j)\right)\right) - \mathbb{V}_i - \mathbb{V}_j$. The output variance due to the triple interaction between the i-th, j-th and k-th variables is $\mathbb{V}_{ijk} = \mathbb{V}\left(\mathbb{E}_{\forall x_l \neq x_i, x_j, x_k}\left(\mathcal{M}(\mathbf{x}|x_i, x_j, x_k)\right)\right) - \mathbb{V}_{ij} - \mathbb{V}_{ik} - \mathbb{V}_{jk} - \mathbb{V}_i - \mathbb{V}_j - \mathbb{V}_k$.

The global sensitivity analysis consist in normalizing the variance due to the interaction terms by the total output variance.

$$S_i = \frac{\mathbb{V}_i}{\mathbb{V}(y)} \quad S_{ij} = \frac{\mathbb{V}_{ij}}{\mathbb{V}(y)} \quad \ldots \tag{4.27}$$

[6] Main effect refers to the effect on the output due to a single variable. These effects can be isolated from the other variables. Note that the main effect are not necessarily linear.
The interaction terms refer to terms that have product between multiple.

Where the main effect Sobol index (S_i) is the fraction of output variance that can be explained by the main effect of the i-th variable and its variation. While the total effect Sobol index is the sum of all the Sobol indexes that contain interactions with the i-th variable ($S_{Ti} = S_i + \sum_{\forall k} S_{ik} + \dots$) and it represents the fraction of variance of the output that is explained by the variance of the i-th variable.

The main effect Sobol index (S_i) is equivalent to the DBGS for a model where the linearized surrogate is a good approximation and when the variables are normally distributed. The total Sobol index is a better measure of the sensitivity as it includes non-linearities and variable interactions.

Three different approaches to calculate the Sobol indexes based on MC samples of the inputs have been proposed and are compared in [173]. Surrogates models can facilitate the computation of the global SA: Sobol indexes can be obtained directly from the PCE coefficients [163] and from the Gaussian RBF weights [174].

[173] Saltelli et al. 2010

[163] Sudret. 2008

[174] Wu et al. 2016

Variance decomposition and Sobol index need to be computed in uncorrelated variables, therefore for a case when the variables are correlated an iso-probability transformation needs to be applied. This means that the Sobol indexes will be estimated for the corresponding uniform variable and not the physical variables them-selves.

For conditionally correlated variables it is important to recognize that the corresponding uniform variable only describes the variability given the previous variables. For example the uniform variable corresponding to the streamwise turbulence intensity σ_1 in the example shown in figure 4.9 only represent the variability for a given wind speed; it does not represent the marginal variability of the σ_1. Regardless of this fact, the Sobol index represent a ratio between the variability in the output due an input with respect the total output variability so no modifications to the equations is required.

GUM example: Log-law ABL vertical extrapolation

For this example, all the sensitivity analysis indexes provide the same information since the model can be linearized. The SA indexes depend on the height of the predicted wind resources, see figure 4.17.

The variability in the measured wind speed u_{80} is the main responsible for the variability of the wind resources at different heights. The second most important variable is the stability. Note that the ABL height and the roughness are not main contributors and therefore these variables could be treated as certain from further analysis. It is important to recognize that this is only valid if the standard deviation of these variables is not increased in the future uses of the model. From this figure, it can be recognized how the importance of modeling the stability grows as the resources are predicted further away from the observation point.

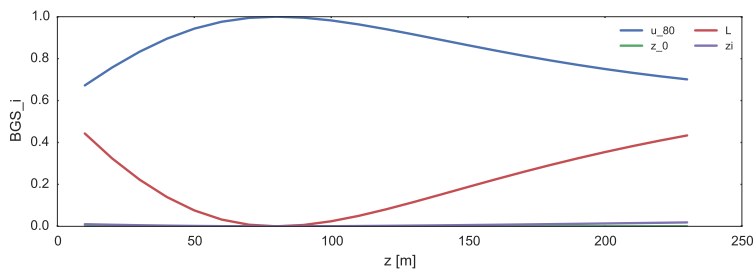

Figure 4.17: indexes for the Log-law ABL vertical extrapolation uncertainty propagation example.

PCE example: Ishigami function

This example shows how the main effect Sobol index does not capture the full picture for models that have periodicity and other types of non-linearities. The Sobol indexes for the Ishigami function with uniform and uncorrelated input variables are presented in table 4.2. The main effect Sobol index do not give all the information because of the periodicity and interaction terms present in the Ishigami function. It can be observed as expected from the results presented in figure 4.7 that the first two variables are equally important in terms of the total effect but not for the main effects. The lack of information that comes from the linear effect SA is clear for the third variable, where it is clear that it is not an important variable in itself but it does have interaction terms with other variables.

	x_1	x_2	x_3
S_i	0.34	0.43	0.00
S_{Ti}	0.57	0.43	0.23

Table 4.2: Sobol Indexes for the Ishigami function with uniform and uncorrelated input variables.

The Sobol indexes for the Ishigami function for the example with correlated variables are presented in table 4.2, note that the Sobol index are given for the corresponding uniform variables after an iso-probabilistic transformation $\mathbf{w}$. In this case as expected from the results presented in figure 4.9, the most important variable is the wind direction while the second one is the wind speed. The turbulence (x_3) has a negligible total and main effects and therefore could be modeled as having a fixed value. This means that the streamwise turbulence fluctuation can be modeled as a function of the wind speed (the expected value $\mathbb{E}(\sigma_1|U)$) and not as a distribution conditioned on the wind speed ($f(\sigma_1|U)$).

Correlated	θ	U	σ_1
Uncorrelated	w_1	w_2	w_3
S_i	0.93	0.07	0.00
S_{Ti}	0.93	0.07	0.00

Table 4.3: Sobol Indexes for the Ishigami function with correlated inputs. Note that the Sobol indexes are given for the corresponding uniform and uncorrelated input variables after an iso-probabilistic transformation $\mathbf{w} = R^{-1}(\mathbf{x})$.

PCE example: Oakley and O'Haggan function

The Sobol indexes for the Oakley and O'Haggan function are presented in the figure 4.18 for the original case without any correlation between the input variables and for the present case with the correlation matrix presented in figure 4.12. As it has been discussed before the correlation between variables considerably modifies the variability of the output; this is a consequence of an accumulation of the effects of multiple inputs covarying. For the correlated example presented in this thesis, it can be concluded that the most important variables are x_0,x_1,x_2,x_3,x_4, while the remaining variables can be treated as certain.

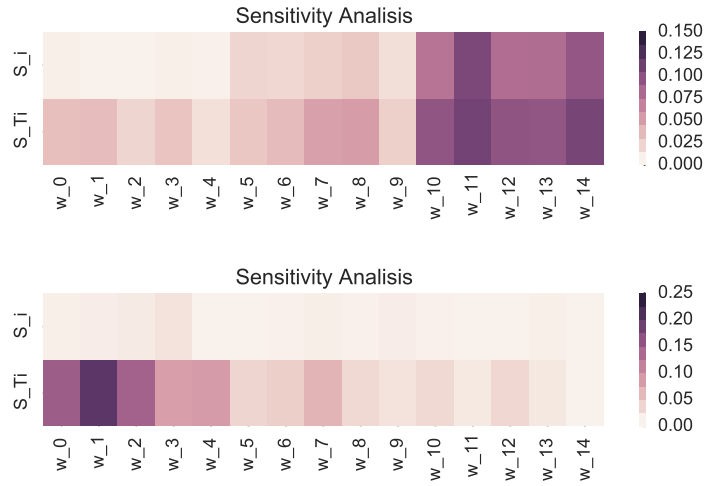

Figure 4.18: Sobol indexes for the Oakley and O'Haggan function (top) original uncorrelated inputs (bottom) correlated inputs example.

How to select the SA method?

If possible Sobol indexes should be used because they are the only global measure for sensitivity analysis that can handle non linear models with arbitrary input variables distributions.

If the model can be linearized and the input variables are normally distributed, then the local derivative based sensitivity index can be used because it is equivalent to the Sobol index.

Screening methods should only be used as rough estimations. They are not a replacement for the Sobol indexes.

4.5 Summary

This chapter has given an overview of the different methods to propagate uncertainty through a model. The examples of uncertainty propagation can be found in `https://github.com/jp5000/Examples_PhD_thesis` [DOI:10.5281/zenodo.204786]. From this chapter the following conclusions can be made:

- Propagation of uncertainty through a computationally efficient model can be done with Monte-Carlo simulations.
- A surrogate model can be used to efficiently propagate the uncertainty through a non-linear model and to obtain global sensitivity analysis.
- An extension of a polynomial response surface that predicts the mean and the uncertainty in the power, the thrust coefficient and D_{eq} on different components of a turbine for realistic inflow conditions has been developed. This methodology is presented in the article [4]. This article is available in chapter B.

[4] Murcia et al. 2016

Chapter 5

Model Calibration and Validation

Model calibration and validation processes share the same problem structure, in which the model prediction capacity is contrasted against measurements. The objective in model calibration is to determine the model parameters while in model validation the objective is to determine the model prediction error. These types of problems are called inverse problems since the model is not used to make predictions but instead information about the model is *inferred* based on the measured pairs $(\tilde{\mathbf{x}}, \tilde{\mathbf{y}})$.

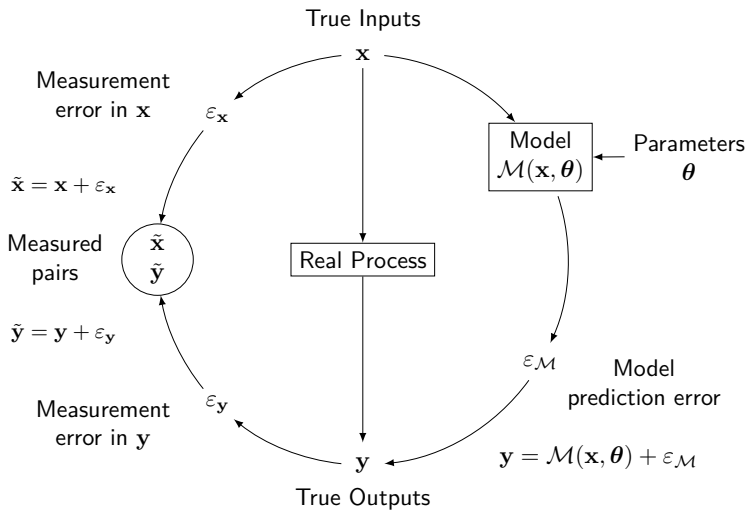

Figure 5.1: Measuring and modeling reality.

In general a calibration or a validation dataset consists of several independent observations of the measured pairs. The notation used in this thesis is: $(\tilde{\mathbf{x}}_{\mathcal{I}}, \tilde{\mathbf{y}}_{\mathcal{I}}) = \{(\tilde{\mathbf{x}}_1, \tilde{\mathbf{y}}_1), (\tilde{\mathbf{x}}_2, \tilde{\mathbf{y}}_2), \dots (\tilde{\mathbf{x}}_{N_{\mathcal{I}}}, \tilde{\mathbf{y}}_{N_{\mathcal{I}}})\}$. Where $N_{\mathcal{I}}$ is the total number of observed pairs in the dataset.

5.1 Model Calibration

There are several methods for model calibration. This section presents them and states their assumptions. Two main groups of methods exist: maximum likelihood estimation and Bayesian calibration. Different methods can be derived from these two classes depending on the assumptions about the measurement uncertainties. Refer to [175] for details and a comparison of calibration methods.

[175] Omlin et al. 1999

5.1.1 Maximum likelihood estimation (MLE)

Maximum Likelihood Estimation (MLE) is a calibration method based on the likelihood function. The likelihood function is defined as the PDF of observing a measured output given the measured inputs and a set of parameters: $\mathcal{L}(\tilde{\mathbf{y}}, \tilde{\mathbf{x}}|\boldsymbol{\theta}) = f(\tilde{\mathbf{y}}|\tilde{\mathbf{x}}, \boldsymbol{\theta})$. The calibration problem is then reduced to an optimization problem in which the parameter estimators maximizes the total likelihood function, see equation 5.1. In this equation the observations are assumed to be independent, therefore the total likelihood is the product of the individual likelihoods for each observed pair.

$$\begin{aligned} \mathcal{L}(\tilde{\mathbf{y}}_{\mathcal{I}}, \tilde{\mathbf{x}}_{\mathcal{I}}|\boldsymbol{\theta}) &= \prod_{i=0}^{N_{\mathcal{I}}} \mathcal{L}(\tilde{\mathbf{y}}_i, \tilde{\mathbf{x}}_i|\boldsymbol{\theta}) = \prod_{i=0}^{N_{\mathcal{I}}} f(\tilde{\mathbf{y}}_i|\tilde{\mathbf{x}}_i, \boldsymbol{\theta}) \\ \hat{\boldsymbol{\theta}} &= \arg\max_{\boldsymbol{\theta}} \mathcal{L}(\tilde{\mathbf{y}}_{\mathcal{I}}, \tilde{\mathbf{x}}_{\mathcal{I}}|\boldsymbol{\theta}) \end{aligned} \tag{5.1}$$

Additionally, MLE requires assumptions about the measurement uncertainty in the inputs $\boldsymbol{\varepsilon}_{\mathbf{x}}$, outputs $\boldsymbol{\varepsilon}_{\mathbf{y}}$ and the model prediction error $\boldsymbol{\varepsilon}_{\mathcal{M}}$ in order to estimate the likelihood function. Classical methods for MLE assume that the observed pairs do not have uncertainty in the inputs. The equation 5.2 describes the deviation between model and observations $\boldsymbol{\varepsilon}$ and it is obtained by re-arranging the modeling and measuring processes shown in figure 5.1.

$$\begin{aligned} \boldsymbol{\varepsilon}_i(\boldsymbol{\theta}) &= \tilde{\mathbf{y}}_i - \mathcal{M}(\tilde{\mathbf{x}}_i, \boldsymbol{\theta}) = \boldsymbol{\varepsilon}_{\mathcal{M}i} + \boldsymbol{\varepsilon}_{\mathbf{y}i} \\ \mathcal{L}(\tilde{\mathbf{y}}_i, \tilde{\mathbf{x}}_i|\boldsymbol{\theta}) &= f(\tilde{\mathbf{y}}_i|\tilde{\mathbf{x}}_i, \boldsymbol{\theta}) = f(\tilde{\mathbf{y}}_i - \mathcal{M}(\tilde{\mathbf{x}}_i, \boldsymbol{\theta})) = f(\boldsymbol{\varepsilon}_i(\boldsymbol{\theta})) \end{aligned} \tag{5.2}$$

MLE is equivalent to the Least Squared Errors (LSE) method when $f(\boldsymbol{\varepsilon}_{\mathcal{I}}(\boldsymbol{\theta}))$ is assumed normal and with the same variance for each observation pair. MLE is equivalent to the Weighted Least Squared Errors (WLSE) method when the $f(\boldsymbol{\varepsilon}_{\mathcal{I}}(\boldsymbol{\theta}))$ is assumed to be a multivariate normal. This equivalence can be proven using the definition of the multivariate normal PDF, see [175] for details. MLE is a more general approach that can be used to describe calibration problems that contain non-normal measurement errors, input measurement uncertainty, model uncertainty, among others.

[175] Omlin et al. 1999

Least squared errors (LSE)

LSE method for calibration consists in finding the parameters that minimize the Residual Sum of Squares (RSS) of the model. LSE assumes that the model calibration will make the deviations of the model follow a normal distribution $\boldsymbol{\varepsilon}_{\mathcal{I}}(\boldsymbol{\theta}) \sim \mathcal{N}(0, \sigma)$. For few problems the LSE calibration can be solved analytically while for most problems it can be solved numerically. Once the parameters have been calibrated a detail description of the distribution of the model deviations $\boldsymbol{\varepsilon}(\hat{\boldsymbol{\theta}})$ is required in order to verify the assumption of no bias and normality.

$$\begin{aligned} RSS(\boldsymbol{\theta}) &= ||\tilde{\mathbf{y}}_{\mathcal{I}} - \mathcal{M}(\tilde{\mathbf{x}}_{\mathcal{I}}, \boldsymbol{\theta})||^2 = \boldsymbol{\varepsilon}_{\mathcal{I}}(\boldsymbol{\theta})^T \boldsymbol{\varepsilon}_{\mathcal{I}}(\boldsymbol{\theta}) \\ \hat{\boldsymbol{\theta}} &= \arg\min_{\boldsymbol{\theta}} RSS(\boldsymbol{\theta}) \end{aligned} \tag{5.3}$$

Weighted least squared errors (WLSE)

WLSE consist in minimizing the Weighted Sum of Squares (WSS), which considers the variance in each measured output. In practice, WLSE assumes that the uncertainty in the output measurement $\boldsymbol{\varepsilon}_{\mathbf{y}\mathcal{I}}(\boldsymbol{\theta}) \sim \mathcal{N}(0, \mathbb{C}_{\tilde{\mathbf{y}}_{\mathcal{I}}})$ follows a multi-dimensional normal distribution, see equation 5.4. This assumption is very general and can represent cases in which each observation has a different variance but are independent, or cases where there is a correlation in the measurement errors of different observations. The covariance $\mathbb{C}_{\tilde{\mathbf{y}}_{\mathcal{I}}}$ can be estimated when the observed pairs are obtained after binning the raw data. This is a common practice in wind energy. In WLSE the model deviations are weighted by the variance in the output measurements.

$$\begin{aligned} WSS(\boldsymbol{\theta}) &= \boldsymbol{\varepsilon}_{\mathcal{I}}(\boldsymbol{\theta})^T \, \mathbb{C}^{-1}_{\tilde{\mathbf{y}}_{\mathcal{I}}} \, \boldsymbol{\varepsilon}_{\mathcal{I}}(\boldsymbol{\theta}) \\ \hat{\boldsymbol{\theta}} &= \arg\min_{\boldsymbol{\theta}} WSS(\boldsymbol{\theta}) \end{aligned} \tag{5.4}$$

5.1.2 Bayesian calibration

Bayesian calibration consists in considering the *prior* knowledge about the parameters as part of the information available to calibrate the model. Here the measurement pairs are considered sources of information or evidence, from which the *prior* knowledge about the parameters can be updated into the *posterior*[1]. The basic problem in Bayesian calibration is summarized in the Bayes theorem, see equation 5.5. In this equation the likelihood function $\mathcal{L}(\tilde{\mathbf{x}}_{\mathcal{I}}, \tilde{\mathbf{y}}_{\mathcal{I}}|\boldsymbol{\theta})$ is the same likelihood function used in MLE, and it gives a measure of how well a set of parameters agree with the observations; the proportional constant that makes equation 5.5 an equality is the normalization constant[2].

[1] In Bayesian statistics the knowledge is characterize by a PDF; therefore narrower distributions are assigned to parameters with less uncertainty.

[2] The normalization constant makes the posterior a PDF i.e. a PDF has unitary integration over all its domain.

$$f_{\text{post}}(\boldsymbol{\theta}|\tilde{\mathbf{x}}_{\mathcal{I}}, \tilde{\mathbf{y}}_{\mathcal{I}}) \propto \mathcal{L}(\tilde{\mathbf{x}}_{\mathcal{I}}, \tilde{\mathbf{y}}_{\mathcal{I}}|\boldsymbol{\theta}) \, f_{\text{prior}}(\boldsymbol{\theta}) \tag{5.5}$$

Maximum a Posteriori (MAP)

Maximum a Posteriori (MAP) calibration method consists in obtaining the set of parameters that maximizes the posterior distribution after a Bayesian update, see equation 5.6.

$$\hat{\boldsymbol{\theta}} = \arg\max_{\boldsymbol{\theta}} \; f_{\text{post}}(\boldsymbol{\theta}|\tilde{\mathbf{x}}_{\mathcal{I}}, \tilde{\mathbf{y}}_{\mathcal{I}}) \tag{5.6}$$

Special case - Calibration with input uncertainty

For some cases it is necessary to build a likelihood function that captures the impact of the different uncertainties in the calibration process. The input uncertainty is characterized by the measurement uncertainty model, $\boldsymbol{\varepsilon}_{\mathbf{x}} \sim f(\mathbf{x}|\tilde{\mathbf{x}})$. The output measurement uncertainty has a similar structure, $\boldsymbol{\varepsilon}_{\mathbf{y}} \sim f(\mathbf{y}|\tilde{\mathbf{y}})$, while the model inadequacy is described as $f(\mathbf{y}|\mathbf{x}, \boldsymbol{\theta})$. The general likelihood function can be seen in equation 5.7 and it consists in marginalizing the effect of the input uncertainty [16]; for this reason this methodology is also known as expected likelihood approach [176]. This likelihood function can be used in MLE or Bayesian calibration techniques.

[16] Huard et al. 2006

[176] Kavetski et al. 2002

$$\begin{aligned}
\mathcal{L}(\tilde{\mathbf{x}}_i, \tilde{\mathbf{y}}_i|\boldsymbol{\theta}) &= \mathcal{L}(\tilde{\mathbf{x}}_i)\, \mathcal{L}(\tilde{\mathbf{y}}_i|\tilde{\mathbf{x}}_i, \boldsymbol{\theta}) \\
&= \int_{\Omega_{\mathbf{x}}} \mathcal{L}(\tilde{\mathbf{x}}_i|\mathbf{x})\, \mathcal{L}(\tilde{\mathbf{y}}_i|\mathbf{x}, \boldsymbol{\theta})\, f(\mathbf{x})\, d\mathbf{x} \\
&= \int_{\Omega_{\mathbf{x}}} f(\tilde{\mathbf{x}}_i|\mathbf{x})\, f(\tilde{\mathbf{y}}_i|\mathcal{M}(\mathbf{x}, \boldsymbol{\theta}))\, f(\mathbf{x})\, d\mathbf{x}
\end{aligned} \tag{5.7}$$

Note that the calibration process requires a prior distribution of the true inputs $f(\mathbf{x})$; and a model inadequacy and input uncertainty propagation likelihood, $f(\mathbf{y}|\mathbf{x}, \boldsymbol{\theta}, \mathcal{M})$. If the model is linearized and the input uncertainties are assumed distributed multivariate normal (or even a linear combination of normals) then equation 5.7 has an analytical closed form, see [16] for an example. If this is not the case then numerical integration using sampling techniques is required. The impact of disregarding input uncertainty in linear model calibration consists in introducing a bias in the estimated parameters [16].

5.1.3 Parameter uncertainty estimation

The last step of the model calibration process is the estimation of the uncertainty in the calibrated parameters. The parameter uncertainty is the result of the uncertainty in the observations. This uncertainty represents the fact that the calibrated parameters are not perfectly known. This section presents different approaches to estimate this uncertainty.

Taylor expansion

Parameter uncertainty estimation can be obtained when it is acceptable to linearize the model and to approximate the uncertainty in the param-

eter estimator with a multi-variate normal distribution with a covariance $\mathbb{C}_{\hat{\boldsymbol{\theta}}}$. A Taylor series expansions of the model response for the parameters is build around the expected parameters $\hat{\boldsymbol{\theta}}$, see equation 5.8. Where $\mathbb{J}_{\hat{\boldsymbol{\theta}}}$ is the Jacobian of the model with respect the parameters; i.e. the local sensitivity of the model to the parameters evaluated at the expected parameters $\hat{\boldsymbol{\theta}}$.

$$\mathcal{M}(\tilde{\mathbf{x}}, \boldsymbol{\theta}) \approx \mathcal{M}(\tilde{\mathbf{x}}, \hat{\boldsymbol{\theta}}) + \mathbb{J}_{\hat{\boldsymbol{\theta}}} \left[\boldsymbol{\theta} - \hat{\boldsymbol{\theta}}\right] \tag{5.8}$$

The WSS can be used to build an unbiased estimator for the variance of $\boldsymbol{\varepsilon}(\hat{\boldsymbol{\theta}})$. Finally, the parameter uncertainty is obtained as a normal distribution if the number of observations in the dataset $N_{\mathcal{I}}$ is larger than the number of parameters to estimate N_p.

$$\begin{aligned} f(\boldsymbol{\theta}) &= \mathcal{N}(\hat{\boldsymbol{\theta}}, \mathbb{C}_{\hat{\boldsymbol{\theta}}}) \\ \mathbb{C}_{\hat{\boldsymbol{\theta}}} &= \frac{WSS}{N_{\mathcal{I}} - N_p} \left(\mathbb{J}_{\hat{\boldsymbol{\theta}}}^T \, \mathbb{C}_{\tilde{\mathbf{y}}} \, \mathbb{J}_{\hat{\boldsymbol{\theta}}}\right)^{-1} \end{aligned} \tag{5.9}$$

From this distribution then confidence intervals and other types of statistics can be computed. The effect of the uncertainty in the parameters to the outputs of the model is obtained as the propagation of the parameter uncertainty:

$$\mathbb{C}_{\mathbf{y}} = \mathbb{J}_{\hat{\boldsymbol{\theta}}} \, \mathbb{C}_{\hat{\boldsymbol{\theta}}} \, \mathbb{J}_{\hat{\boldsymbol{\theta}}}^T \tag{5.10}$$

Two main limitations exist in this approach: the assumption of normally distributed errors and the assumption of null input uncertainty. Extensions exist that address these two issues: if the input uncertainty is considered then the problem of parameter estimation can be extended.

Bootstrap method

Bootstrap method uses the measurements to calculate the joint distribution of model parameters by generating multiple synthetic samples from the calibration dataset. The method assumes a distribution of the model error but it does not assume any form of distribution of the parameters [177]. The procedure to generate the fictitious sample consist in randomly picking (with replacement) individual measured pairs and adding a random realization of the measurement error. A parameter estimation is performed for each of the synthetic datasets. As a result the bootstrap technique produces a distribution of parameter estimators. This technique can be used to estimate parameter uncertainty without assuming their final distributions and due to its simplicity is easy to implement. The main limitation of this method is the requirement for large number of observations in the calibration dataset in order to represent accurately the model in a subset.

[177] Efron. 1979

Bayesian calibration

The posterior distribution obtained in Bayesian calibration represents the uncertainty in the calibration. This property is one of the main advantages of Bayesian calibration.

$$f(\boldsymbol{\theta}) = f_{\text{post}}(\boldsymbol{\theta}|\check{\mathbf{x}}_{\mathcal{I}}, \tilde{\mathbf{y}}_{\mathcal{I}}) \tag{5.11}$$

5.1.4 Example: Analytical model

This example illustrates the differences between the three main calibration methods: LSE, WLSE and Bayesian calibration. Since the model is analytical, the results of the calibration can be verified with the known true parameters. This example assumes that there is no model uncertainty.

The simple analytical model is given by the equation:

$$y = 10\, e^{-a\, x}\, \cos(0.5\, x) \tag{5.12}$$

The true parameter is $a = 0.2$, while the true input distribution used to generate the observations is a Weibull distribution:

$$f(x) = \mathcal{W}(A = 2, k = 10) \tag{5.13}$$

The measurement uncertainties are generated using a normal distribution for the input and the output. The observed pairs are obtained by sampling the true inputs, evaluating the model with the true inputs and adding measurement errors. Two different cases are generated one with low input uncertainty and one with large input uncertainty.

$$\begin{aligned} f(\tilde{x}|x) &= \mathcal{N}(\mu = x, \sigma_x) = x + \mathcal{N}(\mu = 0, \sigma_x) \\ f(\tilde{y}|y) &= \mathcal{N}(\mu = y, \sigma_y) = y + \mathcal{N}(\mu = 0, \sigma_y) \end{aligned} \tag{5.14}$$

Note that the WLSE method does not use the raw observations but it uses the bin averaged observation and the corresponding standard deviation of the error (SEM) as the observation uncertainty.

For the Bayesian calibration method the prior distribution is assumed to be uniform, this means that the posterior only depends on the likelihood function. The likelihood function including input uncertainty in equation 5.7 is approximated using a MC sample of the true input $\mathbf{x}_j \sim f(x)$. This approximation is expressed in equation 5.15, where N is the MC sample size.

$$\begin{aligned} \mathcal{L}(\tilde{\mathbf{x}}_i, \tilde{\mathbf{y}}_i|\boldsymbol{\theta}) &= \int_{\Omega_{\mathbf{x}}} f(\tilde{\mathbf{x}}_i|\mathbf{x})\, f(\tilde{\mathbf{y}}_i|\mathcal{M}(\mathbf{x}, \boldsymbol{\theta}))\, f(\mathbf{x})\, d\mathbf{x} \\ &\approx \frac{1}{N} \sum_{j=1}^{N} f(\tilde{\mathbf{x}}_i - \mathbf{x}_j)\, f(\tilde{\mathbf{y}}_i - \mathcal{M}(\mathbf{x}_j, \boldsymbol{\theta})) \end{aligned} \tag{5.15}$$

Figure 5.2 presents the results when there is low input measurement uncertainty. This is given by a standard deviation of the measurement error of $\sigma_x = 0.5$. In this case the measurement uncertainty in the output

is given by $\sigma_y = 2.0$. Two main conclusions can be made of this case: the bin averaged observations are a good representation of the true model and all the calibration methods show very similar distribution of the parameter. All the calibration methods agree because the assumptions of normally distributed model deviations in LSE and WLSE are fulfilled by having low input measurement uncertainty.

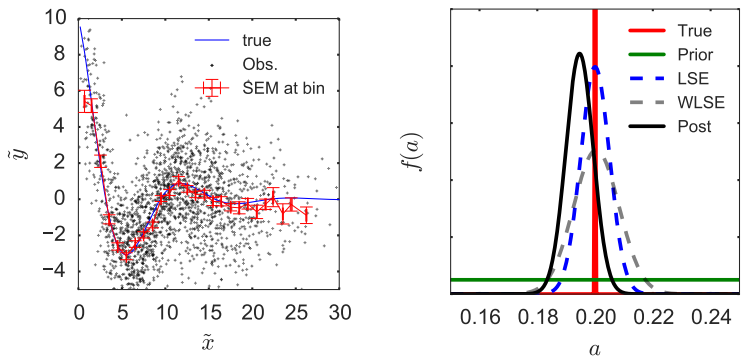

Figure 5.2: Model calibration example with low input uncertainty case (left) Observed pairs, bin averaged observed pairs with their corresponding standard error of the mean (SEM) and true model. (right) Model calibration results.

Figure 5.3 presents the results when there is large input measurement uncertainty: $\sigma_x = 2.0$ and a low measurement uncertainty in the output: $\sigma_y = 2.0$. In this case the bin averaged observations are not a good representation of the true model. Furthermore, there is a bias in the LSE and WLSE calibration methods. This is the consequence of having large input measurement uncertainty. As a consequence of the assumptions of LSE and WLSE, the uncertainty in the measured output is overestimated; this produces larger uncertainty in the parameter than in the case of Bayesian calibration.

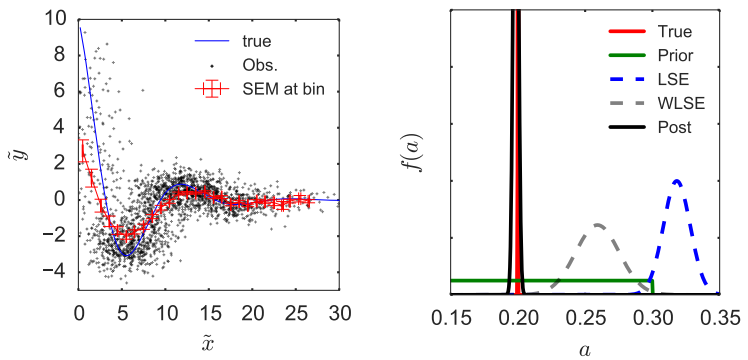

Figure 5.3: Model calibration example with large input uncertainty case (left) Observed pairs, bin averaged observed pairs with their corresponding standard error of the mean (SEM) and true model. (right) Model calibration results.

When to use which model calibration method?

Bayesian calibration is a very powerful method, but it is more computationally expensive than other calibration techniques. For this reason Bayesian calibration should only be used when all the other methods give inconsistent results. One of the main advantages of the Bayesian calibration is the fact that it can handle

dataset with reduced number of observed pairs. It also has the advantage of including the prior information from the experts. This information can speed up the computation by reducing the effective parameter space in which the calibration will search for the parameter. Maximum likelihood estimation is related uses the same information as the Bayesian calibration, the likelihood function and therefore it can be used on the same cases.

Simplified versions of the MLE such as WLSE should be used only when there is evidence that the measurement uncertainty in the inputs is reduced.

5.2 Model Validation

Model validation is a term that has multiple interpretations in the scientific community. When a model is compared against measurements it is not enough to show a plot where the model prediction passes through the error bars (or confidence intervals) of the observations. In this thesis, model validation is defined as the process that builds a statistical model to predict the model prediction error at a given input vector. Most scientific models are only valid under specific conditions, this means that the model prediction error depends on the input variables. In order to make clear this assumption, the notation for model error changes to $\boldsymbol{\varepsilon}_{\mathcal{M}} = \zeta(\mathbf{x})$. Using this notation, one can express the model prediction error for a given observed pair $(\tilde{\mathbf{x}}_i, \tilde{\mathbf{y}}_i)$ in the validation dataset as:

$$\zeta(\tilde{\mathbf{x}}_i) = \tilde{\mathbf{y}}_i + \boldsymbol{\varepsilon}_{\mathbf{y}} - \mathcal{M}(\tilde{\mathbf{x}}_i + \boldsymbol{\varepsilon}_{\mathbf{x}}, \boldsymbol{\theta}) \tag{5.16}$$

Equation 5.16 expresses the model prediction error for a single observation. The main problem with this equation is the fact that the observation errors are unknown and therefore one can not fully compute the model prediction error as a deterministic problem.

Model validation as an uncertainty propagation problem

One way of understanding the construction of the statistical model of the prediction error consists in recasting the validation problem into a propagation of uncertainty problem. One can consider the model prediction error as a model that receives as inputs the measurement/observation errors for the inputs and outputs as well as the model parameters, see figure 5.4. This means that if the experimental/measurement uncertainties are well understood in terms of having a model that predicts their observation errors and if the parameters of the model have been previously calibrated, then the PDF of the prediction error can be obtained by propagating the uncertainties through the model chain.

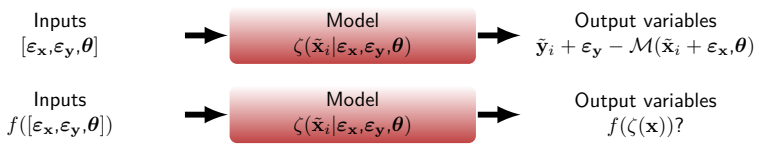

Figure 5.4: Model validation as a propagation of uncertainty problem.

Usually a calibration or a validation dataset includes an estimation of the measurement errors for inputs and outputs. These estimations are expressed as a measurement uncertainty model such as:

$$f(\varepsilon_{\mathbf{x}}) = \mathcal{N}(\mathbf{0}, \mathbb{C}_{\mathbf{x}}) \qquad f(\varepsilon_{\mathbf{y}}) = \mathcal{N}(\mathbf{0}, \mathbb{C}_{\mathbf{y}}) \tag{5.17}$$

Simplified model validation

In general the uncertainties in inputs and parameter are not zero. This produces a combination of the output measurement uncertainty and the propagation of input/parameter uncertainties through the model. If the measurement uncertainties are central, normally distributed, a common approach is to assume that the measurement uncertainty in the output and the propagation of parameter and input uncertainties are uncorrelated. This assumptions implies that the expected model prediction error at the observed input can be estimated as:

$$\mathbb{E}(\zeta(\tilde{\mathbf{x}})) = \tilde{\mathbf{y}} - \mathbb{E}(\mathcal{M}(\tilde{\mathbf{x}} + \varepsilon_{\mathbf{x}}, \boldsymbol{\theta})) \tag{5.18}$$

Simultaneous Validation and Calibration

Simultaneous validation and calibration is often an intractable problem because deviations from the true value of a parameter can be compensated by the model inadequacy term $\zeta(\mathbf{x})$. This means that the parameters and model inadequacy are highly correlated. To be able to solve this problem, Bayesian inference and physical description of the prior distributions for both model parameters and model inadequacy are necessary. This framework is usually referred to as the Kennedy-O'Hagan approach [178][25][179].

In machine learning context every dataset is divided into three groups: a model calibration, a model validation and an evaluation datasets. Some experts propose to use 50% of the data as training (calibration) dataset, 25% of the data is used for validation, and the last 25% of the data is used for final evaluation. The last step consists in checking that the model inadequacy is correctly predicted; this step is a verification of the validation [153]. The process of splitting the data can be done in an aleatory process and repeated several times. This will enable to test that the statistical model for the prediction error is properly estimated.

[178] Kennedy et al. 2001
[25] Higdon et al. 2004
[153] Friedman et al. 2001

5.2.1 Validation regions

The validation of a model is an ongoing process in which several validation cases will be performed for different validation datasets. As a result the

validation process should build a validation region. Its main purpose is to understand the regions where the model can be used with confidence, the regions where the model is not able to capture the physical behavior and the regions where there is evidence to predict how well or badly the model will perform.

[19] Oberkampf et al. 2004

The validation region can be used as a predictive model for the model prediction error at new non-validated input points [19]. The definition of a validation region consists in setting a maximum tolerance values for the model prediction error and for the variance in the prediction of model prediction error[3]. If the number of validation datasets in a region is limited or zero then there is no evidence that will inform us on whether the model could be used there. A model that is used outside the validated region (or in general far away from a validation point) will be penalized as there is more uncertainty about how much model inadequacy should be expected at this application point. See figure 5.5 for a visual example of the process.

[3] A model that has high bias in the model prediction error is clearly not capturing the physics of the process

There are many advantages of knowing the current state of the validation region of a model: a validation region will clearly state the regions in which the users can use the model with reasonably levels of model uncertainty and obtain estimations of these uncertainties. Additionally, a validation region is a planning tool for the design of new experiments that may challenge the models. There is value in increasing the size of the validation regions as it will extend the range of application of the model. Note that the validation region will be different for different models even if the same validation datasets are used, due to the maximum tolerance to the mean model inadequacy.

5.2.2 Example: Validation region for a wake model

Figure 5.5 presents the validation region for NOJ wake model based on Horns Rev 1. This validation region is a generalization of the model prediction error obtained from a validation campaign done using the operational data from two offshore wind plants [3]. The generalization consists in translating the wind direction into a measure of the averaged spacing and number of turbines aligned. This will help to have an estimation of the model prediction error on an different wind plant with an arbitrary layout.

[3] Murcia et al. 2016

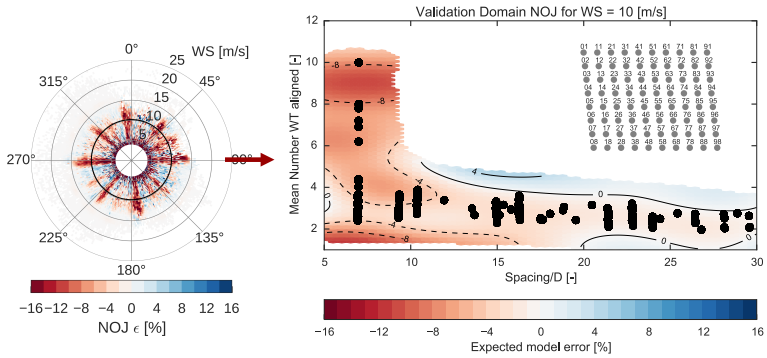

Figure 5.5: An example of model validation region.

This chapter has given an overview of the different methods to do model calibration and model validation. Several examples of model calibration can be found in `https://github.com/jp5000/Examples_PhD_thesis` [DOI:10.5281/zenodo.204786]. The main ideas presented in this chapter are:

- Traditional calibration techniques such as LSE and WLSE failed when there are large uncertainties in the inputs. Special treatment of such uncertainties needs to be considered using alternative definitions of the likelihood function.
- A calibration method that takes into account the uncertainty in the input uncertainties can be implemented for calibration of simple wake models based on SCADA data from multiple offshore wind plant. This is the main objective of the article [5]. This article is available in chapter D.
- Model validation requires to consider the measurements uncertainties in the observations. This chapter introduced a methodology for model validation based on uncertainty propagation. This methodology is used in the articles [3] and [2].

[5] Murcia et al. 2016

[3] Murcia et al. 2016

[2] Murcia et al. 2015

Chapter 6

Conclusions and Future Work

The main focus of this PhD project was the development of a framework to validate models in the wind plant model chain. The classical procedure for estimation of model validation assumes that the uncertainty in the input variables, such as observed wind resources and wake losses, can be propagated through a linearized version of the model chain. This procedure has been adapted to include a more realistic propagation of uncertainty and to include the effect of model prediction errors with a distribution that depends on the input conditions.

Wind resources

Several extensions to the traditional wind rose used to describe the PDF of the wind resources on a site have been studied. Time series as used in the wake model validation articles C and D, continuous conditional distributions as used in the wake model calibration article E and mixture of multivariate normal distributions can be used to describe the joint distributions for wind speed and wind direction without the traditional 30°binning. To include the atmospheric turbulence intensity the normal turbulence model proposed in [30] can be used. A shear distribution conditioned on wind speed and turbulence intensity should be used such as the one proposed by [151]. These two extensions were explored in the article about efficient propagation of uncertainty through an aeroelastic model, article B. From these studies it can be concluded that:

[30] IEC 61400-1. 2005

[151] Dimitrov et al. 2015

- A sequential conditional dependency between the atmospheric variables is a natural way to represent the variability that characterize the wind resources.
- Rosenblatt transformation and other iso-probabilistic transformations can be used to generate samples of arbitrary sizes and are a key element of the methods for efficient propagation of uncertainty.
- In the case when the number of uncertain variables is large ($\sim$100) advanced sampling techniques can be used to obtain a sample; these methods also required a sequential conditional distribution.

Uncertainty in the wind turbine model

One of the main contribution of this thesis is the methodology to capture the uncertainty in the wind turbine model presented in article B. In this article a surrogate of the aeroelastic model of wind turbine is able to predict the distribution of power, thrust coefficient, damage equivalent fatigue loads and extreme loads as a function of several turbulent inflow parameters. The proposed methodology is also able to capture the uncertainty due to different realizations of the turbulent structures in all the outputs of the turbine. This methodology is based on defining a conditional distribution for each of the outputs as a function of the atmospheric turbulent inflow variables. From this study it can be concluded that:

- A surrogate of an aeroelastic wind turbine model based on a conditional distribution for each of the outputs as a function of the atmospheric turbulent inflow variables is an efficient method to capture the turbine response and its corresponding uncertainties.
- The proposed type of surrogates can be used in two-level propagation of uncertainty model chains in order to estimate the uncertainty in AEP and L_{eq}.

Wake model validation

Wake model validation has been implemented using SCADA data from Horns Rev 1 and Nysted offshore wind plants for several of wake models in articles [3] and [2]. The validation methodology takes into account the uncertainty in the undisturbed inflow conditions and the uncertainty in the mean power curve of the turbines. The main objective of these validation campaigns was to understand the distribution of the model prediction error as a function of the inflow variables from which a generalized stochastic model to predict the wake model prediction error can be built. From these studies it can be concluded that:

[3] Murcia et al. 2016
[2] Murcia et al. 2015

- Wake model validation requires to consider the measurement/observation uncertainty in the undisturbed inflow conditions (inputs) and power production (outputs). If these uncertainties are not considered the model prediction error will be overestimated.
- The uncertainty in the AEP prediction is a combination of the distribution of the model prediction error as a function of the inflow conditions, the power curve uncertainty and the probability of the inflow conditions (the PDF of the wind resources).

Wake model calibration

Model calibration of a simple engineering wake model using the SCADA data of four large offshore wind plants is presented in article [5]. This article shows that calibration techniques that consider the uncertainty in the inputs can be implemented to avoid the introduction of a bias in the calibration. Similar calibrations have been performed in the past

[5] Murcia et al. 2016

[109] without considering uncertainty in the undisturbed inflow conditions. The uncertainty in the parameter can be estimated and used to estimate the uncertainty in AEP. From this study it can be concluded that:

[109] Cleve et al. 2009

- Wake model calibration based on least squared errors on individual flowcases does not include the uncertainty in the inflow conditions and therefore, it produces a bias in the estimated parameter.
- Maximum likelihood calibration can be used to include the effect of the uncertainty in the input variables.
- The maximum likelihood parameters obtained from each individual flowcase show a clear structure with respect to the inflow conditions which reveals the existence of a structural model error due to lacks of physics. This fact agrees with the previous wake validation studies.

6.1 Future Work

There are mainly two subjects which have not been investigated in this thesis but that are reasonable next steps of the proposed implementation of the UQ framework:

- A full propagation of uncertainty to predict the uncertainty in the LCoE of an onshore wind plant in the planning stages requires to consider a large number of uncertain variables: the uncertainty in the long term wind resources, the uncertainty in the flow model (including spatial decorrelation), the uncertainty in the wind turbine response operating inside the plant and the uncertainty in the wake model. Efficient propagation methods as the ones presented in this thesis, are necessary to be able to consider these large amount of uncertainties.
- The concept of validation region has been introduced to the field of wake models. This concept promises to be an useful way to communicate the users of a model that the assumptions of the model only hold on a certain subdomain of the input variables space. The uncertainty of the model, represented by the statistical model of the model prediction error, depends on the input variables and is different for every model. This means that, using this information the user could identify the input conditions that require high-fidelity modeling in order to reduce the uncertainty in the final variables such as AEP or LCoE.
- The model validation regions are constructed based on SCADA data from multiple sites. This means that if there is no validation cases for certain conditions, then the model uncertainty predicted by the validation region would be high. This case will enable international agencies to prioritize experiments that fill the gaps of knowledge for the models.

Bibliography

[1] JP Murcia, PE Réthoré, A Natarajan, and JD Sørensen. "How many model evaluations are required to predict the aep of a wind power plant?" In: *Journal of Physics: Conference Series* 625.1 (2015), p. 012030. DOI: 10.1088/1742-6596/625/1/012030 (cit. on p. 7).

[2] JP Murcia, PE Réthoré, KS Hansen, A Natarajan, and JD Sørensen. "A new method to estimate the uncertainty of AEP of offshore wind power plants applied to Horns Rev 1". In: (2015), pp. 161–165 (cit. on pp. 7, 97, 100).

[3] JP Murcia, PE Réthoré, KS Hansen, A Natarajan, and JD Sørensen. "Improved validation of stationary wake models using uncertainty propagation". In: *Wind Energy* (2016), Submitted (cit. on pp. 7, 29, 53, 64, 96, 97, 100).

[4] JP Murcia, PE Réthoré, N Dimitrov, A Natarajan, JD Sørensen, P Graf, and T Kim. "Uncertainty propagation through an aeroelastic wind turbine model using polynomial surrogates". In: *Renewable Energy* (2016), Submitted (cit. on pp. 7, 28, 53, 85).

[5] JP Murcia, PE Réthoré, KS Hansen, OS Rathmann, A Natarajan, and JD Sørensen. "Wake model calibration based on SCADA data considering uncertainty in the inflow conditions". In: *Wind Energy Science* (2016), Submitted (cit. on pp. 7, 29, 97, 100).

[6] Y Wang, P Réthoré, M van der Laan, J Murcia Leon, Y Liu, and L Li. "Multi-fidelity wake modelling based on Co-Kriging method". In: *Journal of Physics: Conference Series*. Vol. 753. 3. IOP Publishing. 2016, p. 032065 (cit. on p. 8).

[7] MP Laan, NN Sørensen, PE Réthoré, J Mann, MC Kelly, N Troldborg, KS Hansen, and JP Murcia. "The k-ϵ-f_P model applied to wind farms". In: *Wind Energy* 18.12 (2015), pp. 2065–2084. DOI: 10.1002/we.1804 (cit. on pp. 8, 47).

[8] C Pavese, T Kim, and JP Murcia. "Design of a wind turbine swept blade through extensive load analysis". In: *Renewable Energy* 102 (2017), pp. 21–34 (cit. on p. 8).

[9] A Meyer, N Troldborg, N Sathe, A Angelou, A Vignaroli, and J Murcia. "Validation of a CFD model with a synchronised triple-lidar system in the wind turbine induction zone". In: *Wind Energy* (2016), Submitted (cit. on p. 8).

[10] EEA. *Trends and projections in Europe 2016 - Tracking progress towards Europe's climate and energy targets*. Tech. rep. European Energy Agency, 2016. eprint: http://www.eea.europa.eu/themes/climate/trends-and-projections-in-europe (cit. on p. 21).

[11] GWEC. *Global Wind Report - Annual Market Update 2015*. Tech. rep. 11. Global Wind Energy Council, 2016. eprint: http://www.gwec.net/wp-content/uploads/vip/GWEC-Global-Wind-2015-Report_April-2016_22_04.pdf (cit. on pp. 21, 31).

[12] Lazzard. *Levelized cost of energy analysis*. Tech. rep. 9.0. 2015. eprint: https://www.lazard.com/media/2390/lazards-levelized-cost-of-energy-analysis-90.pdf (cit. on p. 21).

[13] V Gass, F Strauss, J Schmidt, and E Schmid. "Assessing the effect of wind power uncertainty on profitability". In: *Renewable and Sustainable Energy Reviews* 15.6 (2011), pp. 2677–2683. DOI: 10.1016/j.rser.2011.01.024 (cit. on p. 21).

[14] PE Réthoré, P Fuglsang, GC Larsen, T Buhl, TJ Larsen, and HA Madsen. "TOPFARM: Multi-fidelity optimization of wind farms". In: *Wind Energy* (2013), n/a–n/a. DOI: 10.1002/we.1667 (cit. on pp. 22, 36, 45, 51).

[15] WL Oberkampf, SM DeLand, BM Rutherford, KV Diegert, and KF Alvin. "Error and uncertainty in modeling and simulation". In: *Reliability Engineering & System Safety* 75.3 (Mar. 2002), pp. 333–357. DOI: 10.1016/S0951-8320(01)00120-X (cit. on p. 23).

[16] D Huard and A Mailhot. "A Bayesian perspective on input uncertainty in model calibration. Application to hydrological model "abc"". In: *Water Resources Research* 42.7 (2006). DOI: 10.1029/2005WR004661 (cit. on pp. 24, 90).

[17] ISO and IEC. *98-3:2008. Guide to the expression of uncertainty in measurement (GUM)*. 2008 (cit. on pp. 25, 69).

[18] WL Oberkampf and CJ Roy. *Verification and validation in scientific computing*. Cambridge University Press, 2010. ISBN: 9780521113601 (cit. on p. 26).

[19] WL Oberkampf, TG Trucano, and C Hirsch. "Verification, validation, and predictive capability in computational engineering and physics". In: *Applied Mechanics Reviews* 57.5 (2004), p. 345. DOI: 10.1115/1.1767847 (cit. on pp. 26, 96).

[20] B Biller and S Ghosh. "Multivariate input processes". In: *Handbooks in Operations Research and Management Science* 13 (2006), pp. 123–153. DOI: 10.1016/S0927-0507(06)13005-4 (cit. on pp. 26, 55, 58, 62).

[21] JC Helton and FJ Davis. "Latin hypercube sampling and the propagation of uncertainty in analyses of complex systems". In: *Reliability Engineering and System Safety* 81.1 (2003), pp. 23–69. DOI: 10.1016/S0951-8320(03)00058-9 (cit. on p. 26).

[22] A Saltelli, K Chan, EM Scott, et al. *Sensitivity analysis*. Vol. 134. Wiley New York, 2000. ISBN: 9780471998921 (cit. on p. 26).

[23] A Tarantola. *Inverse Problem Theory and Methods for Model Parameter Estimation*. Philadelphia: SIAM, 2005. ISBN: 0898715725 (cit. on p. 27).

[24] CJ Roy and WL Oberkampf. "A comprehensive framework for verification, validation, and uncertainty quantification in scientific computing". In: *Computer Methods in Applied Mechanics and Engineering* 200.25-28 (2011), pp. 2131–2144. DOI: 10.1016/j.cma.2011.03.016 (cit. on p. 27).

[25] D Higdon, M Kennedy, JC Cavendish, JA Cafeo, and RD Ryne. "Combining field data and computer simulations for calibration and prediction". In: *SIAM Journal on Scientific Computing* 26.2 (2004), pp. 448–466. DOI: 10.1137/S1064827503426693 (cit. on pp. 27, 95).

[26] B Peherstorfer, K Willcox, and M Gunzburger. "Survey of multifidelity methods in uncertainty propagation, inference, and optimization". In: (2016). eprint: http://kiwi.mit.edu/papers/multi-fidelity-survey-peherstorfer-willcox-gunzburger.pdf (cit. on pp. 27, 68, 78).

[27] DONG. *Official Site*. http://www.dongenergy.com/en/media/newsroom/news/articles/dong-energy-wins-tender-for-dutch-offshore-wind-farms. Accessed: 2/12/2016. 2016 (cit. on p. 31).

[28] Vattenfall. *Official Site*. https://corporate.vattenfall.com/press-and-media/press-releases/2016/vattenfall-wins-tender-to-build-the-largest-wind-farm-in-the-nordics/. Accessed: 2/12/2016. 2016 (cit. on p. 31).

[29] MA Miner et al. "Cumulative damage in fatigue". In: *Journal of applied mechanics* 12.3 (1945), pp. 159–164 (cit. on p. 34).

[30] IEC 61400-1. *Wind turbines-part 1: Design requirements*. Tech. rep. Switzerland: International Electrotechnical Commission., 2005 (cit. on pp. 35, 48, 51, 60, 74, 99).

[31] LJ Fingersh, MM Hand, and AS Laxson. *Wind turbine design cost and scaling model*. Tech. rep. National Renewable Energy Laboratory Golden, CO, 2006. eprint: http://www.nrel.gov/docs/fy07osti/40566.pdf (cit. on p. 36).

[32] KW Ayotte. "Computational modelling for wind energy assessment". In: *Journal of Wind Engineering and Industrial Aerodynamics* 96.10 (2008), pp. 1571–1590. DOI: 10.1016/j.jweia.2008.02.002 (cit. on p. 36).

[33] L Landberg, L Myllerup, O Rathmann, EL Petersen, BH Jørgensen, J Badger, and NG Mortensen. "Wind resource estimation—an overview". In: *Wind Energy* 6.3 (2003), pp. 261–271. DOI: 10.1002/we.94 (cit. on p. 36).

[34] J Sanz Rodrigo, RA Chávez Arroyo, P Moriarty, M Churchfield, B Kosović, PE Réthoré, KS Hansen, A Hahmann, JD Mirocha, and D Rife. "Mesoscale to microscale wind farm flow modeling and evaluation". In: *Wiley Interdisciplinary Reviews: Energy and Environment* (2016). ISSN: 2041-840X. DOI: 10.1002/wene.214 (cit. on pp. 36, 38–40).

[35] I Troen and EL Petersen. *European wind atlas*. Vol. 1. 1989. ISBN: 87-550-1482-8(1989)656p (cit. on pp. 36, 37).

[36] I Troen. "A high resolution spectral model for flow in complex terrain". In: *9th symposium on turbulence and diffusion*. 1990, pp. 417–420 (cit. on p. 37).

[37] F Dunkerley, J Moreno, T Mikkelsen, and I Griffiths. "LINCOM wind flow model: Application to complex terrain with thermal stratification". In: *Physics and Chemistry of the Earth, Part B: Hydrology, Oceans and Atmosphere* 26.10 (2001), pp. 839–842. DOI: 10.1016/S1464-1909(01)00095-8 (cit. on p. 37).

[38] P Taylor, J Walmsley, and J Salmon. "A simple model of neutrally stratified boundary-layer flow over real terrain incorporating wavenumber-dependent scaling". In: *Boundary-Layer Meteorology* 26.2 (1983), pp. 169–189. DOI: 10.1007/BF00121541 (cit. on p. 37).

[39] NN Sørensen. "General purpose flow solver applied to flow over hills". PhD thesis. Technical University of DenmarkDanmarks Tekniske Universitet, Risø National Laboratory for Sustainable EnergyRisø Nationallaboratoriet for Bæredygtig Energi, Wind Energy DivisionAfdelingen for Vindenergi, Aeroelastic DesignAeroelastisk Design, 1995 (cit. on p. 37).

[40] KW Ayotte and PA Taylor. "A mixed spectral finite-difference 3D model of neutral planetary boundary-layer flow over topography". In: *Journal of the atmospheric sciences* 52.20 (1995), pp. 3523–3538. DOI: 10.1175/1520-0469(1995)052<3523:AMSFDM>2.0.CO;2 (cit. on p. 37).

[41] M Balogh, A Parente, and C Benocci. "RANS simulation of ABL flow over complex terrains applying an enhanced k-ε model and wall function formulation. Implementation and comparison for Fluent and OpenFOAM". In: *Journal of wind engineering and industrial aerodynamics* 104 (2012), pp. 360–368. DOI: 10.1016/j.jweia.2012.02.023 (cit. on p. 37).

[42] N Wood. "Wind flow over complex terrain: a historical perspective and the prospect for large-eddy modelling". In: *Boundary-Layer Meteorology* 96.1-2 (2000), pp. 11–32. DOI: 10.1023/A:1002017732694 (cit. on p. 38).

[43] A Clerc, M Anderson, and P Stuart. "A systematic method for quantifying wind flow modelling uncertainty in wind resource assessment." In: *Journal of Wind Engineering and Industrial Aerodynamics* 111 (2012), p. 85. DOI: 10.1016/j.jweia.2012.08.006 (cit. on pp. 38, 39, 53).

[44] NG Mortensen, AJ Bowen, and I Antoniou. "Improving WAsP predictions in (too) complex terrain". In: *Proceedings of the 2006 European Wind Energy Conference and Exhibition, Athens*. Vol. 27. 2006 (cit. on p. 39).

[45] R Mickle, N Cook, A Hoff, N Jensen, J Salmon, P Taylor, G Tetzlaff, and H Teunissen. "The Askervein Hill Project: Vertical profiles of wind and turbulence". In: *Boundary-Layer Meteorology* 43.1-2 (1988), pp. 143–169. DOI: 10.1007/BF00153977 (cit. on p. 39).

[46] J Berg, J Mann, A Bechmann, M Courtney, and HE Jørgensen. "The Bolund Experiment, Part I: Flow over a steep, three-dimensional hill". In: *Boundary-layer meteorology* 141.2 (2011), pp. 219–243. DOI: 10.1007/s10546-011-9636-y (cit. on p. 39).

[47] R Chávez Arroyo, J Sanz Rodrigo, and P Gankarski. "Modelling of atmospheric boundary-layer flow in complex terrain with different forest parameterizations". In: *Journal of Physics: Conference Series*. Vol. 524. 1. IOP Publishing. 2014, p. 012119. DOI: 10.1088/1742-6596/524/1/012119 (cit. on p. 39).

[48] J Berg, A Bechmann, M Courtney, T Koblitz, and YV Hristov. "In the wake of Bolund: Benakanahalli - Stratification and complex terrain". In: (2012) (cit. on p. 39).

[49] A Bechmann, NN Sørensen, J Berg, J Mann, and PE Réthoré. "The Bolund experiment, part II: blind comparison of microscale flow models". In: *Boundary-Layer Meteorology* 141.2 (2011), pp. 245–271. DOI: 10.1007/s10546-011-9637-x (cit. on p. 39).

[50] T Koblitz, A Bechmann, J Berg, A Sogachev, N Sørensen, and PE Réthoré. "Atmospheric stability and complex terrain: comparing measurements and CFD". In: *Journal of Physics: Conference Series*. Vol. 555. 1. IOP Publishing. 2014, p. 012060. DOI: 10.1088/1742-6596/555/1/012060 (cit. on p. 39).

[51] J Sanz Rodrigo, P Gancarski, R Chávez Arroyo, P Moriarty, M Chuchfield, JW Naughton, KS Hansen, E Machefaux, T Koblitz, E Maguire, et al. "IEA-Task 31 WAKEBENCH: Towards a protocol for wind farm flow model evaluation. Part 1: Flow-over-terrain models". In: *Journal of Physics: Conference Series*. Vol. 524. 1. IOP Publishing. 2014, p. 012105. DOI: 10.1088/1742-6596/524/1/012105 (cit. on p. 39).

[52] G Svensson, A Holtslag, V Kumar, T Mauritsen, G Steeneveld, W Angevine, E Bazile, A Beljaars, E de Bruijn, A Cheng, et al. "Evaluation of the diurnal cycle in the atmospheric boundary layer over land as represented by a variety of single-column models: the second GABLS experiment". In: *Boundary-layer meteorology* 140.2 (2011), pp. 177–206. DOI: 10.1007/s10546-011-9611-7 (cit. on p. 39).

[53] B Sanderse, SP Van Der Pijl, and B Koren. "Review of computational fluid dynamics for wind turbine wake aerodynamics". In: *Wind Energy* 14 (2011), pp. 799–819. DOI: 10.1002/we.458 (cit. on p. 40).

[54] A Crespo, J Hernández, and ST Frandsen. "Survey of modelling methods for wind turbine wakes and wind farms". In: *Wind Energy* 2.1 (Jan. 1999), pp. 1–24. DOI: 10.1002/(SICI)1099-1824(199901/03)2:1<1::AID-WE16>3.3.CO;2-Z (cit. on p. 40).

[55] H Snel. "Review of aerodynamics for wind turbines". In: *Wind Energy* 6.3 (2003), pp. 203–211. DOI: 10.1002/we.97 (cit. on p. 40).

[56] JN Sørensen. "4 - Wind turbine wakes and wind farm aerodynamics". In: *Wind Energy Systems*. Ed. by JD Sørensen and JN Sørensen. Woodhead Publishing Series in Energy. Woodhead Publishing, 2011, 112–e131. ISBN: 978-1-84569-580-4. DOI: 10.1533/9780857090638.1.112 (cit. on p. 40).

[57] T Göçmen, P van der Laan, PE Réthoré, AP Diaz, GC Larsen, and S Ott. "Wind turbine wake models developed at the technical university of Denmark: A review". In: *Renewable and Sustainable Energy Reviews* 60 (2016), pp. 752–769. DOI: 10.1016/j.rser.2016.01.113 (cit. on p. 40).

[58] G Larsen, H Madsen, T Larsen, and N Troldborg. *Wake modeling and simulation*. Tech. rep. Risø-R-1653(EN). Roskilde, Denmark: Risø-DTU, 2008, p. 28. eprint: http://orbit.dtu.dk/files/3453997/risr-1653.pdf (cit. on p. 42).

[59] CB Hasager, PE Réthoré, LE Jensen, A Peña, and L Rasmussen. "Wind Farm Wake: The Horns Rev Photo Case". In: (2013). DOI: 10.3390/en6020696 (cit. on p. 42).

[60] S Frandsen. *Turbulence and turbulence-generated structural loading in wind turbine clusters*. Tech. rep. January. Roskilde, Denmark: Risø, 2007. eprint: http://orbit.dtu.dk/fedora/objects/orbit:79899/datastreams/file_269c3f19-0001-4e41-b754-b5b322a826cb/content (cit. on p. 43).

[61] AC Fitch, JB Olson, and JK Lundquist. "Parameterization of wind farms in climate models". In: *Journal of Climate* 26.17 (2013), pp. 6439–6458. DOI: 10.1175/JCLI-D-12-00376.1. (cit. on p. 44).

[62] P Volker, J Badger, AN Hahmann, and S Ott. "The Explicit Wake Parametrisation V1. 0: a wind farm parametrisation in the mesoscale model WRF". In: *Geoscientific Model Development* 8.11 (2015), pp. 3715–3731. DOI: 10.5194/gmd-8-3715-2015. (cit. on p. 44).

[63] NO Jensen. *A Note on Wind Generator Interaction*. Tech. rep. Roskilde, Denmark: Risø, 1983. eprint: http://orbit.dtu.dk/files/55857682/ris_m_2411.pdf (cit. on p. 44).

[64] ST Frandsen, RJ Barthelmie, O Rathmann, and SE Larsen. "Analytical modelling of wind speed deficit in large offshore wind forms". In: *Wind Energy* 9.1-2 (2006), pp. 39–53. DOI: 10.1002/we.189 (cit. on p. 44).

[65] M Bastankhah and F Porté-Agel. "A new analytical model for wind-turbine wakes." In: *Renewable Energy: an International Journal* 70 (2014), p. 116. DOI: 10.1016/j.renene.2014.01.002 (cit. on p. 44).

[66] P Gebraad, F Teeuwisse, J Wingerden, PA Fleming, S Ruben, J Marden, and L Pao. "Wind plant power optimization through yaw control using a parametric model for wake effects—a CFD simulation study". In: *Wind Energy* 19.1 (2016), pp. 95–114. DOI: 10.1002/we.1822 (cit. on p. 44).

[67] GC Larsen. *A simple stationary semi-analytical wake model*. Technical Report, Risø-R-1713(EN) August. Risø-DTU, 2009 (cit. on p. 44).

[68] JF Ainslie. "Calculating The Flowfield In The Wake Of Wind Turbines". In: *Journal of Wind Engineering and Industrial Aerodynamics* 27.1 (1987), pp. 213–224. DOI: 10.1016/0167-6105(88)90037-2 (cit. on p. 44).

[69] HA Madsen, GC Larsen, TJ Larsen, N Troldborg, and R Mikkelsen. "Calibration and Validation of the Dynamic Wake Meandering Model for Implementation in an Aeroelastic Code". In: *Journal of Solar Energy Engineering* 132.4 (2010). DOI: 10.1115/1.4002555 (cit. on p. 44).

[70] S Frandsen and ML Thogersen. "Integrated fatigue loading for wind turbines in wind farms by combining ambient turbulence and wakes". In: *Wind Engineering* 23.6 (1999), pp. 327–340 (cit. on p. 44).

[71] DC Quarton and JF Ainslie. "Turbulence in wind turbine wakes". In: *Wind Engineering* 14.1 (1990), pp. 15–23 (cit. on p. 44).

[72] U Hassan. *A wind tunnel investigation of the wake structure within small wind turbine farms*. Tech. rep. ETSU-WN–5113, Energy Technology Support Unit (ETSU), Harwell (United Kingdom), Department of Trade and Industry, 1993 (cit. on p. 44).

[73] A Crespo et al. "Turbulence characteristics in wind-turbine wakes". In: *Journal of Wind Engineering and Industrial Aerodynamics* 61.1 (1996), pp. 71–85 (cit. on p. 44).

[74] LP Chamorro and F Porté-Agel. "A Wind-Tunnel Investigation of Wind-Turbine Wakes: Boundary-Layer Turbulence Effects". English. In: *Boundary-Layer Meteorology* 132.1 (2009), pp. 129–149. DOI: 10.1007/s10546-009-9380-8 (cit. on p. 44).

[75] S Ott, J Berg, and M Nielsen. *Developments of the offshore wind turbine wake model Fuga*. Tech. rep. DTU Wind Energy E-0046. Roskilde, Denmark: Risø-DTU, 2014 (cit. on pp. 44, 47).

[76] A Crespo and J Hernández. "Numerical modelling of the flow field in a wind turbine wake". In: *Proceedings of the 3rd Joint ASCE/ASME Mechanics Conference*. 1989, pp. 121–127 (cit. on p. 44).

[77] J Schepers and S Van der Pijl. "Improved modelling of wake aerodynamics and assessment of new farm control strategies". In: *Journal of Physics: Conference Series*. Vol. 75. 1. IOP Publishing. 2007, p. 012039. DOI: 10.1088/1742-6596/75/1/012039 (cit. on p. 44).

[78] MP van der Laan, NN Sørensen, PE Réthoré, J Mann, MC Kelly, N Troldborg, JG Schepers, and E Machefaux. "An improved k-ϵ model applied to a wind turbine wake in atmospheric turbulence". In: *Wind Energy* (2014). DOI: 10.1002/we.1736 (cit. on p. 44).

[79] D Cabezón, E Migoya, and A Crespo. "Comparison of turbulence models for the computational fluid dynamics simulation of wind turbine wakes in the atmospheric boundary layer". In: *Wind Energy* 14.7 (2011), pp. 909–921. DOI: 10.1002/we.516 (cit. on p. 44).

[80] A El Kasmi and C Masson. "An extended k–ε model for turbulent flow through horizontal-axis wind turbines". In: *Journal of Wind Engineering and Industrial Aerodynamics* 96.1 (2008), pp. 103–122. DOI: 10.1016/j.jweia.2007.03.007 (cit. on p. 44).

[81] R Gómez-Elvira, A Crespo, E Migoya, F Manuel, and J Hernández. "Anisotropy of turbulence in wind turbine wakes". In: *Journal of Wind Engineering and Industrial Aerodynamics* 93.10 (2005), pp. 797–814. DOI: 10.1016/j.jweia.2005.08.001 (cit. on p. 44).

[82] GC Larsen, HA Madsen, K Thomsen, and TJ Larsen. "Wake meandering: A pragmatic approach". In: *Wind Energy* 11.4 (2008), pp. 377–395. DOI: 10.1002/we.267 (cit. on pp. 44, 46).

[83] RE Keck, HA Madsen, G Larsen, M de Maré, S Lee, and MJ Churchfield. "Two improvements to the dynamic wake meandering model: Including the effects of atmospheric shear on wake turbulence and incorporating turbulence build-up in a row of wind turbines". In: *Wind Energy* (2013). DOI: 10.1002/we.1686 (cit. on p. 44).

[84] A Jimenez, A Crespo, E Migoya, and J Garcia. "Advances in large-eddy simulation of a wind turbine wake". In: *Journal of Physics: Conference Series*. Vol. 75. 1. IOP Publishing. 2007, p. 012041. DOI: 10.1088/1742-6596/75/1/012041 (cit. on p. 44).

[85] K Nilsson, S Ivanell, KS Hansen, R Mikkelsen, JN Sørensen, SP Breton, and D Henningson. "Large-eddy simulations of the Lillgrund wind farm". In: *Wind Energy* 18.3 (2015), pp. 449–467. DOI: 10.1002/we.1707 (cit. on p. 44).

[86] YT Wu and F Porté-Agel. "Large-Eddy Simulation of Wind-Turbine Wakes: Evaluation of Turbine Parametrisations". English. In: *Boundary-Layer Meteorology* 138.3 (2011), pp. 345–366. DOI: 10.1007/s10546-010-9569-x (cit. on p. 44).

[87] J Sorensen and W Shen. "Numerical modeling of wind turbine wakes". In: *Journal Of Fluids Engineering-transactions Of The ASME* 124.2 (2002), pp. 393–399. DOI: 10.1115/1.1471361 (cit. on p. 44).

[88] M Churchfield and S Lee. "A Large-Eddy Simulation of Wind-Plant Aerodynamics". In: *50th AIAA Aerospace* January (2012). DOI: 10.2514/6.2012-537 (cit. on p. 44).

[89] S Ivanell, JN Sørensen, R Mikkelsen, and D Henningson. "Analysis of numerically generated wake structures". In: *Wind Energy* 12.1 (2009), pp. 63–80. DOI: 10.1002/we.285 (cit. on p. 44).

[90] N Troldborg, JN Sørensen, and R Mikkelsen. "Actuator line simulation of wake of wind turbine operating in turbulent inflow". In: *Journal of physics: conference series*. Vol. 75. 1. IOP Publishing. 2007, p. 012063. DOI: 10.1088/1742-6596/75/1/012063 (cit. on pp. 44, 46).

[91] SJ Andersen, B Witha, SP Breton, JN Sørensen, RF Mikkelsen, and S Ivanell. "Quantifying variability of Large Eddy Simulations of very large wind farms". In: *Journal of Physics: Conference Series*. Vol. 625. 1. IOP Publishing. 2015, p. 012027. DOI: 10.1088/1742-6596/625/1/012027 (cit. on p. 44).

[92] J Heinz. "Partitioned fluid-structure interaction for full rotor computations using CFD". PhD thesis. Technical University of Denmark, 2013. eprint: http://orbit.dtu.dk/files/87944638/Partitioned_Fluid_Structure_Interaction.pdf (cit. on p. 44).

[93] PE Réthoré, NA Johansen, ST Frandsen, R Barthelmie, K Hansen, L Jensen, MA Bækgaard, and J Kristoffersen. "Systematic wind farm measurement data reinforcement tool for wake model calibration". In: *European Offshore Wind Conference*. 2009 (cit. on p. 45).

[94] RJ Barthelmie, K Hansen, ST Frandsen, O Rathmann, J Schepers, W Schlez, J Phillips, K Rados, A Zervos, E Politis, et al. "Modelling and measuring flow and wind turbine wakes in large wind farms offshore". In: *Wind Energy* 12.5 (2009), pp. 431–444. DOI: 10.1002/we.348 (cit. on p. 45).

[95] R Barthelmie and S Pryor. "An overview of data for wake model evaluation in the Virtual Wakes Laboratory". In: *Applied Energy* 104 (Apr. 2013), pp. 834–844. DOI: 10.1016/j.apenergy.2012.12.013 (cit. on pp. 45, 46).

[96] GJ Taylor. *Wake measurements on the Nibe wind turbines in Denmark*. Tech. rep. Report ETSU WN 5020, Energy Technology Support Unit, National Power-Technology and Environment Center, 1990 (cit. on p. 45).

[97] J Cleijne. *Results of Sexbierum Wind Farm: single wake measurements*. Tech. rep. TNO, 1993 (cit. on p. 45).

[98] E Machefaux, N Troldborg, GC Larsen, J Mann, and H Aagaard Madsen. "Experimental and Numerical study of Wake to Wake Interaction in Wind Farms". In: *Proceedings of EWEA 2012 - European Wind Energy Conference; Exhibition* (2012) (cit. on p. 45).

[99] E Machefaux, GC Larsen, N Troldborg, and A Rettenmeier. "Single Wake Meandering, Advection and Expansion - An analysis using an adapted Pulsed Lidar and CFD LES-ACL simulations". In: *Prodeedings of EWEA 2013* (2013) (cit. on p. 45).

[100] JG Schepers, TS Obdam, and J Prospathopoulos. "Analysis of wake measurements from the ECN Wind Turbine Test Site Wieringermeer, EWTW". In: *Wind Energy* 15.4 (2012), pp. 575–591. DOI: 10.1002/we.488 (cit. on p. 45).

[101] ST Frandsen, L Chacón, A Crespo, P Enevoldsen, R Gómez-Elvira, J Hernández, J Højstrup, F Manuel, and K Thomsen. *Measurements on and modelling of offshore wind farms*. Tech. rep. Risø-R-903(EN), Risø/DTU, 1996 (cit. on p. 45).

[102] R Barthelmie, M Courtney, J Højstrup, and SE Larsen. "Meteorological aspects of offshore wind energy: Observations from the Vindeby wind farm". In: *Journal of Wind Engineering and Industrial Aerodynamics* 62.2 (1996), pp. 191–211. DOI: 10.1016/S0167-6105(96)00077-3 (cit. on p. 45).

[103] RJ Barthelmie, S Pryor, ST Frandsen, KS Hansen, J Schepers, K Rados, W Schlez, A Neubert, L Jensen, and S Neckelmann. "Quantifying the impact of wind turbine wakes on power output at offshore wind farms". In: *Journal of Atmospheric and Oceanic Technology* 27.8 (2010), pp. 1302–1317. DOI: 10.1175/2010JTECHA1398.1 (cit. on p. 45).

[104] KS Hansen, RJ Barthelmie, LE Jensen, and A Sommer. "The impact of turbulence intensity and atmospheric stability on power deficits due to wind turbine wakes at Horns Rev wind farm". In: *Power* November 2011 (2012), pp. 183–196. DOI: 10.1002/we.512 (cit. on p. 45).

[105] P Moriarty, J Sanz Rodrigo, P Gancarski, M Chuchfield, JW Naughton, KS Hansen, E Machefaux, E Maguire, F Castellani, L Terzi, et al. "IEA-Task 31 WAKEBENCH: Towards a protocol for wind farm flow model evaluation. Part 2: Wind farm wake models". In: *Journal of Physics: Conference Series*. Vol. 524. 1. IOP Publishing. 2014, p. 012185. DOI: 10.1088/1742-6596/524/1/012185 (cit. on pp. 45, 46).

[106] K Walker, N Adams, B Gribben, B Gellatly, NG Nygaard, A Henderson, M Marchante Jiménez, SR Schmidt, J Rodriguez Ruiz, D Paredes, et al. "An evaluation of the predictive accuracy of wake effects models for offshore wind farms". In: *Wind Energy* (2015). DOI: 10.1002/we.1871 (cit. on p. 45).

[107] RJ Barthelmie, ST Frandsen, M Nielsen, S Pryor, PE Rethore, and H Jørgensen. "Modelling and measurements of power losses and turbulence intensity in wind turbine wakes at Middelgrunden offshore wind farm". In: *Wind Energy* 10.6 (2007), pp. 517–528. DOI: 10.1002/we.238 (cit. on p. 45).

[108] PE Réthoré, P Fuglsang, GC Larsen, T Buhl, TJ Larsen, and HA Madsen. "TopFarm: Multi-fidelity Optimization of Offshore Wind Farm". In: 2007 (2011) (cit. on p. 45).

[109] J Cleve, M Greiner, P Enevoldsen, B Birkemose, and L Jensen. "Model-based analysis of wake-flow data in the Nysted offshore wind farm". In: *Wind Energy* 12.2 (2009), pp. 125–135. ISSN: 1099-1824. DOI: 10.1002/we.314 (cit. on pp. 45, 101).

[110] NG Nygaard. "Wakes in very large wind farms and the effect of neighbouring wind farms". In: *Journal of Physics: Conference Series*. Vol. 524. 1. IOP Publishing. 2014, p. 012162. DOI: 10.1088/1742-6596/524/1/012162 (cit. on p. 45).

[111] GC Larsen, H Aagaard Madsen, N Troldborg, TJ Larsen, PE Réthoré, P Fuglsang, S Ott, J Mann, T Buhl, M Nielsen, et al. *TOPFARM-next generation design tool for optimisation of wind farm topology and operation*. Tech. rep. Danmarks Tekniske Universitet, Risø Nationallaboratoriet for Bæredygtig Energi, 2011 (cit. on p. 45).

[112] JÅ Dahlberg. *Assessment of the Lillgrund wind farm*. Tech. rep. Vattenfall Vindkraft AB, 2009 (cit. on p. 45).

[113] KS Hansen and D Wind. "WP1 wake model performance validation results for Lillgrund offshore wind farm". In: January (2012), pp. 1–18 (cit. on p. 45).

[114] KS Hansen, PE Réthoré, J Palma, B Hevia, J Prospathopoulos, A Peña, S Ott, G Schepers, A Palomares, M Van der Laan, et al. "Simulation of wake effects between two wind farms". In: *Journal of Physics: Conference Series*. Vol. 625. 1. IOP Publishing. 2015, p. 012008. DOI: 10.1088/1742-6596/625/1/012008 (cit. on p. 45).

[115] NG Nygaard and SD Hansen. "Wake effects between two neighbouring wind farms". In: *Journal of Physics: Conference Series*. Vol. 753. 3. IOP Publishing. 2016, p. 032020. DOI: 10.1088/1742-6596/753/3/032020 (cit. on p. 45).

[116] ES Politis, J Prospathopoulos, D Cabezon, KS Hansen, P Chaviaropoulos, and RJ Barthelmie. "Modeling wake effects in large wind farms in complex terrain: the problem, the methods and the issues". In: *Wind Energy* 15.1 (2012), pp. 161–182. DOI: 10.1002/we.481 (cit. on p. 46).

[117] J Mann. "Wind field simulation". In: *Probabilistic Engineering Mechanics* 13.4 (Oct. 1998), pp. 269–282. DOI: 10.1016/S0266-8920(97)00036-2 (cit. on pp. 46, 50).

[118] M Gaumond, PE Réthoré, S Ott, A Pena, A Bechmann, and KS Hansen. "Evaluation of the wind direction uncertainty and its impact on wake modeling at the Horns Rev offshore wind farm". In: *Wind Energy* 17.8 (2014), pp. 1169–1178. DOI: 10.1002/we.1625 (cit. on pp. 46, 66).

[119] P McKay, R Carriveau, and DSK Ting. "Wake impacts on downstream wind turbine performance and yaw alignment". In: *Wind Energy* 16.2 (2013), pp. 221–234. DOI: 10.1002/we.544 (cit. on p. 47).

[120] IEC 61400-12-1. *Wind turbines-part 12-1: Power performance measurements of electricity producing wind turbine*. Tech. rep. Switzerland: International Electrotechnical Commission., 2005 (cit. on pp. 48, 69).

[121] IEC 61400-12-2. *Wind turbines-part 12-2: Power performance of electricity producing wind turbines based on nacelle anemometry*. Tech. rep. Switzerland: International Electrotechnical Commission., 2013 (cit. on p. 48).

[122] R Wagner, M Courtney, J Gottschall, and PJP Lindelöw. "Accounting for the speed shear in wind turbine power performance measurement". In: *Wind Energy* 14.8 (2011), pp. 993–1004. DOI: 10.1002/we.509 (cit. on pp. 48, 51).

[123] A Clifton and R Wagner. "Accounting for the effect of turbulence on wind turbine power curves". In: *Journal of Physics: Conference Series*. Vol. 524. 1. IOP Publishing. 2014, pp. 12109–12119. DOI: 10.1088/1742-6596/524/1/012109 (cit. on pp. 49, 51).

[124] MOL Hansen, JN Sørensen, S Voutsinas, N Sorensen, and HA Madsen. "State of the art in wind turbine aerodynamics and aeroelasticity". In: *Progress In Aerospace Sciences* 42.4 (2006), pp. 285–330. DOI: 10.1016/j.paerosci.2006.10.002 (cit. on p. 50).

[125] D Simms, S Schreck, M Hand, and L Fingersh. *NREL unsteady aerodynamics experiment in the NASA-Ames wind tunnel: a comparison of predictions to measurements*. Tech. rep. 2001. eprint: http://www.nrel.gov/docs/fy01osti/29494.pdf (cit. on p. 50).

[126] ML Buhl Jr and A Manjock. "A comparison of wind turbine aeroelastic codes used for certification". In: *Conference Paper National Renewable Energy Laboratory, Golden, CO, Report No. NREL/CP-500-39113*. 2006. DOI: 10.2514/6.2006-786 (cit. on p. 50).

[127] F Vorpahl, M Strobel, JM Jonkman, TJ Larsen, P Passon, and J Nichols. "Verification of aero-elastic offshore wind turbine design codes under IEA Wind Task XXIII". In: *Wind Energy* 17.4 (2014), pp. 519–547. DOI: 10.1002/we.1588 (cit. on p. 50).

[128] A Clifton, L Kilcher, JK Lundquist, and P Fleming. "Using machine learning to predict wind turbine power output". In: *Environmental Research Letters* 8.2 (2013). DOI: 10.1088/1748-9326/8/2/024009 (cit. on p. 51).

[129] A Clifton, M Daniels, and M Lehning. "Effect of winds in a mountain pass on turbine performance". In: *Wind Energy* 17.10 (2014), pp. 1543–1562. DOI: 10.1002/we.1650 (cit. on p. 51).

[130] HS Toft, L Svenningsen, W Moser, JD Sørensen, and ML Thøgersen. "Assessment of wind turbine structural integrity using response surface methodology". In: *Engineering Structures* 106 (2016), pp. 471–483. DOI: 10.1016/j.engstruct.2015.10.043 (cit. on p. 51).

[131] I Abdallah, B Sudret, C Lataniotis, JD Sørensen, and A Natarajan. "Fusing simulation results from multifidelity aero-servo-elastic simulators: application to extreme loads on wind turbine". In: (2015). DOI: 10.14288/1.0076137 (cit. on p. 51).

[132] I Abdallah, A Natarajan, and JD Sørensen. "Impact of uncertainty in airfoil characteristics on wind turbine extreme loads". In: *Renewable Energy* 75 (2015), pp. 283–300. DOI: 10.1016/j.renene.2014.10.009 (cit. on p. 51).

[133] P Moriarty. "Database for validation of design load extrapolation techniques". In: *Wind Energy* 11.6 (2008), p. 559. DOI: 10.1002/we.305 (cit. on p. 51).

[134] P Agarwal and L Manuel. "Simulation of offshore wind turbine response for long-term extreme load prediction". In: *Engineering structures* 31.10 (2009), pp. 2236–2246. DOI: 10.1016/j.engstruct.2009.04.002 (cit. on p. 51).

[135] CM Grinstead and JL Snell. *Introduction to probability*. American Mathematical Society., 2012. ISBN: 978-0821894149 (cit. on p. 55).

[136] M Rosenblatt. "Remarks on a multivariate transformation". In: *The annals of mathematical statistics* 23.3 (1952), pp. 470–472. DOI: 10.1214/aoms/1177729394 (cit. on pp. 58, 60).

[137] HS Li, ZZ L u, and XK Yuan. "Nataf transformation based point estimate method". In: *Chinese Science Bulletin* 53.17 (2008), pp. 2586–2592. DOI: 10.1007/s11434-008-0351-0 (cit. on pp. 58, 59).

[138] J Feinberg and HP Langtangen. "Chaospy: An open source tool for designing methods of uncertainty quantification". In: *Journal of Computational Science* 11 (2015), pp. 46–57. DOI: 10.1016/j.jocs.2015.08.008 (cit. on pp. 58, 74).

[139] R Lebrun and A Dutfoy. "An innovating analysis of the Nataf transformation from the copula viewpoint". In: *Probabilistic Engineering Mechanics* 24.3 (2009), pp. 312–320. DOI: 10.1016/j.probengmech.2008.08.001 (cit. on p. 59).

[140] RB Nelsen. *An introduction to copulas*. Springer Science & Business Media, 2007. ISBN: 978-0387-28659-4 (cit. on p. 60).

[141] JM Hammersley. "Monte Carlo methods for solving multivariable problems". In: *Annals of the New York Academy of Sciences* 86.3 (1960), pp. 844–874. DOI: 10.1111/j.1749-6632.1960.tb42846.x (cit. on p. 62).

[142] JH Halton. "On the efficiency of certain quasi-random sequences of points in evaluating multi-dimensional integrals". In: *Numerische Mathematik* 2.1 (1960), pp. 84–90. DOI: 10.1007/BF01386213 (cit. on p. 62).

[143] IM Sobol'. "On the distribution of points in a cube and the approximate evaluation of integrals". In: *Zhurnal Vychislitel'noi Matematiki i Matematicheskoi Fiziki* 7.4 (1967), pp. 784–802. DOI: 10.1016/0041-5553(67)90144-9 (cit. on p. 62).

[144] MD McKay, RJ Beckman, and WJ Conover. "A comparison of three methods for selecting values of input variables in the analysis of output from a computer code". In: *Technometrics* 42.1 (2000), pp. 55–61. DOI: 10.1080/00401706.2000.10485979 (cit. on p. 62).

[145] G McLachlan and D Peel. *Finite mixture models*. John Wiley & Sons, 2004. ISBN: 9780471721185. DOI: DOI:10.1002/0471721182 (cit. on p. 62).

[146] JA Carta, P Ramirez, and C Bueno. "A joint probability density function of wind speed, and direction for wind energy analysis". In: *Energy Conversion And Management* 49.6 (2008), pp. 1309–1320. DOI: 10.1016/j.enconman.2008.01.010 (cit. on p. 63).

[147] J Zhang, S Chowdhury, A Messac, and L Castillo. "A Multivariate and Multimodal Wind Distribution model". In: *Renewable Energy* 51 (2013), pp. 436–447. DOI: 10.1016/j.renene.2012.09.026 (cit. on p. 63).

[148] MG Morgan. "Use (and abuse) of expert elicitation in support of decision making for public policy". In: *Proceedings of the National Academy of Sciences* 111.20 (2014), pp. 7176–7184. DOI: 10.1073/pnas.1319946111 (cit. on pp. 63, 64).

[149] MAF Wagner and JR Wilson. "Graphical interactive simulation input modeling with bivariate Bézier distributions". In: *ACM Transactions on Modeling and Computer Simulation (TOMACS)* 5.3 (1995), pp. 163–189. DOI: 10.1145/217853.217854 (cit. on p. 63).

[150] CF Dietrich. *Uncertainty, calibration and probability: the statistics of scientific and industrial measurement*. CRC Press, 1991 (cit. on p. 65).

[151] N Dimitrov, A Natarajan, and M Kelly. "Model of wind shear conditional on turbulence and its impact on wind turbine loads". In: *Wind Energy* 18.11 (2015), pp. 1917–1931. DOI: 10.1002/we.1797 (cit. on pp. 67, 99).

[152] AI Forrester and AJ Keane. "Recent advances in surrogate-based optimization". In: *Progress in Aerospace Sciences* 45.1 (2009), pp. 50–79. DOI: 10.1016/j.paerosci.2008.11.001 (cit. on p. 68).

[153] J Friedman, T Hastie, and R Tibshirani. *The elements of statistical learning*. Vol. 1. Springer series in statistics Springer, Berlin, 2001. ISBN: 978-0-387-84858-7. DOI: 10.1007/978-0-387-84858-7 (cit. on pp. 68, 95).

[154] AJ Smola and B Schölkopf. "A tutorial on support vector regression". In: *Statistics and computing* 14.3 (2004), pp. 199–222. DOI: 10.1023/B:STCO.0000035301.49549.88 (cit. on p. 69).

[155] TG Dietterich. "Ensemble methods in machine learning". In: *International workshop on multiple classifier systems*. Springer. 2000, pp. 1–15. ISBN: 978-3-540-67704-8. DOI: 10.1007/3-540-45014-9_1 (cit. on p. 69).

[156] S Mekid and D Vaja. "Propagation of uncertainty: Expressions of second and third order uncertainty with third and fourth moments". In: *Measurement* 41.6 (2008), pp. 600–609. DOI: 10.1016/j.measurement.2007.07.004 (cit. on p. 69).

[157] A Peña, T Mikkelsen, SE Gryning, CB Hasager, AN Hahmann, M Badger, I Karagali, and MS Courtney. *Offshore Vertical Wind Shear*. Tech. rep. DTU Wind Energy-E-Report-0005(EN), Technical University of Denmark, 2012. eprint: http://orbit.dtu.dk/files/10591005/DTU_Wind_Energy_E_report_0005.pdf (cit. on p. 70).

[158] M Kelly and SE Gryning. "Long-term mean wind profiles based on similarity theory". In: *Boundary-layer meteorology* 136.3 (2010), pp. 377–390. DOI: 10.1007/s10546-010-9509-9 (cit. on p. 71).

[159] D Xiu. *Numerical methods for stochastic computations: a spectral method approach*. Princeton University Press, 2010 (cit. on p. 72).

[160] W Gautschi. "Algorithm 726: ORTHPOL–a package of routines for generating orthogonal polynomials and Gauss-type quadrature rules". In: *ACM Transactions on Mathematical Software (TOMS)* 20.1 (1994), pp. 21–62 (cit. on p. 72).

[161] OP Le Maître and OM Knio. *Spectral methods for uncertainty quantification: with applications to computational fluid dynamics*. Springer, 2010. ISBN: 978-90-481-3519-6. DOI: 10.1007/978-90-481-3520-2 (cit. on p. 73).

[162] G Blatman and B Sudret. "Adaptive sparse polynomial chaos expansion based on least angle regression". In: *Journal of Computational Physics* 230.6 (2011), pp. 2345–2367. DOI: 10.1016/j.jcp.2010.12.021 (cit. on p. 73).

[163] B Sudret. "Global sensitivity analysis using polynomial chaos expansions". In: *Reliability Engineering & System Safety* 93.7 (2008), pp. 964–979. DOI: 10.1016/j.ress.2007.04.002 (cit. on pp. 73, 82).

[164] T Ishigami and T Homma. "An importance quantification technique in uncertainty analysis for computer models". In: *Uncertainty Modeling and Analysis, 1990. Proceedings., First International Symposium on*. IEEE. 1990, pp. 398–403. DOI: 10.1109/ISUMA.1990.151285 (cit. on p. 73).

[165] F Pedregosa, G Varoquaux, A Gramfort, V Michel, B Thirion, O Grisel, M Blondel, P Prettenhofer, R Weiss, V Dubourg, et al. "Scikit-learn: Machine learning in Python". In: *The Journal of Machine Learning Research* 12 (2011), pp. 2825–2830 (cit. on p. 74).

[166] JE Oakley and A O'Hagan. "Probabilistic sensitivity analysis of complex models: a Bayesian approach". In: *Journal of the Royal Statistical Society: Series B (Statistical Methodology)* 66.3 (2004), pp. 751–769. DOI: 10.1111/j.1467-9868.2004.05304.x (cit. on p. 76).

[167] D Bigoni, AP Engsig-Karup, and YM Marzouk. "Spectral Tensor-Train Decomposition". In: *SIAM Journal on Scientific Computing* 38.4 (2016), A2405–A2439. DOI: 10.1137/15M1036919 (cit. on p. 77).

[168] DS Broomhead and D Lowe. "Multi-variable functional interpolation and adaptive networks". In: *Complex Systems* 2 (1988), pp. 231–255 (cit. on p. 77).

[169] JS Hesthaven, G Rozza, and B Stamm. "Certified reduced basis methods for parametrized partial differential equations". In: *SpringerBriefs in Mathematics* (2015). DOI: 10.1007/978-3-319-22470-1 (cit. on p. 78).

[170] B Iooss and P Lemaître. "A review on global sensitivity analysis methods". In: *Uncertainty Management in Simulation-Optimization of Complex Systems*. Springer, 2015, pp. 101–122. DOI: 10.1007/978-1-4899-7547-8_5 (cit. on p. 81).

[171] MD Morris. "Factorial sampling plans for preliminary computational experiments". In: *Technometrics* 33.2 (1991), pp. 161–174. DOI: 10.1080/00401706.1991.10484804 (cit. on p. 81).

[172] IM Sobol' and S Kucherenko. "Derivative based global sensitivity measures and their link with global sensitivity indices". In: *Mathematics and Computers in Simulation* 79.10 (2009), pp. 3009–3017. DOI: 10.1016/j.matcom.2009.01.023 (cit. on p. 81).

[173] A Saltelli, P Annoni, I Azzini, F Campolongo, M Ratto, and S Tarantola. "Variance based sensitivity analysis of model output. Design and estimator for the total sensitivity index". In: *Computer Physics Communications* 181.2 (2010), pp. 259–270. DOI: 10.1016/j.cpc.2009.09.018 (cit. on pp. 81, 82).

[174] Z Wu, D Wang, P Okolo, F Hu, and W Zhang. "Global sensitivity analysis using a Gaussian radial basis function metamodel". In: *Reliability Engineering & System Safety* (2016). DOI: 10.1016/j.ress.2016.06.006 (cit. on p. 82).

[175] M Omlin and P Reichert. "A comparison of techniques for the estimation of model prediction uncertainty". In: *Ecological Modelling* 115.1 (1999), pp. 45–59. DOI: 10.1016/S0304-3800(98)00174-4 (cit. on p. 88).

[176] D Kavetski, SW Franks, and G Kuczera. "Confronting input uncertainty in environmental modelling". In: *Calibration of watershed models* (2002), pp. 49–68. DOI: 10.1029/WS006p0049 (cit. on p. 90).

[177] B Efron. "Bootstrap methods: another look at the jackknife". In: *The annals of Statistics* 7.1 (1979), pp. 1–26. DOI: 10.1214/aos/1176344552 (cit. on p. 91).

[178] MC Kennedy and A O'Hagan. "Bayesian calibration of computer models". In: *Journal of the Royal Statistical Society: Series B (Statistical Methodology)* 63.3 (Aug. 2001), pp. 425–464. DOI: 10.1111/1467-9868.00294 (cit. on p. 95).

[179] J Brynjarsdóttir and A O'Hagan. "Learning about physical parameters. The importance of model discrepancy". In: *Inverse Problems* 30.11 (2014), p. 114007. DOI: 10.1088/0266-5611/30/11/114007 (cit. on p. 95).

Article A

How many model evaluations are required to predict the AEP of a wind power plant?

How Many Model Evaluations Are Required To Predict The AEP Of A Wind Power Plant?

J P Murcia[1], P E Réthoré[1], A Natarajan[1] and J D Sørensen[2]

[1]DTU Wind Energy, Technical University of Denmark, Risø Campus, Frederiksborgvej 399, 4000 Roskilde, Denmark

[2]Department of Civil Engineering, Aalborg University

E-mail: jumu@dtu.dk

Abstract. Wind farm flow models have advanced considerably with the use of large eddy simulations (LES) and Reynolds averaged Navier-Stokes (RANS) computations. The main limitation of these techniques is their high computational time requirements; which makes their use for wind farm annual energy production (AEP) predictions expensive. The objective of the present paper is to minimize the number of model evaluations required to capture the wind power plant's AEP using stationary wind farm flow models. Polynomial chaos techniques are proposed based on arbitrary Weibull distributed wind speed and Von Misses distributed wind direction. The correlation between wind direction and wind speed are captured by defining Weibull-parameters as functions of wind direction. In order to evaluate the accuracy of these methods the expectation and variance of the wind farm power distributions are compared against the traditional binning method with trapezoidal and Simpson's integration rules.

The wind farm flow model used in this study is the semi-empirical wake model developed by Larsen [1]. Three test cases are studied: a single turbine, a simple and a real offshore wind power plant. A reduced number of model evaluations for a general wind power plant is proposed based on the convergence of the present method for each case.

1 Introduction

The evaluation of the performance of a wind power plant requires to calculate the expected energy production over the years. The most common measure of wind farm performance used in the planning or evaluation stages is the annual energy production. AEP is proportional to the expected mean power over all the possible atmospheric conditions: $AEP = 8760\,\mathbb{E}(P)$ in [W.h]. The expected power is defined in eq. 1.1. The likelihood of occurrence of the different atmospheric conditions is represented by the joint probability density function, $\mathbb{PDF}(u,\theta)$, where u and θ are the Reynolds-averaged wind speed and wind direction.

$$\mathbb{E}(P) = \int_0^{2\pi}\int_0^{\infty} P(u,\theta)\,\mathbb{PDF}(u,\theta)\,du\,d\theta \tag{1.1}$$

The common practice in the wind energy industry is to consider the Reynolds-averaged wind speed variations over the years at a given location to follow a Weibull distribution. On the other hand, the mean wind direction is modeled by defining sectors or bins. Additionally, the correlation between wind direction and wind speed is captured by defining different wind

speed Weibull-parameters for each sector. As a result the wind speed and wind direction are independent in each of the R_θ wind direction sectors: $[\theta_j, \theta_{j+1}]$, see eq. 1.2. In this equation, $\mathbb{P}_j$ is the the probability of occurrence of each sector.

$$\mathbb{PDF}(u,\theta) \approx \mathbb{PDF}(u|\theta \in [\theta_j, \theta_{j+1}])\, \mathbb{PDF}(\theta|\theta \in [\theta_j, \theta_{j+1}])\, \mathbb{P}_j \tag{1.2}$$

This assumptions implies that the mean power can be computed in each sector independently and then weighted averaged with respect $\mathbb{P}_j$.

$$\mathbb{E}(P) \approx \sum_{j=1}^{R_\theta} \mathbb{P}_j \left(\int_{\theta_j}^{\theta_{j+1}} \int_{0}^{\infty} P(u,\theta)\, \mathbb{PDF}(u|\theta \in [\theta_j, \theta_{j+1}])\, \mathbb{PDF}(\theta|\theta \in [\theta_j, \theta_{j+1}])\, du\, d\theta \right) \tag{1.3}$$

There are different approaches to numerically approximate eq. 1.3: trapezoidal and Simpson's integration rules consist in building linear or quadratic interpolation lines between a number of wind speed and direction evaluation points, $P(u_k, \theta_k)$. Such techniques are the common practice in the industry and they can be interpreted as a weighted average of the evaluation points, see eq. 1.4. The weights shown in this equation, w_k, depend on the integration technique and on the $\mathbb{PDF}(u,\theta)$.

$$\mathbb{E}(P) \approx \sum_{j=1}^{R_\theta} \mathbb{P}_j \left(\sum_{k=1}^{N} w_k\, P(u_k, \theta_k) \right) \tag{1.4}$$

Polynomial chaos with semi-spectral collocation techniques can be used to have a higher accuracy prediction to integrals in the same way as presented in eq. 1.4 with a reduced number of model evaluations. The idea originally introduced in [2], presents quadrature rules based on a normal distribution by the construction of an orthonormal polynomial basis with respect the normal probability density function. The generalized polynomial chaos (gPC) techniques presented in [3] expand this technique to uniform, beta and gamma probability distributions. In the present work, data driven polynomial chaos (aPC) techniques introduced in [4] are applied to the Weibull distribution. Furthermore, the multi-element polynomial chaos presented in [5] is implemented in this paper to deal with integrals over multiple regions of wind speed and wind direction.

2 Polynomial Chaos for AEP

2.1 Multi-element Data-driven Polynomial Chaos (MEPC)

PC techniques enables the user to find the statistical properties of a model with a reduce number of simulations. This is achieved by defining a set of polynomials that are used to interpolate the model response. The purpose of using multiple element PC is to separate the integration region into small sub-regions in which the integration variables can be assumed to be independent. In the present section the theory for building quadrature rules is presented. The theory is presented as a tool to integrate the function $f(x)$ under a random variable, x, characterized by its probability density function $\mathbb{PDF}(x)$. The integral is separated over R_x regions, defined by its end points, x_i.

$$\int_{-\infty}^{\infty} f(x)\, \mathbb{PDF}(x)\, dx = \sum_{i=1}^{R_x} \mathbb{P}_i \int_{x_i}^{x_{i+1}} f(x)\, \mathbb{PDF}(x|x \in [x_i, x_{i+1}])\, dx \tag{2.1}$$

An inner product is defined based on the conditional probability density function such that:

$$\mathbb{E}_i(f) = \langle f \rangle_i = \int_{x_i}^{x_{i+1}} f(x)\, \mathbb{PDF}(x|x \in [x_i, x_{i+1}])\, dx \tag{2.2}$$

$$\mathbb{E}_i(f\, g) = \langle f, g \rangle_i = \int_{x_i}^{x_{i+1}} f(x)\, g(x)\, \mathbb{PDF}(x|x \in [x_i, x_{i+1}])\, dx \tag{2.3}$$

A polynomial of order n is defined as:

$$\pi_n(x) = a_{0n} + a_{1n}\, x + ... + a_{nn}\, x^n = \sum_{m=0}^{n} a_{mn}\, x^m \tag{2.4}$$

An orthonormal polynomial basis based on the probability distribution consists in a group of polynomials that are orthogonal and that have unitary norm with respect the inner product defined in eq. 2.3. These conditions are summarized in eq. 2.5-2.6. These equations are recursive as they use the coefficients from the lower order polynomials to find the next one. The first polynomial is assumed to be: $\pi_0(x) = 1$. Furthermore the statistical moments of the truncated distribution, $\mathbb{E}_i(x^m)$, up to the $(2j-1)$-th order are required.

$$\langle \pi_n, \pi_k \rangle_i = 0 = \sum_{m=0}^{n} a_{mn} \langle x^m, \pi_k \rangle_i = \sum_{m=0}^{n} a_{mn} \left(\sum_{l=0}^{k} a_{lk}\, \mathbb{E}_i(x^{m+l}) \right) \quad \forall k < n \tag{2.5}$$

To close this system of equations orthogonality is solved first. This is done by setting the last coefficient of each polynomial to be: $a_{n\,n} = 1$. Finally the polynomials are normalized:

$$\pi_n = \frac{\pi_n}{\sqrt{\langle \pi_n, \pi_n \rangle}} \tag{2.6}$$

Note that the polynomial basis will be different for each region, since each one has a different conditional $\mathbb{PDF}$. The polynomial basis for the i-th region will be denoted as π_{in}.

The fundamental theorem of Gaussian quadrature states that integrals with respect the $\mathbb{PDF}(x)$ can be approximated using only N evaluation points, x_k. The quadrature rules calculate exactly the integral of functions, $f(x)$, that are a polynomial of order equal or smaller than $2N-1$.

$$\mathbb{E}_i(f) = \langle f \rangle_i = \int_{x_i}^{x_{i+1}} f(x)\, \mathbb{PDF}(x|x \in [x_i, x_{i+1}])\, dx \approx \sum_{k=1}^{N} w_k\, f(x_k) \tag{2.7}$$

where the evaluation points, x_k, are the roots of the N-th polynomial in the basis, $\pi_{i\,N}$, and the weights, w_k, are computed as:

$$w_k = \frac{1}{\sum_{n=0}^{N} \left(\pi_{in}(x_k)\right)^2} \tag{2.8}$$

By projecting any function, f, into the orthonormal polynomial basis one can approximate its response as a polynomial. Note that since the method can handle different truncation orders in each region in general there are going to be discontinuities in the polynomial response

between the regions; this does not produce any problem as the integration in each region is done independently.

$$f(x) = \sum_{n=0}^{\infty} \langle f, \pi_{in} \rangle_i \; \pi_{in}(x) \approx \sum_{n=0}^{N} \langle f, \pi_{in} \rangle_i \; \pi_{in}(x) = \sum_{n=0}^{N} c_{in} \, \pi_{in}(x) \quad \forall x \in [x_i, x_{i+1}] \tag{2.9}$$

The coefficients of the function in the polynomial basis, $c_{i\,j}$, can be computed numerically using the Gaussian quadrature rules presented in eq. 2.8; this method is also known as spectral collocation:

$$c_{in} = \langle f, \pi_{in} \rangle_i \approx \sum_{k=1}^{N} w_k \, f(x_k) \, \pi_{in}(x_k) \quad \forall n < N \tag{2.10}$$

Finally the statistical moments of the function can be obtained from its coefficients in the polynomial basis:

$$\mathbb{E}(f) = \sum_{i=1}^{R_x} \mathbb{P}_i \, \mathbb{E}_i(f) = \sum_{i=1}^{R_x} \mathbb{P}_i \, c_{i\,0} \tag{2.11}$$

$$\mathbb{V}(f) = \sum_{i=1}^{R_x} \sum_{k=0}^{N} \mathbb{P}_i \, c_{i\,k}^2 - \mathbb{E}(f)^2 \tag{2.12}$$

It is very important to notice that the polynomial surrogate function is not used for computing neither the $\mathbb{E}(f)$ nor $\mathbb{V}(f)$. In fact, the $\mathbb{E}(f)$ can be computed using the quadrature rule directly as presented in eq. 2.7; which is equivalent to computing only the 0-th order coefficients; and then using eq. 2.11. If the variance is required then all the coefficients in the polynomial basis are computed and used in eq. 2.12.

2.2 MEPC for wind speed and wind direction:

Due to the independence between wind direction and speed inside a direction sector, a polynomial basis can be constructed independently for wind speed and for wind direction. The 2D polynomial basis is then the product between the one dimensional polynomial basis. Similarly the 1D quadrature weights can be used to define the 2D quadrature rules for each sector. A polynomial basis of orders N_u for wind speed and N_θ for wind direction are built by solving the equations 2.5 and 2.6. To build the orthonormal polynomials the statistical moments of the truncated Weibull are required, as well as the truncated moments for the wind direction distribution. Expressions for the truncated statistical moments of the Weibull distribution are presented in [6].

$$\mathbb{E}(P) \approx \sum_{i=1}^{R_u} \sum_{j=1}^{R_\theta} \langle P \rangle_{ij} \, \mathbb{P}_j \, \mathbb{P}_i \tag{2.13}$$

$$\langle P \rangle_{ij} = \int_{\theta_j}^{\theta_{j+1}} \int_{u_i}^{u_{i+1}} P(u, \theta) \, \mathbb{PDF}(\theta | \theta \in [\theta_j, \theta_{j+1}]) \, \mathbb{PDF}(u | u \in [u_i, u_{i+1}]) \, du \, d\theta$$

$$\approx \sum_{k=1}^{N_u} \sum_{l=1}^{N_\theta} w_{jl} \, \nu_{ik} \, P(u_k, \theta_l) \tag{2.14}$$

The notation used is: w_{jl} represents the weight associated to the l-th root of the N_θ-th order polynomial for the wind direction inside the j-th sector. ν_{ik} represents the weight associated to the k-th root of the N_u-th order polynomial for the wind speed inside the i-th sector. The roots and weights are computed independently as in the single variable case from eq. 2.8. Once the polynomial families have been obtained for each sector, one can capture the statistical properties of the power as produced by the random wind speed and wind direction by projecting the power curve function into the 2D polynomial basis:

$$P(u,\theta) \approx \sum_{k=0}^{N_u}\sum_{l=0}^{N_\theta} c_{ijkl}\,\pi_{ik}(u)\,\pi_{jl}(\theta) \quad \forall\theta\in[\theta_j,\theta_{j+1}] \quad \text{and} \quad \forall u\in[u_i,u_{i+1}] \tag{2.15}$$

The coefficients of the power in the polynomial basis can be computed numerically using the quadrature rules:

$$c_{ijkl} = \langle P, \pi_{ik}\pi_{jl}\rangle_{ij} \approx \sum_{k=1}^{N_u}\sum_{l=1}^{N_\theta} w_{jl}\,\nu_{ik}\,P(u_k,\theta_l)\;\pi_{ik}(u_k)\,\pi_{jl}(\theta_l) \tag{2.16}$$

Finally the statistical moments of the power distribution can be obtained from the polynomial basis coefficients:

$$\mathbb{E}(P) = \sum_{i=1}^{R_u}\sum_{j=1}^{R_\theta} \mathbb{P}_i\,\mathbb{P}_j\,(c_{ij00}) \tag{2.17}$$

$$\mathbb{V}(P) = \sum_{i=1}^{R_u}\sum_{j=1}^{R_\theta}\left(\mathbb{P}_i\,\mathbb{P}_j\sum_{k=0}^{N_u}\sum_{l=0}^{N_\theta} c_{ijkl}^2\right) - \mathbb{E}(P)^2 \tag{2.18}$$

3 Single wind turbine case

A single wind turbine case is considered in order to verify the concept of using MEPC techniques to estimate the AEP. For this case the power is only a function of the Weibull distributed wind speed. The wind speed operational range of the wind turbine and optionally the region with rated power are used to define the regions of integration. Some examples of the orthonormal polynomial basis for the truncated Weibull distribution are shown in figure 1, as well as the obtained quadrature points and the polynomial surrogates. In this figure it can be observed that the polynomial response passes through the evaluation points. And it can be expected that oscillations might appear for high polynomial orders, especially for regions with constant power.

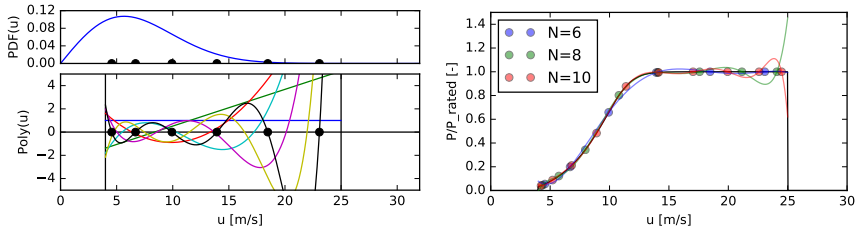

Figure 1. (Left) 6-th order polynomial basis for an individual region Weibull distributed wind speed: $u \in [4, 25]$ [m/s] (Right) Power curve (black line), quadrature evaluation points and polynomial surrogate of the power curve.

Figure 6 shows the convergence for different integration schemes for the relative error of $\mathbb{E}(P)$ and of $\mathbb{V}(P)$ vs. the number of model evaluations used in the integration N. The relative error is calculated with respect the trapezoidal integration rule with 10^5 points. The instabilities in the MEPC quadrature results are produced by the difference in the location of the evaluation points. The location of the evaluation points and the accuracy of the quadrature rules depend on the Weibull parameters because the method depends on the $\mathbb{PDF}(u)$. The benefit obtained for using MEPC is considerable; as it reduced the number of model evaluations from 21 (current common practice) down to 6 model evaluations for similar relatives errors of 0.1% in expected power and variance. Note that the method becomes numerically unstable at high polynomial orders (larger than 10) even with careful handling of number precision because of the large differences in the values of the high order statistical moments, $\mathbb{E}(x^m)$. The results presented in this article use the following python libraries: the polynomial handling class on numpy (http://www.numpy.org), scipy (http://www.scipy.org) for its implementation of the trapezoidal/Simpson's methods and mpmath (http://mpmath.org/doc/current/index.html) for handling the polynomial construction and root finding algorithms with an arbitrary high precision.

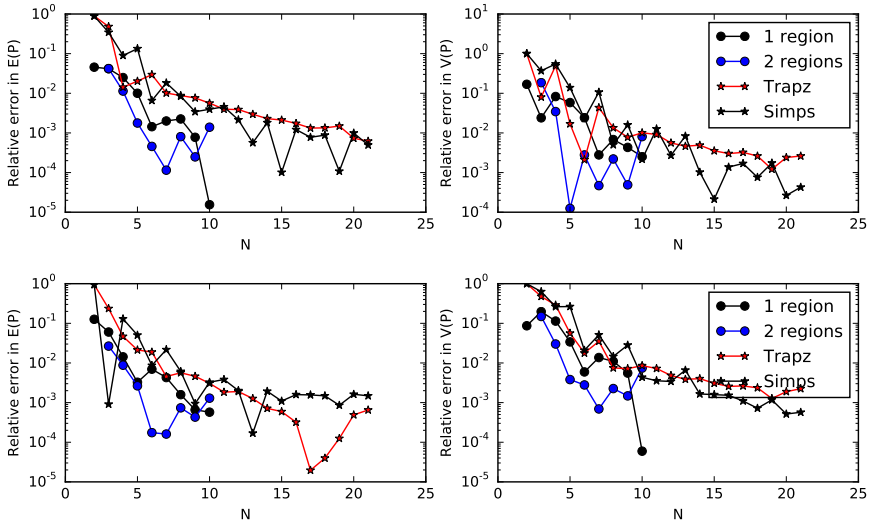

Figure 2. Convergence for different integration schemes vs. number of model evaluations N for the relative error of (left) $\mathbb{E}(P)$ and (right) $\mathbb{V}(P)$. Weibull distribution with shape parameter $k_W = 2$ and scale parameter (Top) $A = 8.0$ [m/s] (Bottom) $A = 10.0$ [m/s].

4 Simple wind power plant case

In this section the multi-element polynomial chaos technique is applied to a simple wind power plant. The power is computed using G. C. Larsen's semi-empirical wake model [1]. The local weather is characterized by a Weibull distributed wind speed and an uniformly distributed wind direction inside each wind direction sector. Note that this type of assumption is the standard in most wind energy flow models such as WAsP. On the other hand, the method proposed in this paper could be applied for an arbitrary distribution of wind direction inside each sector. The only requirement is that the statistical moments are known or computable (some examples of

marginal distributions for wind direction are: Multiple mixture of Von Mises, or kernel density estimated $\mathbb{PDF}$).

Under the assumptions of the present model, the correlation between wind speed and wind direction is modeled by having different parameters of the Weibull distribution as a function of the wind direction sector. The 1D polynomial basis for the wind direction are the Legendre polynomials since the conditional probability density function for the wind direction inside each sector is assumed to be uniform. The final number of evaluation points is the tensorial product (meshgrid combination) of the wind speed and the wind direction quadrature points.

The layout of the simple offshore power plant is shown in figure 3, as well as the power and thrust coefficient curves for the Vestas V80-offshore turbines. The wind rose and Weibull parameters for the site are shown in figure 4.

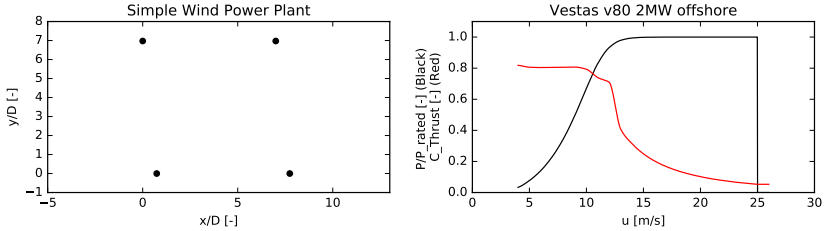

Figure 3. Simple wind power plant: (Left) layout and (Right) power and thrust coefficient curves for the turbines.

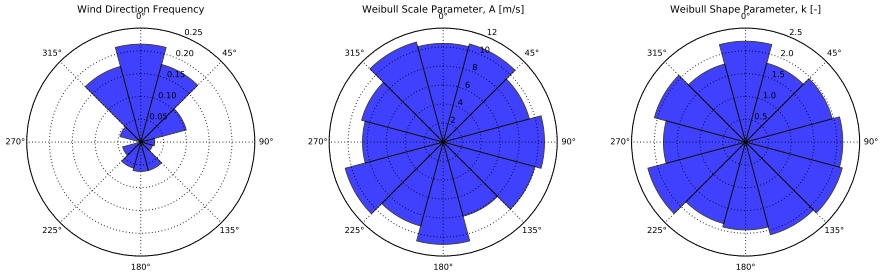

Figure 4. (Left) Wind rose of the site. (Middle) Weibull scale parameter for each sector. (Right) Weibull shape parameter for each sector.

The wind park's power curve , $P(u, \theta)$ is shown in figure 5 (Left). This power curve is computed using 30960 model evaluations: every 0.5 [deg.] and 0.5 [m/s]. This figure additionally shows an example of the resulting polynomial surrogate power curve. It can be observed that the power surrogate captures the rough behavior of power. As expected the polynomial surrogates present oscillations in the region of rated power as well as discontinuities between the regions; this does not cause any problem due to the fact that the integration in each region is done independently and since the oscillations around the *real* power curve cancel out when computing the $\mathbb{E}(P)$ or $\mathbb{V}(P)$. It might be of interest to visualize the polynomial surrogate because if the surrogate presents to many oscillations it means that the order of the polynomial is to high, and a further division of integration region can be executed.

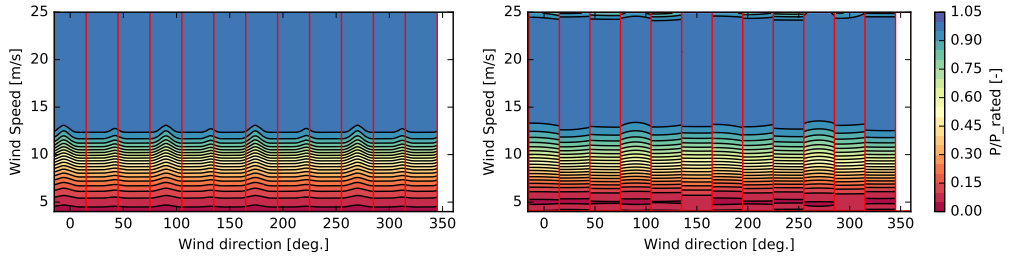

Figure 5. Power plant power curve: (Left) computed from $720 \times 43 = 30960$ model evaluations. (Right) Polynomial surrogate of the power curve order computed in $R_D = 12$ sectors, with $N_u = 8$-th order in wind speed and $N_\theta = 5$-th order in wind direction for a total of $12 \times 5 \times 8 = 480$ simulations.

The convergence of the expected power and of the standard deviation of power normalized by the rated wind farm power are shown in figure 6. The same numerical instabilities produced by the shifting of root locations can be observed. Furthermore it can be observed that the MEPC algorithm converges very fast to the desired values with relatives error of order of 1%. This relative error is computed with respect the predictions with 30960 model simulations and it is show in the figure as the shaded purple region. It is important to remark that surrogates with a low polynomial degree, 2-nd in wind direction per sector and 4-th in wind speed, capture the expected power and its variance within 1% accuracy with around 10 times less model evaluations than the trapezoidal integration scheme used in the traditional binning method. Note that when $R_u = 2$, the regions are defined as: $[4, 14]$ and $[14, 25]$ [m/s], and the order on the rated power region is always $N_u[2] = 1$.

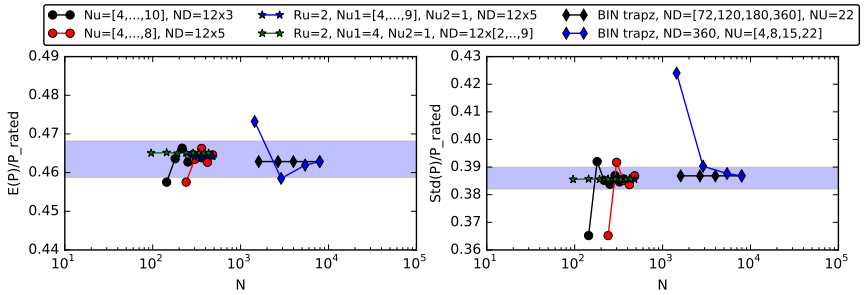

Figure 6. Convergence for different integration schemes vs. number of point evaluation N for the (left) normalized expected power $\mathbb{E}(P)$ and (right) normalized standard deviation of power, $\mathbb{S}(P)$ for number of model evaluations.

5 Real wind power plant case - Horns Rev 1

In this section the multi-element polynomial chaos technique is applied to the Danish offshore wind power plant Horns Rev 1 (HR1) co-owned by Vattenfall and DONG Energy. This wind farm is located in the Western coast of Denmark, at a distance of 9 to 12 [km] from the coast. This plant has has been studied in several articles and it is one of the benchmark cases for wind

turbine wake models. The layout of HR1 is shown in figure 7, along with the power and thrust coefficient curves for the Vestas V80-offshore turbines. The wind rose and Weibull parameters for the site are shown in figure 8.

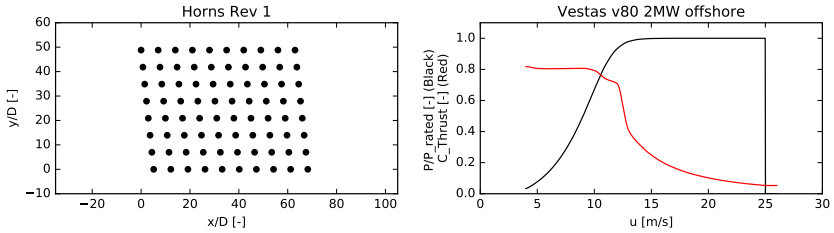

Figure 7. Horns Rev 1 power plant: (Left) layout and (Right) power and thrust coefficient curves for the turbines.

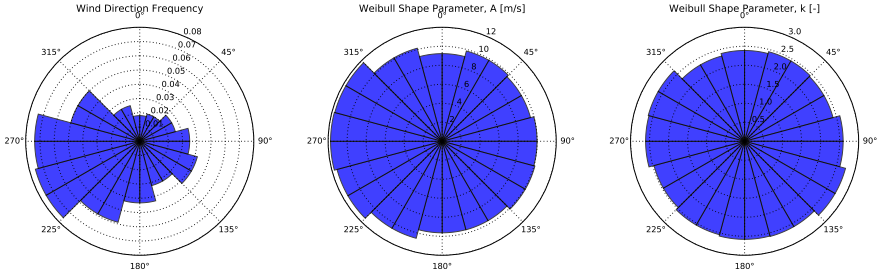

Figure 8. Horns Rev 1 plant: (Left) Wind rose of the site. (Middle) Weibull scale parameter for each sector. (Right) Weibull shape parameter for each sector.

The power curve of Horns Rev 1, $P(u, \theta)$ is shown in figure 9. As in the previous section the power curve is computed using 30960 simulations of G. C. Larsen's model [1]. An example of a polynomial surrogate for the power curve is also presented in this figure. As expected, the polynomial surrogate presents discontinuities between the sectors and it contains oscillations in the region of rated power. As discussed in the previous section, the discontinuities do not cause problems in the computation of AEP because each region is treated individually. Note that the 12 wind direction sectors were divided into 2 regions in order to reduce the degree of the polynomial basis required to capture the dependency on wind direction.

Convergence of power expectation and standard deviation can be observed in figure 10. It can be observed that the MEPC algorithm converges very fast to the desired values with relatives error of order of 1%. This relative error is computed with respect the predictions done using 30960 model simulations and it is show in the figure as the shaded purple region. It is important to remark that surrogates with a low polynomial degree, 2-th in wind direction per sector and 4-th in wind speed, capture the expected power and its variance within 1% accuracy using 10 times less model evaluations than the trapezoidal integration scheme used in the traditional binning method. Note that when $R_u = 2$, the regions are defined as: $[4, 16]$ and $[16, 25]$ [m/s], and the order on the rated power region is always $N_u[2] = 1$.

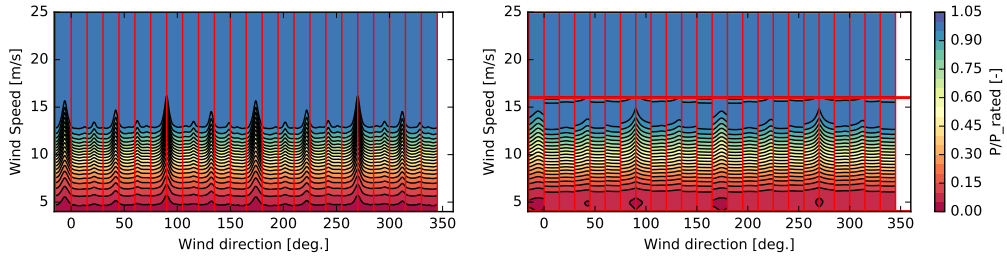

Figure 9. Horns Rev 1 power curve: (Left) computed from $720 \times 43 = 30960$ model evaluations. (Right) Polynomial surrogate of the power curve order computed in $R_D = 24$ sectors, with 3-th order in wind direction and 4-th order in wind speed for a total of $24 \times 3 \times 4 = 288$ simulations.

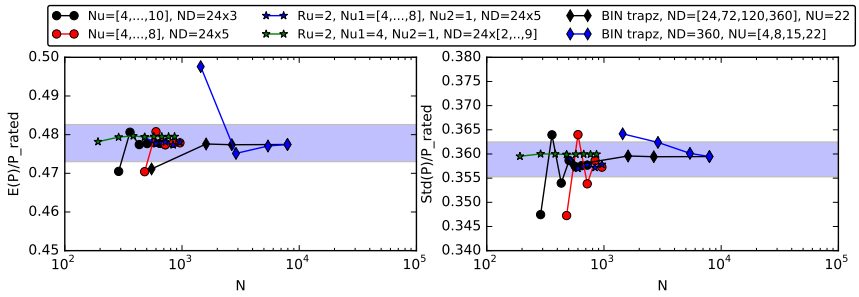

Figure 10. Convergence for different integration schemes vs. number of point evaluation N for the (left) normalized expected power $\mathbb{E}(P)$ and (right) normalized standard deviation of power, $\mathbb{S}(P)$ for number of model evaluations.

6 Discussion

The conceptual methodology of MEPC has been proven as having the potential to handle arbitrary local wind resources probability distributions. The methodology presented in the current paper has been implemented to handle user defined number/machine precision. Despise these efforts the polynomial basis building algorithm presents instabilities for large order of polynomial basis order. The quadrature rules are a fundamental step to find the statistical parameters of the power. Further research is still required to assure stability in the convergence rates of polynomial chaos for arbitrary Weibull distributions.

AEP production calculations with high fidelity flow models are restricted by their large computational requirements, in particular due to the large number of model simulations required to estimate the AEP with a certain level of accuracy. There is a need for methods to reduce the number of model evaluations required to compute power statistics. Furthermore analysis of uncertainty in power production have shown that the uncertainty in AEP can go up to 10% depending on the uncertainty in the input parameters [7]. The minimum requirement of AEP accuracy should be between $0.1 - 1\%$. MEPC method can achieve a relative error in the calculation of AEP smaller than 1% for a reduced number of evaluations. A reduction by a factor of 10 in comparison to current techniques can be achieved using MEPC with $192 = 24 \times 4 \times 2$ model simulations: this accounts for 2 regions of wind speed polynomial basis of orders $N_U = [4, 1]$ and a 2-nd order basis for wind direction.

The presented method is designed to be applied in optimization under uncertainty in which AEP calculations are going to be calculated on every optimization step (possible thousands of times). Each optimization step will propose a new wind power plant layout which makes the use of previous simulations impossible. Building the MEPC surrogate is a fast process, specially if the polynomial basis in wind direction and wind speed are precomputed and stored before the optimization technique. Furthermore, in optimization algorithms the accuracy of the AEP is gradually refined as the objective function increment diminishes, this can be achieved with the present method by increasing the order of the polynomial basis. Consequently a good estimation of AEP with few model simulations can speed up the process of optimization significantly and a more accurate AEP estimation will only be computed for the final steps.

Further investigation of the use of other types of functional basis are planed to be developed such as: (1) the use of polynomial basis for correlated wind velocity vector and turbulence intensity, (2) the use of wavelets for wind speed to deal with the discontinuities in the power curve and (3) a mixtures of polynomials and Fourier series for wind speed, wind direction and turbulence intensity. These techniques promise to have a better estimation of AEP but at the cost of increasing the number of model evaluations in comparison to the method presented in this article.

Acknowledgments
This work was supported by the International Collaborative Energy Technology R&D Program of the Korea Institute of Energy Technology Evaluation and Planning (KETEP), granted financial resource from the Ministry of Trade, Industry & Energy, Republic of Korea. (No. 20138520021140).

References

[1] Larsen G C 2009 A simple stationary semi-analytical wake model Technical report, risø-r-1713(en) Risø-DTU

[2] Wiener N 1938 *American Journal of Mathematics* 897–936

[3] Xiu D and Karniadakis G E 2002 *SIAM Journal on Scientific Computing* **24** 619–644

[4] Oladyshkin S and Nowak W 2012 *Reliability Engineering & System Safety* **106** 179–190

[5] Wan X and Karniadakis G E 2006 *SIAM Journal on Scientific Computing* **28** 901–928

[6] McEwen R P and Parresol B R 1991 *Communications in Statistics-Theory and Methods* **20** 1361–1372

[7] Clerc A, Anderson M, Stuart P and Habenicht G 2012 *Journal of Wind Engineering and Industrial Aerodynamics* **111** 85–94

Article B

Uncertainty propagation through an aeroelastic wind turbine model using polynomial surrogates

Uncertainty propagation through an aeroelastic wind turbine model using polynomial surrogates

Juan Pablo Murcia[a], Pierre-Elouan Réthoré[b], Nikolay Dimitrov[b], Anand Natarajan[b], John Dalsgaard Sørensen[b,c], Peter Graf[d], Taeseong Kim[b]

[a] *jumu@dtu.dk, Department of Wind Energy, Technical University of Denmark. Risø Campus, Frederiksborgvej 399 Building 125. 4000 Roskilde. Denmark*
[b] *Department of Wind Energy, Technical University of Denmark*
[c] *Department of Civil Engineering, Aalborg University*
[d] *National Renewable Energy Laboratory, Colorado USA*

Abstract

In the present work, polynomial surrogates are used to characterize the energy production and lifetime equivalent fatigue loads for different components of the DTU 10 MW reference wind turbine under realistic atmospheric conditions. One of the contributions of the present article is to model the variability caused by different turbulent structures in the inflow. This is done by creating independent surrogates for the mean and standard deviation of each output of the aeroelastic model for different realizations of the turbulent structures. A global sensitivity analysis shows that the turbulent inflow realization has a bigger impact on the total distribution of equivalent fatigue loads than the shear coefficient or yaw miss-alignment. The methodology presented extends the deterministic power and thrust coefficient curves to uncertainty models and adds new variables like damage equivalent fatigue loads in different components of a wind turbine. These surrogate model can then be implemented inside other work-flows such as: estimation of the uncertainty in annual energy production due to wind resources variability and/or robust wind power plant layout optimization. It can be concluded that it is possible to capture the global behavior of a modern wind turbine and its uncertainty under realistic inflow conditions using polynomial response surfaces. The surrogates are a way to obtain power and load estimation under site specific characteristics without sharing the proprietary aero-elastic design.

Keywords: Uncertainty quantification, aeroelasticity, wind turbine model, annual energy production, lifetime equivalent fatigue loads

1. Introduction

The wind turbine design standard IEC 61400-1 [1] provides wind climate specifications which are used as a reference for the structural design of the wind turbines. For achieving type certification of a new turbine model, the designer has to demonstrate that the structural capacity of the turbine is sufficient for withstanding the reference

wind conditions over the entire lifetime of the turbine. Such a demonstration is normally given by dynamic load simulations which characterize the behavior of the turbine under the reference wind conditions. Once certification is achieved, the given turbine model can safely be installed on sites where the wind conditions are identical or more benign than the reference standard conditions. However, in many occasions one or more of the parameters describing the site environmental conditions will be outside the ranges which are sufficiently covered by the IEC reference conditions. In such cases, it is necessary to estimate the actual loads which the turbine will experience over its entire lifetime, by considering the full joint distribution of the variables that describe the turbulent inflow. This is similar to a propagation of uncertainty problem in which the distribution of the atmospheric conditions on the site needs to be propagated through the aeroelastic model of the turbine, see Figure 1.

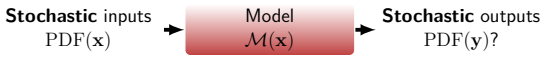

Figure 1: Propagation of uncertainty problem.

If a full design load case setup similar to the IEC 61400-1 design cases is used for that purpose, the problem quickly becomes time-consuming as new dynamic simulations would be required for each site. As an example, the number of simulations required to predict within 1% error the lifetime equivalent fatigue loads on a floating wind turbine can reach up to $3,200,000 = 20^5$ using regular grid-based estimates or in the order of 50,000 using Monte-Carlo (MC) simulation [2]; in this study the inflow conditions (sea/wind fields) are characterized by five stochastic variables. An approach that alleviates these issues is mapping the turbine response to different environmental inputs by means of a fast and accurate surrogate model. Several techniques can be used to predict the behavior of the turbine from a limited set of model evaluations such as: interpolation techniques, response surface techniques, polynomial chaos expansion (PCE), Gaussian process (Kriging) and machine learning techniques.

A quadratic response surface technique based on a circular central composite design has been used to represent the response of a wind turbine to five environmental input parameters [3]. The probability density function (PDF) of the fatigue load in different components of the NREL 5 MW reference turbine has been studied as function of the PDF of four inputs: mean wind speed, yaw error, wind shear exponent and wind veer parameter [4]. A Kriging surrogate has been used as a function of wind speed and turbulent standard deviation to predict the 50 year extreme loads on a 5 MW wind turbine [5]. Two different regression-tree wind turbine surrogates have been developed for power production [6] and for equivalent fatigue loads [7]; these surrogates use machine learning techniques to predict the output of the turbine as a function of wind speed, turbulence intensity and shear exponent.

Polynomial chaos expansion is a methodology used to efficiently propagate input uncertainties through a non-linear model. This methodology consists in building a

polynomial response surface to capture the global dependency of the output as a function of the uncertain inputs. PCE is widely used in the uncertainty quantification field because of its simplicity and fast convergence in comparison to a full MC simulation based on the original model [8, 9, 10, 11, 12]. Furthermore, adaptive PCE training algorithms can be used to obtain a sparse surrogate that minimizes the number of terms that have multiple variable dependency, making the surrogates extremely efficient response surfaces in multiple dimensions [13, 14, 15]. In the case of smooth continuous models with multiple input variables, sparse polynomial chaos expansion methodology is the most efficient technique to build the surrogates in terms of the number of model evaluations required, the number of input dimensions they can handle and the rate of convergence [13].

One of the main difficulties in building a surrogate of an aeroelastic wind turbine model is the fact that the turbulent inflow realization (TIR, i.e. turbulent structures in the flow field) causes variations in the different wind turbine model outputs: such as power, thrust, fatigue and extreme loads in the different components of the turbine. This can be restated as: an aeroelastic wind turbine model has stochastic/non-deterministic outputs. Many studies have analyzed the difficulties of studying fatigue and extreme loads under different turbulent inflow realizations [16, 17, 18, 5, 3]. Different TIR activate different dynamics of the structure and have different control system responses; therefore are an important source of uncertainty in the prediction of the outputs of the model [16]. The high variability in the model response to certain turbulent inflow structures has also been shown to be problematic when MC simulation was used to predict lifetime averages of fatigue loads on a floating wind turbine [2].

1.1. Response to the problem

The aim of the present study is to demonstrate a method for building a quick and accurate surrogate of a wind turbine model that predicts the turbine response as a function of multiple stochastic input variables that describe the turbulent inflow on a site ($\mathbf{x}$). The surrogate for the turbine model is a set of two independent sparse polynomial response surfaces that allow to predict the variability caused by different input variable distributions and by different turbulent inflow field realizations (TIR). One response surface characterizes the expected output with respect TIR: $\hat{y}_{\mathbb{E}}(\mathbf{x}) \approx \mathbb{E}_{\text{TIR}}(y|\mathbf{x})$. The other one describes the standard deviation of the output with respect TIR: $\hat{y}_{\mathbb{S}}(\mathbf{x}) \approx \sqrt{\mathbb{V}_{\text{TIR}}(y|\mathbf{x})}$; which is a model that predicts the uncertainty in the turbine response due to different turbulent structures hitting the turbine. Finally, a sample can be obtained from the normal distribution constructed using the mean and the standard deviation surrogates in order to make a prediction of the variability in the output at a given input point:

$$\hat{y}(\mathbf{x}) \sim \text{Normal}(\hat{y}_{\mathbb{E}}(\mathbf{x}),\, \hat{y}_{\mathbb{S}}(\mathbf{x})) \tag{1}$$

The final surrogate $\hat{y}(\mathbf{x})$ can then be used to obtain distributions of the wind turbine power and loads in a given year whose input parameters (or wind/sea, or

wind/geological) follow the distribution used to train the surrogate PDF($\mathbf{x}$). Since the surrogate is a response surface it can also be used to predict the distribution of the outputs when the input distributions is close but not exactly the distribution used for training the surrogate. This setup is considered a multi-leveled uncertainty propagation and it is the scenario that occurs when there is uncertainty in the parameters that characterize the WS distribution for example. This approach is necessary to estimate the uncertainty in annual energy production and lifetime averaged equivalent fatigue load.

1.2. Article overview

A general overview of the PCE methodology in multiple dimensions is presented in section 2. This section describes the Rosenblatt transformation, the design of experiments used to define the training simulation points, the approach used to train sparse polynomial response surfaces and the logistic transformation used to limit the output. In section 3, the methodology is then applied to the response of the DTU 10 MW reference wind turbine HAWC2 model [19] to turbulent inflow fields characterized by four input parameters. The four input parameters are the 10-min averaged hub height wind speed, the turbulent standard deviation of the instantaneous wind speed in the streamwise component, the shear exponent and the yaw misalignment angle. A study of how many independent realizations of the turbulent inflow field are required to achieve a certain error tolerance in the surrogate is presented in the section 3.7. Finally in section 3.8, the surrogates are used in an example of prediction of the uncertainty in the annual energy production and the uncertainty in lifetime averaged equivalent fatigue loads.

2. Methods

This article proposes the use of two different variable transformations to simplify the polynomial response surface fitting problem, see Figure 2. The first transformation is the Rosenblatt transformation [20], which is used to de-correlate the set of D input variables $\mathbf{x} = (x_0, x_1, \dots x_{D-1})$ into a set of independent uniform variables, $\mathbf{w} = (w_0, w_1, \dots w_{D-1})$. The second transformation is a logistic transformation, and it is used to enforce constraints on the polynomial surrogates [21]. This transformation enables the use of polynomial surrogates in problems where the output has a minimum and/or maximum value. Without the logistic transformation the polynomial surrogates will present oscillations in the regions where the model has a constant output. The power production of a turbine is an example of a variable with a strict upper constraint corresponding to the rated power.

2.1. 1D PCE theory

Consider a model with a single uncertain input (x) and a single output (y). PCE consists in defining a polynomial family that is orthogonal with respect the input distribution, PDF(x). Orthogonal polynomial families with respect the most important

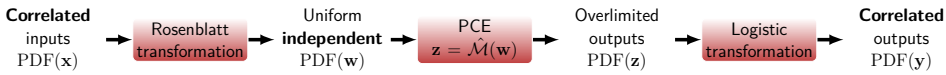

Figure 2: Transformation of variables to build efficient polynomial response surface.

distributions are well known, see table 1. For details on how to define new polynomial basis to an arbitrary input distributions refer to Gautschi et al [22].

Distribution	Polynomial Family
Uniform	Legendre
Normal	Hermite
Exponential	Laguerre

Table 1: Classical orthogonal polynomial families.

The orthogonal polynomials are used to build a polynomial approximation of the output, i.e. a polynomial response surface, see equation 2. Where, $\phi_l(x)$ is the l order orthogonal polynomial, c_l is its correspondent coefficient and M represents the truncation order of the PCE.

$$y(x) \approx \hat{y}(x) = \sum_{l=0}^{M} c_l \, \phi_l(x) \tag{2}$$

There are two different approaches to determine the c_l coefficients:

Semi-Spectral projection consists in using quadrature rules to approximate the inner product definition of the coefficient, see eq. 3. Many quadrature rules exist to approximate the integrals; but all quadrature rules give N_n nodes for model evaluation (x_i) and their corresponding weights (ω_i). Gaussian quadrature rules are widely used because they are accurate for smooth function integration with respect a weight function, in this case the PDF(x), see equation 3.

$$c_l = \langle y, \phi_l \rangle \equiv \int y(x) \, \phi_l(x) \, \mathrm{PDF}(x) \, dx \approx \sum_{i=0}^{N_n} \omega_i \, y(x_i) \, \phi_l(x_i) \tag{3}$$

In general, semi-spectral projection is an efficient method for low number of input dimensions, but the number of model evaluations required grows exponentially with the number of dimensions. Additionally, quadrature rules can be unstable for heavy tailed PDFs such as the Weibull distribution [22].

Point collocation consists in fitting the polynomial basis to a small sample of model evaluations. Traditionally, this fit can be done using least squares algorithm, but some other optimization algorithms can be used to obtain PCE approximations that minimize the number of terms in the surrogate [13, 14, 15]. This techniques are explained in

the section 2.5. In general, point collocation is robust and the advanced optimization algorithms are designed to handle large number of dimensions, to avoid over-fitting and to achieve sparsity in the final surrogate. The present study focuses only in the point collocation techniques since the number of model evaluations required to fit a multiple dimensional PCE is smaller [13] than in other methods.

2.2. Rosenblatt transformation

To build the PCE of a model with multiple correlated inputs ($\mathbf{x}$), it is required to initially transform the correlated input space into an uncorrelated space ($\mathbf{w} = R^{-1}(\mathbf{x})$). In this article, the Rosenblatt transformation is used because the input distribution of the turbulent inflow field parameters are usually defined in a sequence of conditional relationships [20]. Refer to Dimitrov et al [23] and Graf et al [2] for examples of such distributions used for offshore and floating wind turbine fatigue and extreme load analysis.

Since all the variables are transformed into uncorrelated unitary uniform variables then the PCE only requires the use of the Legendre polynomials: $y(\mathbf{x}) = y(R(\mathbf{w})) \approx \hat{y}(\mathbf{w})$.

2.3. Multi-dimensional PCE

A D-dimensional polynomial is constructed as the sum of the product between individual one dimensional polynomials for each of the D uniform input variables, $\mathbf{w} = [w_0, \ldots, w_{D-1}]$. The D-dimensional surrogate is written using a set of multiple indexes $\mathcal{I} \subset \mathbb{N}^D$. An element $J \in \mathcal{I}$ contains the order of the polynomial in each dimension: $J = [l_0, \ldots, l_{D-1}]$. Additionally, the multiple indexes are enumerated, $J \leftrightarrow j \in \mathbb{N}$. A surrogate that contains N_c terms can be written as:

$$y(\mathbf{x}) = y(R(\mathbf{w})) \approx \sum_{j=0}^{N_c-1} c_j \, \boldsymbol{\phi}_j(\mathbf{w}) \tag{4}$$

where an element in the multidimensional polynomial basis is given as:

$$\boldsymbol{\phi}_j(\mathbf{w}) = \phi_{l_0}(w_0) \times \cdots \times \phi_{l_{D-1}}(w_{D-1}) \tag{5}$$

2.4. Training point selection

The Rosenblatt transformation enables the use of multiple variance reduction MC sampling techniques to define the training points of a surrogate [24]. Latin hypercube sampling [25], Sobol sequence [26] and Hammersley sequence [27] are some examples of such techniques. These techniques are designed to sample from the unitary hypercube of D dimensions, i.e. the uniform distributed variables: $\mathbf{w}_i \sim \mathrm{PDF}(\mathbf{w})$. Finally, the Rosenblatt transformation is used to transform each realization in the uniform sample into the correlated input space, $\mathbf{x}_i = R(\mathbf{w}_i) \sim \mathrm{PDF}(\mathbf{x})$.

The number of unknown coefficients c_j in a D-dimensional PCE depends of the total polynomial order of the PCE. The total order is defined as the maximum sum

of the one dimensional orders. If the PCE is truncated to a total order M then the number of unknown coefficients is given by the following combination:

$$N_c = \binom{M+D}{M} = \frac{(M+D)!}{M!\,D!} \tag{6}$$

The number of model evaluations should be between 2 or 3 times the number of unknowns in order to have extra data to test the accuracy of the surrogate and to implement strategies to avoid over-fitting [13]. Note that the maximum order is only used to estimate the number of model evaluations. Advanced regression techniques allow to explore higher order terms [15, 13]. The maximum order M can be increased in order to achieve higher accuracy surrogates but at the cost of having more model evaluations and the requirement of assuring that there is not over-fitting.

2.5. Point collocation and the LASSO problem

The least absolute shrinkage and selection operator (LASSO) problem is a modified least squares optimization problem that adds a term that penalizes the amount of active terms in the surrogate (terms with non zero coefficients). LASSO is used to achieve sparsity and to avoid over fitting in the polynomial surrogate. Additionally, the number of model evaluations required for solving the LASSO problem is smaller in comparison to a least squares regression that has the same maximum total polynomial order [13].

A LASSO problem can be described as finding the set of coefficients c_j that minimizes the sum of squared errors plus the sum of the absolute values of all coefficients (ℓ_1 norm regularization term) [15]:

$$\min_{c_j} \quad \sum_{i=0}^{N-1} \left[\sum_{j=0}^{N_c-1} c_j \boldsymbol{\phi}_j(\mathbf{w}_i) - y(\mathbf{x}_i) \right]^2 + \alpha \sum_{j=0}^{N_c-1} |c_j| \tag{7}$$

where the number of model/surrogate evaluation points N is fixed. Note that the input and surrogate evaluation points are related by the Rosenblatt transformation $\mathbf{x}_i = R(\mathbf{w}_i)$. The maximum number of possible terms of the surrogate N_c is fixed by selecting a maximum total multi-dimensional polynomial order.

The regularization coefficient α controls the amount of active terms in the final solution. Smaller values allow to have more active terms while larger values will prefer final surrogates with few active terms. A sparse surrogate has the advantage of making the evaluation of the multi-dimensional surrogate faster in comparison to the full least squares solution; this advantage becomes critical in high number of input dimensions.

There are two algorithms widely used to solve the LASSO problem: coordinate descent [15] and least angle regression (LAR) [13]. Coordinate decent is used in the present work because it tends to be more stable for high dimensional problems [14]. The reason for this is that coordinate descent operates on a given regularization coefficient instead of exploring the full space of α's as in LAR algorithm.

Cross-validation is used to select the regularization coefficient α that minimizes over fitting of the data. A k-fold cross-validation consists in splitting the dataset into

k groups of data. All the points in k-1 groups are used for training and the remaining group is used for cross-validation. This means that the surrogate fitted using k-1 groups is used to predict the output in each of the elements of the remaining group. The mean squared error of the prediction of the surrogate is then computed. This process is repeated leaving out each individual fold and for multiple regularization parameters. The regularization parameter that gives the lowest mean cross-validation mean squared errors is then selected to train the whole dataset. This translates as selecting the sparse model that performs the best by predicting missing data, i.e. that has less over-fitting.

2.6. Logistic transformation

A logistic transformation is applied to an output of the model in order to avoid oscillations in the regions where the model is constant. In practice this transformation is used to impose strict restrictions on the polynomial surrogates. The transformation consists in applying the *logit* function, $L(p) = \ln\left(\frac{p}{1-p}\right)$, to the model output at the training points $y_i = y(\mathbf{x}_i)$ into the over-shooting variable space: $z_i = L(a_1\, y_i + a_0)$ [21]. Finally, each time the surrogate is evaluated, the prediction of the surrogate is transformed back to the original output space $\hat{y} = (L^{-1}(\hat{z}) - a_0)/a_1$. The constants of the transformation are calibrated in order to impose the constrains of the output and to avoid numerical instabilities that are inherent to the logit function.

2.7. Global sensitivity analysis

Global sensitivity analysis (SA) is a methodology to determine how important each input is to explain the variance of the output. SA can be obtained with a Sobol variance decomposition [28]. In this technique, the variance of the output is explained into the different terms of variance of each of the inputs, in a process similar to the analysis of the variance of experiments (ANOVA) [29]. Total effect Sobol indices are widely used as measures of how much of the variance of a given output is explained by the variance of an input, including possible interactions with other variables. This method is the most recognized method for global sensitivity analysis because it accounts for non-linear dependencies and for interactions between variables [30].

Variance decomposition can be expressed as the sum of the variance of the marginal expected value of a subset of input variables, see eq. 8. Note that this decomposition is not an infinite series expansion, it is truncated to the maximum number of variable interactions.

$$
\begin{aligned}
\mathbb{V}(y) = \sum_{k=0}^{D-1} \mathbb{V}_k + \sum_{k=0}^{D-1}\sum_{l>k}^{D-1} \mathbb{V}_{kl} + \sum_{k=0}^{D-1}\sum_{l>k}^{D-1}\sum_{m>l}^{D-1} \mathbb{V}_{klm} + \cdots + \mathbb{V}_{0\ldots D-1} \\
\mathbb{V}_k = \mathbb{V}\left(\mathbb{E}_{\forall n\neq k}\left(\mathcal{M}(\mathbf{x}|x_k)\right)\right) \\
\mathbb{V}_{kl} = \mathbb{V}\left(\mathbb{E}_{\forall n\neq k,l}\left(\mathcal{M}(\mathbf{x}|x_k, x_l)\right)\right) \\
\mathbb{V}_{klm} = \mathbb{V}\left(\mathbb{E}_{\forall n\neq k,l,m}\left(\mathcal{M}(\mathbf{x}|x_k, x_l, x_m)\right)\right)
\end{aligned}
\tag{8}
$$

The global sensitivity measure is defined by normalizing eq. 8 with the total variance of the output $\mathbb{V}(y)$. From this normalization one can define the Sobol index of a given degree of interaction between input variables as:

$$S_k = \frac{\mathbb{V}_k}{\mathbb{V}(y)} \qquad S_{kl} = \frac{\mathbb{V}_{kl}}{\mathbb{V}(y)} \qquad S_{klm} = \frac{\mathbb{V}_{klm}}{\mathbb{V}(y)} \quad \dots \tag{9}$$

The total effect Sobol index of an input variable x_i is then the sum of all the Sobol indices that include the variable in any interaction:

$$S_{\text{total}\,x_i} = S_i + \sum_{\substack{k=0 \\ k\neq i}}^{D-1} S_{ik} + \dots \tag{10}$$

The sensitivity analysis of the response of the turbine should consider the effect of having different turbulent inflow realizations. The turbulent inflow is modeled with the two independent PCE for the local mean and local standard deviation. Therefore, even though the Sobol indexes could be computed directly from the PCE coefficients, see Sudret et al [31], they would not include the effect of the turbulence inflow realization. To solve this limitation, the approximate method proposed in Saltelli et. al [30] is used to compute the total effect Sobol indexes. This approach estimates the total effect Sobol indexes from a large MC simulation.

3. Results

3.1. Implementation

Several open source implementations of PCE methods are available such as: Chaospy [24], Dakota [32], UQLab [33] and OpenTurns [34]. In the present work we use Chaospy because of its implementation of the Rosenblatt transformation. Additionally, the present work uses the LASSO problem solvers [15] and the cross-validation capabilities available in the open source library Scikit-learn [14]. These capabilities are used inside of Chaospy for general users and are used externally in the present study to gain control over the different stages of the cross-validation.

3.2. Case description

The model consists of the DTU 10 MW reference wind turbine HAWC2 model [35, 19] with Mann turbulent inflow generation [36]. The turbulent inflow conditions are defined using the four variables described in table 2.

The dependency between WS and σ_1 is defined in the Normal Turbulence Model described in the IEC 61400-1 [1]. The present case uses a reference ambient turbulence intensity of a site Class 1A: $\text{TI}_{\text{ref}} = 0.16$. This dependency is given by the local statistical moments of σ_1 as:

$$\begin{aligned} \mathbb{E}(\sigma_1|\text{WS}) &= \text{TI}_{\text{ref}}\,(0.75\text{WS} + 3.8) \\ \mathbb{V}(\sigma_1|\text{WS}) &= (1.4\,\text{TI}_{\text{ref}})^2 \end{aligned} \tag{11}$$

Input	Variable	Distribution	Parameters	
10-min mean hub height wind speed	$x_0 = \text{WS}$	Rayleigh	$\mathbb{E}(\text{WS}) = 10$ m/s	
Std. of the inst. wind speed in the streamwise direction during the 10-min simulation	$x_1 = \sigma_1$	Lognormal	$\mu_{\sigma_1}(\text{WS})$	$\sigma_{\sigma_1}(\text{WS})$
10-min mean shear exponent	$x_2 = \alpha$	Normal	$\mu_\alpha(\text{WS})$	$\sigma_\alpha(\text{WS})$
10-min mean yaw miss-align.	$x_3 = \gamma$	Normal	$\mu_\gamma = 0$	$\sigma_\gamma = 5$ deg.

Table 2: Wind turbine model inputs.

The correlation between α and WS is based on the simplified joint distribution defined by Dimitrov et al [23]:

$$\begin{aligned} \mu_\alpha &= 0.088(\ln(\text{WS}) - 1) \\ \sigma_\alpha &= 1/\text{WS} \end{aligned} \tag{12}$$

Seven different model outputs are considered ($\mathbf{y}$), see table 3. The damage equivalent fatigue loads (EFL) are computed using a rainflow counting algorithm to determine the number of load cycles n_i with their corresponding load range S_i in the 10-min time series of turbine response. The EFL is then weighted using different materials' Wöhler exponent m, see equation 13 by Miner et al [37]. For obtaining 1Hz-equivalent fatigue loads based on 10 minute reference periods, the reference number of load cycles used is $N_{\text{ref}} = 600$.

$$S_{\text{eq}} = \left(\frac{\sum n_i S_i^m}{N_{\text{ref}}} \right)^{\frac{1}{m}} \tag{13}$$

Output	m	Variable
10 minute mean power production	-	P
10 minute mean thrust coefficient	-	CT
EFL blade root flapwise bending moment	12	BRF
EFL tower bottom fore-aft bending moment	4	TBF
EFL tower bottom sidewise bending moment	4	TBS
EFL tower top tilt bending moment	4	TTT
EFL tower top yaw bending moment	4	TTY

Table 3: Wind turbine model outputs.

3.3. Training points

In this study, the number of model evaluations are set to be $N = 2\,N_c$, the maximum order of the polynomial is expected to be $M = 4$ and the number of input

variables is $D = 4$. This leads to 140 total number of model evaluations, i.e. 140 input variables locations for which HAWC2 model is executed, see equation 6. A Hammersley sequence [27] is preferred over other variance reduction methods to generate the training sample in the uniform space as it is a sequence that can be extended to contain larger sample size without changing the previous points [24, 38]. The uniform sample is then transformed into the physical variables using the Rossenblat transformation. A similar approach is used to generate the input sample for a MC simulation; the size of the MC sample is taken to be 80000. The training input sample is shown in Figure 3 as well as a the inputs sample for the MC simulation. Figure 3 is a representation of the multidimensional PDF($\mathbf{x}$): the histograms represent the marginal distributions for each variable, while the plots in the lower diagonal represent the training points and bi-dimensional histograms of the MC sample. The figures in the lower diagonal show the correlations between each pairs of variables as well as the iso-pdf quantiles that enclose 68%, 95% and 99.7% of the data. It can be observed that the training points are more densely distributed in the regions of higher probability of the inputs. This means that the surrogate is better trained in the most likely regions of the input space. 100 different turbulent inflow realizations are generated using the Mann model for each input point, for which the mean and standard deviation of the outputs are obtained. This number is selected to test the accuracy of the prediction of the surrogates when they are trained using a reduced number of TIR as it is defined in the design load cases defined in the standard [1]. The full training sample consists of 140×100 HAWC2 10 minutes simulations.

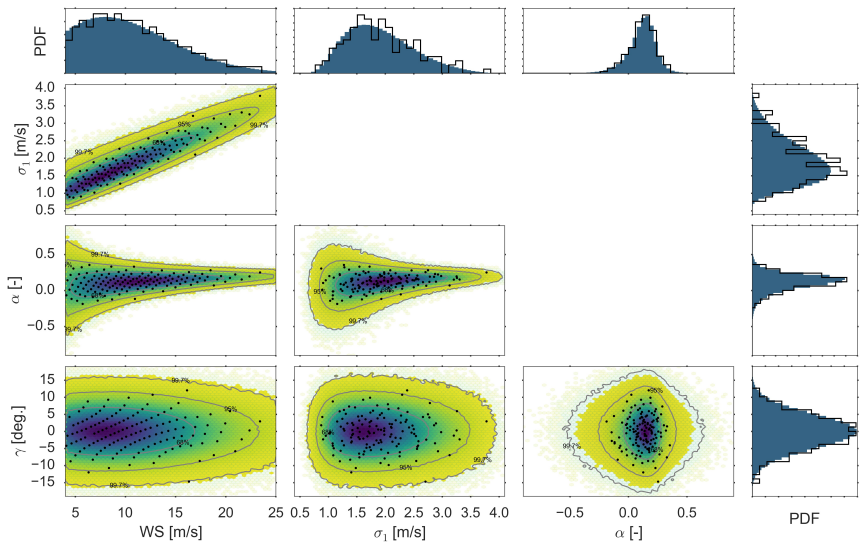

Figure 3: (Black points) Training dataset in the inputs: 140 Hammersley sequence sample of input joint distribution. (Histogram colored hex-bins) 80000 Hammersley sequence MC sample.

3.4. Example of PCE surrogates for individual statistical moments

Some examples of the distribution of $\mathbf{y}_{\mathbb{E}}$ and $\mathbf{y}_{\mathbb{S}}$ [1] are shown in Figure 4. In this figure the black points represent the observed statistic of the output for the training points; while the bi-dimensional histogram represents the obtained distribution of the surrogate for a 80000 MC sample. The observed histogram in the training dataset and the PDF predicted by the surrogate for $\mathbf{y}_{\mathbb{E}}$ and $\mathbf{y}_{\mathbb{S}}$ are shown in the last column in Figure 4. It can be observed that the surrogates accurately capture the global PDF of the model and its dependency with respect to the 4 input variables. The surrogates of the local standard deviations, $\hat{y}_{\mathbb{S}}$, are not able to capture the behavior of some extreme cases, see the extreme points at low wind speeds in the plots for $\mathrm{CT}_{\mathbb{S}}$ and $\mathrm{BRF}_{\mathbb{S}}$. These errors are small in comparison to the overall magnitude of the output; the distribution of the errors of the surrogates and its impact in the final prediction are quantified in section 3.7. These errors can be reduced up to a tolerance level selected by the user by adding more training points (input points with their turbulent inflow realizations). The surrogates are robust enough to predict the frequency of occurrence of extreme values such as the outputs resulting from the input point with largest σ_1, see first and third row in Figure 4. This point seems to be outside the main trend in WS in Figure 4 because it has a large σ_1 and α given its WS, see Figure 3.

3.5. Final surrogate predictions

The surrogates of $\mathbf{y}_{\mathbb{E}}$ and $\mathbf{y}_{\mathbb{S}}$ are combined to estimate the distribution of each individual output of the DTU 10 MW RWT. The prediction is done by sampling the normal distribution constructed using the surrogates of $\mathbf{y}_{\mathbb{E}}$ and $\mathbf{y}_{\mathbb{S}}$, see equation 1. These results are presented in Figure 5 along with the full dataset of HAWC2 simulations. In this figure each cross represents an individual 10-min simulation, therefore the scatter of nearby simulations illustrates the stochasticity in the output of the aeroelastic simulation. The amount of local output variability due to the turbulent inflow realization, varies between outputs and depends on the region of the input space. The effect of the turbulent inflow realization is more important for the fatigue loads than for power and thrust coefficient. Figure 5 also presents the bi-dimensional histogram obtained with a 80000 MC simulation of the surrogate. The distribution predicted by the surrogate captures the dependency and variability of each output with respect the four input variables; the iso-PDF quantiles that encircle the 68%, 95% and 99.7% of the MC sample are also shown in the Figure 5 and they give a visual estimation of how likely are the observations of the output. It can be observed that the surrogate estimates the regions that contribute more on the lifetime fatigue and even gives an estimation of the input region on which the largest damage is to be expected. Additionally the MC simulation on the surrogate gives an estimation of the PDF for each variable, see fifth column in Figure 5.

[1] $P_{\mathbb{S}}$ represents the standard deviation of 100 different realizations of the 10-min averaged power; this variable should not be confused with the standard deviation of the instantaneous power during the 10 minutes of simulation.

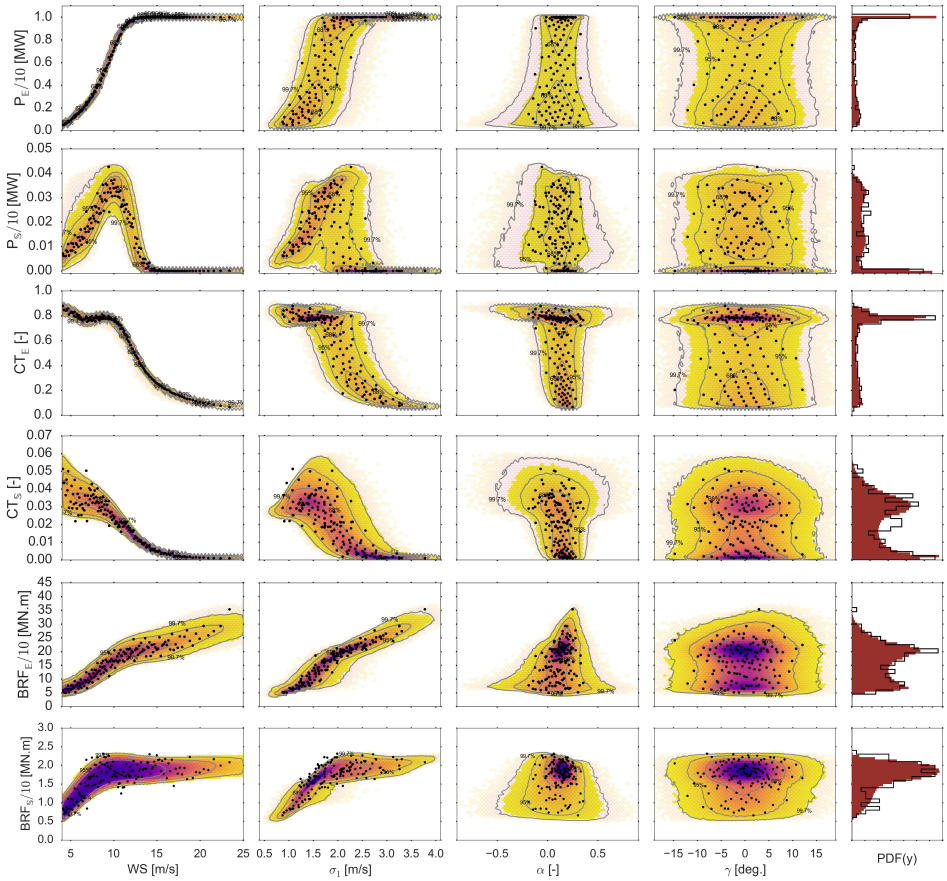

Figure 4: Example of surrogates for individual mean output and std. of the output with respect TIR. (Black points) 140 training points. (Histogram colored hex-bins) 80000 Monte-Carlo simulation on the surrogate. (Contour lines) Iso-PDF lines that encircle 68%, 95% and 99.7% of the Monte-Carlo simulation on the surrogate.

The obtained distribution of power shows a similar behaviour to the operational data of wind turbines; this shows that one of the main drivers for variability in the prediction of power below rated is the TIR. Similarly, the thrust coefficient shows large variability for wind speeds below rated; this large variability can become important for wake models that use the thrust coefficient to predict the strength of the wake of a turbine and its impact on other turbines in a wind farm. The fatigue load blade root and tower top bending moments (BRF, TTT and TTY) show similar dependency on the four input variables and a similar amount of variability due to TIR; this is because they are all driven by the streamwise flow field. The fatigue loads tower bottom bending

moments (TBF and TBS) show a different dependency on the input variables, mainly because they are driven by the thrust and sidewise forces; this two outputs have larger variability at lower WS which generate both the largest and lowest observations.

3.6. Sensitivity analysis

The global sensitivity analysis (SA) for the outputs are presented in Table 4. The total effect Sobol indexes are computed using the approximation presented by Saltelli et al [30]. The total effect Sobol index represents the non-linear influence of the input variable in the total variance of the output. Most of the outputs have a large total Sobol index for the wind speed. WS is clearly the main variable to explain the power and loads in a wind turbine. The SA shows that the power and thrust coefficient can be explained almost fully by the WS, since all the terms in the surrogate have WS dependency.

The variance introduced by the turbulent inflow realization is an important component for all the outputs, it has a higher influence than σ_1 for most outputs. This counter intuitive result is due to the large amount of correlation between WS and σ_1; this causes that a large fraction of the variance of the output generated by σ_1 is already explained by WS. The shear and yaw have reduced effects over most output variables. The yaw miss alignment has reduced total effect because its assumed distribution is centered around zero. The shear exponent becomes important only for capturing the fatigue at the tower top tilt and yaw bending moments (TTT, TTY); while the yaw misalignment becomes important for modeling the fatigue at the tower bottom fore-aft moment (TBF).

	WS	σ_1	α	γ	TIR
P	1.0	2.4×10^{-4}	3.1×10^{-4}	8.1×10^{-5}	3.1×10^{-3}
	1st	3rd	4th	5th	2nd
CT	9.9×10^{-1}	1.2×10^{-3}	1.3×10^{-3}	6.5×10^{-4}	9.8×10^{-3}
	1st	3rd	4th	5th	2nd
BRF	8.8×10^{-1}	5.6×10^{-2}	1.5×10^{-2}	3.4×10^{-3}	6.7×10^{-2}
	1st	3rd	4th	5th	2nd
TBF	5.9×10^{-1}	2.1×10^{-1}	3.6×10^{-4}	1.0×10^{-3}	3.0×10^{-1}
	1st	3rd	5th	4th	2nd
TBS	7.1×10^{-1}	7.6×10^{-2}	2.1×10^{-3}	2.3×10^{-4}	3.0×10^{-1}
	1st	3rd	5th	4th	2nd
TTT	8.7×10^{-1}	7.1×10^{-2}	3.3×10^{-4}	5.7×10^{-4}	7.7×10^{-2}
	1st	3rd	5th	4th	2nd
TTY	8.7×10^{-1}	6.8×10^{-2}	2.2×10^{-4}	9.6×10^{-4}	7.2×10^{-2}
	1st	3rd	5th	4th	2nd

Table 4: Total influence Sobol index.

The sensitivity analysis conditioned on WS for the outputs are presented in Table 5. It can be observed that for power and thrust coefficient the influence of TIR goes from being the main source of variability at WS below rated to become the least important for WS above rated; this result summarizes the influence of the pitch controller enforcing the power and limiting the thrust. The effect of TIR in the fatigue loads is more uniform through all the ranges of operation. Similarly to the global SA , the

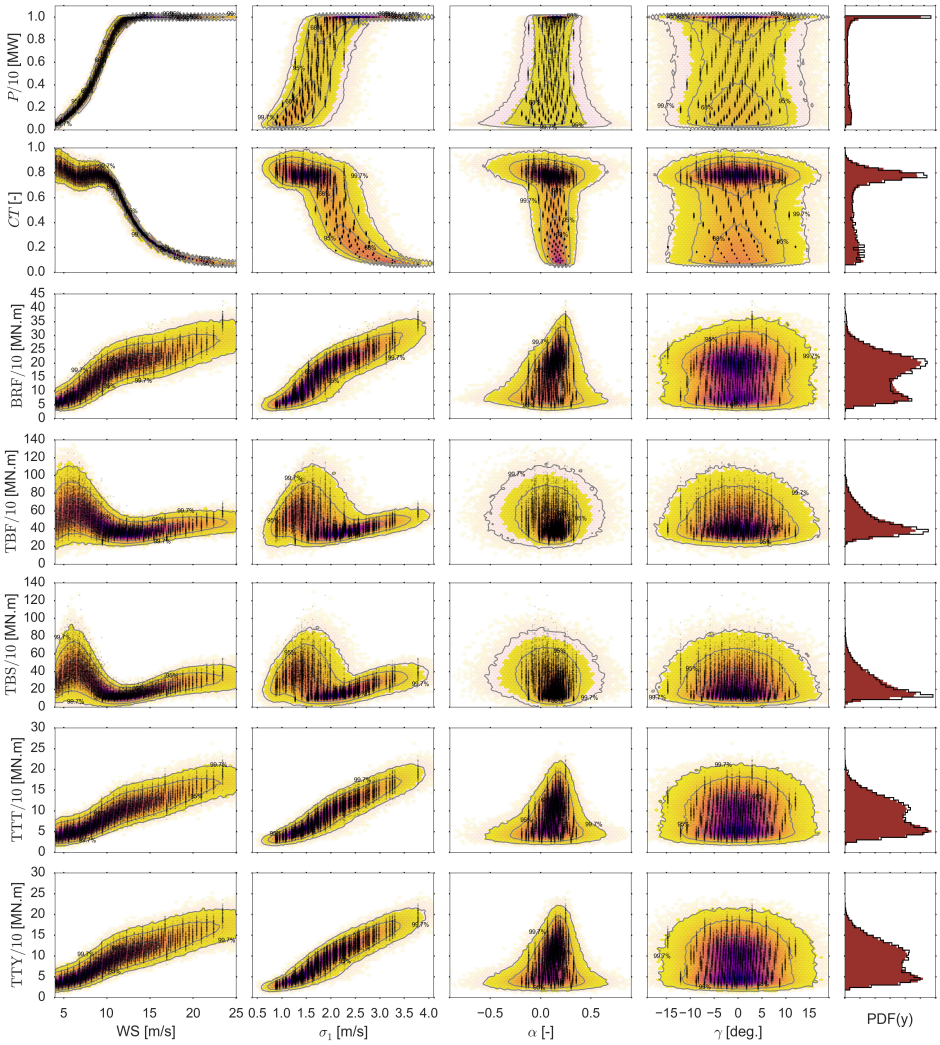

Figure 5: (Black crosses) 10-min HAWC2 simulation for the 140 input sample x 100 turbulent inflow realizations. (Histogram colored hex-bins) 80000 Monte-Carlo simulation of the surrogate. (Contour lines) Iso-PDF lines that encircle 68%, 95% and 99.7% of the Monte-Carlo simulation on the surrogate.

main variables required to explain the equivalent fatigue loads are TIR and σ_1. This is also true for the power and thrust coefficient for WS bellow rated.

	WS=8 ms^{-1}				WS=12 ms^{-1}				WS=16 ms^{-1}			
	σ_1	α	γ	TIR	σ_1	α	γ	TIR	σ_1	α	γ	TIR
P	1.1×10^{-1}	1.4×10^{-1}	2.8×10^{-2}	7.9×10^{-1}	7.8×10^{-2}	3.7×10^{-2}	2.5×10^{-2}	9.8×10^{-1}	3.0	1.6	3.7	9.7×10^{-1}
	3rd	2nd	4th	1st	2nd	3rd	4th	1st	2nd	3rd	1st	4th
CT	5.1×10^{-2}	1.1×10^{-1}	3.7×10^{-2}	8.6×10^{-1}	2.4×10^{-1}	2.1×10^{-1}	1.5×10^{-1}	6.4×10^{-1}	6.1×10^{-1}	4.3×10^{-1}	3.3×10^{-1}	2.0×10^{-1}
	3rd	2nd	4th	1st	2nd	3rd	4th	1st	1st	2nd	3th	4th
BRF	4.8×10^{-1}	3.3×10^{-2}	1.1×10^{-2}	5.0×10^{-1}	3.9×10^{-1}	1.0×10^{-1}	9.2×10^{-3}	5.1×10^{-1}	3.5×10^{-1}	1.8×10^{-1}	2.7×10^{-2}	4.6×10^{-1}
	2nd	3rd	4th	1st	2nd	3rd	4th	1st	2nd	3rd	4th	1st
TBF	3.7×10^{-1}	4.6×10^{-4}	1.9×10^{-3}	6.5×10^{-1}	5.6×10^{-1}	2.1×10^{-3}	1.9×10^{-3}	4.5×10^{-1}	5.2×10^{-1}	3.6×10^{-3}	4.0×10^{-3}	4.8×10^{-1}
	2nd	4th	3rd	1st	1st	3rd	4th	2nd	1st	4th	3rd	2nd
TBS	1.9×10^{-1}	3.2×10^{-3}	6.8×10^{-4}	8.3×10^{-1}	2.4×10^{-1}	8.7×10^{-4}	1.7×10^{-3}	7.8×10^{-1}	2.2×10^{-1}	1.4×10^{-3}	1.5×10^{-3}	7.9×10^{-1}
	2nd	3rd	4th	1st	2nd	4th	3rd	1st	2nd	4th	3rd	1st
TTT	5.6×10^{-1}	2.2×10^{-3}	4.0×10^{-3}	4.5×10^{-1}	4.6×10^{-1}	1.3×10^{-3}	3.6×10^{-3}	5.5×10^{-1}	4.6×10^{-1}	2.5×10^{-3}	3.5×10^{-3}	5.4×10^{-1}
	1st	3rd	4th	2nd	2nd	4th	3rd	1st	2nd	4th	3rd	1st
TTY	5.3×10^{-1}	1.9×10^{-3}	1.9×10^{-3}	4.8×10^{-1}	4.6×10^{-1}	5.6×10^{-4}	4.5×10^{-3}	5.5×10^{-1}	4.7×10^{-1}	1.7×10^{-3}	1.2×10^{-2}	5.3×10^{-1}
	1st	3rd	4th	2nd	2nd	4th	3rd	1st	2nd	4th	3rd	1st

Table 5: Total influence Sobol index at different WS.

3.7. Convergence

A leave-one-out cross-validation (LOO) is done to estimate the distribution of the prediction error of each surrogate as a function of the number of independent turbulent seeds per input points used in the surrogate training. A LOO is a cross validation in which the surrogate is trained leaving on point out. Then, the local statistical moments of the output predicted by the surrogates at the missing point are compared against the statistics computed using the surrogate. In this article, the prediction errors are normalized with respect to the maximum scale of the output variable, which means that the errors represent the fraction of the total scale that should be considered as an extra uncertainty due to the inadequacy of the surrogate. The prediction error for the local mean surrogate is defined as:

$$\epsilon_{y\,\mathbb{E}} = \frac{y_{\mathbb{E}}(\mathbf{x}_{LO}) - \hat{y}_{\mathbb{E}}(\mathbf{x}_{LO})}{\max(y)} \tag{14}$$

while the prediction error for the local standard deviation surrogate is defined as:

$$\epsilon_{y\,\mathbb{S}} = \frac{y_{\mathbb{S}}(\mathbf{x}_{LO}) - \hat{y}_{\mathbb{S}}(\mathbf{x}_{LO})}{\max(y)} \tag{15}$$

The convergence of the prediction error of the statistical moments is shown in Figure 6. It can be seen that all the prediction errors tend to be distributed around zero and their standard deviations converge as the number of turbulent inflow realizations per input are increased. The errors converge to the distribution of the errors to the current surrogate. New input points need to be added to the training data set in order to further narrow the converged distribution of surrogate errors. In this figure the outliers are the extreme cases of selecting seeds with similar outputs, therefore, they are those cases

that have large errors in the statistical moments. Finally, the converged distribution can be used to estimate the uncertainty in the final prediction of the output as:

$$\hat{y}(\mathbf{x}) \sim \text{Normal}(\hat{y}_{\mathbb{E}}(\mathbf{x}) + \epsilon_{y\,\mathbb{E}}\, max(y), \quad \hat{y}_{\mathbb{S}}(\mathbf{x}) + \epsilon_{y\,\mathbb{S}}\, max(y)) \tag{16}$$

where the errors of the surrogates can be sampled from the distribution predicted using LOO cross validation, see Figure 6:

$$\epsilon_{y\,\mathbb{E}} \sim \text{Normal}(\mathbb{E}(\epsilon_{y\,\mathbb{E}}), \mathbb{S}(\epsilon_{y\,\mathbb{E}})) \quad \epsilon_{y\,\mathbb{S}} \sim \text{Normal}(\mathbb{E}(\epsilon_{y\,\mathbb{S}}), \mathbb{S}(\epsilon_{y\,\mathbb{S}})) \tag{17}$$

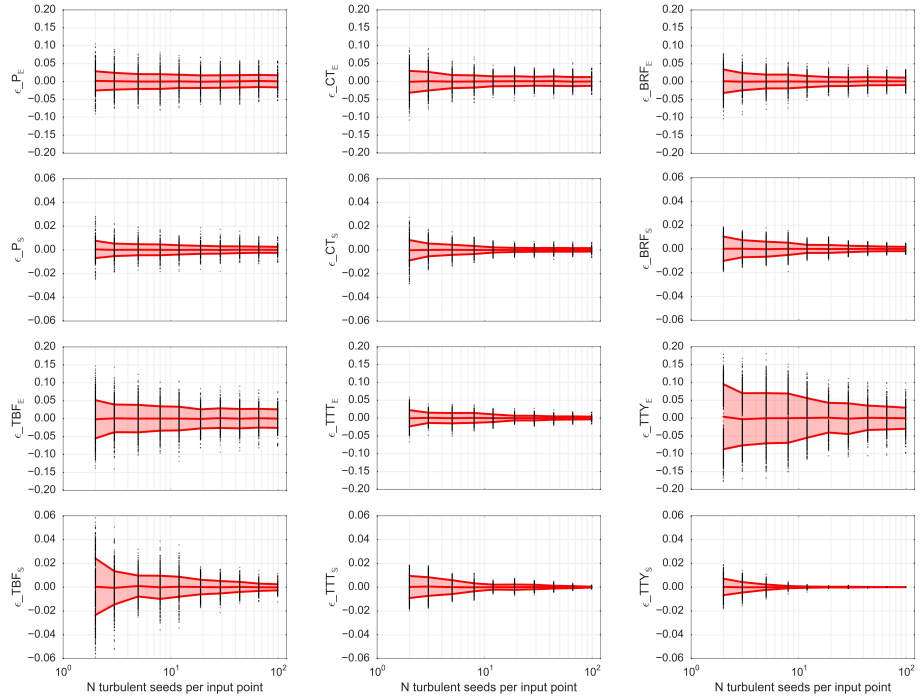

Figure 6: Convergence of the LOO cross-validation prediction error as a function of the number of turbulent seeds per input point used in PCE training. (Pink area) One standard deviation confidence interval around the mean $\mathbb{E}(\epsilon) \pm \mathbb{S}(\epsilon)$.

3.8. Example of using the surrogates for the estimation of the uncertainty in annual energy production and lifetime equivalent fatigue loads

This section presents an example to illustrate the use of the surrogates of the DTU 10 MW RWT to estimate the uncertainty in the distribution of expected energy production and of equivalent fatigue loads $\mathbb{E}_{\mathbf{x}}(\mathbf{y})$ in a given return period; here the

averaging period is either 1 year or 20 years. In this example a single turbine is planned to operate in a location from which the uncertainty in the wind resources has been estimated before hand. This uncertainty can represent the year-to-year variability, the effect of the long-term correction, uncertainty in the wind resources assessment tool, among other sources of uncertainty. The propagation of uncertainty is done in two steps as described in the Figure 7. The inner level predicts the distribution of the turbine outputs PDF($\mathbf{y}$) given a joint distribution of the turbulent inflow parameters PDF($\mathbf{x}$) . In the outer level the uncertainty in the resources is propagated through the inner level to estimate the distribution of the expected value of each output.

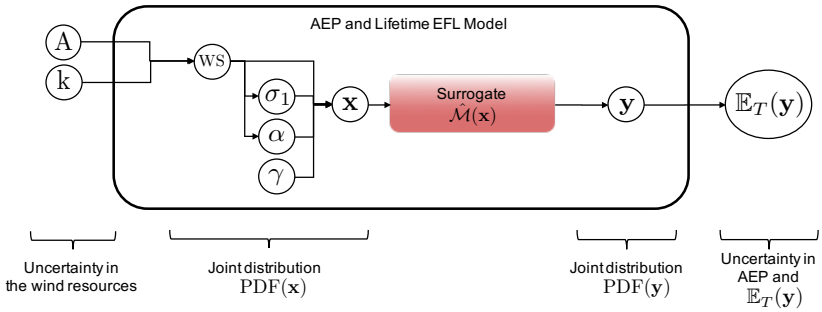

Figure 7: 2 levels of propagation of uncertainty.

The distribution of the variability of the wind resources is presented in the table 6. The main difference with the distribution used for training the surrogates is the fact that the WS follows a Weibull distribution with uncertain shape and scale parameters. This distribution of the Weibull parameters is used to characterize the variability/uncertainty in the wind resources. Nevertheless, the conditional distributions of σ_1, α and γ with respect WS follow the same dependency described in the table 2.

Variable	Distribution	Parameters	
A	Normal	$\mu_A = 9$	$\sigma_A = 0.5$ m/s
k	Normal	$\mu_k = 2$	$\sigma_k = 0.1$
$x_0 = \text{WS}$	Weibull	scale= A	shape= k
$x_1 = \sigma_1$	Lognormal	μ_{σ_1}(WS)	σ_{σ_1}(WS)
$x_2 = \alpha$	Normal	μ_α(WS)	σ_α(WS)
$x_3 = \gamma$	Normal	$\mu_\gamma = 0$	$\sigma_\gamma = 5$ deg.

Table 6: Uncertainty in wind resources.

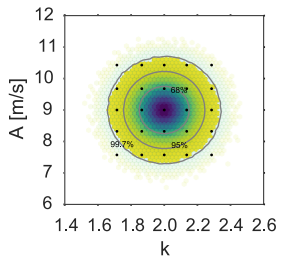

Figure 8: Joint distribution of the Weibull parameters and semi-spectral projection nodes for outer level propagation of uncertainty.

The propagation of uncertainty in the outer level is done using both a 1000 MC sample and a PCE with semi-spectral projection, for which a total of 25 Weibull parameters nodes are evaluated with their corresponding Gaussian quadrature weights, see Figure 8 and equation 3. Each node or element of the outer level MC sample represents a realization of the wind resources in a given year. For each of these nodes, a large inner level sample of the inputs of the surrogate, $\mathbf{x} = [\mathrm{WS}, \sigma_1, \alpha, \gamma]$, is generated. The size of the inner level MC sample is the number of 10-min cases in a year, $365 \times 24 \times 6 = 52,560$ cases. The power and EFL are evaluated using the surrogate and the mean power and mean EFL for a given year are calculated $\mathbb{E}_{\mathbf{x}}(\mathbf{y})$. Each individual surrogate evaluation has its own realization of the local distribution of the outputs due to the turbulence inflow realization, see equation 1. Additionally, the effect of the errors of the surrogate are considered, by sampling the distribution of the errors for each evaluation of the outputs, see equation 16. There is no differences in the distributions of $\mathbb{E}_{\mathbf{x}}(\mathbf{y})$ obtained using the surrogate or the ones obtained including the uncertainty of the surrogate due to the large sample size of the inner level (52 560); this means that the errors of the surrogate cancel out when computing their mean on a given year.

A 1000 MC sample of the distribution of one year $\mathbb{E}_{\mathbf{x}}(\mathbf{y})$ is generated using the PCE of the outer level in order to have an equivalent database of 1000 years as the one obtained in the outer MC simulation. A bootstrap of the outer level sample is used to estimate the variation in the expected value during 20 years of operation. This means that the average of 20 randomly selected years is computed for several realizations of 20 years. The central limit theorem is also used to estimate the distribution of the average of 20 randomly selected (independent) years. The distributions of the 1 year and 20 years capacity factor and expected equivalent fatigue loads are presented in Figure 9. It can be observed how the 20-year-averaged distribution has a narrower distribution, $\sigma_{20yr} = \sigma_{1yr}/\sqrt{20}$. Note that the yearly distribution of average output is required in order to estimate the uncertainty in the 20-year-averaged output. In this example coefficient of variations ($\mathrm{CoV} = \sigma/\mu$) of 5.6% for the scale parameter and 5% for the shape parameter of the WS distribution give a coefficient of variation of 2.4% in AEP and a 9.5% in year-to-year expected power production. The coefficient of variation in the 20-year-averaged BRF is 1.8% while the CoV of the year-to-year expected BRF is 6.1%. The CoV for the TBF are 0.5% for the 20-year-averaged and 2.0% for the year-to-year variation. Note that this coefficients of variations will be increased if the correlation between the WS and the other turbulent inflow parameters changes from year to year.

4. Discussion

The present article presents a methodology to implement sparse polynomial surrogates for aeroelastic wind turbine models. PCE are widely used in the uncertainty quantification field due to their efficiency to compute the statistical properties of the output and because the sensitivity analysis is obtained without any additional effort. The main two limitations in the use of PCE for wind energy are: (1) The input at-

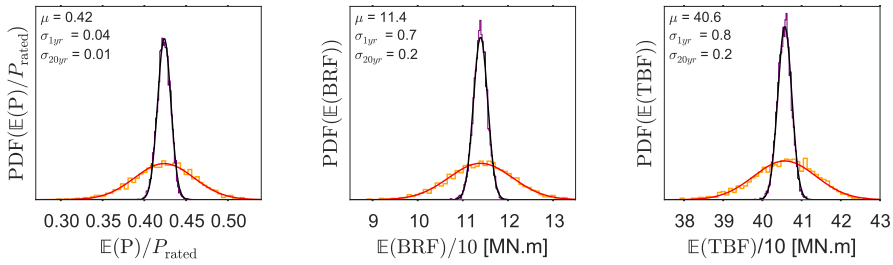

Figure 9: Distribution of the capacity factor and of the expected BRF and TBF equivalent loads. (Red) PCE distribution of the 1 year expected output. (Orange) 1000 MC sample of the 1 year expected output. (Black) Central limit distribution of 20-year-averaged output. (Purple) 1000 Bootstraps of the 20-year-averaged output.

mospheric parameters are usually jointly distributed with several layers of dependency (2) Some of the output have discontinuities and/or are restricted to certain values (e.g. only positive). The present article has shown how to solve these two problems: the implementation of an iso-probabilistic transformation to de-correlate the inputs, and the use of a logistic transformation to implement restrictions on the outputs. The benefits of using the logistic transformation can be seen in Figure 4, note that the polynomial surrogates do not present oscillations in the constant regions.

The final surrogate can be used to generate an output sample that covers the full output space, and that will predict the general details of the distributions of the outputs. One of the main limitations of the present surrogates is that the local distribution of the output is assumed to be normal, this is not the case for the operating region close to rated wind speed. Since this assumption only affects the turbulent inflow realization, it is considered to be an acceptable approximation. The local distributions of most outputs are not normal in reality, because the wind turbine controller has different strategies in each operating region, which creates skewness in the local distributions.

The results presented in this article show that there are multiple dependencies between the input variables as well as between inputs and outputs. Such complicated inter-dependencies are difficult to capture when applying other methods such as interpolation or Gaussian processes. For example, advanced interpolation methods such as radial basis functions will not account for the likelihood of an extreme training point and will generate trends that always pass through all the model observations. This behavior penalizes the capacity of the surrogate to generalize and to predict the output in new conditions. The sparse PCE are ideal for this class of problems because the k-fold cross validation is a step inside the training. Additionally, the correlations between the outputs are fully captured when using the presented surrogates; this occurs because each of the outputs has a dependency on the inputs. The full pair plot of the training dataset and the resulting surrogate for all inputs and outputs is presented in the extra

material accompanying this article.

The final results presented in Figures 5 and 9 show a promising new approach to communicate the performance characteristics of a wind turbine between the turbine manufacturers and project developers. The wind turbine producers normally do not share the detailed structural and aerodynamic model information of their products due to intellectual property concerns. As a result, often the wind project planners and operators do not have the full information about the expected performance of a turbine at the site they are developing. Furthermore, typically there is no model for the uncertainty of the turbine performance. A possible application of the multiple polynomial surrogates of a wind turbine could involve fitting the model by the manufacturer, and consequent distribution of the surrogate to users and clients. With this approach, project developers could get an useful tool for assessing site feasibility including uncertainty estimation, while not requiring access to detailed engineering models. Consequently, the use of more refined site assessment can potentially lead to improved overall estimation of levelized cost of energy and its uncertainty.

Obtaining the PDF(P) and PDF(EFL) is useful as they can be used for uncertainty estimation of the levelized cost of energy on a yearly basis. The surrogates can be evaluated on a long time series of the local wind resources (in multiple variables) such as the ones predicted by wind resource forecast (WRF) models without considerable extra computational effort. The power surrogate can then predict the annual variation of energy production while the EFL can be used to estimate the operation and maintenance costs. Such a probabilistic output can be the input to a decision support tool.

A surrogate of the DTU 10 MW RWT within a 4-dimensional turbulent inflow parameter space can be built using only 140 input cases (with multiple turbulent inflow realizations per case) and can be used to predict the distribution of the power, thrust coefficient and equivalent fatigue loads on the turbine. In contrast, traditional approaches require in the order of 20^4 gridsearch/interpolation (full factorial design with 20 points per dimension) or $10^5 - 10^6$ variance reduction MC sample of the inputs [23]. Furthermore, the present approach enables to build an uncertainty model around the 10 minutes performance of the turbine that captures the effect of the turbulent inflow realization.

The combined PCE surrogate approach can also be used to improve traditional conservative designs in which a worst case scenario for shear and turbulence intensity is considered. The fast evaluation of the joint probability distributions for loads based on the surrogate model opens possibilities for performing structural reliability analysis and probability based design.

5. Conclusions

In the present study, a polynomial surrogate model of wind turbine fatigue loads and energy output was defined and demonstrated for the DTU 10 MW reference wind turbine. Using only 140 input cases was found to be sufficient for building a surrogate

of the DTU 10MW model within a 4-dimensional turbulent inflow parameter space. The presented approach was demonstrated as an efficient alternative of the traditional techniques for characterizing the global behavior of an aeroelastic wind turbine model under multiple uncertain turbulent inflow parameters.

The surrogate has enable to perform a global sensitivity analysis on the DTU 10 MW turbine. This study showed that the hub height wind speed is the most important variable to predict the power of the turbine, followed by the turbulent inflow realization (TIR); this is a consequence of the correlation between turbulence intensity, shear and hub height wind speed. The turbulence intensity is of similar importance as the TIR in the prediction of blade root flapwise (BRF), and tower top tilt (TTT) and yaw (TTY) equivalent fatigue loads.

The surrogate can be used in a two-level propagation of uncertainty example. In the example presented in this article the year-to-year variability in the shape and scale parameters of the hub height wind speed Weibull distribution are propagated into a variation of AEP and of lifetime equivalent fatigue loads. Coefficient of variations of 5.6% for the scale and of 5% for the shape parameters give a coefficient of variation of 2.4% in AEP, of 1.8% in lifetime $\mathbb{E}(BRF)$ and of 0.5% in lifetime $\mathbb{E}(TBF)$.

6. Acknowledgments

This work was supported by the International Collaborative Energy Technology R&D Program of the Korea Institute of Energy Technology Evaluation and Planning (KETEP), granted financial resource from the Ministry of Trade, Industry & Energy, Republic of Korea. (No. 20138520021140). The authors will like to thank Michael McWilliam for the suggestion of the use of logistic transformations to enforce strict restrictions to the polynomial surrogates.

References

[1] I. E. Commission, et al., Iec 61400-1: Wind turbines part 1: Design requirements, International Electrotechnical Commission.

[2] P. A. Graf, G. Stewart, M. Lackner, K. Dykes, P. Veers, High-throughput computation and the applicability of monte carlo integration in fatigue load estimation of floating offshore wind turbines, Wind Energy.

[3] H. S. Toft, L. Svenningsen, W. Moser, J. D. Sørensen, M. L. Thøgersen, Assessment of wind turbine structural integrity using response surface methodology, Engineering Structures 106 (2016) 471–483.

[4] A. Natarajan, N. Dimitrov, P. H. Madsen, J. Berg, M. C. Kelly, G. C. Larsen, J. Mann, D. R. Velerst, J. Dalsgaard Srensen, H. Toft, I. Abdallah, N.-J. Tarp-Johansen, T. Krogh, J. Strdahl, C. Eriksson, E. Jrgensen, F. Klint, L. Thesbjerg, Demonstration of a basis for tall wind turbine design, EUDP project final report, Tech. Rep. E-0108, Technical University of Denmark, Department of Wind Energy, Roskilde, Denmark (2016).

[5] I. Abdallah, A. Natarajan, J. D. Sørensen, Influence of the control system on wind turbine loads during power production in extreme turbulence: Structural reliability, Renewable Energy 87 (2016) 464–477.

[6] A. Clifton, L. Kilcher, J. Lundquist, P. Fleming, Using machine learning to predict wind turbine power output, Environmental research letters 8 (2) (2013) 024009.

[7] A. Clifton, M. Daniels, M. Lehning, Effect of winds in a mountain pass on turbine performance, Wind Energy 17 (10) (2014) 1543–1562.

[8] C. Soize, R. Ghanem, Physical systems with random uncertainties: chaos representations with arbitrary probability measure, SIAM Journal on Scientific Computing 26 (2) (2004) 395–410.

[9] O. Le Maıtre, O. Knio, H. Najm, R. Ghanem, Uncertainty propagation using wiener–haar expansions, Journal of computational Physics 197 (1) (2004) 28–57.

[10] S.-K. Choi, R. V. Grandhi, R. A. Canfield, C. L. Pettit, Polynomial chaos expansion with latin hypercube sampling for estimating response variability, AIAA journal 42 (6) (2004) 1191–1198.

[11] M. Berveiller, B. Sudret, M. Lemaire, Stochastic finite element: a non intrusive approach by regression, European Journal of Computational Mechanics/Revue Européenne de Mécanique Numérique 15 (1-3) (2006) 81–92.

[12] D. Xiu, J. S. Hesthaven, High-order collocation methods for differential equations with random inputs, SIAM Journal on Scientific Computing 27 (3) (2005) 1118–1139.

[13] G. Blatman, B. Sudret, Adaptive sparse polynomial chaos expansion based on least angle regression, Journal of Computational Physics 230 (6) (2011) 2345–2367.

[14] F. Pedregosa, G. Varoquaux, A. Gramfort, V. Michel, B. Thirion, O. Grisel, M. Blondel, P. Prettenhofer, R. Weiss, V. Dubourg, et al., Scikit-learn: Machine learning in python, The Journal of Machine Learning Research 12 (2011) 2825–2830.

[15] R. Tibshirani, Regression shrinkage and selection via the lasso, Journal of the Royal Statistical Society. Series B (Methodological) (1996) 267–288.

[16] P. Moriarty, Database for validation of design load extrapolation techniques, Wind Energy 11 (6) (2008) 559.

[17] A. Natarajan, D. R. Verelst, Outlier robustness for wind turbine extrapolated extreme loads, Wind Energy 15 (5) (2012) 679–697.

[18] C. Tibaldi, L. C. Henriksen, C. Bak, Investigation of the dependency of wind turbine loads on the simulation time, in: European Wind Energy Conference & Exhibition 2014, 2014.

[19] C. Bak, R. Bitsche, A. Yde, T. Kim, M. H. Hansen, F. Zahle, M. Gaunaa, J. P. A. A. Blasques, M. Døssing, J.-J. Wedel Heinen, et al., Light rotor: The 10-mw reference wind turbine, in: EWEA 2012-European Wind Energy Conference & Exhibition, 2012.

[20] M. Rosenblatt, Remarks on a multivariate transformation, The annals of mathematical statistics 23 (3) (1952) 470–472.

[21] P. Y. Simard, Y. A. LeCun, J. S. Denker, B. Victorri, Transformation invariance in pattern recognitiontangent distance and tangent propagation, in: Neural networks: tricks of the trade, Springer, 1998, pp. 239–274.

[22] W. Gautschi, Algorithm 726: Orthpol–a package of routines for generating orthogonal polynomials and gauss-type quadrature rules, ACM Transactions on Mathematical Software (TOMS) 20 (1) (1994) 21–62.

[23] N. Dimitrov, A. Natarajan, M. Kelly, Model of wind shear conditional on turbulence and its impact on wind turbine loads, Wind Energy 18 (11) (2015) 1917–1931. doi:10.1002/we.1797.

[24] J. Feinberg, H. P. Langtangen, Chaospy: An open source tool for designing methods of uncertainty quantification, Journal of Computational Science 11 (2015) 46–57.

[25] M. D. McKay, R. J. Beckman, W. J. Conover, A comparison of three methods for selecting values of input variables in the analysis of output from a computer code, Technometrics 42 (1) (2000) 55–61.

[26] I. M. Sobol', On the distribution of points in a cube and the approximate evaluation of integrals, Zhurnal Vychislitel'noi Matematiki i Matematicheskoi Fiziki 7 (4) (1967) 784–802.

[27] J. M. Hammersley, Monte carlo methods for solving multivariable problems, Annals of the New York Academy of Sciences 86 (3) (1960) 844–874.

[28] I. M. Sobol, Global sensitivity indices for nonlinear mathematical models and their monte carlo estimates, Mathematics and computers in simulation 55 (1) (2001) 271–280.

[29] S. E. Maxwell, H. D. Delaney, Designing experiments and analyzing data: A model comparison perspective, Vol. 1, Psychology Press, 2004.

[30] A. Saltelli, P. Annoni, I. Azzini, F. Campolongo, M. Ratto, S. Tarantola, Variance based sensitivity analysis of model output. design and estimator for the total sensitivity index, Computer Physics Communications 181 (2) (2010) 259–270.

[31] B. Sudret, Global sensitivity analysis using polynomial chaos expansions, Reliability Engineering & System Safety 93 (7) (2008) 964–979.

[32] M. S. Eldred, A. A. Giunta, B. G. van Bloemen Waanders, S. F. Wojtkiewicz, W. E. Hart, M. P. Alleva, DAKOTA, a multilevel parallel object-oriented framework for design optimization, parameter estimation, uncertainty quantification, and sensitivity analysis: Version 4.1 reference manual, Citeseer, 2007.

[33] S. Marelli, B. Sudret, UQLab: a framework for uncertainty quantification in MATLAB, ETH-Zürich, 2014.

[34] G. Andrianov, S. Burriel, S. Cambier, A. Dutfoy, I. Dutka-Malen, E. De Rocquigny, B. Sudret, P. Benjamin, R. Lebrun, F. Mangeant, et al., Open turns, an open source initiative to treat uncertainties, risks n statistics in a structured industrial approach, in: Proceedings of ESREL, 2007.

[35] T. J. Larsen, A. M. Hansen, How 2 HAWC2, the user's manual, Risø National Laboratory, 2007.

[36] J. Mann, Wind field simulation, Probabilistic Engineering Mechanics 13 (4) (1998) 269 – 282. doi:10.1016/S0266-8920(97)00036-2.

[37] M. A. Miner, et al., Cumulative damage in fatigue, Journal of applied mechanics 12 (3) (1945) 159–164.

[38] S. Hosder, R. W. Walters, M. Balch, Efficient sampling for non-intrusive polynomial chaos applications with multiple uncertain input variables, in: Proceedings of the 48th AIAA/ASME/ASCE/AHS/ASC Structures, Structural Dynamics and Materials Conference, AIAA paper, Vol. 1939, 2007.

Article C

A new method to estimate the uncertainty of AEP of offshore wind power plants applied to Horns Rev 1

A new method to estimate the uncertainty of AEP of offshore wind power plants applied to Horns Rev 1

Juan P. Murcia
PhD. Student, Dept. of Wind Energy, Technical University of Denmark

Pierre E. Réthoré
Senior Researcher, Dept. of Wind Energy, Technical University of Denmark

Kurt S. Hansen
Professor, Dept. of Wind Energy, Technical University of Denmark

Anand Natarajan
Senior Scientist, Dept. of Wind Energy, Technical University of Denmark

John D. Sørensen
Professor, Department of Civil Engineering, Aalborg University

Abstract: The present article proposes a framework for validation of stationary wake models that wind developers can use to predict the energy production of a wind power plant more accurately. The application of this framework provides a new way to quantify the uncertainty of annual energy production predictions. Additionally this methodology enables the fair comparison of different wake models. Furthermore the methodology enables the estimation of how much information can be obtain from a measurement dataset to quantify model inadequacy. In the present work the proposed framework is applied to the Horns Rev 1 offshore wind power plant. The model uncertainty of a modified N. O. Jensen wake model under uncertain undisturbed flow conditions was studied. Evidence of model inadequacy is found in terms of a bias in the predicted AEP distribution. It was found that the use of the official power curve compensates the errors in the wake model, as a consequence a larger uncertainty of the overall model is predicted. Furthermore a study of wake model benchmarking based on filtered flow cases indicates that measurement uncertainty in the wind speed and wind direction is large enough to obtain any evidence of model inaccuracy even for the simplest wake models.

Keywords: Uncertainty quantification, offshore wind power plant, power predictions, wake model, SCADA data reanalysis

1. Introduction

There is a need in the wind energy industry for better predictions of wind farm power production. In particular investors and financial institutions are interested in understanding the uncertainty of production predictions in order to help them take better decisions about investing in a particular wind energy project. Previous efforts for wake model benchmarking and validation using offshore wind plant supervisory control and data acquisition (SCADA) data have been performed in the past, some examples are the work of Barthelmie et. al. [1], Hansen et. al. [5], Gaumond et. al. [4], Peña et. al. [12], Réthoré et. al. [13] and Moriarty et. al. [10] . These studies were based on the filtering of the measurements database into wind speed and wind direction bins, also called flow cases. All the publications pointed out that due to the large uncertainties in the inflow conditions it has not been possible to obtain statistical evidence about model inaccuracy. Furthermore the large number of wake models that have been evaluated produce a wide spread of power production predictions for apparently simple flow cases.

In general filtering of SCADA databases is still a common practice and uncertainties in the inflow conditions are usually disregarded. The limitations of filtering the flow cases in terms of wind direction uncertainty has been studied in Gaumond et. al. [4]. It was concluded that for large enough wind direction bins (around 30 [deg]) an accurate prediction of the mean power production can be done even with the most simple models. In contrast for narrow wind direction bins, the power production can not be accurately predicted if the wind direction uncertainty is neglected. Additionally the flow cases that have been used in the literature reduce the observed data to only the very few cases in which all the wind turbines (studied) are available and under normal operation. Réthoré et. al. [14] reported that for a wind power plant with 80 turbines only between 9 to 20% of the observations can be used. This limited number of observations has made it challenging to conclude about the uncertainty in annual energy production (AEP) predictions due to the low representation of the flow cases observed in which all turbines are under normal operation.

1.1. Objectives of the present study

The present study has the following objectives:

(1) To map the wake model prediction error for a given wind power plant energy production as a function of the uncertain undisturbed flow conditions.

(2) To estimate the wake model uncertainty to predict the mean power production of a given wind power plant when there is measurement uncertainties in each variable.

(3) To estimate the uncertainty of AEP of a given wind power plant. It is important to remark that in the present work uncertainty in AEP refers to the probability density function or distribution of possible annual energy production and not just the standard deviation around its expected value.

1.2. Model validation under uncertainty

The present work follows the framework for verification, validation and uncertainty quantification of computer codes presented by Roy and Oberkampf [15]. This framework is very relevant for wind energy since it proposed a division

between epistemic uncertainty (uncertainties that are due to lack of knowledge but that could be reduced e.g. individual measurement uncertainties, statistical uncertainty due to limited sample size and model uncertainty) from the aleatory uncertainty (uncertainties that can not be reduced e.g. real wind speed and real wind direction distribution during a time period). In this framework multiple realizations of the epistemic uncertainty of the inputs are sampled for each individual realization of the aleatory uncertainty of the inputs. By evaluating the model in each of this cases one can predict a set of distributions of the output. A similar approach is done for the possible realizations of the observed output: multiple realizations of the epistemic uncertainty are sampled for each realization of the aleatory uncertainty of the output. Roy and Oberkampf [15] and Ferson et. al. [3] have proposed the use of the area validation metric to compare the distributions of model predictions and measured outputs under measurement uncertainty. These articles argue that the area validation metric is a good estimator of the model uncertainty. In order to study the impact of measurement uncertainty and model uncertainty in the prediction of AEP it is important to be able to separate the natural (aleatory) variability of the flow resources from the measurement (epistemic) uncertainty of each individual 10-minutes measurement.

2. Methodology

2.1. Inputs/output measurements

The SCADA data was processed following the methodology for data reinforcement that has been described by Réthoré et. al. [14] in order to remove calibration shifts through time. In particular nacelle position sensors tend to have calibration shifts due to the inability to use magnetic north tracking close to large generators. Turbines are forced to perform a full 360 [deg.] turn to recalibrate the nacelle position signal. It is important to recognize that an individual turbine yaw angle signal is not an accurate estimator of the undisturbed wind direction. The settings of the yaw controllers are not known and therefore the yaw signal contains yaw errors and time dependency (filtering) due to the controller reaction time. The present work assumes that a large scale averaged undisturbed wind direction can be estimated from multiple yaw sensors, because the individual yaw errors of each turbine compensate each other.

Wind speed

The undisturbed wind speed (WS) was estimated using the average of the nacelle anemometers on the free flow operating turbines at each 10-minutes period. This average represents a spatially averaged undisturbed wind speed. Individual signals were checked for measurement quality before the averaging process was applied, which means that the number of available wind speed signals varied for each 10-minutes. The quality check consisted in comparing each individual upstream nacelle anemometer with the raw spatially averaged undisturbed wind speed. Periods that showed uncommon behavior (time increasing standard deviation) were removed.

Two additional corrections were applied to the undisturbed wind speed based on multiple nacelle anemometers. The nearby met masts hub height anemometers were used to fit a non-linear nacelle transfer function (NTF). This transfer function was used to correct the estimated wind speed for flow distortion due to the nacelle geometry and due to blade shadowing. The procedure followed is inspired in the procedure described in the IEC standard 64100-12-2 (2013) [7]. The difference with respect the standard lies in the fact that the spatial average undisturbed wind speed was used instead of a single nacelle located anemometer.

Finally an air density correction was applied following the IEC standard 64100-12-1 (2005) [6]. This correction scales the wind speed by the ratio of the current air density (10-min. mean) and the standard atmosphere air density to the one third power. This correction is recommended for normalization of power/wind speed measurements for pitch controlled wind turbines [6]. The 10-minutes mean density was estimated following the IEC standard and used the 10 min. mean barometer, air temperature, and water temperature signals.

The elicitation of the uncertainty of the undisturbed wind speed was done following the IEC standard [7]. The sources of uncertainty considered are shown in table 1. The air density correction uncertainty is the result of propagation of barometer, temperature and humidity measurement uncertainties trough the air density correction equation [7]. The large scale structures uncertainty was predicted using the trend inside the 10-minutes by computing the difference between the two consecutive undisturbed wind speeds [11]. All sources of uncertainty were assumed to be independent and normally distributed. It is important to remark that the uncertainty is estimated for each individual 10-minutes period.

Source	Type	Ref.
Calibration	B	[7]
Operation	B	[7]
Mounting	B	[7]
Data acquisition resolution	B	[7]
NTF correction	B	[7]
Air density correction	B	[7]
Large scales structures	B	[11]
Statistical	A	[7]

Table 1: Sources of uncertainty in spatially averaged undisturbed wind speed.

Note that type B uncertainties need to be normalized by applying a coverage factor of $1/\sqrt{3}$. The total uncertainty was evaluated using eq. 1 (this equation uses a general notation for any measured variable x). In this equation the left term contains the type A uncertainty estimated using N sensors and the term on the right is the combination of multiple type B uncertainties. Finally the real value of the wind speed is assumed distributed normal around the average of the multiple sensors, eq. 2 (this equation uses a general notation for any measured variable x).

$$U_x^2 = \left(\frac{std(x)}{\sqrt{N}}\right)^2 + \sum\left(\frac{U_{Bi}}{\sqrt{3}}\right)^2 \quad (1)$$

$$x_{real} \sim Normal\left(\bar{x}, U_x\right) \quad (2)$$

Wind direction

The undisturbed wind direction was estimated using the average of the nacelle positions signals of the free wind operating wind turbines. Individual signals were checked for calibration shifts [14] and for quality of the measurement. Each individual upstream nacelle position signal was re-calibrated based on the wind power plant layout and the power deficit of the first wake operating turbine. This procedure has been introduced by Réthoré et. al. [14].

The spatially averaged undisturbed wind direction (WD) obtained from the average of the multiple available nacelle positions showed a dependency on the wind speed. A correction based on the bias between WD and the wind vane at hub height at the nearby meteorological masts was fitted through a non-linear transfer function following the recommendations presented in the IEC standard 64100-12-2 (2013) [7]. The correction for the wind direction consisted in removing the bias as a function of wind speed.

The elicitation of the uncertainty of the undisturbed wind direction followed the IEC standard [7] and is estimated for each individual 10-minutes period. The sources of uncertainty considered are shown in table 2. The total uncertainty was calculated using eq. 1, while the real value of the wind direction is assumed normally distributed, eq. 2.

Source	Type	Ref.
In-situ re-calibration	B	[7]
Yaw signal resolution	B	[7]
Data acquisition resolution	B	[7]
Sensor alignment	B	[7]
NTF correction	B	[7]
Large scales structures	B	[11]
Statistical	A	[7]

Table 2: Sources of uncertainty in spatially averaged undisturbed wind direction.

Power

The total power production was computed by assuming that the turbines not available under normal operation produce null power. Furthermore it was assumed that a considerable reduction of the thrust coefficient occurs under down-regulation and that the wake deficits can be neglected. The power measurement uncertainty is estimated for each 10-minutes observation following the standard [6]. The sources of uncertainty considered are shown in table 3. The total uncertainty was calculated using eq. 1, while the real value of the power is assumed normally distributed, eq. 2.

Source	Type	Ref.
Calibration	B	[7]
Current transducer	B	[7]
Voltage transducer	B	[7]
Data acquisition resolution	B	[7]

Table 3: Sources of uncertainty in power measurements.

Power curve

The present study used two different power curves: the official power curve and the experimental power curve. The experimental power curve was obtained following the recommendations of the IEC standard [7]. Since SCADA databases include a large number of turbines the experimental power curved was obtained by aggregating multiple upstream wind turbines power measurements as a function of the undisturbed wind speed (for a valid wind direction sector).

Availability

The prediction of normal operation was performed individually to each turbine following the outlier detection methodology presented in [14]. This procedure used the pitch angle and normalized power curve in order to detect when a turbine is not under normal operation conditions. The obtained wind turbine availability is a combination of the actual availability, down regulation conditions and measurement sensor errors.

2.2. Modeling

Wake model

The present work could be applied to any wake model. The wake model used in the present study is a modified N. O. Jensen (NOJ) model [8]. The modified NOJ model was selected for its simplicity and because it is a model still used in the industry. The model assumes a linear wake expansion coefficient (k_j) of 0.05 for offshore conditions. In contrast to the original NOJ model, the modified model includes a near wake expansion from 1-D momentum theory occurring at the rotor disc; further more the wake deficits are scaled by the local hub height wind speed at the wake generating wind turbine instead of the undisturbed wind speed. Finally the wake deficits are aggregated with linear superposition. The model used in the present study is open source and is available at https://github.com/DTUWindEnergy/FUSED-Wake along other wake models such as the original NOJ [8] and G. C. Larsen semi-empirical wake model [9].

The model used in this study has as inputs the undisturbed wind speed, the undisturbed wind direction, the power and thrust coefficients curves, the wind power plant layout, the linear wake expansion coefficient and the availability for each turbine. As a result the model predicts the power produced by each turbine.

It is important to note that the model was executed for each of the 10-minutes inputs. The wake model was run assuming that the unavailable turbines are not running (for which the idle thrust coefficient was used) during the 10-minutes period.

Propagation of input uncertainties

A Monte Carlo simulation based on LHS sampling was used to study the effect of input uncertainty in the power distribution prediction. Each 10-minute distribution of the real wind direction and wind speed are considered independent due to their epistemic nature [15]. 100 different possible realizations of the real undisturbed flow conditions during the 3 years of analysis were calculated. This enabled to separate the aleatory component of the wind resources from the epistemic uncertainty of the measurement/estimation of undisturbed flow conditions. The present approach can be summarized as a full time series reanalysis with detailed availability and uncertainty for each 10-minutes period.

Power measurement uncertainty sampling

A Monte Carlo simulation based on a 100 LHS sample was used to study the effect of the measurement uncertainty in the observed power distribution. This approached produced 100 possible realization of the real active power through the three years of analysis.

2.3. Model validation

Area validation metric

A validation metric describes a methodology to compare an experimental distribution of a variable (with measurement uncertainty) with the result of the propagation of input measurement uncertainties through a model. In the current work the area validation metric was used to characterized the error in the prediction of the expected power of the wind power plant (U_{model}). The area validation metric quantifies the model uncertainty by comparing the median rank based cumulative density function (CDF) of the measured and predicted powers, and not only their mean values [3].

Due to the (epistemic) measurement uncertainty, the CDF of the total power measurements is defined as the region between the worst and best realization of the real power. Similarly when the uncertainty in the inputs is propagated through the model then the predicted CDF of total power becomes the region between the worst and best realizations of the model. The area validation metric is the absolute area between the two regions. If there is no are between the two regions there is no evidence of model uncertainty. This could mean that the model is very accurate or that there is too much uncertainty in the inputs. In the present work several comparisons of flow cases were done that illustrate how to use this validation metric in power production and annual energy production predictions.

The area validation metric is used to predict the confidence interval of any quantile of the output [15]. Therefore it can be used to estimate the expected model error in the prediction of the annual energy production. It is important to understand model uncertainty as an epistemic uncertainty, this means that it produces uncertainty around the predicted distribution of power. This means that it captures an additional uncertainty in the prediction of power that is independent of the input uncertainties. Figure 1 shows an example of area validation metric applied to two models that use the mean wind speed to predict the mean power. It can be observed that there is measurement uncertainty that causes the distributions to be regions. It can be seen that the model on the left gives a better estimation of the mean power (at CDF(P)$= 0.5$), but both models are equally bad at modeling the power distribution. It is expected that such models will deviate significantly from case to case depending on the actual wind resources. Therefore the model uncertainty should be similar for both models. The area validation metric in both cases is around 45 [MW]. Finally the confidence interval that includes the mean power can be estimated as the distribution obtained by the input uncertainty propagation (blue region at CDF(P)$= 0.5$) and an additional bias (uniformly distributed) given by the validation metric:

$$\mathbb{E}(P_{WF\,real}) \in \overbrace{PDF(\mathbb{E}(P_{WF\,model}))}^{\text{Input Unc.}} \pm \overbrace{U_{model}}^{\text{Model Unc.}} \qquad (3)$$

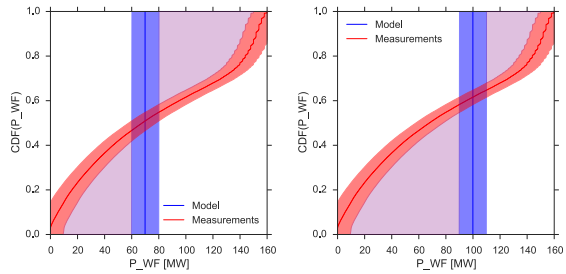

Figure 1: Example of area validation metric for CDF(P) for two models that use the mean wind speed to predict the mean power. First model prediction: $\mathbb{E}(P_{WF\,real}) \in [60, 80] \pm 45 = [15, 125]$ [MW]. Second model prediction: $\mathbb{E}(P_{WF\,real}) \in [90, 100] \pm 45 = [45, 145]$ [MW].

Boot-strapping AEP

In the present work the classical bootstrap technique [2] was used to predict the probability distribution of AEP. This technique consists in building a sample of artificial but probable years of climate, therefore it is sampling the variation (aleatory uncertainty) of the undisturbed wind. A single realization of a year was built by randomly picking a year out of the three available in the database for each of the 10-minutes periods in a given year. This was done keeping the date and time for the observation. The wind speed, wind direction, measured power, predicted power, and its respective uncertainties were chosen together. The statistical uncertainty due to a limited number of bootstrap sample was studied by following the convergence in the standard deviation of the AEP.

The bootstrapped sample is representative of the actual climate as it contains all the long term correlations such as the daily, the synoptic (high and low pressure driven patterns) and seasonal variations. The bootstrapped sample was used to evaluate the distribution of possible AEP. Finally the area validation metric based on CDF(P) was used to predict the confidence interval for the AEP. Note that this validation metric considered the area validation metric for $\mathbb{E}(P_{WF})$ (section 2.3) and the propagation of uncertainties in the undisturbed wind speed and direction through the model (section 2.2).

3. Results

3.1. Test case: Horns Rev 1

Horns Rev 1 is a Danish offshore wind power plant coowned by Vattenfall AB (60%) and DONG Energy AS (40%). It is located 14 [km] from the Danish west coast (fig. 2). The total rated power is 160 [MW]. The power plant consists of 80 Vestas V80-2.0 [MW] wind turbines, see figure 3. The power plant started operation in 2002 and is still operating in 2015.

The present work has been done using 3 years (2005-2007) of measurements from the SCADA database of the power plant. The database contains 10-minutes mean, max., min. and standard deviation for power, nacelle anemometer, nacelle position (orientation), pitch angle and rotational speed for each individual wind turbine. The present study also uses signals from the nearby meteorological mast (M2, M6, M7). Anemometers at 70 [m] height, wind vane at 68 [m]

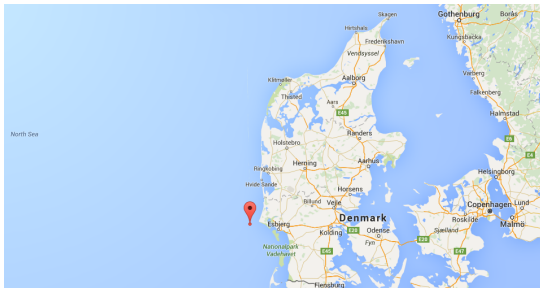

Figure 2: Location of the Horns Rev 1 offshore wind power plant. Image taken the 6th of October 2015 at http://maps.google.com.

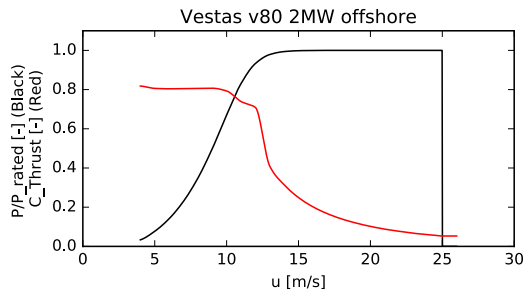

Figure 3: Vestas V80-2.0 [MW] official power curve (black line) and thrust coefficient curve (red line). April 2007 reported curves taken from the WAsP power curve database at http://wasp.dk

height, barometer sensor, air and water temperatures measurements. In the present work the available nacelle position and anemometer sensors of the free flow operating turbines were used to predict the undisturbed wind conditions. The estimation of the undisturbed wind conditions was done independently in four different undisturbed wind direction sectors, see figure 4.

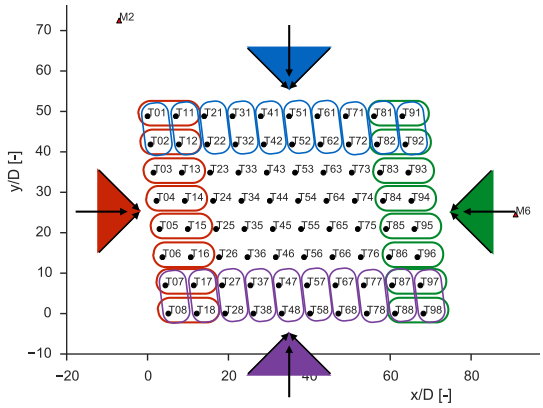

Figure 4: Selected benchmark case in Horns Rev 1. The colored area represents undisturbed wind directions. The sensors used for predicting the undisturbed flow conditions are circled and color coded.

Wind speed

Figure 5 presents an example of the transfer function correction based on the anemometer located at the top of the met mast M6 (height of 70 [m]). Note that the distance between meteorological mast and each nacelle anemometer is larger than the limit recommended in the IEC standard 64100-12-1 (2013) [7]: $4D$. Nacelle transfer functions were independently produced using M2, M6, M7 top anemometers and individual nacelle anemometers in order to asset the effect of the assumptions, similar transfer functions were obtained (not shown).

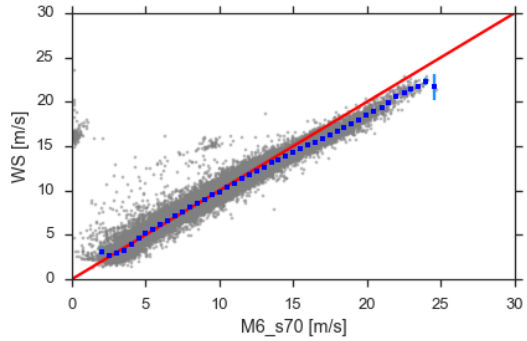

Figure 5: Nacelle transfer function between top anemometer at M6 and the large scale averaged undisturbed wind speed for the Eastern sector.

It is important to remark that the authors had not access to any information about the calibration, mounting, quality, maintenance of any of the anemometers in the wind farm. To compensate for this the uncertainty estimation is conservatively estimated. The elicitation of the uncertainty of the undisturbed wind speed is shown in table 4. This table does not present the type A uncertainty or the large scale uncertainty, since they are computed independently for each 10-min period.

Source	Type	Value
Calibration	B	0.25 [m/s]
Operation	B	class: 1.7A
Mounting	B	0.2%
Data acquisition resolution	B	0.05 [m/s]
NTF correction	B	2 %

Table 4: Estimated uncertainty in spatially averaged undisturbed wind speed.

Wind direction

An example of the nacelle position signal re-calibration based on the layout and the power deficit procedure is shown in fig. 6 for the turbines 04 and 14. In this figure the difference between the two blue lines represents the bias in the wind direction for the nacelle position senor of turbine 04.

The NTF correction for the wind direction consisted in removing the bias as a function of wind speed. Figure 7 shows the bias between the large scale averaged wind direction and the wind vane located at M6 at 68 [m] height. Similar results were obtained for M2 and M7.

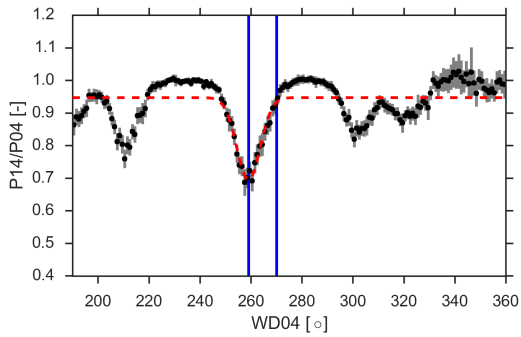

Figure 6: Nacelle position sensor for turbine 04 re-calibration based on the power ratio of turbines 14 and 04.

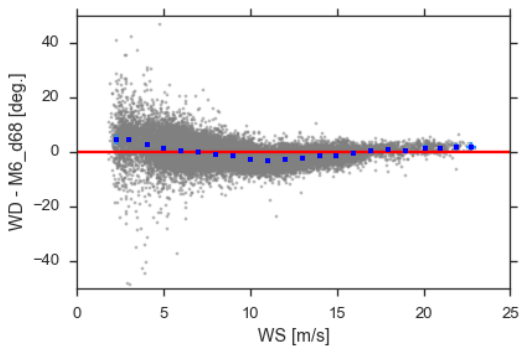

Figure 7: Undisturbed wind direction bias with respect to the wind vane at M6 at 68 [m] height as a function of the undisturbed wind speed for the Eastern sector.

A conservative elicitation of the uncertainty in the undisturbed wind direction was done following the standard for single nacelle anemometer uncertainty [7], table 5. This table does not present the type A uncertainty or the large scale uncertainty, since they are computed independently for each 10-min period.

Source	Type	Value
In-situ calibration	B	3 [deg]
Yaw signal resolution	B	2.5 [deg]
Data acquisition resolution	B	0.05 [deg]
Sensor alignment	B	1 [deg]
NTF correction	B	1 [deg]

Table 5: Estimated uncertainty in spatially averaged undisturbed wind direction.

Power

The estimated power measurement uncertainty for each 10-minutes observation is presented in table 6. Note that the power transducers have not been calibrated since installation, and it is observed that the zero power values changes between 1-2 % with reference to rated power.

Source	Type	Value
Calibration	B	2 %
Current transducer	B	2 %
Voltage transducer	B	0.9 %
Data acquisition resolution	B	2 [kW]

Table 6: Estimated uncertainty in power measurements.

Power curve

The official power curve and the multiple turbine averaged experimental power curve are presented in figure 8. Note that a simple site correction for the power curve based on the annual average turbulence intensity captures the obtained experimental power curve.

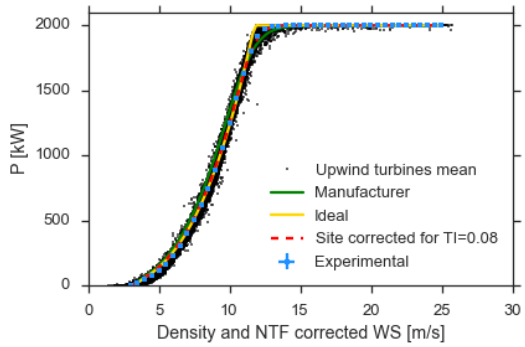

Figure 8: Official power curve and experimental power curve.

3.2. Time series of the main variables

An example of the time series of the undisturbed wind speed, wind direction, total availability, measured total power and model predicted power are presented in Figure 9. In this figure the colored areas represent the 99% confidence intervals for each of the variables. These confidence intervals include all sources of uncertainties and they should be understood as the region in which the real value lies. It is important to remark that the predicted power confidence interval is the result of the input uncertainty propagation process. This figure superficially reveals a good agreement between measurements and predictions.

Furthermore, figure 9 suggest that the confidence intervals predicted by the propagation of input uncertainty are larger than the ones caused by the measured power uncertainty. Note that the confidence intervals in the measured variables reveal that the uncertainty analysis is done for each time period. Some periods of non-available data can also be identified from this figure. Moreover the expected model prediction is build by averaging the 100 realizations of power for each 10-minutes (black line in the lower frame in figure 9).

3.3. Wind farm power rose: experimental and modeled

An example of the wind farm power rose is presented in figure 10 for a single realization of the input uncertainty during the 3 years and for a single realization of the output uncertainty during the 3 years. This figure demonstrates that

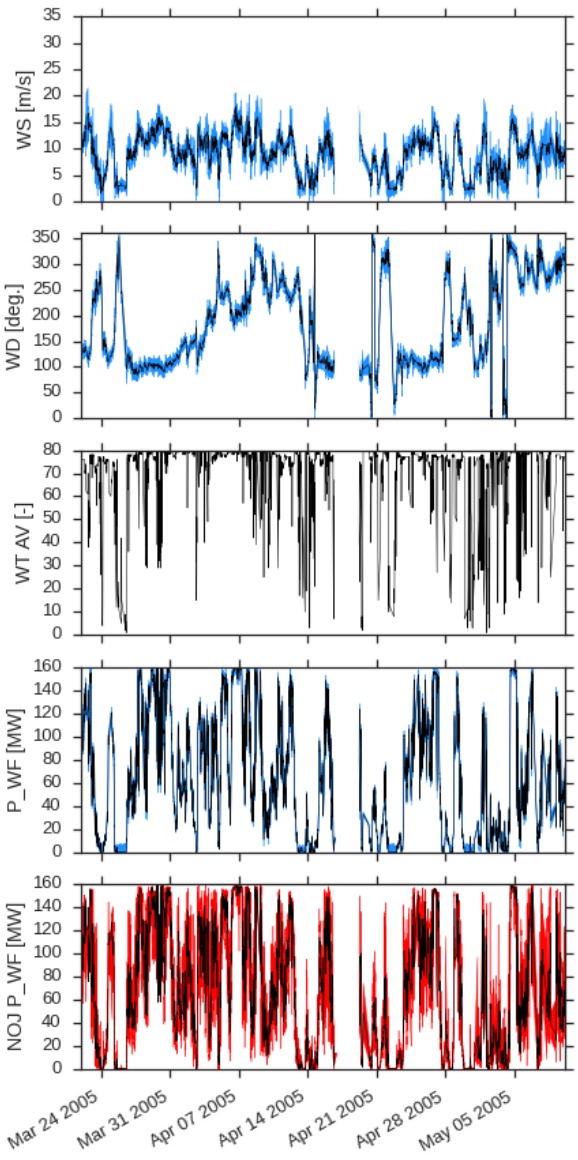

Figure 9: Example of time series of WS, WD, total availability and P_{WF} time series with 99% confidence intervals (colored areas).

the use of the actual available turbines improves the amount of data available to compare the performance of wind farm flow models.

In order to compare the level of agreement the first step is to analyze the distribution of the prediction error, see figure 11. This figure contrast the power prediction error as a function of the input variables for two cases. Using the official power curve (left frame in figure 11) produces an over-prediction of power at wind directions with less coherent wind turbine alignment; on the contrary, an under-prediction of power occurs at the wind directions of main turbine alignment. The prediction errors of the model that used the experimental power curve show a consistent under-prediction of power through the whole wind rose.

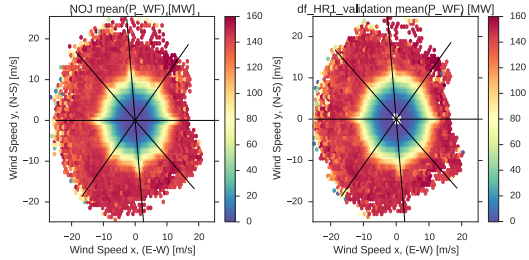

Figure 10: Wind farm power rose for (left) the model predictions based on a single realization of the inputs (right) a single realization of power measurements.

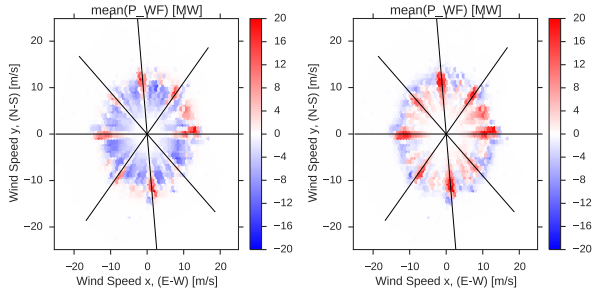

Figure 11: Power prediction error rose for a single realization of input uncertainty (left) official power curve (right) experimental power curve. Positive errors means power under-prediction (red areas) while negative errors represent power over-predictions (blue areas).

3.4. Model uncertainty for total plant expected power

The area validation metric was applied to the cumulative density function of the power, this validation metric gives an uncertainty estimation for the prediction of mean power production ($\mathbb{E}(P_{WF})$). The CDF of both measured and predicted power are shown in figure 12. Note that the CDFs presented in this figure are the areas between all the possible realization of both predicted power and measured power. It can be observed that the measurement uncertainty has negligible influence in the area validation metric. Figure 13 presents the comparison using the experimental power curve.

From figures 12 and 13, it can be observed that using the official power curve produces an over-prediction of powers below 90 [MW]. The opposite effect is observed when the experimental power curve is used: the power is under-predicted of powers below 90 [MW]. The obtained validation metrics normalized by the experimental mean power were 3% for the official power curve case, and 2% for the model that uses the experimental power curve. This suggests that the model uncertainty is lower if the experimental curve is used. The resulting model uncertainty estimations imply that using the NOJ model with the experimental power curve will

predict the actual mean power with an error of $\pm 2\%$. It is important to highlight that the area validation metric is given in absolute value, which means that it does not hold the sign of the bias. The reason for this is that due to the epistemic nature of model uncertainty, the modeler does not know before hand whether the model over-predicts the power or under-predicts it. Furthermore, the area validation metric penalizes a model that might predict the mean by compensating under-predictions with over-predictions [3].

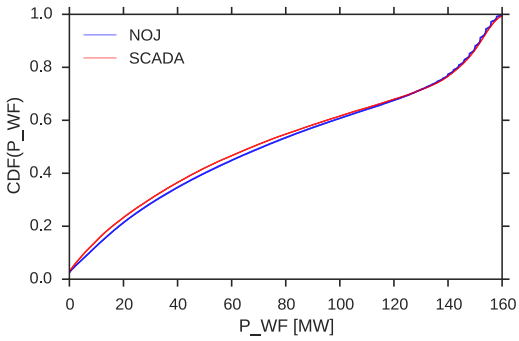

Figure 12: Area metric for CDF(P): $U_{model} = 3\% \, \mathbb{E}(P_{WF\,SCADA})$.

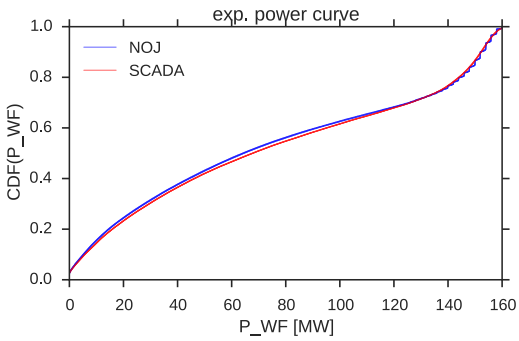

Figure 13: Area metric for CDF(P) using the experimental power curve: $U_{model} = 2\% \, \mathbb{E}(P_{WF\,SCADA})$

3.5. Model validation for AEP

The probability density function (PDF) of the AEP of 1000 possible years of inflow climate is presented in figure 14. This figure shows the distribution of a single realization of measurement uncertainty in the inputs (for the model), of a single realization of output uncertainty (for the SCADA database) and the aggregated distributions of AEP that include all possible realization of the measurement uncertainties. The single realization cases show peaks in the distribution which create variation in the prediction of the mean AEP (expected AEP, or P_{50}). It can also be observed that there is a bias in the model prediction of the expected AEP. This bias is due in part to the over-prediction of power caused by the official power curve. Finally it can be observed that the overall shape of the PDF of the AEP is well captured by the model. It can be concluded that the shape of the PDF of AEP only depends on the realization of the climate in the given year (bootstrapped sample).

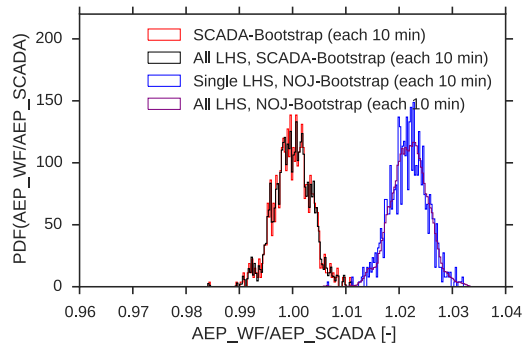

Figure 14: AEP distribution of 1000 possible years (bootstrap) with measurement uncertainties.

The final step is to combine the CDF of model AEP with the model uncertainty that was computed in section 3.4. This process is shown in figure 15. The combination of input uncertainty propagation through the model with the expected model uncertainty gives an expected range of AEP distributions. In this figure the blue are represents the range of possible CDF predicted by propagating of input uncertainties, while the green area includes the 3% model uncertainty. It can be observed that the actual distribution of AEP based on the SCADA data (red area) lies inside the predicted range (green area).

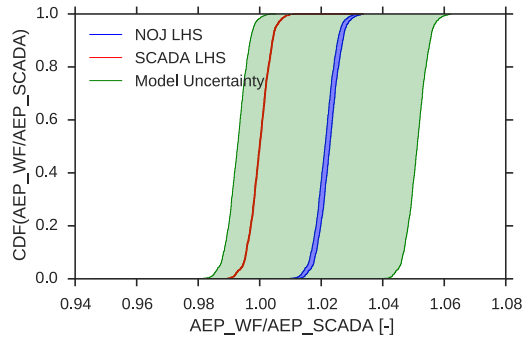

Figure 15: AEP cumulative probability distribution of 1000 possible years (bootstrap) with measurement uncertainties and wake model uncertainty.

The same procedure was repeated for the NOJ model using the experimental power curve. The probability density function of the AEP of 1000 possible years of inflow climate is presented in figure 16. This figure shows an under-prediction of the AEP. The confidence interval presented in figure 16 is a more accurate estimation of the actual bias of the NOJ model. The reason for this is the fact that the use of the experimental power curve minimizes the compensation caused by the over-prediction of the official power curve.

The combination of the CDF of model AEP with the model uncertainty is shown in figure 17 for the NOJ model with

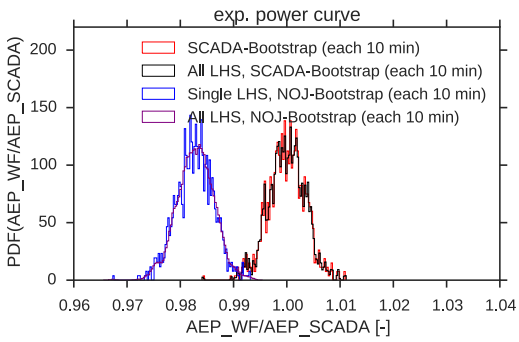

Figure 16: AEP distribution of 1000 possible years (bootstrap) with measurement uncertainties. NOJ model with experimental power curve.

the experimental power curve. The combination of input uncertainty propagation through the model with the expected model uncertainty gives an expected range of AEP distributions. It can be observed that the actual distribution of AEP based on the SCADA data lies inside the predicted region.

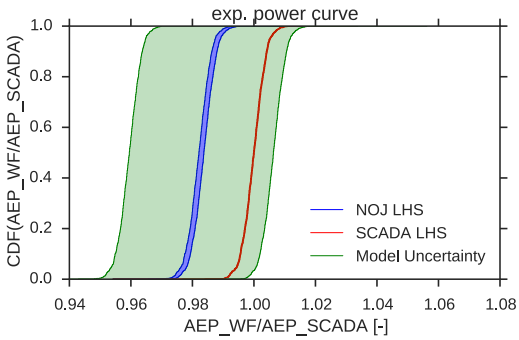

Figure 17: AEP cumulative probability distribution of 1000 possible years (bootstrap) with measurement uncertainties and wake model uncertainty. NOJ model with experimental power curve.

4. Discussion

The present framework can explain the difficulties seen in the previous wake model benchmarking campaigns. The main issue is the effect of input uncertainty in wind speed and direction in the binning process. As a consequence several of the observations obtained when filtering very narrow flow cases have actual values of wind speed and wind directions outside the bin. To show an example of the consequences of this miss-placement, the SCADA and modeled databases were filtered for an undisturbed wind direction inside [270, 272.5] [deg.] and a wind speed inside [10, 10.5] [m/s]. Figure 18 show the resulting regions of power distribution. These results reveal that due to the propagation of input uncertainty there is a null area validation metric when the model uses the official power curve. This can be interpreted as a lack of evidence of a model inadequacy in this flow case. This lack of evidence is not because of a perfect model but due to the large uncertainty in the inputs of the model.

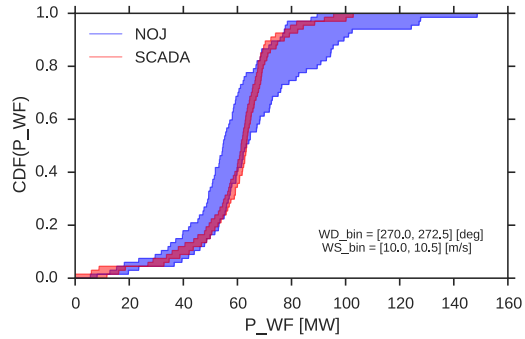

Figure 18: Area validation metric for CDF(P) for an individual flow case is null.

Figure 19 shows a similar analysis using the experimental power curve. In this case there is a relative model uncertainty of 3%. This evaluation of model inadequacy as a function of wind speed and wind direction requires to consider the measurement uncertainty in undisturbed flow conditions and in power.

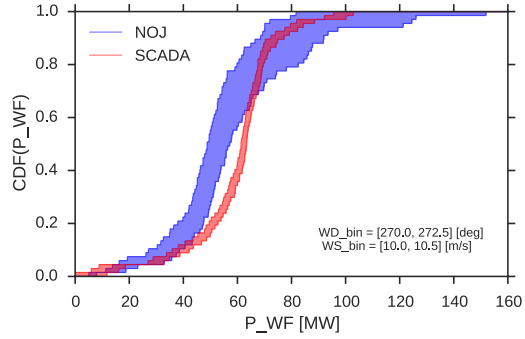

Figure 19: Area validation metric for CDF(P) for an individual flow case experimental power curve. 3%.

4.1. Further work for a full wind power plant AEP uncertainty prediction

The use of area validation metrics for power prediction distributions with uncertainty for each individual turbine inside the wind farm is planed. This study will conclude with the construction of a response surface that captures the dependency of the model uncertainty as a function of the wind speed and wind direction for each individual turbine (wake model validation region). From this results a predictive tool can be generalized such that the SCADA data from Horns Rev 1 could be use to predict the uncertainty on AEP prediction for an offshore wind power plant with an arbitrary layout. The proposed framework could be used to benchmark different wake models and to obtain individual validation regions for each model. This two aspects are the focus of the IEA-task 31.

The added uncertainty that come from modeling the power plant at full availability and by applying a percentage of operating turbines for each 10-minutes period will be studied using the area validation metric methodology. Finally the model discretization uncertainty will be quantified. This means to understand the effect of creating a wake model response database using a limited number of model evaluations.

5. Conclusions

A bias in the modified NOJ wake model prediction of annual energy production has been identified. The size and sign of this bias depends on whether the official or experimental power curve is used. The use of the official power curve makes it hard to identify the errors in the wake model, due to the errors in the turbine model. The use of the official power curve gives a larger uncertainty of the overall model based on the area validation metric of total power cumulative density function. The use of an experimental power curve or a site corrected turbulence intensity power curve indicate a lower level of superposition of turbine and wake model errors.

The standard deviation of the AEP distribution was found to be well captured by the NOJ model. It can concluded that it mainly depends on the realizations of the possible one-year wind climates and it can be more accurately predicted if the measurement uncertainty is taken into account.

Furthermore an explanation to the problem of wake model benchmarking based on filtered flow cases indicates that the measurement uncertainty in the wind speed and wind direction is large enough that there is no statistical evidence about the accuracy of the wake model if the official power curve is used. On the contrary there is statistical evidence of model inadequacy for a narrow flow case if the experimental power curve is used. Further work is planed in which the distribution of model prediction error (model uncertainty) as a function of both wind speed and wind direction for individual wind turbine power is studied.

Acknowledgments

This work was supported by the International Collaborative Energy Technology R&D Program of the Korea Institute of Energy Technology Evaluation and Planning (KETEP), granted financial resource from the Ministry of Trade, Industry & Energy, Republic of Korea. (No. 20138520021140). The authors thank DONG Energy AS and Vattenfall AB for the access to the SCADA data of Horns Rev 1.

Nomenclature

AEP	Annual energy production
CDF	Cumulative probability density function
$\mathbb{E}(x)$	Expected value of a random variable x
LHS	Latin hyper-cube sampling
PDF	Probability density function
SCADA	Supervisory control and data acquisition

References

[1] Barthelmie, R. J., Pryor, S., Frandsen, S. T., Hansen, K. S., Schepers, J., Rados, K., Schlez, W., Neubert, A., Jensen, L., and Neckelmann, S. (2010). "Quantifying the impact of wind turbine wakes on power output at offshore wind farms." *Journal of Atmospheric and Oceanic Technology*, 27(8), 1302–1317.

[2] Efron, B. (1979). "Bootstrap methods: another look at the jackknife." *The annals of Statistics*, 7(1), 1–26.

[3] Ferson, S., Oberkampf, W. L., and Ginzburg, L. (2008). "Model validation and predictive capability for the thermal challenge problem." *Computer Methods in Applied Mechanics and Engineering*, 197(29), 2408–2430.

[4] Gaumond, M., Réthoré, P.-E., Ott, S., Peña, A., Bechmann, A., and Hansen, K. S. (2014). "Evaluation of the wind direction uncertainty and its impact on wake modeling at the horns rev offshore wind farm." *Wind Energy*, 17(8), 1169–1178.

[5] Hansen, K. S., Barthelmie, R. J., Jensen, L. E., and Sommer, A. (2012). "The impact of turbulence intensity and atmospheric stability on power deficits due to wind turbine wakes at Horns Rev wind farm." *Power*, (November 2011), 183–196.

[6] IEC et al. (2005). "Iec 61400-12-1-2005 wind turbines-part 12-1: Power performance measurements of electricity producing wind turbine." *Switzerland: International Electrotechnical Commission*.

[7] IEC et al. (2013). "Iec 61400–12-2, wind turbines: part 12–2: Power performance of electricity producing wind turbines based on nacelle anemometry." *Switzerland: International Electrotechnical Commission*.

[8] Katic, I., Højstrup, J., and Jensen, N. O. (1986). "A simple model for cluster efficiency." *EWEC*, number October, 407–410.

[9] Larsen, G. C. (2009). "A simple stationary semi-analytical wake model." *Technical Report, Risø-R-1713(EN) August 2009*, Risø-DTU.

[10] Moriarty, P., Rodrigo, J. S., Gancarski, P., Chuchfield, M., Naughton, J. W., Hansen, K. S., Machefaux, E., Maguire, E., Castellani, F., Terzi, L., et al. (2014). "Iea-task 31 wakebench: Towards a protocol for wind farm flow model evaluation. part 2: Wind farm wake models." *Journal of Physics: Conference Series*, Vol. 524, IOP Publishing, 012185.

[11] Ott, S., Berg, J., and Nielsen, M. (2014). "Developments of the offshore wind turbine wake model Fuga." *Report No. DTU Wind Energy E-0046*, Risø-DTU, Roskilde, Denmark.

[12] Peña, A., Réthoré, P.-E., and Rathmann, O. (2014). "Modeling large offshore wind farms under different atmospheric stability regimes with the Park wake model." *Renewable Energy*, 70(June), 164–171.

[13] Réthoré, P.-E., Hansen, K. S., Larsen, G. C., Larsen, T. J., Ott, S., Rathmann, O., Penña, A., and Hasager, C. B. (2013). "Benchmarking of wind farm scale wake models in the eera - dtoc project." *Proceedings of the 2013 International Conference on Aerodynamics of Offshore Wind Energy Systems and Wakes (ICOWES2013)*.

[14] Réthoré, P. E., Johansen, N. A., Frandsen, S. T., Hansen, B. K. S., Jensen, L. E., and Kristoffersen, R. (2009). "Systematic wind farm measurement data reinforcement tool for wake model calibration .." *EOW Conference 2009*, 1–10.

[15] Roy, C. J. and Oberkampf, W. L. (2011). "A comprehensive framework for verification, validation, and uncertainty quantification in scientific computing." *Computer Methods in Applied Mechanics and Engineering*, 200(25-28), 2131–2144.

Article D

Improved validation of stationary wake models using uncertainty propagation

WIND ENERGY
Wind Energ. 2015; **00**:1–19
DOI: 10.1002/we

RESEARCH ARTICLE

Improved validation of stationary wake models using uncertainty propagation

Murcia JP [1], Réthoré PE [1], Hansen KS [1], Natarajan A [1], Sørensen JD [1,2]

[1] DTU Wind Energy, Technical University of Denmark, Risø Campus, Frederiksborgvej 399, 4000 Roskilde,Denmark
[2] Aalborg University, Department of Civil Engineering, Sofiendalsvej 11, Building: 11-214, 9200 Aalborg SV, Denmark

ABSTRACT

This study introduces an improved method for the validation of wake models used for power generation predictions from an arbitrary offshore wind plant. The method describes a standard way to analyze the SCADA data of an offshore wind plant. Key elements in the new method are: first, the majority of flow cases are used in the validation. This element contrasts the current wake model validation based on filtering the measurements for fully operational plant conditions and based on a specific wind speed and direction flow case. Second, the method accounts for the uncertainties in the undisturbed wind speed and direction, as well as in the wind turbine performance. Operational data of two Danish offshore wind plants are used as validation cases. The power production prediction of four different stationary wake models is closer to the observed production when uncertainties in the undisturbed wind velocity, power measurement and wind turbine performance are taken into account. Finally, the new methodology is used to identify the weaknesses of the most widely used wake models, to explain the inconsistency of AEP predictions among different offshore wind plants and will lead to an improved estimation of annual energy production of offshore wind plants.

KEYWORDS

Wind turbine wake model, uncertainty quantification, model validation, annual energy production, offshore wind power plant.

Correspondence

Technical University of Denmark, Risø Campus, Building 101, Frederiksborgvej 399, 4000 Roskilde,Denmark. E-mail: jumu@dtu.dk

Received . . .

NOMENCLATURE

AEP	Annual energy production	TI	Mean turbulence intensity
AV	No. turbines available in 10-min	$\overline{u}$	10-min mean axial wind speed at hub height
C_T	Thrust coefficient	u'	Instantaneous axial wind speed at hub height turbulent component
$\mathbb{E}$	Mean or expected value		
L	Wake loss	U_x	Total uncertainty of the variable x
LHS	Latin hyper-cube sampling	$U_{x\,A}$	Type A uncertainty in the variable x
LSS	Large scale turbulent structures	$U_{x\,B\,i}$	Type B uncertainty in the variable x due to the uncertainty source i
N_{MC}	Size of Monte Carlo sample		
N_T	Number of turbines	$\mathbb{V}$	Variance
N_{ts}	Number of timestamps in the database	WD	Spatially averaged undisturbed wind direction
P_{exp}	Experimental power curve. Obtained from the average of multiple upstream turbines	WS	Spatially averaged undisturbed wind speed
		ϵ	10-minute relative prediction error
P_{ref}	Reference power curve used in the turbine model	ϵ_i	10-minute relative prediction error turbine i
P_i	10-min mean power turbine i	ϵ_L	Wake loss relative prediction error
P_{WF}	10-min mean total plant power	η	10-min power plant efficiency
SCADA	Supervisory control and data acquisition	η_i	10-min turbine i efficiency

Prepared using weauth.cls [Version: 2010/06/17 v1.00]

1. INTRODUCTION

Estimating the uncertainty in the prediction of power production of large wind plants is one of the main aspects that the wind energy industry needs to improve in order to reduce the cost of energy. A reduction in the uncertainty of the estimation of energy yield will cause as a consequence a reduction in the interest rates and financial costs associated to a wind energy project [1]. Wake loss prediction has been reported as one of the main sources of uncertainty in the prediction of the annual energy production of large offshore wind plants, [2]. Several wake models are used in the industry to predict the energy yield of wind plants such as: low fidelity engineering models, mid fidelity linearized, parabolized or unmodified RANS CFD models and high fidelity LES models. Wake model validation using offshore wind plant supervisory control and data acquisition (SCADA) databases has been performed in the past in multiple studies [3, 4, 5, 6, 7, 8, 9]. In all these studies the SCADA database is filtered based on a wind speed and direction bin, also called flow case. Walker et al [3] analyzed the performance of several wake models with respect to the SCADA data from five offshore wind farms. This paper is the first analysis to present the wind plant efficiency as a function of the wind speed and direction, although these results were published for large wind direction bins (30 deg.). Moriarty et al [4] published the results of the benchmarking campaign, IEA Task 31 Wakebench, that concluded that there is no clear improvement in the power production prediction of wake models of higher fidelity; this is explained as an effect of the large uncertainties in the validation datasets. Most of the studies disregarded the effect of the measurement uncertainty in the binning process before filtering the database. Furthermore, most authors recognize that due to the large uncertainty in the undisturbed flow conditions little can be said about the inadequacy of wake models. Gaumond et al [5] presented a methodology to improve the prediction capacity of stationary wake models by considering the uncertainty in the wind direction. They concluded that it is important to consider the uncertainty in the undisturbed flow conditions if a comparison with the measurements is to be performed for narrow wind direction sectors. In addition to the flow case filtering, only the cases in which the full power plant is under normal operation have been used for model validation. This additional filter reduces the number of observations to a fraction of the database.

Recently, Nygaard et al [10] reported that the Jensen wake model does not show a consistent wake loss relative prediction error on a large set of offshore wind plants. This study showed that the prediction error of AEP in offshore wind plants is site dependent. We believe that the reason for this inconsistency is the fact that most stationary wake models are design to work on large wind direction sectors and therefore they compensate areas of under-estimation with the areas of over-estimation of wake losses inside the wind direction sectors. The frequency of occurrence of the under-estimations and over-estimations flow cases depends on the wind rose of the site, hence the total prediction error of AEP is site dependent. In order to improve the accuracy of a wake model it is therefore required to understand how the power prediction error is distributed as a function of the undisturbed wind speed and wind direction for narrow flow cases.

The present study has the objective of identifying the wake model prediction error for narrow flow cases. In general, the power prediction error is a mixture of many sources of error: undisturbed wind velocity measurement uncertainty that causes binning errors, wind turbine model uncertainty, wake model error and power measurement uncertainty. This article presents a methodology that accounts for the effect of the uncertainty in each 10-minute mean undisturbed wind speed and wind direction in the long term AEP estimation. Additionally, the uncertainty in the wind turbine model is also considered. Finally, a comparison of model validation with and without uncertainty shows how the treatment of uncertainty improves the estimation of power production in narrow wind direction flow cases and reveals the limitations of current engineering wake models.

The present work can be considered as an extension of the work of Walker et al. [3], although the present study was done before this paper was published. The main difference is that in this article we have decided to focus on the distribution of relative prediction error over very narrow flow conditions for the plant and individual turbines. This allows a better understanding of the limitations of stationary wake models that are not usually reported in the literature. The present work differs from the result presented by Gaumond et al [5] in the fact that more uncertainties have been considered in this study; the power curve is not used as a proxy measurement of the wind speed, additionally the uncertainty in wind direction has been treated in a different manner: we consider that the turbulence fluctuations of the wind direction inside the averaging time should be captured/modeled by stationary wake models, and therefore the uncertainties considered are the uncertainties due to larger scales. The approach presented in this article can help to understand the bias in the prediction of AEP presented by Nygaard et al [10] and by Mortensen et al [2]. In these articles the prediction of AEP in multiple offshore wind plants was reported to have different biases and it is therefore the result of the plant layout and of the local climate. The present article proves that each wind rose will weight the frequency of occurrence of over-prediction regions with under-prediction regions which creates an overall different expected value of the error in wake loss prediction.

Wind Energ. 2015; **00**:1–19 © 2015 John Wiley & Sons, Ltd.
DOI: 10.1002/we
Prepared using weauth.cls

2. METHODOLOGY

The methodology introduced in the present study can be divided into three steps: initially the SCADA measurements of the wind plant are post-processed to determine the observed inputs and observed outputs and their correspondent uncertainties. The second step consists in setting-up a wind plant model and to propagate the input uncertainties through the model. Finally the validation of the model is performed by computing the distribution of the power prediction errors as function of the undisturbed wind velocity (speed and direction).

2.1. SCADA data processing

The requirements of the SCADA dataset of a wind plant to be used for the validation of stationary wake models are: First, it must contain the 10-minute statistics of the sensors located in each individual turbine in the plant such as nacelle anemometer, nacelle position or orientation, power production, rotational speed and pitch angle. Second, the site must include at least one reference meteorological mast in order to perform the nacelle flow distortion and density corrections to the undisturbed wind velocity. The main assumption is that the 10-minute upstream/undisturbed wind velocity is uniform across the plant; this assumption is done to reduce the number of uncertain inflow variables down to two: the spatially averaged wind speed and wind direction. This treatment has the main limitation of disregarding the local inflow conditions for each turbine which can be caused by local wind resource variability inside the plant and/or due to blockage effects. These assumptions are reasonable in the case of offshore plant design since the models should account for the blockage effects. Therefore, the SCADA data is used to determine the 10-minute averages of the input and output variables of a wake model: undisturbed wind speed, undisturbed wind direction, individual wind turbine availability and individual turbine power production. The SCADA data post-processing follows the methodology presented by Murcia et al [11]. The expected values and the correspondent uncertainty of each input and output variable is estimated independently for each 10-minute time-stamp.

Wind speed

The nacelle anemometers of the upstream and undisturbed turbines are averaged to predict a spatially averaged undisturbed wind speed for each 10-minute case. The undisturbed and spatially averaged wind speed are corrected using a nonlinear nacelle transfer function (NTF) as described in the IEC standard 61400-12-1 (2013) [12, 11]. This correction is done with respect to the hub height anemometer located in the nearby met. masts for valid wind direction sector. The spatially averaged undisturbed wind speed (WS) is also corrected for density variations following the IEC 61400-12-1 (2005) standard [13]. The total uncertainty in WS (U_{WS}) has two main components of uncertainty. Type A uncertainty is the variability that can be observed using the standard deviation of the mean of the multiple upstream turbine nacelle anemometers used in the average. Type B uncertainties are additional sources of uncertainty that can not be observed and therefore they are estimated using standards, instrument information and empirical relationships.

Type A measurement uncertainty of WS is estimated based on the number of upstream nacelle anemometers available in each specific 10-minute: $U^2_{\mathrm{WS}\,A} = \mathbb{V}(\mathrm{WS})/N$. Different sources of type B measurement uncertainty are estimated and combined assuming no correlation. This is done following the procedure presented in the IEC standard [12]. The sources of uncertainty considered are: anemometer calibration, operation and mounting, data acquisition resolution, NTF correction and air density correction. Finally, the uncertainty due to the large scale turbulent structures (LSS) is estimated as the absolute difference between the current and previous 10-minute average WS. This considers that the undisturbed flow is not uniform over the averaging time but that there are trends that are being advected downstream in such a way that the most downstream part of the plant will experience the previous timestamp undisturbed flow while the most upstream turbines experience the current timestamp WS. The effect of the LSS is important because a stationary wake model only captures turbulent scales within the 10 minutes, consequently the LSS trends are a source of WS uncertainty. Finally the wind speed is assumed normally distributed around the estimated value and with standard deviation equal to the total uncertainty, see Equations 1 and 2 (these equations use a general notation for any measured variable x: type A uncertainty $U_{x\,A}$, type B uncertainties due to i-th source $U_{x\,B\,i}$ and uncertainty due to LSS $U_{x\,\mathrm{LSS}}$).

$$U_x^2 = U_{x\,A}^2 + \sum \left(\frac{U_{x\,B\,i}}{\sqrt{3}} \right)^2 + U_{x\,\mathrm{LSS}}^2 \qquad (1)$$

$$x \sim \mathcal{N}\left(\overline{x}, U_x\right) \qquad (2)$$

Wind direction

Each nacelle position sensor of the turbines located in the outer edge of the plant is calibrated using the power ratio between the upstream and the first wake operating turbine and the layout of the wind power plant. The nacelle position sensors of the upstream turbines are then combined to predict a spatially averaged undisturbed wind direction (WD).

The type A measurement uncertainty in WD is computed based on the number of upstream nacelle position sensors available. Different sources of type B uncertainties were considered independent and combined following the procedure

presented in the IEC standard [12]: The sources of type B WD uncertainty considered are: in-situ calibration, yaw signal resolution, data acquisition resolution and sensor alignment. Finally, the WD uncertainty due to the large scale turbulent structures is estimated as the absolute difference between two consecutive 10-minute averages.

Power

The uncertainty in the measurement of the 10-minute average power for each individual turbine is considered independent from each other. The uncertainty is estimated using multiple independent type B sources: uncertainties due to power calibration, current transducer operation, voltage transducer operation and data acquisition resolution. The uncertainty of the power produced by the full plant is determined by the combination of the uncertainty of each turbine. This means that the number of uncertain variables related to power measurement is equal to the number of turbines in the wind plant.

Availability

Each turbine is identified as functioning under normal operation in each 10-minute case using its rotational speed, pitch angle and power measurements. This procedure followed the outliers recognition algorithm presented by Réthoré et al [14]. The power production of turbines under down-regulation is forced to be zero. This is equivalent to assuming that the down-regulated turbines were not available.

2.2. Wind plant flow modeling

In this study the stationary wind plant flow models are executed for each individual 10-minute flow condition. A stationary wind plant flow model requires post-processing the single wake models in order to include the effects of partial wakes and wake aggregation, see Figure 1. Wake meandering is not captured by such models, although turbulent fluctuations inside the averaging time are supposed to be modeled.

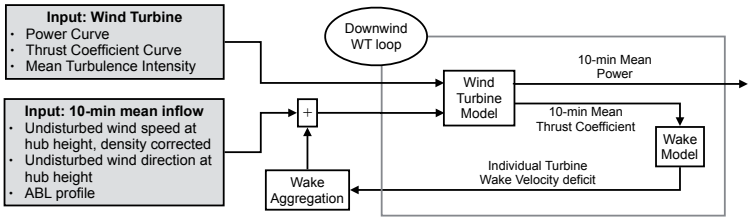

Figure 1. Offshore wind plant flow model diagram.

Wind turbine model

The wind turbine model consists of the power and thrust coefficient curves. The power and thrust coefficient curves are obtained from the official curves reported by the manufacturer and are based on the hub height wind speed [12]. A site correction for the official power curve is required in the planning stages since operational conditions like shear, ambient turbulent intensity or yaw miss alignment will affect the power and thrust curves. Additionally, this correction needs to include operation under wakes or partial wakes; to do so the turbine model uses the rotor averaged wind speed instead of the hub height wind speed in the power and C_T interpolation.

The official power curve is corrected to the site considering an ideal turbine response model. The ideal turbine response, P_{ideal}, assumes a constant power coefficient for powers below rated power, and constant power afterwards, Equation 3. The constant power coefficient for below rated wind speeds is the maximum power coefficient that can be derived from the official power curve, $C_{P\,max}$. This power coefficient is corrected by a power extraction factor, f_p, in order to model the power losses due to the yaw/tilt errors that deviate from the standard turbine.

$$P_{ideal}(\mathrm{WS}) = \begin{cases} \frac{1}{2}\rho\, A\, f_p\, C_{P\,max}\, \mathrm{WS}^3 & \text{if } P_{ideal} \leq P_{rated} \\ P_{rated} & \text{if } P_{ideal} \geq P_{rated} \end{cases} \tag{3}$$

The site correction uncertainty model assumes that the instantaneous axial hub height wind speed is normally distributed with a standard deviation given by the normal turbulence model on the site, Equation 4. Here $\mathbb{E}(\sigma_u|\mathrm{WS})$ is described in the IEC 61400-1 standard [15] as shown in Equation 5. The power curve at the site is the expected power given a hub height wind speed. In the present study the expected site correction is approximated using a Monte-Carlo sample of size N_{MC}, see Equation 6.

$$u' \sim \mathcal{N}(0, \mathbb{E}(\sigma_u|\mathrm{WS})) \tag{4}$$

$$\mathbb{E}(\sigma_u|\mathrm{WS}) = \mathrm{TI}_{ref}\,[0.75\,\mathrm{WS} + 3.8] \tag{5}$$

$$P_{site}(\mathrm{WS}) = \mathbb{E}(P|\mathrm{WS}) = \int_{-\infty}^{\infty} P_{ideal}(\mathrm{WS} + f\,u')\,\mathrm{PDF}(u'|\mathrm{WS})\,du' \approx \sum_{i=0}^{N_{MC}} \frac{P_{ideal}(\mathrm{WS} + f\,u_i')}{N_{MC}} \tag{6}$$

Note that the turbine is not able to capture the total turbulent kinetic energy of the flow because the turbine has a time response lag. The factor of turbulent energy extraction (f) depends on the operational region, control strategy and inertia of the wind turbine. For simplicity, the uncertainty in the site corrected power curve is built by combining 3 uniformly distributed variables that characterize the site and turbine performance: maximum power coefficient reduction factor f_p inside [0.8,0.9], a factor of turbulent energy extraction f inside [0.75,0.85], and a reference turbulence intensity between [0.07, 0.11]. These values are selected to produce a similar variation of the power production to the one observed in multiple upstream turbines as a function of WS.

A model for the uncertainty for thrust curves is built using a Gaussian process distributed around the manufacturer reported thrust coefficient with a squared exponential autocorrelation function with a characteristic velocity scale of 8 $m\,s^{-1}$ and a standard deviation of 5% of the thrust coefficient at a given wind speed. These values are selected to account for variations in the thrust coefficient curve that are smooth and consistent with the larger variability in C_T at lower wind speeds due to the dynamic response of a turbine to different turbulent structures.

Wake model

A wake model predicts the velocity field caused by the wake of a single turbine based on its thrust coefficient and flow conditions such as: ambient turbulence intensity, stability, etc. Each wake model uses a wake aggregation procedure that is responsible for combining the velocity deficits from different upwind turbines to predict the observed wind distribution seen by a downwind turbine. An overview of the models is presented in Table I. None of the models consider yaw misalignment effects on the direction of wake advection. All the models in the present study, with the exception of FUGA, are open source and are available at [16]. In order to avoid an unfair comparison of the models, the parameters for all the models are calibrated to minimize the sum of squares of the relative errors based on Horns Rev 1 database.

Model	Main Assumptions	Inputs (10-min. averages)	Parameters
NOJ [17]	Top-hat velocity deficit	Undisturbed wind velocity	Wake expansion coefficient
	Linear wake expansion	Power/thrust coef. curves	$k_j = 0.04$
	Quadratic wake superposition	Availability	
GAU [18]	Gaussian velocity deficit	Undisturbed wind velocity	wake expansion coefficient
	Linear wake expansion	Power/thrust coef. curves	$k_s = 0.03$
	Linear wake superposition	Availability	
GCL [19]	Self-similar velocity deficit	Undisturbed wind velocity	Mean turbulence intensity
	Wake expansion of order 1/3	Power/thrust coef. curves	TI $= 0.09$
	Linear wake superposition	Availability	
FUGA [20]	Linearized CFD	Undisturbed wind velocity	Mean ABL stability
	RANS/eddy viscosity	Power/thrust coef. curves	Horns Rev 1: $\zeta_0 = 0$, neutral
		Availability	Nysted: $\zeta_0 = 1.0 \times 10^{-7}$, neutral/stable

Table I. Wake models overview.

In the Jensen model (also called Park or Katic, NOJ) [17], the wake velocity deficit profile is assumed to be a top-hat profile that expands linearly with the distance from the wake generating turbine. Furthermore, this model does not update the thrust coefficient of the wake operating turbines. Partial wakes are considered by redistributing the wake deficit hitting part of the turbine over all the rotor area. The squared root of the sum of the squared deficits is used as wake aggregation. In the present study the wake expansion parameter used was 0.04.

Bastankhah et al [18] assume a Gaussian axial wake velocity deficit and a linear wake expansion. This model is an empirical approximation as it does not solve the axisymmetrical turbulent thin shear layer equations, neither continuity equation nor momentum equations. Partial wakes are considered by replacing the hub height wind speed in the turbine model by a rotor equivalent wind speed. This model uses linear wake deficit superposition. The wake expansion parameter used for this model was 0.03.

In the Larsen model (GCL) [19], the wake velocity deficit is assumed to be axisymmetric and self-similar, and a solution of the the turbulent thin shear layer equations is obtained analytically. The assumption of self-similarity of the axial velocity

wake deficit gives a wake expansion of order 1/3. The pressure term in the wake momentum equation is neglected and the Reynolds stresses are replaced using Prandtls mixing length theory. This model uses as a boundary condition an empirical relation for the wake diameter at a downstream distance of 9.6 rotor diameters. The empirical relation gives the far wake diameter as a function of the thrust coefficient and the ambient turbulent intensity. The Larsen model considers partial wakes by computing a rotor equivalent wind speed. Linear wake aggregation is used for multiple wakes superposition. The site average turbulence intensity used in the present study was 0.09.

FUGA [20] is a linearized CFD wake model based on the semi-spectral small perturbation linearization of the steady RANS equations with an eddy viscosity closure for the Reynolds stresses. Additionally, in order to have a grid-less flow solver, the flow variables are Fourier transformed in the horizontal components. Monin-Obukhov similarity theory is used to describe the vertical distribution of the undisturbed flow as a function of atmospheric stability. Partial wakes are considered by using a rotor equivalent wind speed. Linear wake superposition is a consequence of the RANS linearization. The stability parameter, $\zeta_0 = z_0/L$, used in the present study was set to $\zeta_0 = 0$, neutral atmospheric boundary layer, for the Horns Rev 1; while in Nysted, it was set to $\zeta_0 = 1.0 \times 10^7$, which corresponds to a neutral/stable ABL.

Model Verification

Model verification consists in quantifying the errors in the solution of the mathematical equations that describes the physics of the model. In the case of stationary wake models two errors are introduced in the power prediction: errors due to not considering the actual turbine availability and errors due to the interpolation of a precomputed database of flow cases.

The wind power plant models handle turbine availability in two possible ways: by considering the available turbines in each of the 10-min timestamps as the only turbines generating power and wakes $P_{\text{WF model}}$, and by scaling the fully available plant power production $P_{\text{WF model Full AV}}$ with the fraction of turbines available. The relative error due to availability is defined in Equation 7. The distribution of the relative error due to availability for Horns Rev 1 is presented in the Figure 2. This error is normalized with respect to the gross power predicted using the experimental power curve without wakes, $N_T\, P_{\text{exp}}$. The availability error is only important in the region bellow rated where the wake losses are overestimated when assuming the scaled full available power; the errors due to availability are reduced when only the flow cases in which at least 95% of the turbines are operating under normal conditions (AV>=76 for Horns Rev 1). See Figure 2.

$$\epsilon_{\text{AV}} = \frac{P_{\text{WF model}} - [\text{AV}/N_T]P_{\text{WF model Full AV}}}{N_T\, P_{\text{exp}}} \tag{7}$$

Additionally, a database of the power produced by a fully available plant is interpolated to predict the power on a given 10-minute condition. The interpolation of a precomputed database reduces the number of full model evaluations required in the analysis. A two-dimensional cubic spline is used for model interpolation. The convergence of the absolute interpolation error as a function of the number of evaluation points on the NOJ model is presented in Figure 2 (right); the interpolation error is defined in Equation 8. This figure shows how the mean absolute error decreases exponentially with the increase of number of model evaluations. In the present study the fully available models databases were evaluated using $\Delta\text{WD} = 2^\circ$ and $\Delta\text{WS} = 1.5\, m\, s^{-1}$, which corresponds to 1800 model evaluations, see Figure 2 (center).

$$\epsilon_{interp} = \frac{P_{\text{WF interp}} - P_{\text{WF model Full AV}}}{N_T\, P_{\text{exp}}} \tag{8}$$

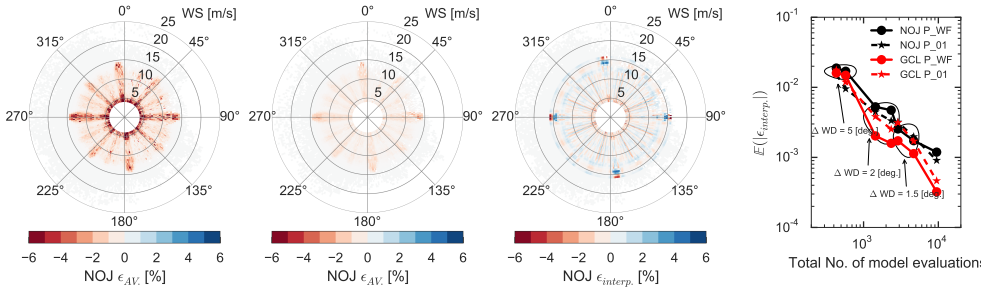

Figure 2. Model verification in Horns Rev 1. (Left) Error due to individual turbine availability for all cases. (Center left) Error due to individual turbine availability for at least 95% availability. (Center right) Model interpolation error for a database build with $\Delta\text{WD} = 2^\circ$ and $\Delta\text{WS} = 1.5\, m\, s^{-1}$. (Right) Convergence of the mean absolute model interpolation error.

DOI: 10.1002/we
Prepared using weauth.cls

2.3. Model validation

This section describes the process of stationary wake model validation, which consists in quantifying the prediction error of a model with respect to a measurement dataset, see Figure 3. In order to accurately estimate the model prediction error it is required to consider the uncertainties in the input and output variables. The uncertainties in the input and output variables are sampled to estimate candidates of their true values. The true inputs are used in the model evaluation. Finally, the measured and predicted output variables are compared and the prediction error is computed. In the last step, each prediction error is assigned back to the observed inputs; by doing that the effect of misplacing an observation in the wrong WS, WD bins is considered.

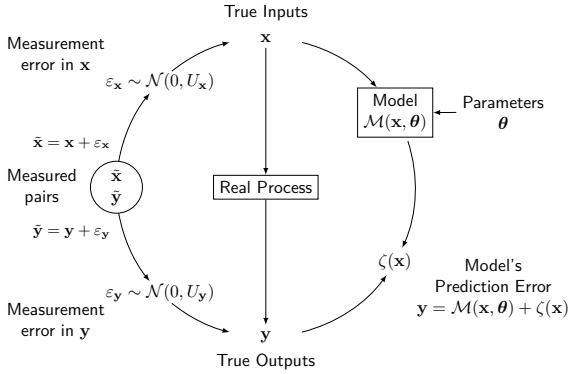

Figure 3. Model validation diagram. Modified from [21]

Input/Output uncertainty sample

A Monte-Carlo sample of the each individual 10-minute inputs (WS, WD) and outputs (observed power for each turbine) is generated. This sample represents possible realizations of their true value. The uncertainty in each variable and for each 10-minute case are considered independent. A Latin-Hypercube sampling (LHS) is used to generate an unitary uniformly distributed sample for a number of variables equal to the total number of inputs and outputs times the number of timestamps in the database: $[N_T + 2]N_{ts}$. LHS is used because it assures that the obtained sample captures the target variability and assures the independence among the variables [22]. This uniform sample is then transformed into the normal distribution obtained in the uncertainty characterization using the inverse of the cumulative density function for each variable. As a result, 50 independent realizations of the WS, WD and P_i time series are obtained; each one has a length equal to the number of 10-minute stamps available in the years of SCADA data.

Wind turbine model uncertainty sample

A sample of 20 independent site corrections for the wind turbine model (power and thrust coefficient curves) is generated by performing the site correction described in Equations 4, 5 and 6 for a 20 LHS of the three uncertain parameters of the correction: f_p, f and TI_{ref}. The combination of input/output sample and turbine model sample gives a total of 1000 independent realizations of possible input/output variables true value.

Input uncertainty propagation

Model results are evaluated for each case in the inputs sample by interpolation of the power database under a fully available plant generated using one of the turbine model realizations. The power prediction is then scaled using the fraction of turbines available at the given 10-minute time-stamp. As a result 1000 independent time series for the power produced in each turbine are predicted. Each realization of power time-series lasts the number of available years in the SCADA data.

Validation metric

The relative prediction error based on the total wind power plant is used to compare the power measurements with the model predictions, see Equation 9. This error metric is defined since it represents a prediction error in power plant efficiency for a given 10-minute case η, hence its distribution over WS and WD can be studied. The relative prediction error consists of a power prediction error normalized by the gross or wake-less power. The gross power is predicted using the reference power curve used in the wind turbine model; when the uncertainties are not considered the reference power curve is the experimental power, which is obtained by averaging the power produced by the upstream turbines as a function

of the spatially averaged undisturbed wind speed, WS. The normalization of the power prediction error by the gross power has the effect of removing the dependency of the wind speed in this error metric. Similarly, the relative prediction error metric for an individual wind turbine power is used for model validation of individual turbine performance. Equation 10 shows this metric for turbine i.

$$\epsilon = \eta_{\text{meas}} - \eta_{\text{model}} = \left(1 - \frac{P_{\text{WF meas}}}{N_T\, P_{\text{ref}}}\right) - \left(1 - \frac{P_{\text{WF model}}}{N_T\, P_{\text{ref}}}\right) = \frac{P_{\text{WF model}} - P_{\text{WF meas}}}{N_T\, P_{\text{ref}}} \tag{9}$$

$$\epsilon_i = \eta_{i\ \text{meas}} - \eta_{i\ \text{model}} = \left(1 - \frac{P_{i\,\text{meas}}}{P_{\text{ref}}}\right) - \left(1 - \frac{P_{i\,\text{model}}}{P_{\text{ref}}}\right) = \frac{P_{i\,\text{model}} - P_{i\,\text{meas}}}{P_{\text{ref}}} \tag{10}$$

In order to have a global measure for model comparison and to have a metric to compare with the literature, the wake loss for the total plant is defined in Equation 11. The wake loss relative prediction error is defined in Equation 12. Note that the metrics for wake loss compute the expected gross and the expected net powers individually; hence these metrics are not equivalent to the expected value of the 10-minute plant efficiency distribution, $\mathbb{E}(\eta)$, nor to its expected relative efficiency prediction error, Equation 13. A similar validation approach as the one proposed by Walker et al [3] is used. The approach consists of weighting the results using a reference wind speed distribution characteristic of Northern sea climate (Rayleigh with a mean wind speed of 9.5 $m\,s^{-1}$) and a wind direction uniformly distributed. This approach is necessary because the wind resources in the validation period are different to the long term resources and because the actual long term wind climate at the sites have proprietary restrictions.

$$L = 1 - \frac{\mathbb{E}(P_{\text{WF}})}{\mathbb{E}(N_T\, P_{\text{ref}})} \tag{11}$$

$$\epsilon_L = 1 - \frac{L_{\text{model}}}{L_{\text{meas}}} \tag{12}$$

$$\epsilon_{E\eta} = 1 - \frac{\mathbb{E}(\eta_{\text{model}})}{\mathbb{E}(\eta_{\text{meas}})} = \frac{\mathbb{E}(\epsilon)}{\mathbb{E}(\eta_{\text{meas}})} \tag{13}$$

3. MEASUREMENTS

The described methodology is applied to two Danish offshore wind plant cases, see Figure 4. Horns Rev 1 is a 160 MW plant, located in the western shore of Denmark, 14 km away from the coast. Horns Rev 1 is co-owned by Vattenfall AB (60%) and by DONG Energy AS (40%). It consists of 80 Vestas V80-offshore 2 MW wind turbines. The spacing between turbines is 7 rotor diameters in both alignment directions. Horns Rev 1 started operation in 2002 and is still operating in 2015. This study uses 3 years (2005-2007) of measurements from its SCADA database.

Nysted is a 166 MW plant located in the south-eastern coast of Denmark, south of Sjaelland, located 10.5 km from the coast. It is also known as Rødsand I. Nysted is co-owned by PensionDanmark (50%), DONG Energy SA (42.75%) and Stadtwerke Lübeck GmbH (7.25%). It consists of 72 Siemens (formerly Bonus Energy AS) B82-2300 kW offshore wind turbines. The spacing between turbine are 5.9 and 10.4 rotor diameters. Nysted started operation in 2003 and is still operating in 2015. 2.5 years (May 2004 to December 2006) of SCADA measurements are used in this study.

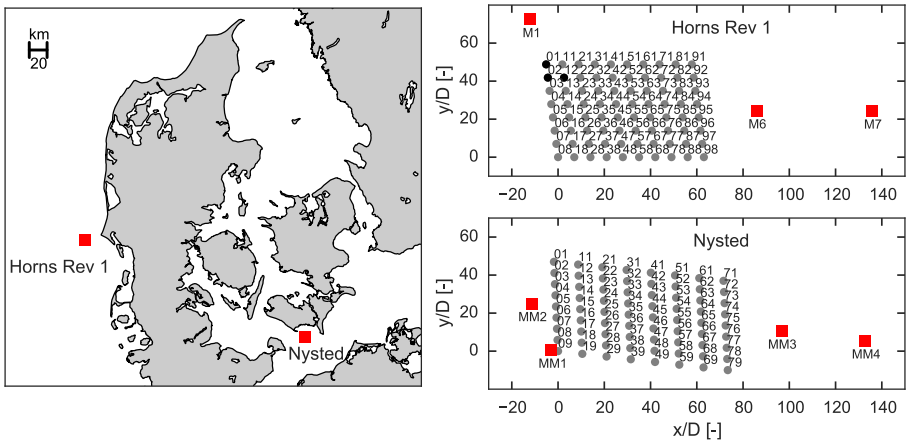

Figure 4. Location and layout of Horns Rev 1 and Nysted. Dark markers indicate the turbines selected for individual analysis.

3.1. Case 1: Horns Rev 1

The measurement uncertainty estimation has been conservative because the authors had no access to the information about calibration, mounting, quality, maintenance of any of the sensors in the wind farm. The uncertainty assumptions for Horns Rev 1 are presented in Table II. Note that the Type A, Type B due to density correction and the LSS uncertainties are not indicated in this table because they are computed for each individual 10-minute case. The sample of the uncertainty model in the power and thrust coefficient curves is shown in Figure 5. In this figure the official curves and the experimental power curve obtained using the SCADA database are also shown. The realizations of possible power curves cover the experimental power curve. It can also be observed that the main source of uncertainty in the turbine model is due to the thrust coefficient uncertainty.

Variable	Source	U_{Bi}
WS	Calibration	0.25 $m\,s^{-1}$
	Operation	class: 1.7A
	Mounting	0.2%
	Data acquisition resolution	0.05 $m\,s^{-1}$
	NTF correction	2 %
WD	In-situ calibration	3°
	Yaw signal resolution	2.5°
	Data acquisition resolution	0.05°
	Sensor alignment	1°
	NTF correction	1°
P	Calibration	2 %
	Current transducer	2 %
	Voltage transducer	0.9 %
	Data acquisition resolution	2 kW

Table II. Assumed measurement uncertainty for Hors Rev 1.

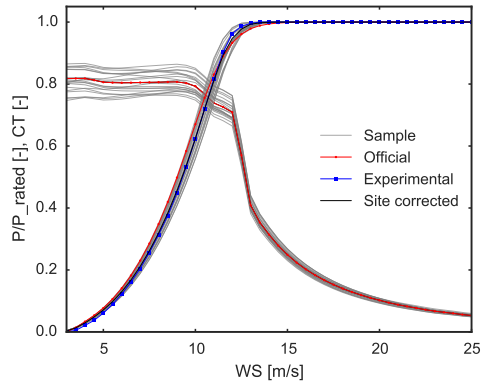

Figure 5. Power curve and thrust coefficient curve Horns Rev 1.

3.2. Case 2: Nysted

As in Horns Rev 1 case, the measurement uncertainty estimation has been conservative because the authors had no access to the information about the calibration, mounting, quality, maintenance of any of the sensors in the wind farm. The sample of the uncertainty model in the power and thrust coefficient curves for Nysted is shown in Figure 6. The official curves and the experimental power curve obtained using the SCADA database are also shown in this figure. Note that the experimental power curve predicts larger powers for wind speeds lower than 6 $m\,s^{-1}$. This is caused by the fact the the B82-2300 turbine operates at two rotational speeds one for low wind speeds and one for large wind speeds.

Variable	Source	U_{Bi}
WS	Calibration	0.25 $m\,s^{-1}$
	Operation	class: 1.7A
	Mounting	0.2%
	Data acquisition resolution	0.05 $m\,s^{-1}$
	NTF correction	2 %
WD	In-situ calibration	3°
	Yaw signal resolution	2.5°
	Data acquisition resolution	0.05°
	Sensor alignment	1°
	NTF correction	1°
P	Calibration	2 %
	Current transducer	2 %
	Voltage transducer	0.9 %
	Data acquisition resolution	2 kW

Table III. Assumed measurement uncertainty for Nysted.

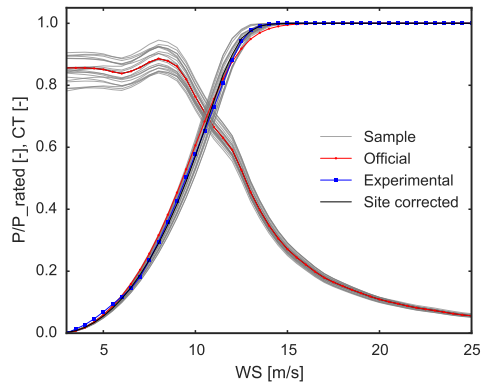

Figure 6. Power curve and thrust coefficient curve Nysted.

4. RESULTS

4.1. Case 1: Horns Rev 1

The observed total plant power production at Horns Rev 1 is shown in Figure 7. The mean observed power production and its standard deviation is depicted for three different levels of filtering of the SCADA database. Filtering the database to have full plant availability considerably reduces the number of observations that can be used to study the distribution of power production, see first column Figure 7. Accepting all observed availability cases produces a large variance in the power production, second column in Figure 7, that hides the actual variability caused by having different wake conditions. The observed power for the selected filtering level (95% minimum plant availability, AV>=76 for Horns Rev 1) shows a clear pattern of wake deficits for the main directions of alignment and a clear pattern of variation of power due to the different wake conditions, see third column Figure 7. The different wake conditions are due to the different stability and ambient turbulence intensity in each observed flow case. Furthermore, the fourth column in Figure 7 summarizes the LHS obtained for WS, WD and P. This distribution places a flow case on each candidate true value of WS, WD and P, and therefore gives an idea of the scale of the effect of miss-placing an observation in the power polar plot.

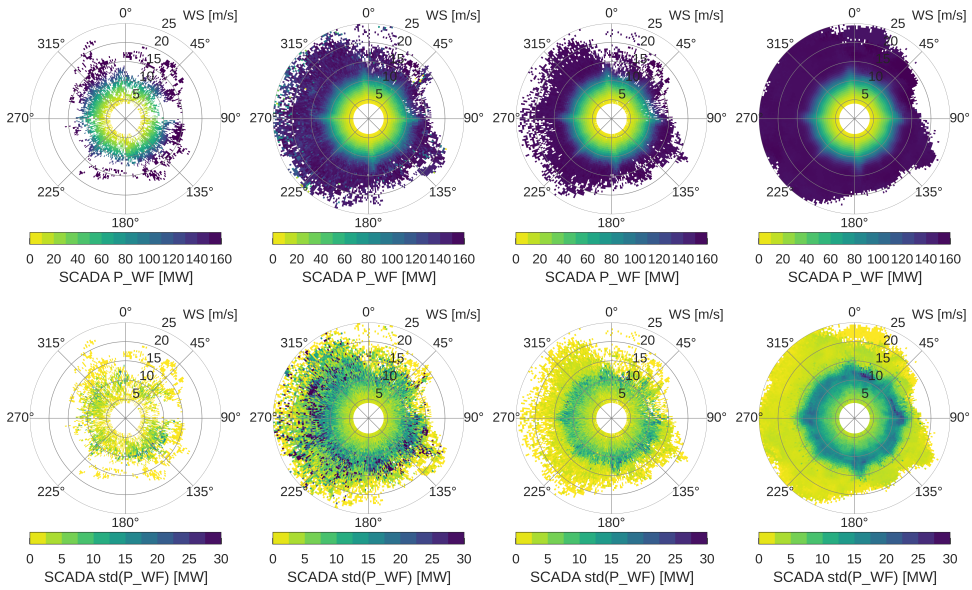

Figure 7. Observed power production at Horns Rev 1. (Top row) Expected power for each bin, (bottom row) standard deviation of power for each bin. (Left) For fully available plant, (center left) for all the database, (center right) for at least 95% available plant without uncertainties, (right) for at least 95% available plant with LHS of the candidate true values of WS, WD and P uncertainties.

Relative prediction error

The distribution of the relative prediction error for each of the wake models without considering uncertainties is shown in the top row of Figure 8. All the models under-predict the power production for the wind directions in which there is a large number of turbines aligned. Additionally, all models show evidence of error compensation when the wind direction is binned in 30° sectors as there are regions of both under-prediction and over-prediction. The relative prediction error validation metric does not depend on the wind speed, besides the clear separation in each turbine operational region: below cut-in, below rated and above rated.

The distribution of the relative prediction error for each of the wake models when the uncertainties in WS, WD and P are considered is presented in the central row in Figure 8; note that this relative prediction error does not consider the uncertainty in the turbine model (site correction) but uses the experimental power curve and the official thrust curve. All the models show lower prediction errors when WS, WD and P uncertainties are considered; note that the color scale in the two bottom rows in the Figure 8 have narrower ranges than the one in the top row. In particular, after propagation of uncertainties the models do not compensate the regions of under-predictions with the regions of over-prediction as in

the comparison without uncertainties. Moreover, the maximum errors continue to be in the main directions of alignment. Similar results are obtained when both WS, WD, P and wind turbine model uncertainties are considered. These results are shown in the bottom row of Figure 8. The relative prediction error is not considerably changed by introducing the uncertainties in the wind turbine model. The main difference are the larger over-prediction errors for wind speeds lower than 6 $m\,s^{-1}$ which are a consequence of having a site corrected power curve that predicts higher power than the experimental power curve, see Figure 5. The errors due to coastal effects can also be seen when uncertainties are considered for GCL and FUGA models; these effects occur when the wind direction comes from the East: [60,90]°. In those directions the coast creates an internal boundary layer that generates a higher ambient turbulent intensity and, consequently, increases the mixing in the wake. For this reason coastal effect creates regions of model under prediction of power.

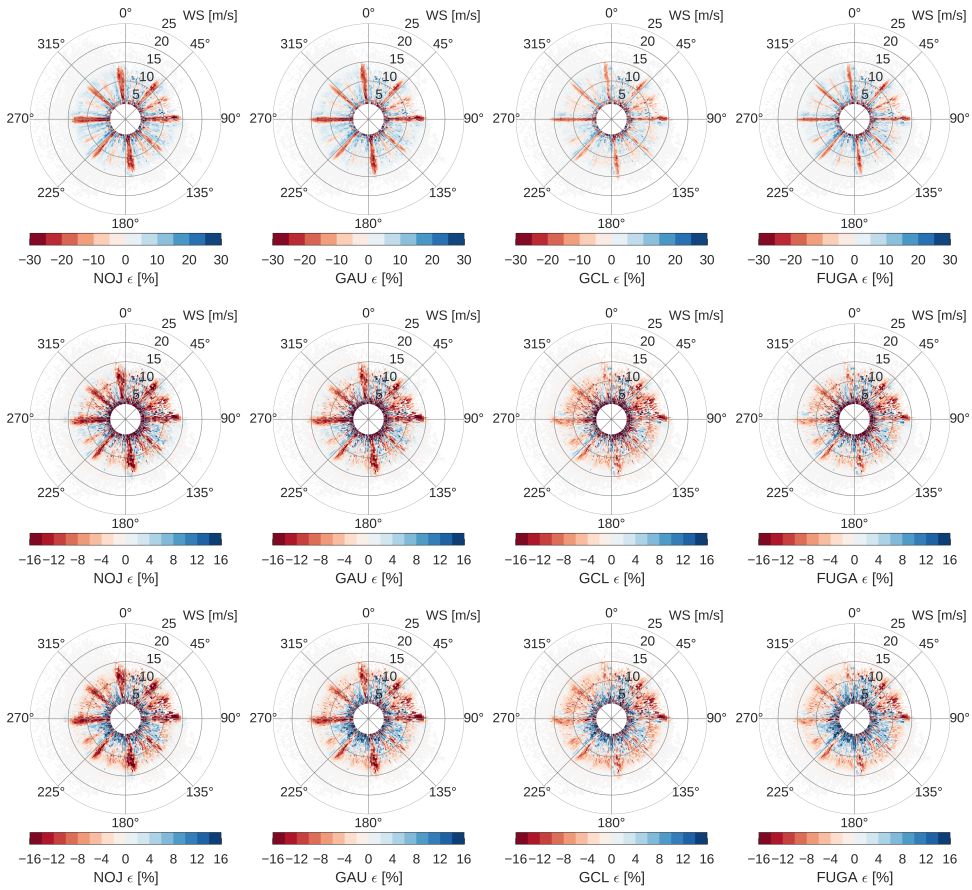

Figure 8. Relative prediction error distribution at Horns Rev 1 for at least 95% availability (top row) without considering uncertainties and using experimental power curve and official thrust coefficient curve (central row) considering uncertainties in WD, WS and P and using experimental power curve and official thrust coefficient curve (bottom row) considering uncertainties in WD, WS, P and turbine model. The colorbar scales of the top and bottom rows are different for clarity.

Wake loss validation

The resulting wake loss predictions and their relative errors are presented in Table IV for all the models with and without considering uncertainties. Here, several different wind direction distributions are used to estimate the wake losses. The cases 1 and 2 use an uniform wind rose, WD $\sim \mathcal{U}(0, 360)$. Case 1 has no availability filter while case 2 filters the database for 95% availability (AV>=76 for Horns Rev 1). Comparing these two cases shows that the wake losses reported

in the literature include the losses due to availability, down-regulation and instrument errors; as a consequence, there is an overestimation of the wake losses. Additionally, for cases 1 and 2, the propagation of uncertainty does not influence the prediction of wake losses. The site correction of the turbine model and its correspondent uncertainty model have a larger impact in the expected efficiency than in the wake losses; the reason for this is that the amount of power produced in the region where the site corrections divers from the experimental performance (WS$<6m\,s^{-1}$) is reduced, while the efficiency prediction error is a normalized power prediction error and therefore scale up the effect of this region.

The other cases in Table IV represent metrics for single wind direction sector of various widths. The relative error on the wake loss is low for larger sectors independent of the propagation of uncertainty but the error increases as the sector width is reduced, see cases 5 to 7. This is caused by the error compensation that happens in larger WD sectors, but that does not occur in narrower WD sectors. Additionally, cases 3 and 4 show that the error compensation changes when a wind direction sector is moved by 5°; this rotation of the wind direction sector is equivalent to have the same layout placed in a slightly different climate. The reason for this change in wake loss estimation is that the new sector includes a region where there are larger prediction errors. Moreover, the errors are considerably larger when the the reference wind direction sector includes a direction of main turbine alignment, cases 5 to 7. Table IV shows that the relative error on the wake loss is overestimated when the uncertainty in the flow conditions are neglected; a better estimation of this prediction error is obtained after propagation of uncertainty for narrower WD sectors.

			No uncertainty and experimental power curve				WS, WD, P uncertainties and experimental power curve				WS, WD and P uncertainties and wind turbine model uncertainty			
WD Sector	Variable	SCADA	NOJ	GAU	GCL	FUGA	NOJ	GAU	GCL	FUGA	NOJ	GAU	GCL	FUGA
1) $\mathcal{U}(0,360)$ AV>= 0	L [%]	15.4	15.7	15.6	15.7	15.3	15.8	15.7	15.7	15.3	15.8	15.8	15.7	15.3
	ϵ_L [%]		-2	-1	-1	1	-2	-2	-2	1	-2	-2	-1	1
	$\mathbb{E}(\eta)$ [%]	15.6	16.2	16.0	16.0	15.6	16.2	15.9	15.9	15.7	15.9	15.6	15.5	15.3
	$\epsilon_{E\eta}$ [%]		-4	-3	-3	0	-4	-2	-2	-1	-2	0	1	2
2) $\mathcal{U}(0,360)$ AV>= 76	L [%]	11.5	11.8	11.7	11.7	11.3	11.8	11.7	11.7	11.2	11.7	11.7	11.5	11.0
	ϵ_L [%]		-3	-2	-2	2	-3	-2	-2	2	-2	-2	-1	4
	$\mathbb{E}(\eta)$ [%]	11.4	12.2	11.9	11.9	11.5	12.1	11.8	11.8	11.7	11.8	11.4	11.3	11.2
	$\epsilon_{E\eta}$ [%]		-7	-4	-4	-1	-6	-4	-4	-3	-4	0	1	2
3) $\mathcal{U}(195,225)$ AV>= 76	L [%]	9.9	10.4	10.0	10.0	9.9	10.2	9.8	9.8	9.6	10.2	9.9	9.7	9.5
	ϵ_L [%]		-5	-1	-1	1	-3	1	1	3	-3	0	2	4
	$\mathbb{E}(\eta)$ [%]	11.4	12.5	11.9	11.7	11.6	12.1	11.4	11.3	11.4	11.8	11.1	10.9	11.0
	$\epsilon_{E\eta}$ [%]		-10	-4	-3	-2	-6	0	1	0	-4	3	4	4
4) $\mathcal{U}(200,230)$ AV>= 76	L [%]	10.6	10.6	10.2	10.1	10	10.5	10.1	10	9.8	10.3	10.1	9.8	9.6
	ϵ_L [%]		0	4	5	6	1	4	5	7	3	5	8	9
	$\mathbb{E}(\eta)$ [%]	12.4	12.8	12.3	12	11.9	12.6	12.0	11.8	11.8	12.3	11.6	11.3	11.3
	$\epsilon_{E\eta}$ [%]		-3	1	3	4	-2	3	5	5	1	6	9	9
5) $\mathcal{U}(255,285)$ AV>= 76	L [%]	13.1	14.3	14.7	14.1	13.5	14.3	14.6	14.0	13.4	15.0	15.4	14.7	14.1
	ϵ_L [%]		-9	-12	-7	-2	-8	-11	-7	-2	-14	-17	-12	-8
	$\mathbb{E}(\eta)$ [%]	14.6	16.3	16.6	16.1	15.4	16.2	16.4	15.9	15.4	15.9	16	15.3	14.8
	$\epsilon_{E\eta}$ [%]		-12	-14	-10	-5	-11	-12	-9	-5	-9	-10	-5	-1
6) $\mathcal{U}(265,275)$ AV>= 76	L [%]	18.5	26.6	27.1	23.5	23.3	23.0	23.4	20.8	20.4	22.1	22.6	19.8	19.4
	ϵ_L [%]		-44	-47	-28	-26	-25	-27	-13	-10	-20	-22	-7	-5
	$\mathbb{E}(\eta)$ [%]	19.7	30.5	30.4	26.5	26.6	26.0	26.1	23.4	23.2	25.7	25.4	22.5	22.3
	$\epsilon_{E\eta}$ [%]		-55	-54	-35	-35	-32	-32	-19	-18	-30	-29	-14	-13
7) $\mathcal{U}(267.5,272.5)$ AV>= 76	L [%]	19.7	29.7	32.3	29.4	29.3	24.8	25.6	22.8	22.5	22.6	23.5	20.6	20.3
	ϵ_L [%]		-51	-64	-49	-48	-26	-30	-16	-14	-14	-19	-4	-3
	$\mathbb{E}(\eta)$ [%]	21.0	33.8	35.7	32.5	32.9	28.0	28.4	25.5	25.5	27.8	27.7	24.5	24.5
	$\epsilon_{E\eta}$ [%]		-61	-70	-55	-57	-33	-35	-21	-21	-32	-32	-17	-17

Table IV. Wake loss validation at Horns Rev 1 based on uniform wind direction and Rayleigh distributed wind speed (mean 9.5 $m\,s^{-1}$).

Uncertainty in power production prediction

The standard deviation of the total plant power production at Horns Rev 1 is shown in Figure 9 for all the models. The prediction of the variability of power at a given WS and WD is neglected when the power prediction is done without considering uncertainties. The distributions of variance in power predicted considering the uncertainties in WS, WD and

P with and without uncertainty in the site correction of the wind turbine model are similar for all the models and are close to the measured variance of power, see center left plot in Figure 7. The predicted standard deviation of power after propagation of uncertainty is consistently larger for wind speeds around 8 $m.s^{-1}$; this is the region with a balance of high thrust coefficient and high wind speed, and it is the region where the wake velocity deficits are larger. The predicted power variance distributions show a clear pattern of larger values for the directions of turbine alignment such as 90°, 175°, 270° and 355°; this is due to the fact that in these locations the uncertainty in wind direction has a larger effect in the variance of the predicted power. This effect is less important in the observed standard deviation of power from the SCADA database.

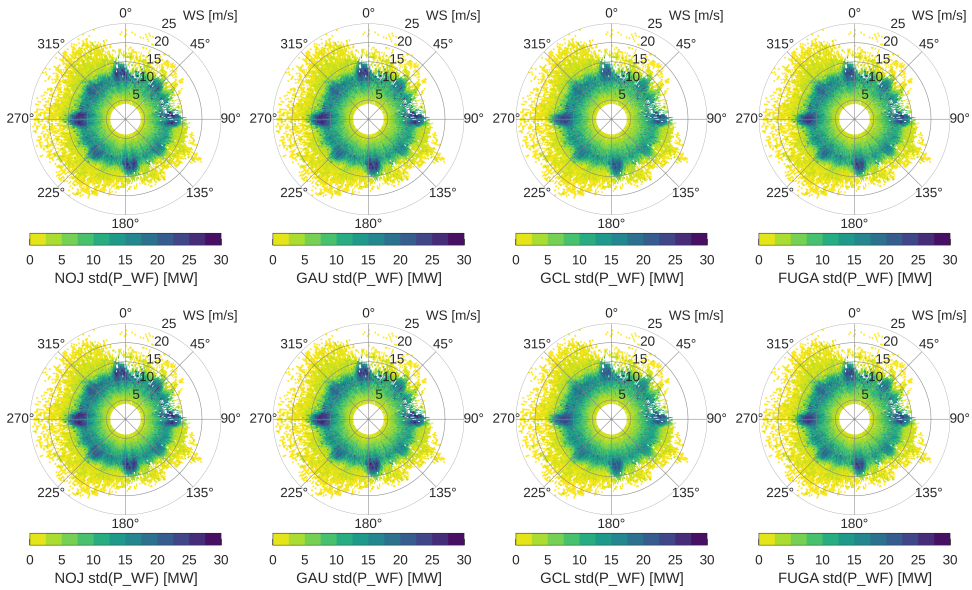

Figure 9. Standard deviation of power production at Horns Rev 1 predicted with different models for at least 95% available plant (top row) considering uncertainties in WD, WS and P using experimental power curve and official thrust coefficient curve (bottom row) considering uncertainties in WD, WS, P and turbine model.

4.2. Case 2: Nysted

The observed total plant power production at Nysted along its standard deviation are shown in Figure 10. Just as in the Horns Rev 1 case, the effect of filtering the database for availability in the size of the validation database can be observed. A lower coverage of flow cases is obtained when filtering for the fully available plant for Nysted in comparison to Horns Rev 1. The observed power for the selected filtering level (95% minimum plant availability, AV>=68 for Nysted) shows a clear pattern of wake deficits for the main directions of alignment and a clear pattern of variability of power due to the different atmospheric conditions that changes the wake conditions, see third column Figure 10. Finally, the fourth column in Figure 10 summarizes the LHS obtained for WS, WD and P. This distribution places a flow case on each candidate true value of WS, WD and P, and therefore gives an idea of the scale of the effect of miss-placing an observation in the power polar plot.

Relative prediction error

The relative prediction error distribution in Nysted for each of the wake models without considering uncertainties are shown in the top row of Figure 11. Similarly to Horns Rev 1 case, all the models under-predict the power production for the wind directions in which there is a large number of turbines aligned. It can also be seen that there are large errors due to coastal effects when the wind direction comes from the north: [315,45] °. In the same way as in Horns Rev 1, the sectors where the model under-predicts the power are compensated with the regions of over-prediction. The relative prediction error distribution for each of the wake models considering both input and output uncertainties are shown in Figure 11. The prediction errors are overestimated when the validation is done without considering uncertainty; note that the color scale in the bottom row in the Figure 6 has a narrower range than the one in the top row. As expected for northern wind directions,

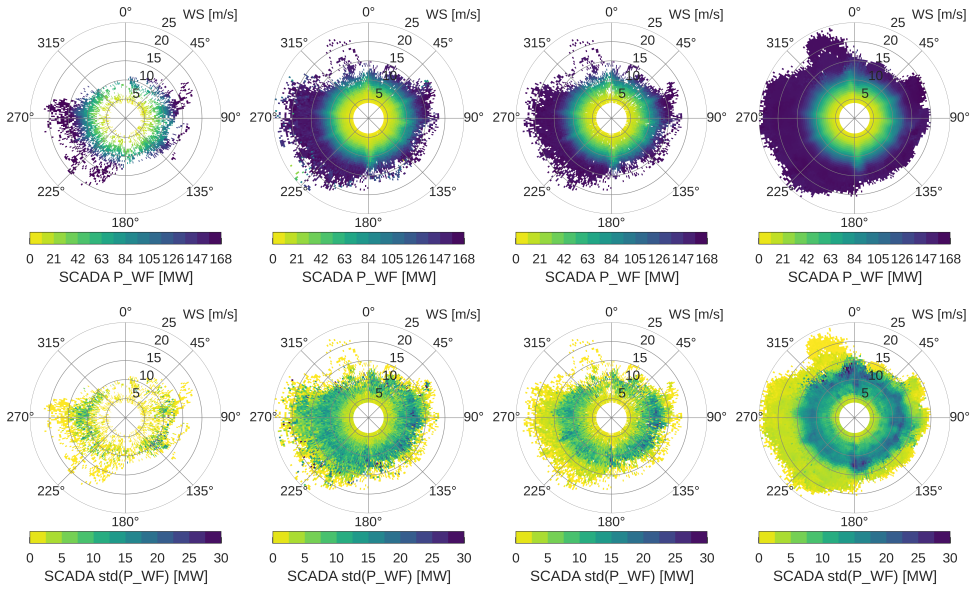

Figure 10. Observed power production at Nysted. (Top row) Expected power for each bin, (bottom row) standard deviation of power for each bin. (Left) For fully available plant, (center left) for all the database, (center right) for at least 95% available plant without uncertainties, (right) for at least 95% available plant with LHS of the candidate true values of WS, WD and P uncertainties.

the coastal effects produce large under-predictions and these effects are not reduced by considering model WS, WD, P and turbine model uncertainty. All the models show a region of under-prediction for wind speeds lower than 6 $m\,s^{-1}$. This is the result of the under-prediction in the expected power curve in this region, see Figure 6. These errors do not occur in the top figure because the experimental power curve is used to produce the results without considering uncertainty.

4.3. Individual turbine validation

The turbines 01, 02, 12 from Horns Rev 1 are selected for individual analysis because they include the main operation conditions: blockage effects, individual wake, double wake, staggered multiple wakes and aligned multiple wakes; each of these wake operation modes can be seen with different turbine spacings for different WD. Figure 12 shows the relative prediction error for turbine 01, with and without considering uncertainties. It can be seen that the blockage effect causes two speed up regions [20,80]$^\circ$ and [190,250]$^\circ$; all the models under-predict the power in these two sectors. A reduced coastal effect can also be seen in the sector [60,80]$^\circ$; this effect is not as pronounced as seen in Nysted because the distance to the shore is larger at Horns Rev 1, 14 [km]. As expected all models under-predict the power for the main directions of turbine alignment; the under-prediction error is larger for narrower turbine spacings than diagonal alignments. Figure 12 shows that NOJ over-predicts the power for staggered multiple wakes, e.g. sectors between [100, 120]$^\circ$ and [135,160]$^\circ$. Similar over-predictions are seen for GAU model, while GCL and FUGA show smaller errors.

Figure 13 shows the relative prediction error for turbine 02, with and without considering uncertainties. It can be seen that the blockage effect causes a speed up regions [190,250]$^\circ$; all the models under-predict the power in this sector. This figure also shows the capacity of a single model to capture a single wake condition: NOJ and GAU models seem to under-predict the single wake in the [350, 360]$^\circ$ sector, while GCL and FUGA properly reproduce it. The single wakes in the sector [0, 60]$^\circ$ show a combination of the blockage effect seen in the upstream turbine 01 and single wake errors. This turbine shows similar multiple wake behavior in the sector [90,180]$^\circ$ as mentioned for turbine 01. Figure 14 shows the relative prediction error for turbine 12, with and without considering uncertainties. It can be seen that NOJ and GAU models seem to under-predict the double wakes conditions shown in the sectors [350, 360]$^\circ$ and [30, 60]$^\circ$, while GCL and FUGA show a more accurate response.

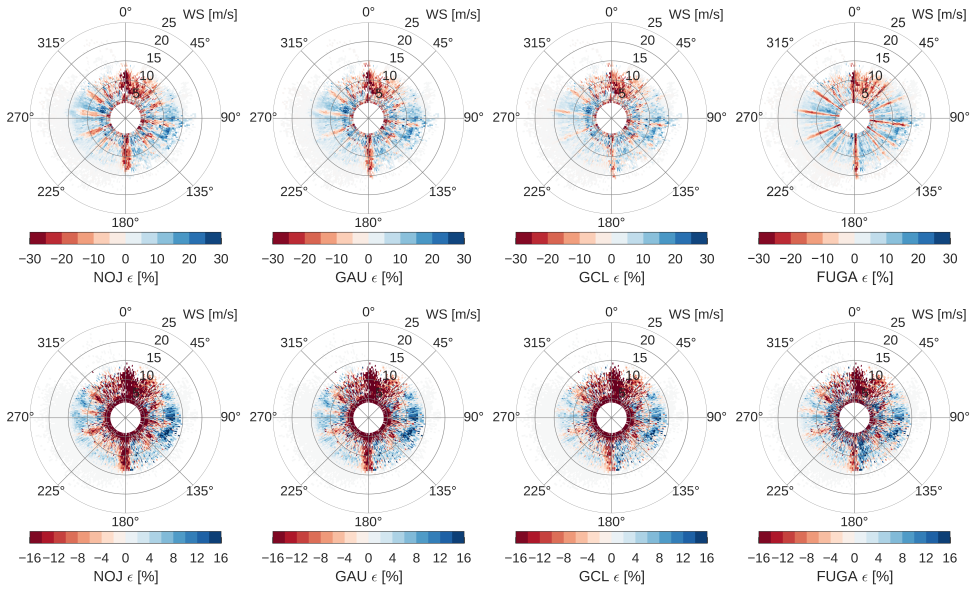

Figure 11. Relative prediction error distribution for different wake models at Nysted for at least 95% availability (top) without considering uncertainties and using experimental power curve and official thrust coefficient curve (bottom) considering uncertainties in WD, WS, P and turbine model. The colorbar scales of the top and bottom rows are different for clarity.

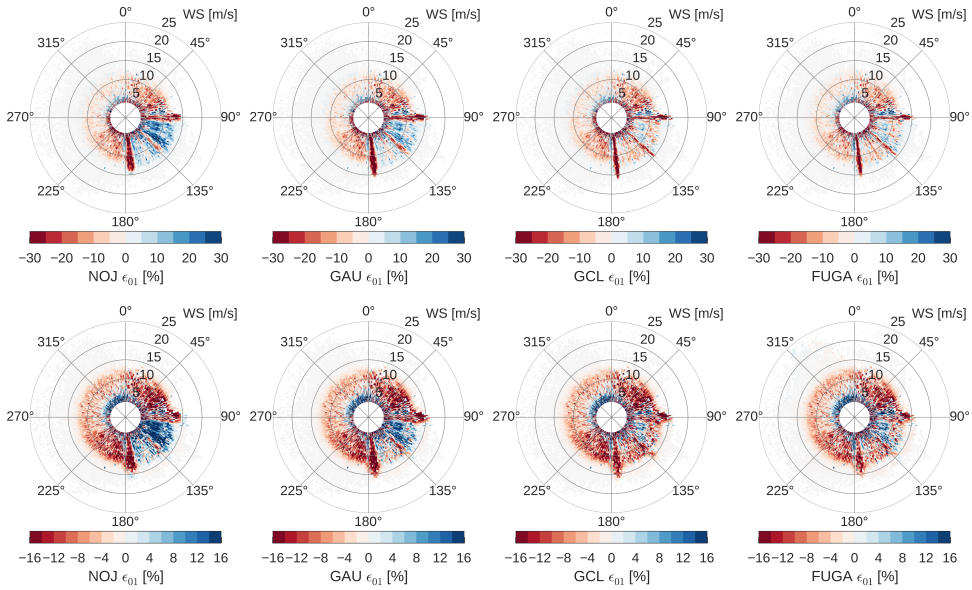

Figure 12. Relative prediction error for different wake models for turbine 01 in Horns Rev 1 for at least 95% availability (top) without considering uncertainties and using experimental power curve (bottom) considering uncertainties in WD, WS, P and turbine model.

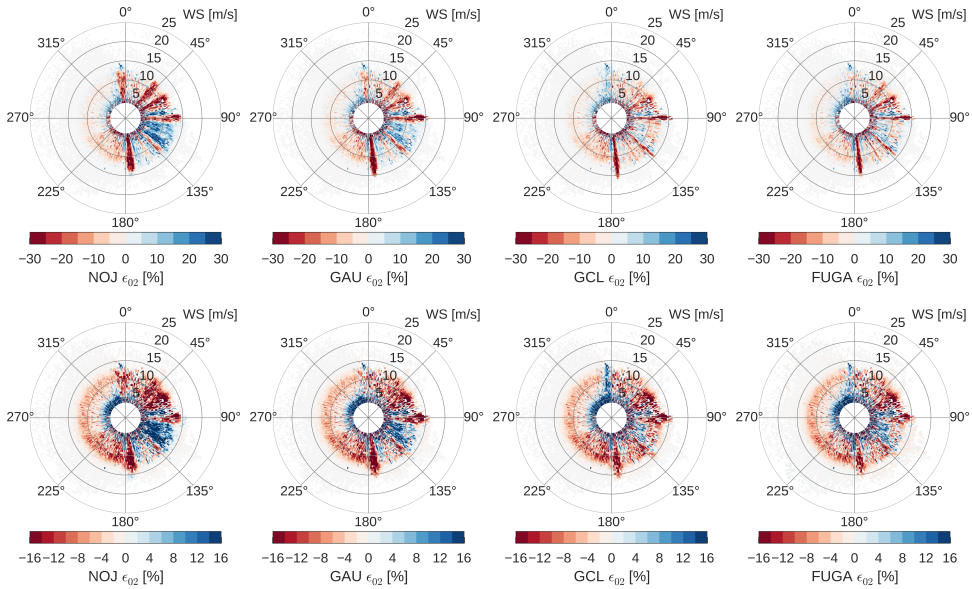

Figure 13. Relative prediction error for different wake models for turbine 02 in Horns Rev 1 for at least 95% availability (top) without considering uncertainties and using experimental power curve (bottom) considering uncertainties in WD, WS, P and turbine model.

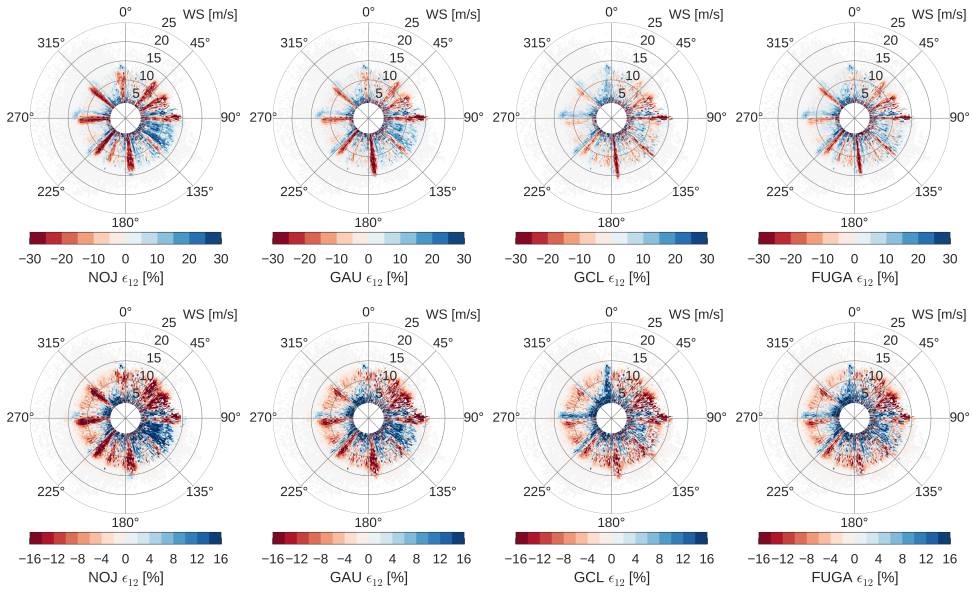

Figure 14. Relative prediction error for different wake models for turbine 12 in Horns Rev 1 for at least 95% availability (top) without considering uncertainties and using experimental power curve (bottom) considering uncertainties in WD, WS, P and turbine model.

Wind Energ. 2015; **00**:1–19 © 2015 John Wiley & Sons, Ltd.
DOI: 10.1002/we
Prepared using weauth.cls

5. DISCUSSION

In the present study the methodology follows the framework of model verification, validation and uncertainty quantification proposed by Oberkampf [23]. Monte-Carlo Latin hypercube sampling is used to propagate uncertainties because it is a reduced variance method that allows one to explore all the uncertain variables and to force them to be independent with a reduced sample size. The uncertainty in the power measurement of each turbine is considered as an individual uncertain variable, therefore the number of uncertain variables that were sampled in the present analysis is the number of turbine models plus WS and WD; for a total $N_T + 2$. Note that the power curve and thrust curve realizations were obtained independently.

The uncertainty assumptions made in the present article are conservative. An improved validation case can be constructed in the cases in which more detailed measurements have been conducted.

It has also been observed that sampling the wind velocity uncertainty does not modify the wind rose (i.e. joint PDF of WS and WD) because the relative frequency of occurrence of each WS and WD instance is still centered in the expected value of the wind velocity for a given 10-minute time-stamp. This does produce a mixture of the cases that creates a smoothing effect, which captures the effects of miss-placing observations in the power or error polar plots. The wind rose figures have not been presented because the weather resources are commercially sensitive.

The uncertainty model for the wind turbine performance on site has proven to capture the main effects. A more detailed model can be constructed using aero-elastic codes to simulate the time response to different turbulent inflow conditions and obtain a more detailed information about the capacity of a given turbine/controller to extract the additional energy available in turbulent flow. Note that additional information is required to perform this type of simulation such as elastic properties and aerodynamic planform of the blade, control algorithm and set points; this type of information is usually not publicly available.

An improvement in the accuracy of the prediction of power production of stationary wake models can be achieved by propagating the undisturbed wind velocity and wind turbine model uncertainties. The improvement is significant as the maximum park relative prediction error in the directions of main turbine alignment is reduced from -20% to -5% for Horns Rev 1, see Figure 8. Under-predictions in these aligned directions result because of the lack of two physical phenomena neglected by these wake models. First, the turbulence added by a wake generating turbine modifies the turbulence intensity and wake mixing inside the wind plant; this effect is very important when turbines are perfectly aligned. Second, these wake models do not consider how the inflow conditions impact wake meandering and wake development; an example of these conditions are the atmospheric stability and actual ambient turbulence intensity experienced in each 10-minutes. Interestingly, the prediction error distribution in Horns Rev 1 obtained after propagation of WS, WD, P and turbine model uncertainties does not differ considerably from the one obtained neglecting the turbine model uncertainty. The main difference is the over-prediction of power for wind speeds lower than 6 $m\,s^{-1}$ in Figure 5. This over-prediction is cause by the over-estimation of the site corrected power curve predicted using the turbine model uncertainty, see Figure 5. The opposite effect can be seen in Nysted as the power curve is under-predicted for wind speeds lower than 6 $m\,s^{-1}$ by the turbine model due to the change in the rotational speed of the B82-2300 turbine in this regime, see Figure 10. The improvement in the accuracy is also observed in the individual turbine power predictions, figures 12, 13, 14. In particular, it can be observed that for multiple wakes conditions the error on an individual turbine is reduced. All the models present large errors for wind speeds lower than 4 $m\,s^{-1}$, this is mainly due to the fact that the start up of a turbine is a dynamical procedure that the stationary power curve is not able to capture. The errors obtained in the start up regime are not shown for clarity.

Error compensation for 30° sectors can be observed in both the global wake loss error metric, see Table IV, and in the relative prediction error distributions. The error compensation is responsible for the site dependent inconsistency in the prediction of AEP. Table IV show how weighting the results using a different wind resources creates a large variability in the wake loss error metric. The low errors obtained for most models are the result of the error compensation that occurs in such a symmetric layout as Horns Rev 1. Error compensation does not occur in narrower WD sectors. Moreover, using the relative prediction error distribution enables one to obtain a better understanding of the distribution of the errors for the total wind plant and for each individual turbine.

The present study shows that there is a need for blockage effect sub-model in order to reduce the errors in the power performance prediction for the outermost turbines. Furthermore, there is also a need for an improvement in the treatment of the coastal effects as it is seen to produce the largest errors in the Nysted case. The coastal effects are the combination of two related aspects: the inner boundary layer development due to the change from land to water surface roughness; and an increase ambient turbulence intensity that increases the amount of mixing. The model parameters should be calibrated in order to minimize these under-predictions. We believe that power prediction errors due to coastal effects can be reduced by adding a flow solver that is responsible for the prediction of the internal boundary layer. Another option is to calibrate the wake model parameters as a function of the distance from the shore and ambient turbulence intensity, although calibration disregards the physics and will be more prone to errors.

Computational time and disk space usage are some of the limitations of using the approach presented inside a wind plant layout optimization problem. The computational time to build the fully available plant power database is negligible for the models used in this article, 5-7 [μs] of total cpu wall time in a single core. The model interpolation used to generate a 3 year realization of power production in the plant takes between 7-10 [μs] and uses around 180 MB of disk space. The required time to compute all the results presented in this article took 80000 [μs] wall time; and required 720 GB of disk space. There is an overhead in computational time caused by the large size of the files and is related to move, open, read, process and close such files. One of the most difficult problems to solve is how to post process the databases of this size, which exceeds memory on all current computers. In the present article each 3 year realization of WS, WD, P and turbine model for a single model is analyzed individually and in parallel; the results were aggregated in a final step for each individual output variable (i.e. P_WF, P_01, P_02, P_12).

The presented methodology can be used to reduce the uncertainty of AEP predictions in the planning stages. An initial step is to include the measurement uncertainties in the wind resource assessment; then, an uncertainty model of the performance of the turbines in the desired site should be included as it is done in figures 7 and 10. Additionally, a propagation of the inputs uncertainties through simple engineering models have been proved to reduce the expected errors in the power production predictions.

6. CONCLUSIONS

The present work has introduced a simple method to model the uncertainty of the site performance of a wind turbine. This model needs to be further investigated, verified with respect detailed aero-elastic simulations; and validated against measurements in other offshore and onshore sites.

It has been observed that the reason why the simple engineering models predict the total plant power production for large wind direction sectors of 30° is due to the fact that the wake models produce error cancellation in Horns Rev 1; furthermore, this is responsible for the lack of consistency in the prediction of AEP among different offshore wind plant projects in which the layouts are not as symmetric as Horns Rev 1, and in which the wind roses weight the errors unevenly. The cancellation of errors can be avoided using the methodology introduced in this article. The present approach does not solve the limitations of the studied models to predict the power of an individual turbine inside a wind plant.

A validation domain can be built by fitting a Gaussian process to the error distribution for each model and by parameterizing the wind power plant layout into multiple geometrical parameters. The validation domains of the most commonly used wake models can be built and tested by dividing the operational data into training and testing subsets. These domains can be used to predict the model error independently from the input uncertainties for wind power plant with an arbitrary layout. This approach can be used to improve the estimation of annual energy production of an arbitrary offshore power plant.

Further work needs to be done in order to improve the accuracy of wake models to capture coastal and obstruction effects. In general, simple engineering models do not capture individual turbine power performance. In particular, a detailed sub-model for the obstruction effect is required if the simple models are to be used to optimize wind plant layouts; while the coastal effect can be included in most engineering models by recalibrating the wake model parameters based on the SCADA data of different plants with different distances from the coast.

ACKNOWLEDGEMENT

This work was supported by the International Collaborative Energy Technology R&D Program of the Korea Institute of Energy Technology Evaluation and Planning (KETEP), granted financial resource from the Ministry of Trade, Industry & Energy, Republic of Korea. (No. 20138520021140). We would like to thank DONG Energy AS and Vattenfall AB for the access to the SCADA data, Ebba Dellwik, Paul van der Laan and the anonymous reviewers for their contributions to this manuscript.

REFERENCES

1. Gass V, Strauss F, Schmidt J and Schmid E. 2011. *Assessing the effect of wind power uncertainty on profitability*. Renewable and Sustainable Energy Reviews, 6(15), 2677-2683. DOI: 10.1016/j.rser.2011.01.024.
2. Mortensen NG, Nielsen M, Jørgensen H. 2015. *Comparison of Resource and Energy Yield Assessment Procedures 2011-2015: What have we learned and what needs to be done?*. EWEA Annual Conference and Exhibition 2015.

3. Walker K, Adams N, Gribben B, Gellatly B, Nygaard NG, Henderson A, Marchante Jimémez M, Schmidt SR, Rodriguez Ruiz J, Paredes D and Harrington G. 2015. *An evaluation of the predictive accuracy of wake effects models for offshore wind farms*. Wind Energy. DOI: 10.1002/we.1871.
4. Moriarty P, Rodrigo JS, Gancarski P, Chuchfield M, Naughton JW, Hansen KS, Machefaux E, Maguire E, Castellani F, Terzi L, and others. 2014. *IEA-Task 31 WAKEBENCH: Towards a protocol for wind farm flow model evaluation. Part 2: Wind farm wake models.* Journal of Physics: Conference Series, 524(1), 012185, DOI: 10.1088/1742-6596/524/1/012185.
5. Gaumond M, Réthoré PE, Ott S, Peña A, Bechmann A, and Hansen KS. 2014. *Evaluation of the wind direction uncertainty and its impact on wake modeling at the horns rev offshore wind farm.* Wind Energy, 17(8), 11691178. DOI: 10.1002/we.1625
6. Réthoré PE, Hansen KS, Larsen GC, Larsen TJ, Ott S, Rathmann O, Peña A, and Hasager C B. 2013. *Benchmarking of wind farm scale wake models in the EERA-DTOC project.* Proceedings of the 2013 International Conference on Aerodynamics of Offshore Wind Energy Systems and Wakes (ICOWES2013).
7. Peña A, Réthoré PE, and Rathmann O. 2014. *Modeling large offshore wind farms under different atmospheric stability regimes with the Park wake model.* Renewable Energy, 70(June), 164171. DOI: 10.1016/j.renene.2014.02.019.
8. Barthelmie RJ, Pryor S, Frandsen ST, Hansen KS, Schepers J, Rados K, Schlez W, Neubert A, Jensen L, and Neckelmann S. 2010. *Quantifying the impact of wind turbine wakes on power output at offshore wind farms*. Journal of Atmospheric and Oceanic Technology, 27(8), 1302-1317. DOI: 10.1175/2010JTECHA1398.1.
9. Hansen KS, Barthelmie RJ, Jensen LE, and Sommer A. 2012. *The impact of turbulence intensity and atmospheric stability on power deficits due to wind turbine wakes at Horns Rev wind farm.* Wind Energy, 15(1), 183196. DOI: 10.1002/we.512.
10. Nygaard NG. 2015. *Systematic quantification of wake model uncertainty*. EWEA Offshore Conference, Copenhagen.
11. Murcia JP, Réthoré PE, Hansen KS, Natarajan A, Sørensen JD. 2015. *A new method to estimate the uncertainty of AEP of offshore wind power plants applied to Horns Rev 1*. EWEA Annual Conference and Exhibition 2015, 161-165.
12. IEC. 2013. *IEC 61400-12-2 Wind turbines-part 12-2: Power performance of electricity producing wind turbines based on nacelle anemometry.* Switzerland: International Electrotechnical Commission.
13. IEC. 2005. *IEC 61400-12-1 Wind turbines-part 12-1: Power performance measurements of electricity producing wind turbine.* Switzerland: International Electrotechnical Commission.
14. Réthoré PE, Johansen NA, Frandsen ST, Hansen KS, Jensen LE, and Kristoffersen R. 2009. *Systematic wind farm measurement data reinforcement tool for wake model calibration.* European Offshore Wind (EOW)Conference 2009, 110.
15. IEC. 2013. *IEC 61400-1 Wind turbines-part 1: Design requirements.* Switzerland: International Electrotechnical Commission.
16. Réthoré PE, and Murcia JP. 2014. *FUSED-Wake: open source stationary wake models repository available at: https://github.com/DTUWindEnergy/FUSED-Wake*
17. Katic I, Højstrup J, and Jensen NO. 1986. *A simple model for cluster efficiency.* European Wind Energy Association Conference and Exhibition, EWEA October 1986, 407410.
18. Bastankhah M, and Porté-Agel F. 2014. *A new analytical model for wind-turbine wakes*. Renewable Energy, 70, 116-123. DOI: 10.1016/j.renene.2014.01.002.
19. Larsen GC. 2009. *A simple stationary semi-analytical wake model.* Risø. Technical Report, Risø-R-1713(EN).
20. Ott S, Berg J, and Nielsen M. 2014. *Developments of the offshore wind turbine wake model Fuga.* Report No. DTU Wind Energy E-0046, Risø-DTU, Roskilde, Denmark.
21. Huard D, and Mailhot A. 2006. *A Bayesian perspective on input uncertainty in model calibration: Application to hydrological model "abc"*. Water Resources Research, 42(7). DOI: 10.1029/2005WR004661.
22. McKay MD, Beckman RJ, Conover WJ. 2000. *A comparison of three methods for selecting values of input variables in the analysis of output from a computer code*. Technometrics, 42(1), 5561. DOI:10.1080/00401706.2000.10485979.
23. Oberkampf WL, Trucano TG, and Hirsch C. 2004. *Verification, validation, and predictive capability in computational engineering and physics.* Applied Mechanics Reviews, 57(5), 345-384. DOI: 10.1115/1.1767847

Article E

Wake model calibration based on SCADA data considering uncertainty in the inflow conditions

Wake Model Calibration Based On SCADA Data Considering Uncertainty In The Inflow Conditions

Juan Pablo Murcia[1], Pierre-Elouan Réthoré[1], Kurt Schaldemose Hansen[1], Ole Steen Rathmann[1], Anand Natarajan[1], and John Dalsgaard Sørensen[1,2]

[1]Department of Wind Energy, Technical University of Denmark. Risø Campus, Frederiksborgvej 399. 4000 Roskilde. Denmark

[2]Department of Civil Engineering, Aalborg University

Correspondence to: Juan Pablo Murcia (jumu@dtu.dk)

Abstract. The uncertainty in the power production of a wind power plant is one of the main sources of uncertainty in the estimation of the annual energy production for large offshore wind energy projects. At the same time, the wind plant operators have large databases of operational data that could be used to enhance the performance of engineering wake models and to estimate the model uncertainty. One of the main limitation of this process is the fact that these operational databases contain large amounts of noise. Parameter calibration can be used to capture some of the model uncertainty by determining the uncertainty in the model parameter(s). Maximum likelihood calibration techniques can be designed for wake model validation because they can handle uncertainties in both input and output variables. In the present study an implementation of a maximum likelihood estimation has been tested with several analytical examples in which the measurement uncertainty is modeled as a normally distributed random noise. The proposed calibration methodology is able to accurately reconstruct the parameter distribution. At the same time, the analytical examples show that calibration based on least squared errors produces bias in the estimation of the parameter because it neglects the effect of the input uncertainty in a non-linear model. Operational data from four different offshore plants are used to calibrate a simple stationary wake model (Jensen model with linear wake superposition). The results show how the wake expansion parameter has narrower distribution for the more uniform plants. Additionally the wake expansion parameter depends on the wind direction for each site, from which it can be conclude that the mean stream-wise turbine spacing and the number of turbines aligned influence the wake expansion parameter.

1 Introduction

The design of modern large offshore wind plants consist in defining the layout that maximizes the annual energy production (AEP). This requires to estimate the long term local wind resources and the wake induced energy losses. AEP estimation requires the prediction of the power production of a power plant as a function of the undisturbed wind speed (WS) and wind direction (WD). This estimation uses uses a wind turbine model that usually consist of a power and thrust coefficient curves (as a function of the hub height wind speed), and a wake model that captures the power losses with respect the wind direction. The wake models have a highly non-linear behavior with respect the wind direction because its sinusoidal (cyclic) nature. Advanced

wake models are computationally expensive and experienced modelers are required to setting up such simulations, therefore engineering models are commonly used by the industry to design modern offshore wind projects.

Operational data from offshore wind plants is available to the project developers and operators, and such data could be used to enhance the performance and accuracy of engineering wake models. Several studies have performed model comparisons to most of the wake models available today with respect to operational data from wind plants like Horns Rev 1, Nysted, Lillgrund, Rødsand II, among others (Moriarty et al., 2014; Walker et al., 2015; Nygaard, 2014; Nygaard and Hansen, 2016; Murcia et al., 2016). One of the main conclusions of such model comparison campaigns is that due to the uncertainty in the estimation of the undisturbed wind speed and wind direction the comparisons can only be done after binning the data into large wind direction bins ($30°$). Due to this averaging of very different conditions most models make predictions within the expected variability of the observed binned power and, therefore, no practical conclusions have been made about the model uncertainty of the most commonly used wake models. Parameter calibration techniques can be used to partially capture the uncertainty in a model by estimating the uncertainty in the model parameters that minimize the power prediction error.

Calibration of engineering wake models has been done in the past using SCADA data (Cleve et al., 2009) and using a reduced number of large eddy simulations (LES) (Madsen et al., 2010; Bastankhah and Porté-Agel, 2014); but the uncertainty in the calibration parameters is rarely discussed in literature. Traditional calibration methods such as least squared errors calibration (LSE)have been proven to fail to estimate the optimal parameter and its uncertainty for measurements with large input uncertainty (Huard and Mailhot, 2006). A bias in the parameter estimation is introduced if the model has large non-linearities with respect an uncertain input variable. Both conditions are present in wake models since there is a large non-linear behavior of the wake models with respect the wind direction and because of the fact that estimating the undisturbed wind conditions based on operational data has large uncertainty. Maximum likelihood estimation can be used because it can handle uncertainties in both input and output variables (Clark, 2005; Kavetski et al., 2002).

This article introduces the methodology calibration in Section 2. Additionally we explore the benefits of maximum likelihood estimation for analytical cases that have a similar structure as simple engineering wake models; a one dimensional and a two dimensional analytical cases are presented in Section 3. Finally, the wind plants, wake models and the operational data used in this article are presented in Section 4, while the final results of the calibration are presented in Section 6 and discussed in Section 7.

2 Methodology

It is required to understand the flow of information that is available in a model calibration problem in order to understand the concepts behind the different calibration methods and their assumptions. Figure 1 shows the different variables that play a role in such a problem. The real physical process that relates the true inputs ($\mathbf{x}$) and the true outputs ($\mathbf{y}$) is the phenomena that needs to be predicted. The real process is modeled using the model ($\mathcal{M}(\mathbf{x}, \boldsymbol{\theta})$) and a set of parameters ($\boldsymbol{\theta}$). Note that the model is not necessarily perfect and there might be a model discrepancy or a model's prediction error ($\varepsilon(\mathcal{M})$). Synchronized measurement of both the inputs and the outputs gives a measured pair ($\tilde{\mathbf{x}}, \tilde{\mathbf{y}}$), but there are errors in the measurement of both the

input ($\varepsilon_{\mathbf{x}}$) and output variables ($\varepsilon_{\mathbf{y}}$). This measurement errors can not be known and therefore need to be modeled as random variables using information from the instruments, experimental setup and the estimation procedure for each variable. In this article we have assumed that the measurement errors are normally distributed around zero, are independent and have a standard deviation $\sigma_{\mathbf{x}}$ for the inputs and $\sigma_{\mathbf{y}}$ for the outputs. This measurement model can be generalized to a correlated case for the inputs $\varepsilon_{\mathbf{x}} \sim \mathcal{N}(0, \mathbb{C}_{\mathbf{x}})$ and outputs $\varepsilon_{\mathbf{y}} \sim \mathcal{N}(0, \mathbb{C}_{\mathbf{y}})$; or to a non-normal distributed measurement errors when it is necessary. All this variables are present for every single observed pair which in the case of operational data of wind plants is usually a single 10-minute average of the inflow conditions and power production.

Model calibration is the problem of determining the distribution of parameters that makes the model agree with the evidence brought by the set of measured pairs. It is common practice to assume that the model prediction error is also normally distributed when performing a model calibration; in this way the calibrated parameters will make the model agree with the observations without accounting for model inadequacy (dependency of the model prediction error on the inputs). This is of course only valid if the model is is able to follow the observations.

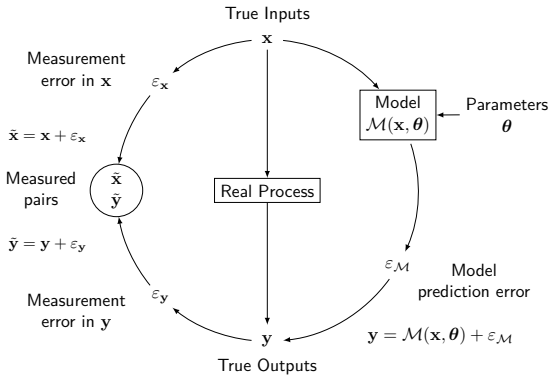

Figure 1. Modeling and measuring reality. Diagram modified from Huard and Mailhot (2006).

2.1 Weighted least squared errors calibration (WLSE)

Model calibration is usually performed solving the weighted least squared errors optimization problem. In this approach the input uncertainty is neglected and the output uncertainty is considered to vary from each of the N observation pairs ($\sigma_{\mathbf{y}\,i}$). The sum of the squares of the prediction errors $\sum_i (\tilde{\mathbf{y}}_i - \mathcal{M}(\tilde{\mathbf{x}}_i, \boldsymbol{\theta}))^2$ are weighted by $\mathbf{W}$, a matrix whose diagonal contains the inverse of the output variance for each observation $\sigma^2_{\mathbf{y}\,i}$ for the single output case or the inverse of the outputs covariance for multiple outputs case $\mathbf{W} = \mathbb{C}_{\mathbf{y}}^{-1}$. These weights make the observations with less uncertainty more important for the total calibration.

The optimization problem consists in finding the parameter that minimizes the weighted sum-of-squares (WSS) between the observed output and the model prediction evaluated at the observed input. Depending on the complexity of the model

this optimization problem can be solved analytically or numerically using iterative algorithms such as the *lmdif* and *lmder* algorithms implemented in the Minpack library by Moré et al. (1980).

$$\boldsymbol{\theta}_{\text{WLSE}} = \underset{\boldsymbol{\theta}}{\text{argmin}} \left((\tilde{\mathbf{y}} - \mathcal{M}(\tilde{\mathbf{x}}, \boldsymbol{\theta}))^T \mathbf{W} (\tilde{\mathbf{y}} - \mathcal{M}(\tilde{\mathbf{x}}, \boldsymbol{\theta})) \right) = \underset{\boldsymbol{\theta}}{\text{argmin}}(\text{WSS}(\boldsymbol{\theta})) \tag{1}$$

In order to determine the uncertainty in the parameters obtained from this calibration technique the model is linearized around the expected parameter ($\boldsymbol{\theta}_{\text{WLSE}}$) using a Taylor expansion and the Jacobian ($\mathbb{F}$) with respect the parameters:

$$\mathcal{M}(\tilde{\mathbf{x}}, \boldsymbol{\theta}) \approx \mathcal{M}(\tilde{\mathbf{x}}, \boldsymbol{\theta}_{\text{WLSE}}) + \mathbb{F}\left[\boldsymbol{\theta} - \boldsymbol{\theta}_{\text{WLSE}}\right] \tag{2}$$

Finally, the parameter estimator are then normally distributed $\boldsymbol{\theta} \sim \mathcal{N}(\boldsymbol{\theta}_{\text{WLSE}}, \mathbb{C}_{\boldsymbol{\theta}_{\text{WLSE}}})$; while the covariance of the parameters can be estimated using equation 3. Here p represents the number of parameters.

$$\mathbb{C}_{\boldsymbol{\theta}_{\text{WLSE}}} = \frac{\text{WSS}(\boldsymbol{\theta}_{\text{WLSE}})}{N - p - 1} \left(\mathbb{F}^T \, \mathbb{C}_{\mathbf{y}} \, \mathbb{F} \right)^{-1} \tag{3}$$

When the measurement campaign includes uncertainties in the inputs the WLSE can be performed on the actual observations assuming that the input uncertainty is negligible. Another option is to perform the WLSE for the input-binned model and observations; this is the most common practice in the wind energy field.

2.2 Maximum likelihood estimation

Maximum likelihood estimation is a calibration method based on the likelihood function. The likelihood function is defined as the PDF of observing a measured output given the measured inputs and a set of parameters: $\mathcal{L}(\tilde{\mathbf{y}}, \tilde{\mathbf{x}} | \boldsymbol{\theta}) = \text{PDF}(\tilde{\mathbf{y}} | \tilde{\mathbf{x}}, \boldsymbol{\theta})$. The calibration problem is then reduced to an optimization problem in which the parameter estimators maximizes the total likelihood function, see equation 4. In this equation the observations are assumed to be independent, therefore the total likelihood is the product of the individual likelihoods for each observed pair. The notation used to represent all the observed pairs is: $I \equiv \{0, \ldots, N_I\}$.

$$\begin{aligned} &\mathcal{L}(\tilde{\mathbf{y}}_I, \tilde{\mathbf{x}}_I | \boldsymbol{\theta}) = \prod_{i=0}^{N_I} \mathcal{L}(\tilde{\mathbf{y}}_i, \tilde{\mathbf{x}}_i | \boldsymbol{\theta}) = \prod_{i=0}^{N_I} \text{PDF}(\tilde{\mathbf{y}}_i | \tilde{\mathbf{x}}_i, \boldsymbol{\theta}) \\ &\hat{\boldsymbol{\theta}} = \text{argmax}_{\boldsymbol{\theta}} \, \mathcal{L}(\tilde{\mathbf{y}}_I, \tilde{\mathbf{x}}_I | \boldsymbol{\theta}) \end{aligned} \tag{4}$$

The likelihood of an observed pair that includes uncertainty in the input requires special treatment. It is estimated by marginalizing the distribution of the true (and unknown) inputs, see equation 5. This procedure is equivalent to applying a convolution of the uncertain inputs to the likelihood function.

$$\mathcal{L}(\tilde{\mathbf{x}}_i, \tilde{\mathbf{y}}_i | \boldsymbol{\theta}) = \mathcal{L}(\tilde{\mathbf{x}}_i) \, \mathcal{L}(\tilde{\mathbf{y}}_i | \tilde{\mathbf{x}}_i, \boldsymbol{\theta}) = \int_{\Omega_{\mathbf{x}}} \mathcal{L}(\tilde{\mathbf{x}}_i | \mathbf{x}) \, \mathcal{L}(\tilde{\mathbf{y}}_i | \mathbf{x}, \boldsymbol{\theta}) \, \text{PDF}(\mathbf{x}) \, d\mathbf{x} = \int_{\Omega_{\mathbf{x}}} \text{PDF}(\tilde{\mathbf{x}}_i | \mathbf{x}) \, \text{PDF}(\tilde{\mathbf{y}}_i | \mathcal{M}(\mathbf{x}, \boldsymbol{\theta})) \, \text{PDF}(\mathbf{x}) \, d\mathbf{x} \tag{5}$$

Here $\mathcal{L}(\tilde{\mathbf{x}}_i|\mathbf{x}) = \mathrm{PDF}(\varepsilon_{\mathbf{x}})$ represents the input measurement error; while $\mathcal{L}(\tilde{\mathbf{y}}_i|\mathbf{x},\boldsymbol{\theta})$ captures both the output measurement error ($\varepsilon_{\mathbf{y}}$) and the model prediction error ($\varepsilon(\mathcal{M})$). Analytical expressions of the likelihood can be found for linear models and when the true inputs can be modeled as a mixture of multi-dimensional normal distributions; an example of this approach can be seen in Huard and Mailhot (2006). When the model is non-linear it is required to use a Monte-Carlo (MC) approximation to the definition of the Likelihood function. Here a MC sample is defined with respect the $\mathrm{PDF}(\mathbf{x})$ for each measured pair using N nodes for model evaluation $\mathbf{x}_{\text{node}} \sim \mathrm{PDF}(\mathbf{x})$ at a given model parameter.

$$\mathcal{L}(\tilde{\mathbf{x}}_i,\tilde{\mathbf{y}}_i|\boldsymbol{\theta}) = \int_{\Omega_{\mathbf{x}}} \mathrm{PDF}(\tilde{\mathbf{x}}_i|\mathbf{x})\,\mathrm{PDF}(\tilde{\mathbf{y}}_i|\mathcal{M}(\mathbf{x},\boldsymbol{\theta}))\,\mathrm{PDF}(\mathbf{x})\,d\mathbf{x} = \int_{\Omega_{\mathbf{x}}} f_i(\mathbf{x},\boldsymbol{\theta})\,\mathrm{PDF}(\mathbf{x})d\mathbf{x} \approx \sum_{\text{node}=1}^{N} \frac{f_i(\mathbf{x}_{\text{node}},\boldsymbol{\theta}))}{N} \tag{6}$$

In wake model calibration the model parameters will depend on additional atmospheric variables such as stability and ambient turbulence intensity; this means that there is not a single unknown set of true parameter but an unknown distribution of parameters that describes their variability. Therefore, the purpose of the calibration is to determine the distribution of the parameters. In order to fulfill this requirement in this article the maximum likelihood parameter for each measured pair is estimated individually. The variation shown in the most likely parameter gives an estimation of parameter uncertainty.

$$\boldsymbol{\theta}_{i\,\mathrm{MLE}} = \underset{\boldsymbol{\theta}}{\operatorname{argmax}}\left(\mathcal{L}(\tilde{\mathbf{x}}_i,\tilde{\mathbf{y}}_i|\boldsymbol{\theta})\right) \tag{7}$$

The procedure consists in defining a design of experiments for the parameter space $\Omega_{\boldsymbol{\theta}}$. Then to evaluate the likelihood for each observation pair. Each observation has a different maximum likelihood parameters ($\boldsymbol{\theta}_{i\,\mathrm{MLE}}$). The $\boldsymbol{\theta}_{i\,\mathrm{MLE}}$ is finally binned as a function of the inputs to capture the parameter variability between different observations.

3 Analytical examples

To verify that the calibration methodology works an analytical example was designed in which the model, the parameter variability and the true inputs distribution are known. For each of the cases a normally distributed noise is added for both input and output variables to model the measurements errors. Finally a calibration is performed with the noisy observations.

The implementation of the MC samples for the true inputs uses the Rosenblatt transformation (Rosenblatt, 1952) and were implemented using the Python library Chaospy (Feinberg and Langtangen, 2015).

The model is a simple analytical function that shows non-linearities with respect a cyclic variable similar to a wind direction (x_0), a smooth behavior with respect the remaining input variable (x_1) and with respect the model parameter (a):

$$y(x) = 10\,e^{-a\,x_1}\,\cos(0.5\,x_0) \tag{8}$$

Additionally, we considered variability in the single model parameter: $a \sim \mathcal{N}(\mu_a,\sigma_a)$. The joint distribution of the inputs is characterized by a conditional dependency (or Rosenblatt transformation (Rosenblatt, 1952)) in such a way that x_0 is the

independent variable and follows a cyclic distribution: $\mathrm{PDF}(x_0) = VonMisses(\mu = 3\pi/2., \kappa = \pi/6.)$; and a conditionally dependent distribution for x_1: $\mathrm{PDF}(x_1|x_0) = Weibull(A = 2, k = 10\cos(x_0))$. Finally, the measurement errors for the inputs and output are normally distributed around their true value: $\mathrm{PDF}(\tilde{x_0}|x_0) = \mathcal{N}(x_0, \sigma_{x_0})$, $\mathrm{PDF}(\tilde{x_1}|x_1) = \mathcal{N}(x_1, \sigma_{x_1})$ and $\mathrm{PDF}(\tilde{y}|x) = \mathcal{N}(y(x), \sigma_y)$.

The true input distribution used in this example is presented in Figure 2 as well as the true input and output dependency. Several samples where generated using different amounts of input uncertainty and model parameter variability. The effect of the input uncertainty in the distribution of the bin-averaged observed output at different input bins is presented in Figure 2. Similarly to the single dimensional example when the input uncertainty is high the bin-averaged observed output (and it's standard error of the mean, SEM) does not capture the true process. This is because the mean at a bin includes observations whose true inputs belong to another bin. This biasing effect only occurs when the model is non-linear and when the size of the input uncertainty is relatively high with respect to the non-linearity of the model. This can be seen in the fact that the uncertainty in x_1 does not cause biasing since the model is smooth in this variable. The bin size in this Figure 2 is 12 deg. for x_0 and 1 [m/s] for x_1, note that the bins shown in this plot are hexagonal, which means that they group observations that are the nearest to the bin center.

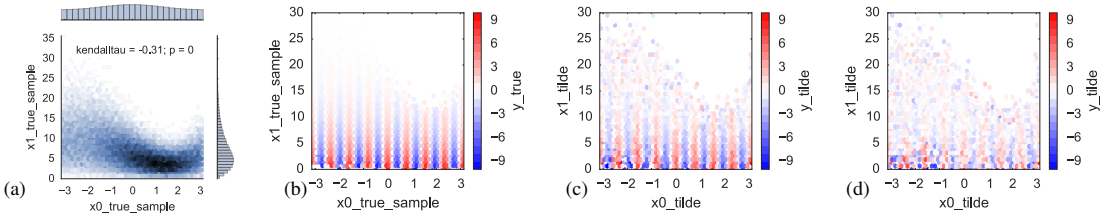

Figure 2. Two cases of uncertainty in the inputs for the 2-dimensional analytical model: (a) True input joint distribution. (b) True pairs. (c) Observed pairs for intermediate input uncertainty, case B2. (d) Observed pairs for high input uncertainty, case B4.

The calibration methodologies are applied for several cases with different uncertainties and true inputs distribution estimation. Table 1 summarizes the results obtained for each case, while Figure 3 shows a comparison between the different calibration approaches and the true parameter distribution for some example cases. It can be observed that calibration using weighted least squared errors based on the raw observations or based on the binned observations and model produce a bias in the parameter distribution. The dark blue line represents the distribution of the total likelihood without considering the parameter uncertainty as in equation 5. The variation in the bin-averaged maximum likelihood parameter is used to estimate the parameter variability missing.

To understand the effect of not knowing the distribution of the true inputs. This distribution was fitted using the noisy observations. This procedure consisted in fitting the marginal distribution of x_0 initially. Then a Weibull fit is done to the x_0-bin observations for the $\mathrm{PDF}(x_1|x_0)$, this produces the Weibull parameters that depend on x_0. In this article, maximum likelihood probability density function fits were used.

	Uncertainties			PDF($\mathbf{x}$)	WLSE Bins		MLE	
	σ_{x_0}	σ_{x_1}	σ_y		μ_a	σ_a	μ_a	σ_a
Case B0	0.5° (0.5°)	0.5 (0.5)	1.0 (1.0)	True (True)	0.206 (0.2)	0.002 (0.0)	0.199 (0.2)	0.001 (0.0)
Case B1	0.5° (0.5°)	0.5 (0.5)	1.0 (1.0)	True (True)	0.206 (0.2)	0.002 (0.01)	0.199 (0.2)	0.023 (0.01)
Case B2	5° (5°)	0.5 (0.5)	1.0 (1.0)	True (True)	0.270 (0.2)	0.004 (0.0)	0.202 (0.2)	0.001 (0.0)
Case B3	5° (5°)	0.5 (0.5)	1.0 (1.0)	True (True)	0.270 (0.2)	0.004 (0.01)	0.202 (0.2)	0.017 (0.01)
Case B4	10° (5°)	0.5 (0.5)	1.0 (1.0)	True (True)	0.270 (0.2)	0.004 (0.01)	0.202 (0.2)	0.017 (0.01)
Case B5	5° (5°)	0.5 (0.5)	1.0 (1.0)	Fitted (True)	0.270 (0.2)	0.004 (0.01)	0.202 (0.2)	0.017 (0.01)
Case B6	10° (5°)	0.5 (0.5)	1.0 (1.0)	Fitted (True)	0.270 (0.2)	0.004 (0.01)	0.202 (0.2)	0.017 (0.01)
Case B7	10° (10°)	0.5 (0.5)	1.0 (1.0)	True (True)	1.081 (0.2)	0.051 (0.01)	0.201 (0.2)	0.021 (0.01)

Table 1. MLE results for cases with different uncertainties and true inputs distribution estimation for the 2-dimensional analytical model. True values used to generate the observations are in brackets.

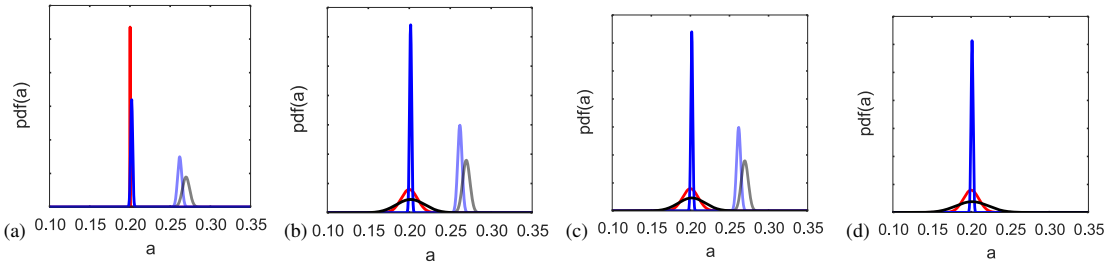

Figure 3. Two cases of uncertainty in the inputs for the 2-dimensional analytical model: (a) Case B2 (b) Case B3 (c) Case B5 (d) Case B7. The *red* line represents the true parameter distribution. The *light grey* line represents parameter distribution obtained from WLSE on the 15°-binned observations and model. The *light blue* line represents parameter distribution obtained from WLSE on the raw data. The *dark blue* line represents the total MLE distribution (equation 5). The *black* line represents the distribution of the MLE for each observation (equation 7).

4 MLE for wake model calibration

Wake model calibration using SCADA data has been done in the past Cleve et al. (2009). In this study the wake expansion parameter of the Jensen model was calibrated using least squares errors for every 10 minutes observations, with the assumption of negligible uncertainty in the inflow conditions: undisturbed wind speed and wind direction. In a similar process we propose to perform a maximum likelihood estimation for each 10 minutes observations in a process that considers the variation of the estimated inflow conditions from multiple turbines. Furthermore, we propose that the wake expansion parameter should be treated as uncertain, since there is large variability in its estimation.

4.1 Model

Jensen's model is one of the most popular wake models among engineering applications due to its simplicity, computational speed and robustness. The model was originally presented by Jensen (1983) and later on it was published in an academic article by Katic et al. (1986). This model assumes a top-hat wake velocity deficit profile that expands linearly with the distance from the rotor. Additionally it uses a global momentum balance to relate the rotor's thrust coefficient to the velocity deficit in the far wake resulting in the expression for the axial velocity deficit. Jensen's model does not consider the near wake expansion but assumes that the linear expansion starts immediately after the rotor. Because of this assumption, Jensen's model only fulfills continuity equation in the wake. The combination of the wakes generated by multiple upstream rotors is done using the squared root of the sum of the squared deficits in the original Jensen model (NOJ) and using linear wake superposition in a modified version used for comparison (MNOJ). Partial wake are considered by scaling the velocity deficit intensity by the ratio of the area affected by the wake with respect the rotor area.

The wake model is evaluated in steps of 2 degrees for the wind direction, in steps of 1 [m/s] in wind speed and in steps of 0.005 for the wake expansions. The model results are the interpolated using linear interpolation, see Figure 4.

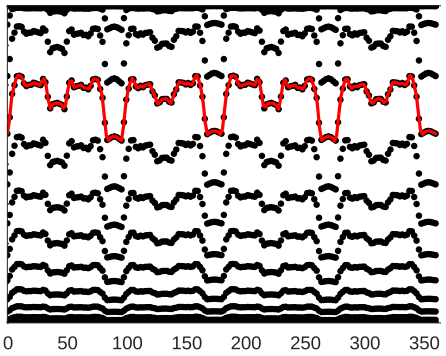

Figure 4. An example of model evaluation and interpolation for Horns Rev 1.

4.2 Measurements

The measurements of four offshore wind plants are used in the present study, see Figure 5. Horns Rev 1 is a 160 MW plant located 14 km away from the western coast of Denmark. It is owned by Vattenfall AB (60%) and by DONG Energy AS (40%). The 80 Vestas V80-offshore 2 MW wind turbines are aligned in a structured grid with 7 rotor diameters of spacing in both alignment directions. This study uses 3 years (2005-2007) of measurements from its SCADA database. Previous studies on this wind farm can be found in Barthelmie et al. (2010)Hansen et al. (2012)Moriarty et al. (2014)Walker et al. (2015).

Nysted is a 165.6 MW plant located 10.5 km away from the south-eastern coast of Denmark. Nysted is co-owned by PensionDanmark (50%), DONG Energy SA (42.75%) and Stadtwerke Lübeck GmbH (7.25%). The 72 Siemens (formerly

Bonus Energy AS) B82-2300 kW offshore wind turbines are aligned in a structured grid with 5.9 and 10.4 rotor diameters of spacing. 2.5 years (May 2004 to December 2006) of SCADA measurements are used in this study. Previous studies on this wind farm can be found in Barthelmie et al. (2009)Barthelmie et al. (2010)Cleve et al. (2009)Nygaard (2014)Walker et al. (2015).

Lillgrund is a 110.4 MW plant located 10 km away from the western coast of Sweden. It is owned by Vattenfall AB (100 %). The 48 Siemens SWT-2.3-93 wind turbines are aligned in a semistructured grid with only 3 rotor diameters of spacing and 2 rotors missing in the center of the layout. The layouts and some examples of the available sensors throughout each wind plant can be seen in Figure 5. Previous studies on this wind farm can be found in Hansen and Wind (2012)Walker et al. (2015)

Anholt is a 400 MW plant located 20 km away form the eastern coast of Denmark. It is owned by DONG Energy SA . Anholt is conformed by 111 Siemens SWT-3.6-120 turbines. This plant is characterized by its large size (over 20 km) and for its non structured layout that maximizes the number of turbines located in the outer border of the wind plant. A previous study on this wind farm can be found in Nygaard (2014).

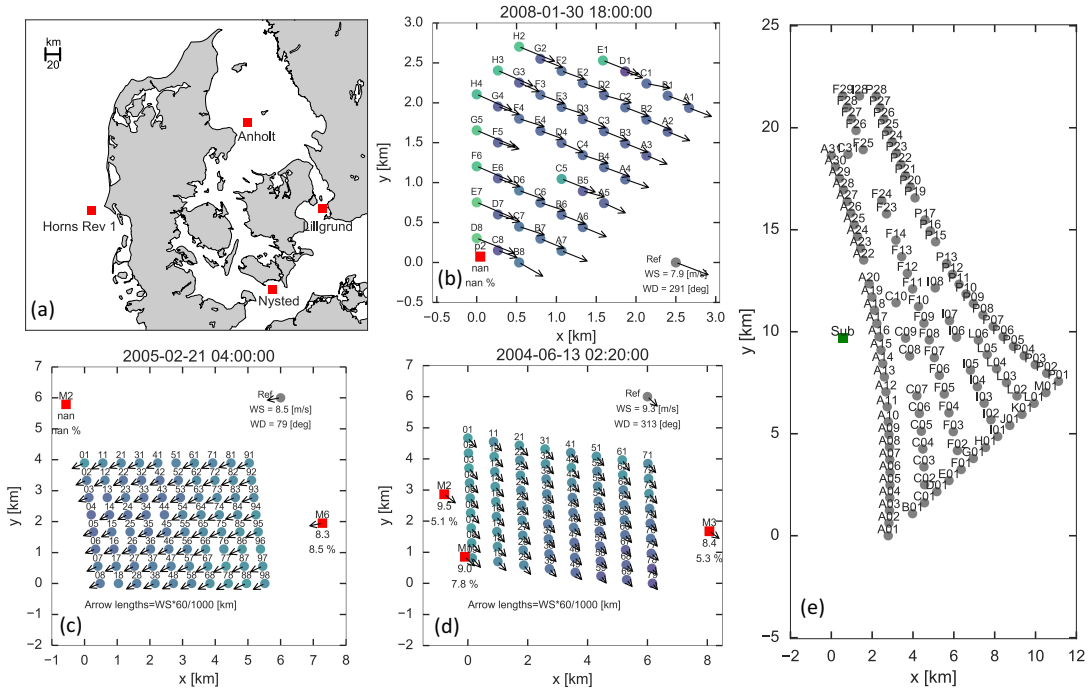

Figure 5. (a) Wind plants locations. (b) Lillgrund layout. (c) Horns Rev 1 layout. (d) Nysted layout. (e) Anholt layout. Each layout shows an example of the available sensors for a given 10 minutes flowcase.

The analysis of the operational data in order to determine the undisturbed wind speed and wind direction used in this work has been previously presented in Murcia et al. (2015, 2016). In this approach it is assumed that multiple nacelle anemometer and nacelle positions sensors from the plant can be averaged to estimate the undisturbed wind speed and velocity as well as its corresponding uncertainties. The estimated undisturbed inflow conditions are corrected for nacelle flow distortion using the nearby met masts available. This estimation is done for every single 10 minutes, and it assumes the same uncertainty sources and magnitudes as in Murcia et al. (2016). The calibration database is build from each wind plant SCADA database by filtering the flowcases in order to have at least 95% of the turbines under normal operation and in order to have inflow conditions in which there are wakes losses ($4 < \mathrm{WS} < 15\ \mathrm{ms}^{-1}$); the calibration dataset of observed power production as a function of the undisturbed wind speed and wind direction for each plant can be seen in Figure 6. The wind resources have bin fitted from all the observations in the database using a moving window maximum likelihood Weibull fit for the wind speed conditioned on the wind direction, and a polynomial fit for the cumulative density function of the wind direction. The resulting fits for the undisturbed wind resources can be seen in Figure 7.

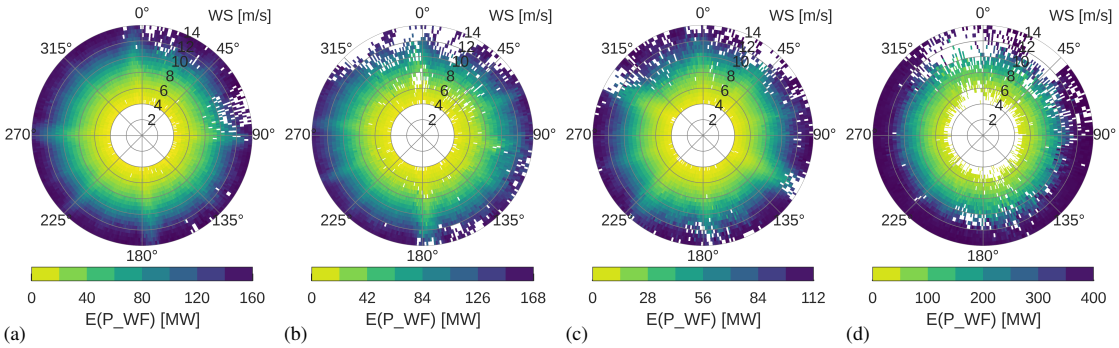

Figure 6. Observed power production at (a) Horns Rev 1, (b) Nysted and (c) Lillgrund. (d) Anholt.

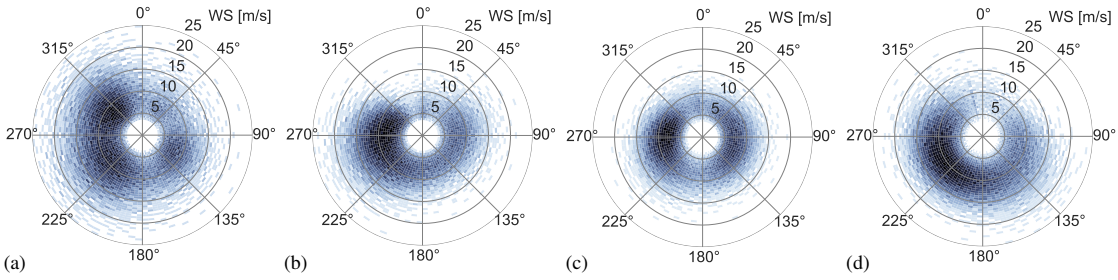

Figure 7. Fitted wind resources at (a) Horns Rev 1, (b) Nysted and (c) Lillgrund. (d) Anholt.

5 Likelihood estimation

Figure 8 presents an example of the estimation of the likelihood function using a Monte-Carlo approximation. This figure illustrates the MLE method for a single 10 minutes observation in Horns Rev 1 and for a single parameter. Note that the likelihood function needs to be estimated for a range of possible parameters. Figure 9 shows the broad distribution of likelihood functions for every 10-minute observations. In this example it can be seen that due to the non-linearities in the wake model with respect to the wind direction there are many local maximums in the wake expansion parameter. The highlighted example likelihood function (in red) has a narrower local-maximum likelihood wake expansion around 0.05, and a broader global-maximum likelihood wake expansion around 0.085. This means that the model allows for multiple solutions that agree with predicted total power production.

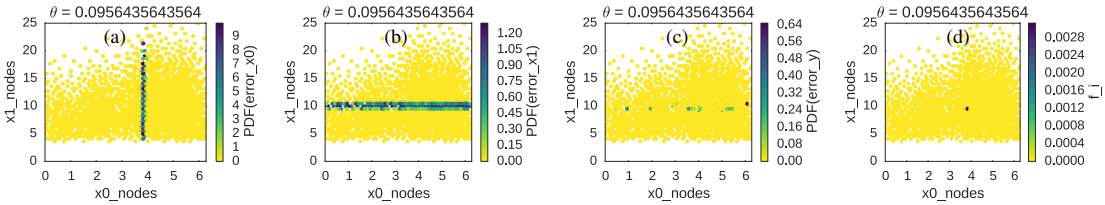

Figure 8. Example of the estimation of the likelihood function (equation 7) for a 10 minute case in Horns Rev 1. (a) Candidate true wind directions that agree with the observed wind direction. (b) Candidate true wind speeds that agree with the observed wind speeds. (c) Candidate model predictions that agree with the observed total power production. (d) Product of (a), (b) and (c): likelihood density function.

6 Calibration Results

The wake expansion calibration has been applied for the four wind plants. The final results of the calibration are summarized in Figure 10. Here the mean wake expansion parameter is estimated using the $30\,^{\circ} \times 1\ \mathrm{ms}^{-1}$ bin-averaged maximum likelihood wake expansion. The variability in the maximum likelihood parameters averaged over different bins is a good estimation for the parameter variability. The wake expansion variability is smaller for Horns Rev 1 and Lillegrund because these wind farms are symmetrical and it contains similar spacings in both main directions of alignment. In Nysted and Lillgrund the wake expansions shows a larger variability. The aggregation of the data from all the plants is done simply by combining the bin-averaged wake expansions into a single dataset. It can be observed that the aggregated wake expansion calibration gives a mean parameter of 0.058 with an standard deviation of 0.007 or a coefficient of variation (COV) of 12%.

The maximum likelihood wake expansion binned as a function of the inflow conditions are presented for the three wind plants in Figure 11. It can be observed that the maximum likelihood wake expansion is a function of the wind direction and it does not depend on the wind speed besides by the fact that the wakes are not present in above rated wind speeds. In particular it can be observed that for all the plants the maximum likelihood wake expansion is larger for the main directions of alignment. The directions in which the main spacing is smaller produce a larger wake expansion.

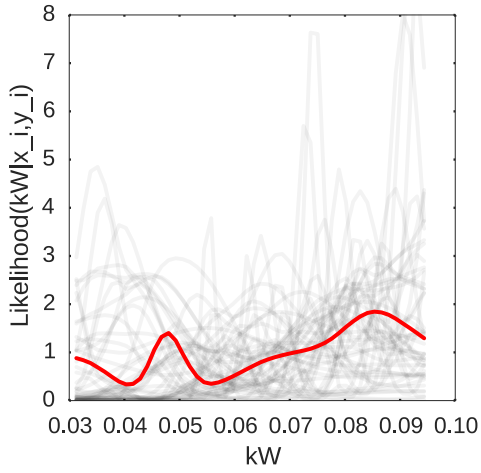

Figure 9. Likelihood function for the wake expansion parameters in the range [0.003, 0.095] for 100 10-minute cases at Horns Rev 1. One of the likelihood functions is highlighted for contrast.

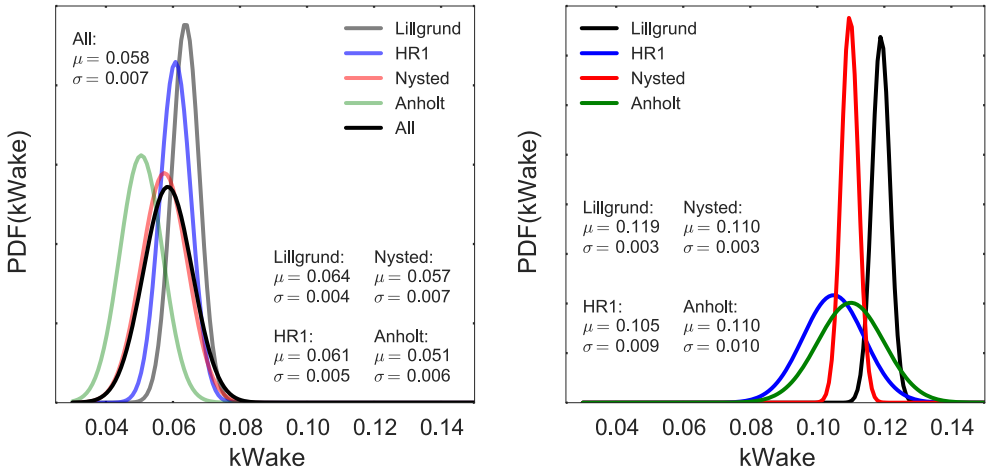

Figure 10. Wake expansion distribution for (left) Maximum likelihood estimation. (right) Weighted least squares of binned model and observations.

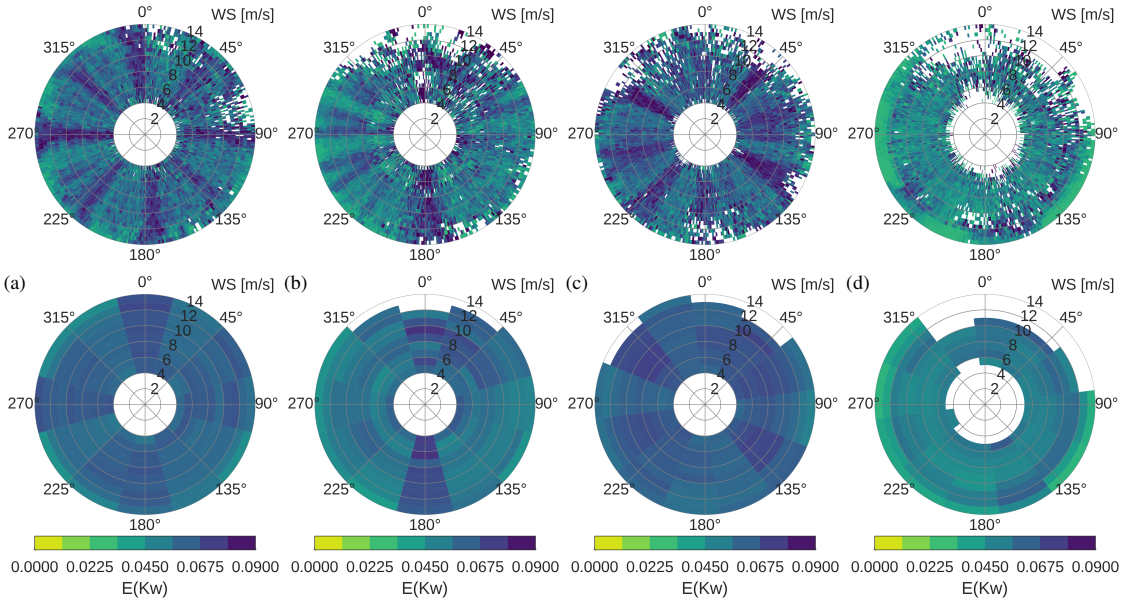

Figure 11. Maximum likelihood wake expansion dependency on the the inflow for two different bin sizes (a) Horns Rev 1 (b) Nysted (c) Lillgrund. (d) Anholt.

7 Estimation and reduction of AEP uncertainty

The problem of estimating the uncertainty in AEP given the results of the calibration consists in propagating the uncertainty of the wake expansion parameter though the AEP estimation. Since the model is very fast, then the distribution of AEP is obtained with a Monte-Carlo simulation of wake expansion parameters, see Figure 12.

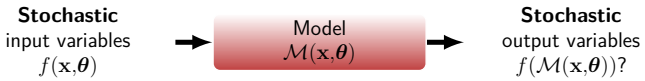

Figure 12. Propagation of uncertainty in the parameters $\boldsymbol{\theta}$ and in the wind resources $\mathbf{x}$.

The resulting distribution of the capacity factor (CF) for each wind plant are presented in figure 13. The spread of the CF distribution depends on the layout, since each plant has different turbine spacings and wind resources. The uncertainty in CF presented in this article is related only due to uncertainty in the wake expansion parameter; it does not consider uncertainty in the wind resources, nor uncertainty in the thrust coefficient or power curve.

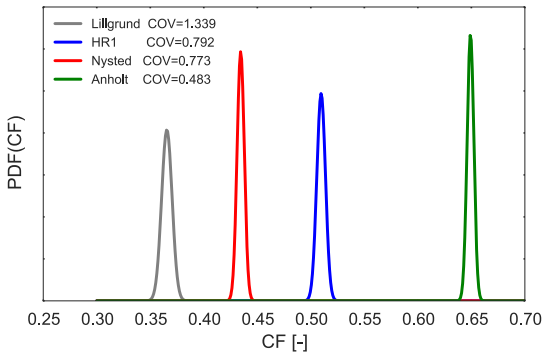

Figure 13. Uncertainty in the capacity factor of each wind plant due to the parameter uncertainty.

In order to reduce the uncertainty in AEP that comes from having a 12% COV in the model parameter one could exploit the fact that the resulting calibration of the NOJ model seems to be dependent on the wind turbine spacing and the amount of turbines aligned. It can be observed that the variability of the wake expansion for a given sector is reduced in comparison to the global variability over all the conditions. This means that one could use an estimation of the number of turbines aligned and their stream-wise spacing to predict the distribution of wake expansion parameters expected from the current calibration databases.

8 Conclusions

The conclusions of this article are:

1. Least squared errors calibration fails when there is large input uncertainty relative to the non-linearity of the model; for these cases the resulting parameter estimation contains large bias. This effect can not be removed by binning both the observations and the model into large input bins, because of the aliasing effect that the input uncertainty has on the binned averaged observations.

2. The proposed maximum likelihood estimation calibration is able to properly calibrate a model based on measurement campaigns in which the input uncertainty is high and that contains parameter variability such as the SCADA data of large offshore wind plants.

3. The obtained distribution of the wake expansion parameter depends on the wind direction, in particular the wake expansion parameter depends on whether the direction is a main direction of alignment and whether the stream-wise turbine spacing in that direction is large or not.

4. The uncertainty in AEP due to model uncertainty for the NOJ model with linear wake superposition can be reduced by defining a dependency with respect the spacing for those wind direction bins with large number of turbine aligned.

Acknowledgements. This work was supported by the International Collaborative Energy Technology R&D Program of the Korea Institute of Energy Technology Evaluation and Planning (KETEP), granted financial resource from the Ministry of Trade, Industry & Energy, Republic of Korea. (No. 20138520021140). We would like to thank DONG Energy AS and Vattenfall AB for the access to the SCADA data.

References

Barthelmie, R. J., Hansen, K., Frandsen, S. T., Rathmann, O., Schepers, J., Schlez, W., Phillips, J., Rados, K., Zervos, A., Politis, E., et al.: Modelling and measuring flow and wind turbine wakes in large wind farms offshore, Wind Energy, 12, 431–444, doi:10.1002/we.348, http://onlinelibrary.wiley.com/doi/10.1002/we.348/abstract, 2009.

Barthelmie, R. J., Pryor, S., Frandsen, S. T., Hansen, K. S., Schepers, J., Rados, K., Schlez, W., Neubert, A., Jensen, L., and Neckelmann, S.: Quantifying the impact of wind turbine wakes on power output at offshore wind farms, Journal of Atmospheric and Oceanic Technology, 27, 1302–1317, doi:10.1175/2010JTECHA1398.1, http://journals.ametsoc.org/doi/abs/10.1175/2010JTECHA1398.1, 2010.

Bastankhah, M. and Porté-Agel, F.: A new analytical model for wind-turbine wakes, Renewable Energy, 70, 116–123, 2014.

Clark, J. S.: Why environmental scientists are becoming Bayesians, Ecology letters, 8, 2–14, 2005.

Cleve, J., Greiner, M., Enevoldsen, P., Birkemose, B., and Jensen, L.: Model-based analysis of wake-flow data in the Nysted offshore wind farm, Wind Energy, 12, 125–135, doi:10.1002/we.314, http://dx.doi.org/10.1002/we.314, 2009.

Feinberg, J. and Langtangen, H. P.: Chaospy: An open source tool for designing methods of uncertainty quantification, Journal of Computational Science, 11, 46–57, 2015.

Hansen, K. S. and Wind, D.: WP1 wake model performance validation results for Lillgrund offshore wind farm, pp. 1–18, 2012.

Hansen, K. S., Barthelmie, R. J., Jensen, L. E., and Sommer, A.: The impact of turbulence intensity and atmospheric stability on power deficits due to wind turbine wakes at Horns Rev wind farm, Power, pp. 183–196, doi:10.1002/we.512, http://onlinelibrary.wiley.com/doi/10.1002/we.512/abstract, 2012.

Huard, D. and Mailhot, A.: A Bayesian perspective on input uncertainty in model calibration: Application to hydrological model "abc", Water Resources Research, 42, 2006.

Jensen, N.: A note on wind turbine interaction, Risoe National Laboratory, Roskilde, Denmark, Technical Report No. M-2411, 1983.

Katic, I., Højstrup, J., and Jensen, N. O.: A simple model for cluster efficiency, in: European Wind Energy Association Conference and Exhibition, pp. 407–410, 1986.

Kavetski, D., Franks, S. W., and Kuczera, G.: Confronting input uncertainty in environmental modelling, Calibration of watershed models, pp. 49–68, 2002.

Madsen, H. A., Larsen, G. C., Larsen, T. J., Troldborg, N., and Mikkelsen, R.: Calibration and validation of the dynamic wake meandering model for implementation in an aeroelastic code, Journal of Solar Energy Engineering, 132, 041 014, 2010.

Moré, J. J., Garbow, B. S., and Hillstrom, K. E.: User guide for MINPACK-1, Tech. rep., CM-P00068642, 1980.

Moriarty, P., Rodrigo, J. S., Gancarski, P., Chuchfield, M., Naughton, J. W., Hansen, K. S., Machefaux, E., Maguire, E., Castellani, F., Terzi, L., et al.: IEA-Task 31 WAKEBENCH: Towards a protocol for wind farm flow model evaluation. Part 2: Wind farm wake models, in: Journal of Physics: Conference Series, vol. 524, p. 012185, IOP Publishing, 2014.

Murcia, J. P., Réthoré, P.-E., Hansen, K. S., Natarajan, A., and Sørensen, J. D.: A new method to estimate the uncertainty of AEP of offshore wind power plants applied to Horns Rev 1, in: EWEA Annual Conference and Exhibition 2015, pp. 161–165, 2015.

Murcia, J. P., Réthoré, P.-E., Hansen, K. S., Natarajan, A., and Sørensen, J. D.: Improved validation of stationary wake models using uncertainty propagation, Wiley Online Library, 2016.

Nygaard, N. G.: Wakes in very large wind farms and the effect of neighbouring wind farms, in: Journal of Physics: Conference Series, vol. 524, p. 012162, IOP Publishing, 2014.

Nygaard, N. G. and Hansen, S. D.: Wake effects between two neighbouring wind farms, in: Journal of Physics: Conference Series, vol. 753, p. 032020, IOP Publishing, 2016.

Rosenblatt, M.: Remarks on a multivariate transformation, The annals of mathematical statistics, 23, 470–472, 1952.

Walker, K., Adams, N., Gribben, B., Gellatly, B., Nygaard, N. G., Henderson, A., Marchante Jimémez, M., Schmidt, S. R., Rodriguez Ruiz, J., Paredes, D., et al.: An evaluation of the predictive accuracy of wake effects models for offshore wind farms, Wind Energy, 2015.

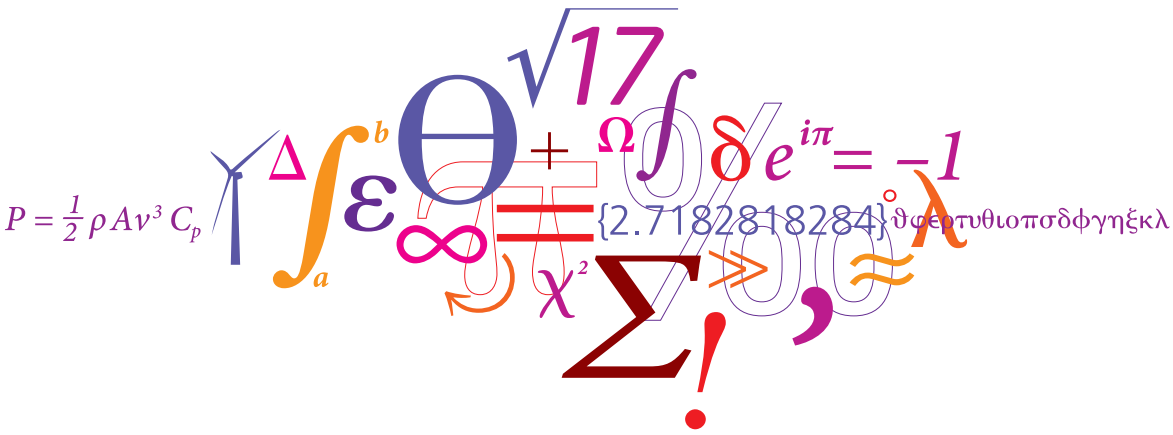
$P = \frac{1}{2}\rho A v^3 C_p$
$\Delta \int_a^b \varepsilon \Theta \sqrt{17} + \Omega \int \delta e^{i\pi} = -1$
{2.7182818284}ϑφερτυθιοπσδφγηξκλ
$\chi^2 \sum ! \gg \approx \lambda$